Theses and Dissertations   Graduate School

2017

EVALUATION OF THE REGIONAL DRUG DEPOSITION OF NASAL DELIVERY DEVICES USING IN VITRO REALISTIC NASAL MODELS

Mandana Azimi
Virginia Commonwealth University

EVALUATION OF THE REGIONAL DRUG DEPOSITION OF NASAL DELIVERY DEVICES USING *IN VITRO* REALISTIC NASAL MODELS

A dissertation submitted in partial fulfillment of the requirements for the degree of
Doctor of Philosophy at Virginia Commonwealth University

by

Mandana Azimi

Pharm.D., Tabriz University of Medical Science, Iran, 2006
Director: Michael Hindle, Ph.D., Professor
Department of Pharmaceutics

Virginia Commonwealth University
Richmond, Virginia
May, 2017

ACKNOWLEDGEMENT

I would like to extend my warmest gratitude to my parents and my sisters, without whom I would not be in this position that I am today.

Last, but certainly not least, I would like to acknowledge my dearest husband, Ali, for his support, sacrifice, encouragement, and staying by my side through this endeavor. Without him, it was impossible to finish this dissertation, and I am the luckiest woman on the earth!

LIST OF CONTENTS

LIST OF FIGURES

XII

LIST OF TABLES

GLOSSARY OF ABBREVIATIONS

°C	Celsius
3D	Three dimensional
AD	Anterior + drip
AIC	Akaike information criterion
ANDA	Abbreviated new drug application
ANOVA	Analysis of variance
API	Active pharmaceutical ingredients
AR	Allergic rhinitis
AUC	Area under curve
BE	Bioequivalence
BIC	Bayesian information criterion
BID	Twice a day
C	Concentration of drug in the bulk fluid
CF	Cystic fibrosis
CFD	Computational fluid dynamics
C_{max}	Maximum serum concentrations
CPF	Ciprofloxacin betaine

CRS	Chronic rhinosinusitis
CRSM	Mucus secretion in CRS
CRSsNP	CRS without nasal polyposis
CRSwNP	CRS with nasal polyposis
Cs	Saturation solubility of the drug in the boundary layer
CT scan	Computerized tomography
CTAB	Cetyltrimethyl ammonium bromide
D	Nasal spray actuation during nasal inhalation
DF	Degrees of freedom
Dmax	The longest diameter measured on spray pattern image
Dmin	The shortest diameter measured on spray pattern image
DOE	Design of experiment
DPI	Dry powder inhaler
dQ/dt	Dissolution rate
DSC	Differential scanning calorimetry
DSD	Droplet size distribution
DUSA	Dosage unit sampling apparatus
DV10	Maximum particle diameter below which 10% of the sample volume exists
DV50	Maximum particle diameter below which 50% of the sample volume exists

DV90	Maximum particle diameter below which 90% of the sample volume exists
E	Nasal inhalation started at the end of nasal spray actuation
EEG	Excipient enhanced growth
EMEM	Eagle's minimum essential medium
ESS	Endoscopic sinus surgery
F	Respiratory filter
hr	Hour
Kg	Kilogram
kHz	kilohertz
LAS	Liquid anti-solvent precipitation
LCC	Liquid covered culture
$Lmin^{-1}$	Liter per minute
LOD	Limit of detection
LOQ	Limit of quantitation
MBC	Minimal bactericidal concentration
MCC	Mucociliary clearance
mg	Milligram
mgL^{-1}	Milligram per Liter
MIC	Minimum inhibitory concentration

MIC90	Minimum Inhibitory Concentration required to inhibit the growth of 90% of organisms
min	Minute
mL	Milliliter
mm	Millimeter
MMAD	Mass median aerodynamic diameter
MP	Middle passages
MRI	Magnetic resonance imaging
ms	Millisecond
n	Number
NGI	Next Generation Impactor
NI	Absence of inhalation airflow
NSP	Nasal spray product
PD	Pharmacodynamic
Ph. Eur. 5.0	European Pharmacopoeia commission 5.0
PIBCA	Poly isobutyl cyanoacrylate
PIFR	Peak inspiratory flow rate
PK	Pharmacokinetic
PD	Pharmacodynamic
pMDI	Pressurized metered dose-inhaler

PSD	Particle size distribution
PTFE	Polytetrafluoroethylene
PVF	Polyvinylidene fluoride
PVP	Polyvinylpyrrolidone
Q	Volumetric flow
R	Airflow resistance
R^2	Coefficient of determination
R^2 Adj	Adjusted R squared
RMSE	Root mean square error
RSD	relative standard deviation
SA	Surface area
SA/V	Surface area to volume ratio
SD	Standard deviation
SDS	Sodium dodecyl sulfate
Sec	Second
SI	Slow inhalation
SPECT	Single-photon emission computed tomography
$t_{1/2}$	Half-life
TEER	Transepithelial electrical resistance

TGA   Thermogravimetric analysis

Tukey's HSD   Tukey's honestly significance test

TW   Transwell

Tween80   Polysorbate 80

USP   U.S. Pharmacopeia

VCU   Virginia Commonwealth University

ABSTRACT

EVALUATION OF THE REGIONAL DRUG DEPOSITION OF NASAL DELIVERY DEVICES USING *IN VITRO* REALISTIC NASAL MODELS

By Mandana Azimi, Pharm.D.

A dissertation submitted in partial fulfillment of the requirements for the degree of Doctor of Philosophy at Virginia Commonwealth University.

Virginia Commonwealth University, 2017
Major director: Michael Hindle, Ph.D.
Professor, Department of Pharmaceutics

The overall objectives of this research project were i) to develop and evaluate methods of characterizing nasal spray products using realistic nasal airway models as more clinically relevant *in vitro* tools and ii) to develop and evaluate a novel high-efficiency antibiotic nanoparticle dry powder formulation and delivery device. Two physically realistic nasal airway models were used to assess the effects of patient-use experimental conditions, nasal airway geometry and formulation / device properties on the delivery efficiency of nasal spray products. There was a large variability in drug delivery to the middle passages ranging from 17 – 57 % and 47 – 77 % with respect to patient use conditions for the two nasal airway geometries. The patient use variables of nasal spray position, head angle and nasal inhalation timing with respect to spray actuation were found to be significant in determining nasal valve penetration and middle passage deposition of Nasonex®.

XXX

The developed test methods were able to reproducibly generate similar nasal deposition profiles for nasal spray products with similar plume and droplet characteristics. Differences in spray plume geometry (smaller plume diameter resulted in higher middle passage drug delivery) were observed to have more influence on regional nasal drug deposition than changes to droplet size for mometasone furoate formulations in the realistic airway models.

Ciprofloxacin nanoparticles with a mean (SD) volume diameter of 120 (10) nm suitable for penetration through mucus and biofilm layers were prepared using sonocrystallization technique. These ciprofloxacin nanoparticles were then spray dried in a PVP K30 matrix to form nanocomposite particles with a mean (SD) volume diameter of 5.6 (0.1) µm. High efficiency targeted delivery of the nanocomposite nasal powder formulation was achieved using a modified low flow VCU DPI in combination with a novel breathing maneuver; delivering 73 % of the delivered dose to the middle passages. A modified version of the nasal airway model accommodating Transwell® inserts and a Calu-3 monolayer was developed to allow realistic deposition and evaluation of the nasal powder. The nanocomposite formulation was observed to demonstrate improved dissolution and transepithelial transport (flux = 725 ng/h/cm^2) compared to unprocessed ciprofloxacin powder (flux = 321 ng/h/cm^2).

CHAPTER 1
BACKGROUND AND INTRODUCTION

1.1   Anatomy and physiology of the nose

The nose has a number of major functions including i) heating, humidification of inspired air and gas exchange, ii) olfaction and iii) particulate filtration [1-3].

The nasal cavity is divided into two separate left and right chambers by the nasal septum with a total volume of approximately 15 mL and surface area (SA) of around 150 cm^2 for each side [4]. Each chamber can be segmented in three parts of i) the nasal vestibule which covers the area inside the nostril, ii) the olfactory region which is located in the roof of the nasal cavity with an approximate SA of 15 cm^2 on each side and iii) the respiratory region [1]. The nasal vestibule is covered with a keratinized, non-ciliated squamous epithelium which is not suitable for drug absorption. The nasal valve area, located posterior to the nostril (approximately 2 cm away), has a very small surface area of 0.3 cm^2 and is at a 90º angle toward the nasal floor. The nasal valve area is the primary flow-limiting segment of the upper respiratory airway and it introduces up to 75 % of the total resistance against the inspired air flow. It also causes change in the flow rate and direction of airflow during inhalation [4, 5]. The nasal valve area connects the anterior nose region to the respiratory region containing the nasal turbinates which are attached to the sidewall of the nasal cavity. The turbinates are three projections (Figure 1.1) referred to as the inferior, middle and superior turbinates. Turbinates have bony structures with a ciliated respiratory epithelium lining (these include pseudostratified columnar epithelium, ciliated and non-ciliated columnar cell with microvilli and cilia) and serve the purpose of heating and humidifying of inspired air with

their increased mucosal surface area and blood flow. There is laminar airflow in the nasal valve during normal nasal breathing at flow rate of 15 Lmin^{-1} which corresponds to an air velocity of 18 m/s. In turbinate regions, a reduced air velocity of 2-3 m/s facilitates warming and humidification of the inhaled air to about 34ºC and 100% relative humidity in the nasopharynx region [2].
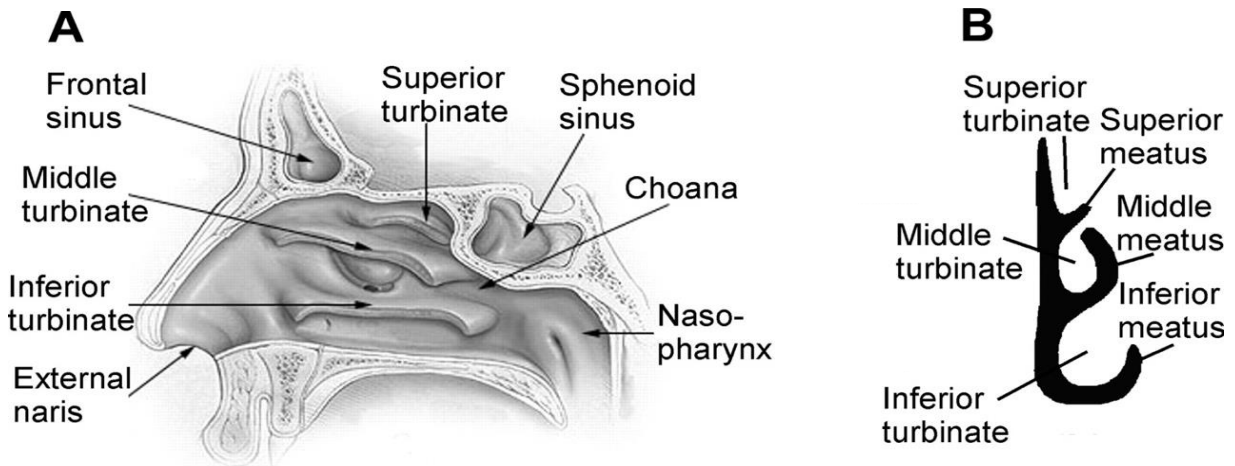
Figure 1. 1. Schematic view of the nasal cavity (A) sagittal cross section and (B) coronal cross section [6]

The area underneath each turbinate is called the meatus. The middle meatus is where the paranasal sinuses such as frontal, maxillary and ethmoidal sinuses drain into the nasal cavity. The paranasal sinuses are air-filled cavities and they function to lighten the skull and increase the resonance of sound [3].

Nasal mucociliary clearance (MCC) is one of the most important defense mechanisms to protect against potentially harmful airborne contaminants. MCC can also acts as an obstacle for nasal drug delivery since it may clear drug formulations prior to their absorption. MCC consists of two major components, the mucus blanket and the ciliated epithelium. The secretion product of

goblet cells, submucosal glands and fluid transported across the epithelium in the respiratory region forms a 2-phase mucus layer with a total thickness of about 10 - 15 µm. The mucus sol (watery) layer covers the epithelium and the gel layer is exposed to air covering the entire nasal cavity regions to efficiently filter inhaled particles in the range of 3 - 10 µm [2, 5]. The gel-like mucus properties are due to the content of mucins (high molecular weight glycoproteins) composed of 80 - 90% carbohydrate, 20% protein containing 1 - 2% sulfate bound to oligosaccharide side chains. The matrix format of mucus is formed by water molecules binding to these oligosaccharide side chains which also lubricates and protects the mucosal surfaces. Except in the inferior turbinate region where the mucus transport is directed toward the anterior region, in the remaining respiratory area, with the aid of cilia (5 µm shafts) beating at an average of 6 mm/min, and the mucus blanket, particles entrapped are propelled posteriorly toward the nasopharynx, throat and then the gastrointestinal tract [5]. The cilia beat also moves mucus secretions into the paranasal sinuses such as frontal, maxillary and ethmoidal sinuses through their narrow openings called ostia, located in the middle meatus (in the area under the middle turbinate).

1.2 Intranasal drug delivery

Drugs are administered intranasally for the local treatment of disorders including nasal allergy, congestion, sinusitis and infections. Sinusitis is a prevalent disease in the United States, which   is characterized by persistence (up to 4 weeks) of sinonasal mucosal inflammation due to allergies, viral or bacterial infection and inhaled irritants. It can progress to chronic rhinosinusitis (CRS) characterized by the accumulation of highly viscoelastic mucus and loss of cilia, obstruction of the nasal airways and sinuses which may stimulate further inflammation, creation of nasal polyps, olfactory dysfunction, headache, and breathing problems. CRS is one of the major chronic

diseases which affect 15% of the US population. These disorders can be treated using nasal delivery systems delivering antihistamines, mast-cell inhibitors, anticholinergics, corticosteroids or by treatment with systemic antibiotics [7].

Nasal delivery can also be used as a non-invasive means of systemic delivery of medications with poor oral absorption, low bioavailability, and slow onset of action [4]. By avoiding first pass metabolism and due to rapid absorption, peptides, vaccines and pain relief medications have been administered via the nose for systemic purposes. There are number of emergency medications that can be delivered intranasally for controlling pain or seizures, inducing sedation and for treating opioid overdose [8]. In addition, nose to brain delivery of small molecules and macromolecules deposited in the olfactory region through olfactory nerve and branches of the trigeminal nerve have been considered for "nose-to-brain" transport. Generally, drugs need to reach to the mucosal surface of the respiratory region to exert their pharmacological actions in the treatment of local and systemic diseases via the nasal route [7].

1.2.1   Factors influencing nasal drug delivery

The physicochemical properties of the drug and formulation together with the nasal anatomy and physiology play an important role in delivering drugs to their site of action and their absorption following nasal administration. Small lipophilic drugs can cross the nasal epithelium via transcellular and paracellular (diffusion or receptor mediated) routes. It has been reported that nasal administration of lipophilic drugs such as propranolol, progesterone, pentazocine and fentanyl demonstrated rapid and complete absorption [9, 10]. For more polar compounds, incomplete absorption from the nasal mucosa results in low bioavailability, with values as low as 10% for small molecular weight drugs and less than 1% for peptides such as insulin, calcitonin and leuprolide [9]. The poor absorption can be explained by a combination of low membrane

4

permeability, efficient drug clearance from the nasal cavity due to MCC and finally for peptides and proteins some degree of enzymatic degradation. One strategy that has been employed to improve absorption has involved formulation with excipients such as absorption enhancers or mucoadhesive agents to increase residence time in the nasal cavity. The intranasal delivery of morphine utilizing chitosan as a mucoadhesive agent, and also its ability to temporarily open tight junctions, enhanced the drug's bioavailability by 6 times compared to the initial formulation. Further improvements in the formulation resulted in an 80 % bioavailability and rapid decline in breakthrough pain during a Phase II clinical trial in cancer patients [9, 11].

For efficient nasal delivery for treatment of local disease within the nose, medication needs to reach the middle passages where the middle meatus, and the superior and middle turbinates are located with minimal delivery to the lower respiratory tract and the lungs. The anatomical barriers for efficient delivery include the presence of the nasal valve with its small surface area and right angle bend. For sinus drug delivery, this is even more challenging, as drug must penetrate through the small sinus ostia which are in the range of 3 - 5 mm in diameter. These ostia are often blocked in sinusitis, and the sinuses remain a poorly ventilated region that makes them difficult to reach. Moreover, the presence of mucociliary clearance results in translocation of drug to the posterior region of the nasal cavity and nasopharynx within 10 - 30 min. This requires that poorly soluble drugs such as corticosteroids must be dissolved within this short time window [2, 7, 8]. In addition to the complex geometry of the nasal cavity, there is significant inter and intra-subject variability with respect to race, sex and age, along with the variability associated with nasal septal deviation or the presence of the nasal cycle which can result in increased variability in delivered dose [12-14].

The primary site of drug deposition is also highly dependent upon the delivery system, formulation (liquid, gel or powder) and patient administration technique. The drug concentration and volume (in case of liquid formulations) must be optimized to maximize respiratory epithelial coverage and reduce removal of the formulation by dripping from the nose or mucociliary clearance. The presence of local irritaion or disease in the nose also needs to be considered; for example in nasal atrophy and severe vasomotor rhinitis the capacity for nasal drug absorption is reduced which results in drug dripping out of the nose or down the back of the throat for liquid formulations, thus reducing bioavailability [8]. Changes in airflow pattern within the nasal cavity depending upon device insertion location within the nostril have been reported to result in varying drug distribution in the nasal cavity which makes the release point of medication one of the important factors that needs to be considered [15].

1.2.2   Assessment of the regional nasal drug deposition

Ideally, to assess drug deposition, distribution and clearance of nasal delivery systems *in vivo*, two-dimensional imaging such as scintigraphy (gamma camera imaging), three-dimensional imaging using CT, single-photon emission computed tomography (SPECT) or endoscopic visualization with an aerosolized dye are the gold standards [7, 16-18]. However, these methods are expensive, time consuming, mostly qualitative or at best, semi-quantitative, and there can be risks due to radiation. Probably most importantly, for use from a regulatory perspective, they require the incorporation of a radiolabel agent which may not distribute homogeneously in suspension formulations and represents an altered form of the proposed commercial formulation [2]. It is considered important that deposition studies to establish local delivery are performed on the unmodified proposed commercial formulation for regulatory purposes. As an alternative, employing a realistic nasal *in vitro* geometric model to assess the deposition pattern of nasal spray

products would be an inexpensive and efficient alternative to these studies during product development and evaluation and would allow testing with the unmodified proposed commercial formulation. The assessment of both new and generic nasal spray products would benefit from the use of clinically meaningful *in vitro* methods to assess the delivery efficiency of nasal drug products.

1.2.3   Use of realistic airway geometries

Nasal airway models have historically been used for assessing the deposition efficiency of submicron and micron size particles in nasal airways to evaluate environmental exposure to airborne materials or for simulation of nasal airflow dynamics [19] and heat and humidity transport in the nasal cavity [20-26]. Advanced imaging techniques including magnetic resonance imaging (MRI) [27] and computed tomography (CT) enable improved accuracy in the measurement of nasal airway dimensions of human subjects compared to measurements derived from casts obtained post-mortem from human cadavers resulting in more accurate models [25, 28]. Rigid or soft airway models can now be produced with realistic nasal geometries and dimensions using stereolithography [29].

It should be noted, however, that these models have some limitations including the absence of a nasal mucociliary clearance process and the models may not reflect the *in vivo* physiology of different nasal disease states. Also, these models lack the dynamic capacity for altering the size and tonicity for the nasal valve region during nasal breathing and nasal cycling (dynamic and irregular change in nasal passages caliber and alternating congestion and decongestion) [25]. In addition, for rigid models, small sized nostrils may restrict the positioning of the nasal spray within the nostril. Lastly, application of organic solvents on the surface of the nasal model for extraction

of administered poorly soluble steroid drug formulations may results in extraction and dissolution of plastic resin and change in the nasal airway dimensions over time.

Attempts to validate nasal models have used methods to measure the pressure drop across the model and compare the total deposition efficiency in the model with *in vivo* deposition data [20, 23, 30, 31]. Table 1.1 summarizes the nasal airway geometries that have been used for assessing the delivery efficiency of nasal sprays and the developed standardized and average nasal models.

Table1.1 Human nasal models: Model origin and regions of interest

Nasal Model type	Data Source	Nasal Region Segments	Ref
Idealized model	Derived from CT scans of 10 infants aged 3–18 months	One part model	[32]
Average model	Derived from CT scans of 30 healthy adults aged 17-78, Does not consider the shape deviation in the nasal cavity	3 sections: anterior nose, middle passage and nasopharynx regions	[6]
	Derived from CT scans of 26 healthy adults aged 17-70, Considers the variations in nasal passages	3 sections: anterior nose, middle passage and nasopharynx regions	[33]
	Derived from CT scans of 3 healthy adults aged 31-53, Considers the variations in nasal passages	3 sections: anterior, middle and posterior cavity	[14]
Individual "typical" model			
Bespak	Derived from CT scan of healthy female	5 sections: anterior nose, anterior turbinates, posterior turbinates, olfactory and nasopharynx regions	[34]
Boehringer Ingelheim	Derived from CT scan of 40-year-old healthy Caucasian male	5 sections: anterior nose, inferior, middle and superior turbinates, and nasopharynx regions	[35]

Koken	Cast derived from human cadaver	2 sections: divided into left and right nasal cavity One part model with access to maxillary sinuses	[19, 36-38]
NC1	Cast model derived from a human cadaver	One part model	[39]
NC2	Replica constructed from CT scan of NC1	One part: nose-throat model	[40]
Saint	Derived from CT scan of 9-month-old Caucasian female	3 sections: anterior nose, middle passage and nasopharynx regions	[41]
VCU model 1 (also, used by Lovelace and CIIT Center for Health Research)	Derived from MRI scan of nonsmoking, 53-year old Caucasian male with no pathophysiological Conditions	2 sections: anterior nose, middle passage and nasopharynx regions	[21, 31, 42, 43]
VCU model 2	Derived from CT scan of healthy 20-year old female	2 sections: anterior nose, middle passage and nasopharynx regions	[44]

The use of a physically realistic model, compared to the current FDA *in vitro* methodology, may offer insights into the predicted deposition pattern of nasal spray products within the nose. However, it is important to consider a number of issues as we look to harmonization and standardization of the methodology. From a regulatory method perspective, one important issue is the identification of single or multiple model airway geometries that can be made available to the scientific community. To date, however, several different models have been described and are summarized in Table 1. Options available include, the development of an idealized nasal airway geometry, similar to the infant nasal airway described by Javaheri et al. [32], the use of composite "average" human nasal airways [6, 33] or the use of an individual "typical" human nasal airway

based on average airway geometries [21, 31, 34-36, 39, 41]. The infant idealized nasal and throat models were able to mimic average deposition in multiple anatomical models by including simplified features of the anatomical airways, and an average value of representative characteristic dimensions that captures the variability among multiple anatomical models [32, 45]. A new developed average model was obtained by the use of a deformable template method for aligning and averaging the nasal airway geometry from computed tomography (CT) scans of 26 individuals where there were good agreement between the landmark locations between input CT scan of individual and the average model [33]. At Virginia Commonwealth University (VCU), our two nasal airway models are constructed from an MRI scan and a CT scan of non-smoking 53-year old man and a 20-year old female, respectively. For VCU nasal model 1, the dataset was originally reported by Guilmette et al. [46] and been used in a number of nasal particle deposition experiments [29, 43] and simulations [47]. For VCU nasal model 2 the CT scan data was obtained from VCU Medical Center. In order to measure regional drug deposition in the model, the nasal cast was divided into the anterior/nostril, middle passage and nasopharynx regions [48]. The VCU nasal model 1 was also complimented by the development of three additional nasal models that seek to address the issue of disease state and population variability during testing. The 'Average', 'Constricted1', and 'Constricted 2' models were developed from 12 CT scans of adults ranging from 19 to 60 years at VCU to form a set of nasal anatomies that span the expected range of surface area to volume ratios found in the adult population [44]. In addition to defining the airway geometric model, it is also important to define the regions of interest, if regional deposition is to be investigated. Table 1.1 shows the nasal regional segments employed by a series of nasal airway geometries, with the most significant difference being the divisions made to the middle passages. The Lovelace [31] and Boehringer Ingelheim [35] models segment the middle passage horizontally

into the inferior, middle and superior turbinates, while the Bespak model [34] is segmented vertically into the anterior and posterior regions. The VCU *in vitro* model considers the total middle passage deposition [21], but has been segmented in previous CFD studies in multiple ways. The nasal airway models are manufactured from a variety of polymer resins with the VCU model being made from Accura ClearVue resin (3D Systems, Inc., Rock Hill, SC); solvent resistant resins from which deposited drug can be completely recovered are essential.

These models have been used to study the effects of device and formulation characteristics, nasal airway variability and nasal spray administration methods on the nasal deposition pattern [42]. However, the conclusions reached about the importance of these variables are often inconsistent. Guo et al., [36] found no significant effect when assessing the presence and absence of constant inhalation airflow on regional deposition of nasal spray formulation, whereas Trows et al., [35] observed greater deposition in nasal vestibule, middle and upper turbinates when administering a nasal spray during inhalation. These observations may be due to the differing experimental protocols used to perform the studies or the different *in vitro* nasal models with different geometries. In addition, there is a lack of standardization for segmentation of the middle passages and the region of interest in middle passages such as turbinate area is often segmented differently. In this research, using *in vitro* nasal airway models, the effect of formulation and device variables, administration technique and inter-subject variability in the geometry of the nasal cavity can be assessed for developing new and generic nasal spray products. However, *in vivo* validation may be needed to establish *in vitro – in vivo* correlations.

1.2.4 Intranasal delivery devices

Intranasal delivery of aqueous solution and suspension formulations can be achieved using a rhinyle catheter, dropper, unit dose pipette, mechanical spray pump such as a squeeze bottle, unit

dose or multiple dose metered dose spray pump, pMDI and nebulizer. Powder formulations can be delivered via a nasal powder inhaler and nasal insufflator. However, among all devices mentioned above, the metered dose nasal spray is the most popular option [2, 7].

1.2.4.1 Metered dose nasal sprays

Nasal drug delivery using solution and suspension metered dose nasal spray products has been employed widely for both local (e.g. corticosteroids for CRS) and systemic therapeutic effects (e.g. sumatriptan for migraine). The metered dose pump typically delivers 100 μL (25 – 200 μL) per spray as single or multiple dose delivery systems. The therapeutic ingredient can be dissolved or suspended in a formulation along with excipients such as buffering agents, osmolality modifiers, wetting agents, bio-adhesive polymers or viscosity enhancers, and preservatives [49]. New designs of nasal sprays use a collapsible bag, a movable piston or compressed gas to compensate for the delivered liquid, reducing the need for incorporating preservative in the formulations. Other approaches use filters for reducing contaminations in the incoming air to the spray pump, or utilize the oligodynamic activity of a silver wire in the tip of the actuator or a silver coated spring and ball (antiseptic properties of silver ion released in the formulation) [50].

The droplet size and plume properties exiting from most nasal sprays depends on the pump design and the actuator orifice, formulation properties and applied actuation force, together with the swirl effect and break-up length. On nasal spray actuation, by applying force and creating pressure, the liquid formulation is transferred from the dip tube and exits from the spray orifice under the action of both radial and axial forces [51]. A swirling thin sheet of liquid exiting from the nozzle breaks up after a few millimeters into "ligaments" before forming the droplets (break-up length). This forms a hollow spray cone with droplets mainly at the periphery. The spray angle

diameters (Dmax and Dmin) are typically 2 to 3 cm measured at 1.0 to 2.5 cm from the spray nozzle. For a spray pump, inserted at a depth of 10 - 15 mm into the nostril, only a small portion of the plume can penetrate deep into the nasal cavity [52]. In addition, it has been suggested that there are 90% of particles or droplets larger than 10 μm and nearly 80 % of particles larger than 5 μm that will impact within the nasal cavity [53]. Most nasal sprays produce droplets larger than 40 μm and usually in the size range of 30 to 120 μm [54, 55]. Therefore, due to the presence of the nasal valve with its small surface area compared to the spray plume geometry and the high initial velocity of the emitted plume from the nasal spray, the majority of drug impacts on the anterior nose with only a small fraction penetrating into the middle passages. Moreover, it has been shown that within 15 to 30 minutes, more than 50% of the formulation delivered by a nasal spray will be cleared from the nose by mucociliary clearance which further reduces the formulation efficacy [4].

1.2.5 Development of generic nasal sprays

FDA received the first generic nasal spray application or abbreviated new drug application (ANDA) in 1978 and by the end of 2013, 85 nasal spray drug product ANDAs had been submitted to the FDA. Based on FDA reports, the average number of nasal spray ANDA submissions in the past 10 years (2003-2013) is six applications per year. FDA has established guidance for pharmaceutical manufacturers to assist in the development of generic nasal spray solution products and to establish equivalence between test and reference products. This guidance includes demonstration of equivalent *in vitro* performance shown by *in vitro* tests including determination of droplet size distributions using laser diffraction, determination of the % of drug < 10 µm using cascade impaction and characterization of the spray plume angle and spray pattern [56]. In addition, manufacturers must show formulation sameness and device comparability between the test and reference products to ensure similarity. However, in case of nasal spray suspension

products the FDA indicated that equivalence should be established based on a 'weight of evidence' approach through equivalent *in vitro* test performance, equivalent systemic exposure demonstrated with a pharmacokinetic (PK) study and equivalent local delivery based on a pharmacodynamic (PD) or clinical endpoint study. In addition, device similarity and formulation sameness should be demonstrated. These additional steps for the suspension formulations are required due to the complexity of suspension formulations and potential differences in the suspending drug particle characteristics (e.g. size, crystallinity) altering the rate and extent of drug availability locally at the nasal sites of action and in the systemic circulation following absorption. Nasal suspension formulations can contain more than one suspended component and current particle sizing technologies are limited in their ability to adequately characterize the particle size distribution (PSD) of the active ingredient in the presence of other suspended excipients.

Despite the established use of a number of *in vitro* characterization methods, Suman *et al.* [52] recognized that these *in vitro* tests were capable of discriminating between different nasal spray products, the differences did not necessarily translate to differences *in vivo* nasal deposition and absorption. While it appears that these tests are useful as quality control tests for assessing nasal spray performance, in practice, the confined anatomy of the nose makes it extremely unlikely that an emitted spray formulation develops into the fully developed plume, and therefore, the clinical relevance of such *in vitro* methodologies is doubtful [17].

1.2.5.1 Comparison of device nasal drug delivery efficiency

Nasal drops and vapors are the oldest and simplest nasal delivery systems. Nasal drops can be administered via a pipette. The main limitations of these delivery devices is the lack of precision in the administered dose and required complex administration maneuvers. Penetration of the

formulation through the nasal valve region is superior for drops compared to the nasal spray pump. However, administration of drops requires a head – down body position which results in poor patient compliance [57]. Nasal liquid formulations can also be delivered using a fine catheter by a trained person to the desired site. A hydrofluoroalkane (HFA) based pressurized metered dose-inhaler (pMDI) delivery system for beclomethasone dipropionate (QNasal, Teva Respiratory, LLC) has recently been developed in the USA [58]. Similar to nasal spray products, the pMDI produces localized deposition on the anterior non-ciliated nose as the emitted plume has an even larger velocity than the nasal spray plume [18]. However, the amount of drug loss due to dripping from the anterior nose and the deposition fraction in the throat are reduced and less variable with an overall higher drug retention and slower clearance compared to Nasonex® and Flonase® nasal spray products when administered to patients with allergic rhinitis [18].

Small volumes administered by nasal sprays (20 - 200 µL) are suitable for potent drugs (such as corticosteroids) and can be formulated as suspensions or solutions. Previously, for treatment of local infection in the nose, nebulizers have been used. Nebulizer delivery of antibiotics provided an increased drug penetration through the nasal valve region due to their small droplet size (often 3µm) [59, 60]. With respect to drug clearance, no differences in MCC rate for drugs administered by nebulizer or by nasal sprays was observed. However, nebulizers can deliver drugs to the olfactory region and upper portion of the nasal cavity where the MCC is slower. The limitation of using nebulizers is the large potential of lung drug delivery [17]. However, sonic jet nebulizers have shown improved results for sinus delivery of antibiotics [60].

Powder formulations can offer longer retention in the nasal cavity by the addition of mucoadhesive excipients to the formulation. In addition, they absorb moisture from the nasal lining fluid and may adsorb to the surfaces. Nasal powders have been administered via powder spray

devices similar to liquid sprays, or by breath-actuated inhalers (using patient inspiratory effort to aerosolize powder and delivery dose to the nasal cavity) and nasal insufflators devices with connected mouth and nose pieces [61].

1.2.6 Use of antibiotics in chronic rhinosinusitis

Chronic rhinosinusitis (CRS) is a common chronic disease of the nasal airways and paranasal sinuses affecting approximately 10 - 15% of the US population [62, 63]. The etiology of CRS is not completely clear, but it is believed that one or more factors, such as anatomical obstruction due to high mucus secretion, accumulation of bacterial or fungal infection in the sinuses, or allergies result in a chronic inflammation of the nasal airways. The most widely employed classification of CRS divides the disease into two classes, CRS with nasal polyposis (CRSwNP) and CRS without nasal polyposis (CRSsNP), on the basis of the presence or absence of bilateral nasal polyps as confirmed with nasal endoscopy. The main organisms in CRS include *Staphylococcus aureus, Enterobacteriaceae spp.*, and *Pseudomonas spp.*, and less commonly *Streptococcus pneumoniae, Haemophilus influenza*, and beta hemolytic streptococci [64-66]. In patients who had previous sinus surgery, *Pseudomonas aeruginosa* is a frequent cause of sinusitis. In addition, in cystic fibrosis (CF) patients the most dominant organism isolated from sinuses is *Pseudomonas aeruginosa* [67]. There is a high rate of endoscopic sinus surgery (ESS) in North America due to ineffective drug treatment options [62].

The main therapies for CRS include topical nasal irrigation, nasal steroids and oral antibiotics [68]. The first-line agent for treatment of acute sinusitis is extended use of antibiotics such as amoxicillin/clavulanic acid. However, a double-blind study including 251 CRS patients with major infection of *S. pneumonia, S. aureus* and *Haemophilus influenza* compared the effectiveness of ciprofloxacin and amoxicillin/clavulanic acid (500mg BID (two times a day) for

9 day for each treatment) and the results showed that ciprofloxacin was as effective as amoxicillin/clavulanic acid. There was a similar clinical cure rate of 58.6 % and 51.2% and bacterial eradication of 88.9 % vs 90.5%, respectively, for ciprofloxacin vs. amoxicillin/clavulanic acid [69]. A clinical study also assessed the effect of oral administration of ciprofloxacin in 56 patients with CRS (30 patients were diagnosed with bacterial infection, mostly with *S. pneumonia, S. aureus and Haemophilus influenza*). These patients were given 500 mg of ciprofloxacin orally, BID, for 9 months. The bacterial infection was eradicated in 90% of the cases with the bacterial infection and cure rate greater for these patients compared to patients with no evidence of infection (83 % and 71 %, respectively) [70].

Despite the main use of antibiotics for treatment of CRS being administered systemically, there are studies which have examined the use of local delivery of antibiotics. Vaughan et. al [71] assessed the effect of nebulized ciprofloxacin for a duration of three weeks in patients with CRS with previous sinus surgery who were positive for bacterial infection by *S. aureus and Pseudomonas aeruginosa.* The dose of ciprofloxacin was 90 mg twice a day. The results showed that patients treated with nebulized ciprofloxacin had 11-16 infection free weeks compared to the standard therapy (average of 6 weeks). A clinical trial was conducted using nebulized levofloxacin (125 mg-twice a day) for 14 days to assess its efficacy in treatment of CRS for patients with a history of bilateral endoscopic sinus surgery [72]. The device used was the NasoNeb nebulizer (MedInvent, LLC, Medina, OH), which is a pulsating nebulizer. The device produces an aerosol with a droplet size of 23.3 microns and no particles smaller than 15 microns. It is designed to deliver between 0.2 to 15 mL of liquid formulation [73]. The manufacturers website indicated that "NasoNeb-delivered levofloxacin demonstrate a reduction in total bacterial abundance in a randomized, controlled trial of chronic sinusitis patients".

However, using nebulizer delivery systems, the drawbacks are lower formulation stability and long nebulization time, the need for rigorous cleaning after each use to reduce the risk for contamination, and they are relatively bulky to carry around. Improved physicochemical and microbial stability can be accomplished by formulation of nasal powders. Also, for nasal sprays, inadequate distribution of the particles produced by nasal spray pumps limit the therapeutic effects for topical and systemic applications. Nasal powder formulation is a viable system for less potent drugs (needing higher doses) and for delivery of therapeutics such as antibiotics with greater distribution in posterior nasal cavity.

It has been suggested that inhaled micro-antibiotic formulation would be entrapped in the biofilm produced by Pseudomonas aeruginosa in CF patients [74-76]. The biofilm produced by bacteria was shown to be a complicated 3D heterogeneous mesh with holes ranging from 100 nm to 500 nm, therefore drug formulation should be small enough to travel through the mesh [77, 78]. The mucus secretion in CRS patients (CRSM) are also highly viscous due to excess mucin secretion and release of DNA and actin from degenerating neutrophils. Based on the mobility of different sized PEGylated particles, the average pore size of fresh CRSM has been reported to be at least 150 ± 50 nm [76]. Therefore, one approach for successful powder antibiotic delivery to the nasal cavity may involve formation of a matrix of nanoparticles which releases the primary nanoparticles upon deposition in nasal fluid. This possibility has been investigated in this dissertation.

1.2.6.1   Ciprofloxacin

Ciprofloxacin, a fluoroquinolone, is a broad-spectrum antibiotic first introduced in 1980 and was effective against a wide variety of Gram-negative and Gram-positive bacteria. It is a

zwitterion and exhibits poor solubility at physiologic pH = 7.4 [79, 80]. The solubility curve for ciprofloxacin is shown in Figure 1.2 as a function of pH [79]. The change in solubility with respect to pH can be explained by formation of different species at respective pH (Figure 1.3). Based on Figure 1.2, the lowest solubility values are observed in the pH region around 7.4. Higher solubility is observed at pH values < 5.9 and > 8.9. The dominant species at pH values lower than 5.9, are the soluble ciprofloxacin$^+$ species (ciprofloxacin ion with + charge) and at pH higher than 8.9 are the soluble ciprofloxacin$^-$ (ciprofloxacin ion with - charge) species. The pH range from 5.9 (pKa1) to 8.9 (pKa2) contains three different species producing the lowest solubility in water at pH 7.4 due to the dominant presence of the ciprofloxacin zwitterion species which is neutral (Figure 1.3) [80]. Therefore, ciprofloxacin is more soluble when present as either its cation or anion forms.

The bactericidal action of ciprofloxacin results from interfering with replication, transcription repair and recombination of bacterial DNA by inhibition of the enzymes topoisomerase II (DNA gyrase) and topoisomerase IV followed by formation of complexes of quinolone-enzyme-DNA leading to the production of cellular poisons and cell death. The drug's carboxyl group and ketone moiety have been suggested to be involved in its binding to the bacterial DNA/DNA-gyrase complex and to facilitate its penetration into the cells (Figure 1.3) [81, 82]. The MIC for 90% of the *P.aeruginosa* strains (MIC90) for ciprofloxacin was shown in several studies to be around 0.25 mgL^{-1}. A previous study of ciprofloxacin pharmacokinetics for normal subjects demonstrated that the drug was rapidly absorbed after oral administration and that levels in plasma were well above the MICs for *Enterobacteriaceae, Haemophilus influenzae, P. aeruginosa*, and *Staphylococcus aureus*. Maximum serum concentrations (C$_{max}$) were attained 1 to 2 hours after oral dosing. C$_{max}$ after 12 hours dosing with 250, 500, or 750 mg are 0.1, 0.2, and 0.4 µg/mL, respectively. The serum elimination half-life (t$_{1/2}$) in subjects with normal renal function was

approximately 4 hours. Serum concentration - dose proportionality was observed up to a dose of 1000 mg [83, 84]. After oral administration of ciprofloxacin 750 mg twice a day, drug concentration measured in the nasal and saliva secretion on days 4 to 6 of therapy were reported as 1.84 ± 0.91 µg/mL and 1.29 ± 0.91µg/mL with peak and trough serum concentration of 2.56 ± 1.80 µg/mL and 0.97 ± 0.81 µg/mL [85]. In another study the concentration of ciprofloxacin in the nasal secretion of healthy subjects was measured after 750 mg BID administration for 2 days. Specimens were collected 2, 5 and 8 hr after the last dose. The mean concentration in nasal secretion after two and eight hours were 0.27 ± 0.4 µg/mL and 0.04 ± 0.03 µg/mL, respectively [86].
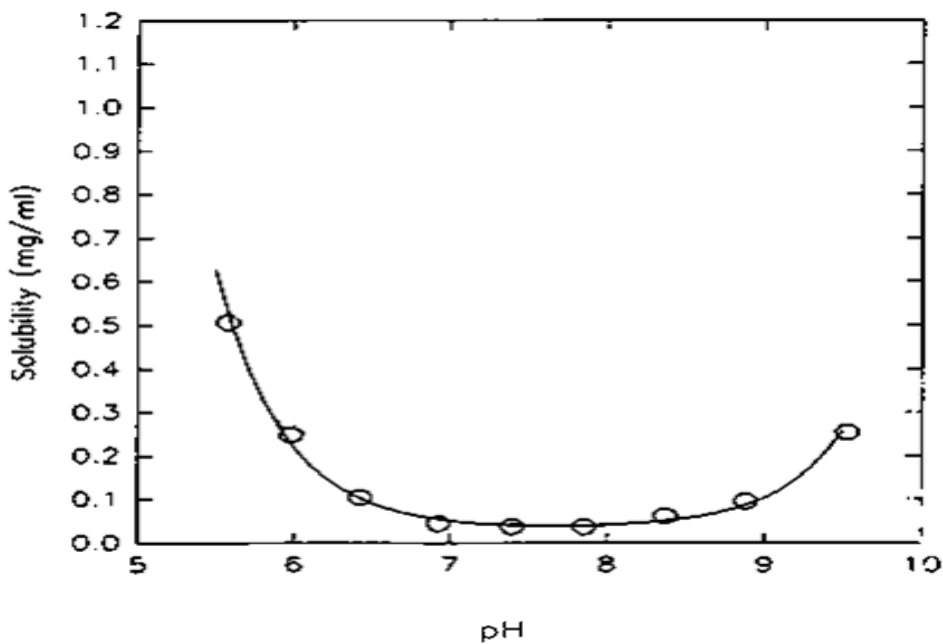
Figure 1.2. Ciprofloxacin solubility profile as a function of pH at 25ºC [79]
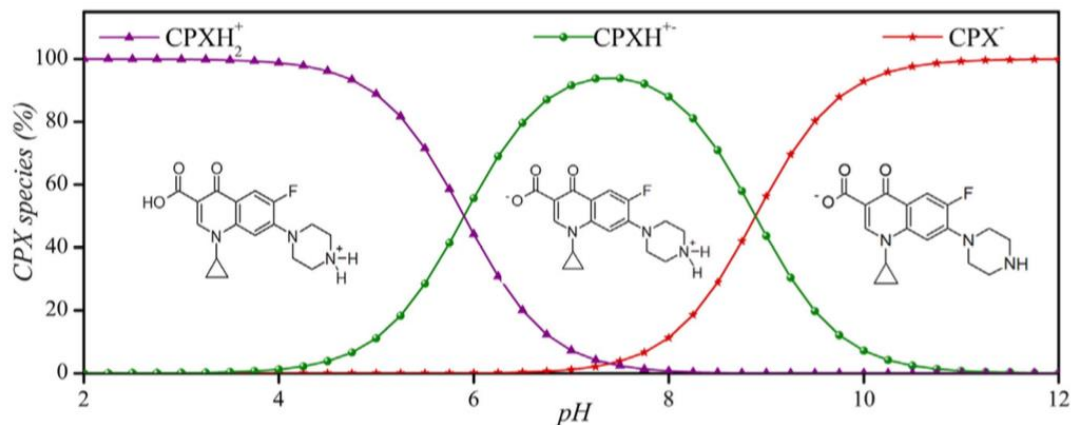
Figure 1.3. Ionization of ciprofloxacin (shown as CPX on diagram) as a function of pH [80]

Intratracheal administration of a micronized suspension (50% < 3µm and 90% < 7µm) of ciprofloxacin betaine showed prolonged half-life ($t_{1/2}$) of 13.5 hr in the lungs vs <1hr and 1.96 hr compared with ciprofloxacin hydrochloride and ciprofloxacin suspension. Differences in half-life were perhaps due to differences in the dissolution rate of the betaine and hydrochloride forms, together with particle size [87]. Also in development is a powder formulation of ciprofloxacin for inhalation in a dry powder inhaler (PulmoSpheres[TM] Technology by Novartis with particle size of ≤5 µm). This formulation uses ciprofloxacin betaine and is currently in Phase III clinical trials for the treatment of bronchiectasis in non-CF patients [88]. For this formulation, the mean deposition of ciprofloxacin in the trachea/bronchi and alveolar space was 22.3 % and 17.2 % of the total dose, respectively, with moderate inter-subject variability being observed [89]. This antibiotic formulation exhibits markedly reduced systemic absorption, thus enhancing its local action and potentially minimizing side effects. The dual formulation of liposomal ciprofloxacin, Pulmaquin, finished Phase 3 clinical trial study [90]. This product is a mixture of extended-release ciprofloxacin mixed with a small amount of ciprofloxacin dissolved in an aqueous medium developed for the management of chronic lung infections with Pseudomonas aeruginosa in

21

subjects with non-cystic fibrosis bronchiectasis and cystic fibrosis patients. The minimum inhibitory concentration (MIC) for ciprofloxacin against gram positive and negative bacteria is reported to be in the range of 0.008 to 1.0 µg/mL and minimal bactericidal concentration (MBC) does not generally exceed this range by a factor of more than 2 [83, 84]. Fluoroquinolones including ciprofloxacin generally exhibit concentration-dependent antimicrobial effectiveness and drug concentration above the MIC or Peak/MIC of >10 and concentration–time curve (AUC/MIC) ratios of >125 have been identified as possible pharmacodynamic predictors of clinical and microbiological outcome as well as the development of bacterial resistance. However, there are contradictory results for the role of time dependency of ciprofloxacin [91].

A nanocomposite powder formulation of ciprofloxacin which releases the ciprofloxacin nanoparticles upon deposition on the nasal fluid may be useful in the enhanced local treatment of the infections in the nose such as CRS as nanoparticles may show faster penetration in the high viscoelastic mucus mesh and biofilms produced by bacteria in the CRS patients.

1.3   Dry powder and nanoparticle nasal delivery strategies

1.3.1   Next generation dry powder delivery devices

The Breath–Powered Bi Directional^{TM} device is a new nasal technology for delivery of nasal powders in which patients exhaling through the device mouthpiece deliver powder particles into an airstream through a delivery tube to one nostril in which the tube is sealed. Powders will be swept entirely around the nasal septum, and any un-deposited powder will escape from the other nostril. Lung delivery is prevented by simultaneous oral exhalation into the device that creates a positive pressure in the oropharynx so the soft palate will close therefore separating the nasal and oral cavities. Clinical studies showed that the device delivered more drug to the upper and middle

posterior passages compared to a conventional nasal spray pump (54% vs 16%, respectively) [61]. Sumatriptan, zolmitriptan, oxytocin and butorphanol are in the pipeline for systemic delivery and fluticasone for topical delivery using this device [92]. Compared to conventional nasal sprays, a similar bi-directional breath actuation technique for nasal powders produced superior distribution in upper and middle posterior part of the nasal cavity. In general, dry powders have the advantage of longer stability compared to liquid formulation with no need for addition of preservatives (which are often locally irritant); they are also more portable and suffer from less risk of microbial contamination. A phase III clinical trial for nasal administration of 16 mg sumatriptan (Onzetra® Xsail®, OptiNose) for pain relief in migraine was completed using the bi-directional approach, demonstrating the feasibility of using powder delivery to administer milligram quantities of drug to the nose.

1.3.2 Nanoparticle formation strategies

For drugs to be pharmacologically active they first need to dissolve at the absorption site (for local and systemic effects) and then be taken up into local cells or transferred to the systemic circulation [93]. However, many new pharmacologically active compounds exhibit low solubility and permeability [94-96]. Classical approaches to increase drug dissolution rate include the use of co-solvents, complex or salt formation, addition of surfactant, and pH adjustment [97]. Particle size reduction is another technique that can be used to enhance dissolution rate which is achieved by increasing the surface area according to the Noyes-Whitney equation:

$$\frac{dQ}{dt} = \frac{D}{h} S(C_s - C) \qquad \text{Equation 1.1}$$

where the dissolution rate, $\frac{dQ}{dt}$, is directly proportional to the diffusion coefficient of the drug, D, the available surface area, S, and the difference between saturation solubility of the drug in the boundary layer, C_s, and concentration of drug in the bulk fluid, C. As particle size decreases, surface area increases which leads to improved dissolution rates. To achieve this increased dissolution, one approach is by the production of nanoparticles for pharmaceutical formulation. These particles have a size below 1 µm, typically a few hundred nanometers [98].

Particles in nano- scale can be made by top-down methods, starting with larger particles and breaking them down into smaller particles. This approach uses methods such as ball milling, jet milling, wet milling and high pressure homogenization. The alternative is a bottom-up approach, starting from atomic level with further assembly process and formation of nanostructures. The later approach uses methods such as crystallization, precipitation and solvent evaporation techniques including spray drying and freeze drying or a combination of these technologies. Finally, a combination of a bottom-up technology such as freeze drying with a top-down method such as high pressure homogenization can be also employed [97, 99-101].

Common top-down processes are wet ball milling and high pressure homogenization in which the larger drug particles are broken down to very small drug nanocrystals. Drug is suspended into an aqueous or organic dispersion medium containing surfactants or polymeric stabilizers and particle size reduction happens through attrition using media milling or a high-pressure homogenizer which repeatedly forces the drug suspension through a very thin gap (typically about 25 µm) at extremely high velocity. Depending on the physicochemical properties of the drug and the processing parameters, different milling time and homogenization cycles can be applied. In

contrast to the bottom-up technologies, almost any poorly soluble drug can be processed using these methods [101, 102].

The bottom-up methods have the advantage of producing smaller particle sizes (below 100 nm) usually by controlled precipitation, while top-down methods often require larger energy input and are more time consuming. In addition, controlling the particle size, morphology and surface characteristics seems to be more feasible by a bottom-up approach such as crystallization, even though any un-desirable solvent residue must be removed [99]. However, it is noted that the top-down processes such as high pressure homogenization and wet ball milling are most commonly used in pharmaceutical industry [97].

1.3.2.1 Liquid anti-solvent precipitation

Liquid anti-solvent precipitation has been used widely for preparation of nanometer and micrometer sized drugs. This technique involves introducing a homogenous drug solution into an anti-solvent. As the solutions mix, a meta-stable supersaturated solution is produced followed by drug nucleation and crystal growth. The crystal growth occurs by condensation, coagulation and agglomeration of particles.

In classical nucleation theory a multicomponent system initially exists as a single phase [103, 104]. However, by changing the boundary conditions such as temperature, pressure or mixing with a secondary component the free energy changes and is favorable to phase separation. The particles, at atomic, ionic or molecular level, of one component coalesce and form nuclei of the separating solid phase in the liquid or gaseous media. The free energy of a spherical nucleus with radius r can be described as in Equation 1.2.

$$\Delta G = \Delta G_S + \Delta G_V = 4\pi r^2 \gamma + \frac{4}{3}\pi r^3 \Delta G_v \qquad \text{Equation 1.2}$$

Where the ΔG_s is the excess free energy between the surface of particle and the bulk of particle

and ΔG_v is the excess free energy between a very large particle and the solute in the solution. γ is

the interfacial tension at solid-liquid interface and ΔG_v is the difference in free energy per unit

volume between the two phases. These two terms of ΔG_S and ΔG_V (as shown in Figure 1.4) have

opposite signs, so as r increases ΔG passes the maximum. The maximum value or ΔG_{cr} critical

free energy corresponds to nucleus with radius r* defining the minimum size of stable nucleus.

Particle smaller than this size dissolve in a liquid media to reduce the free energy and particles

larger than r* continue to grow.

r* $= -2\,\gamma/\Delta Gv$ \qquad\qquad Equation 1.3

From equations 1.2 and 1.3

$$\Delta G_{cr} = \frac{16\,\pi\,\gamma^3}{3\,(\Delta Gv\,)^2} \qquad \text{Equation 1.4}$$

The rate of nucleation (the number of nuclei formed per unit time per volume, *J*, is then can be

defined as

$$J = A \exp\left(-\frac{\Delta G_{cr}}{kT}\right) \qquad \text{Equation 1.5}$$

k is the Boltzmann's constant, T is the absolute temperature.

From equations 1.4 and 1.5

$$J = \left(A\,exp\,\frac{16\,\pi v^2\,\gamma^3}{3\,(kT)^3\,(\ln(1+S))^2}\right) \qquad \text{Equation 1.6}$$

A is the pre-exponential factor (10^{32} to 10^{36}) and depends on the crystal growth mechanism at the particle surface.
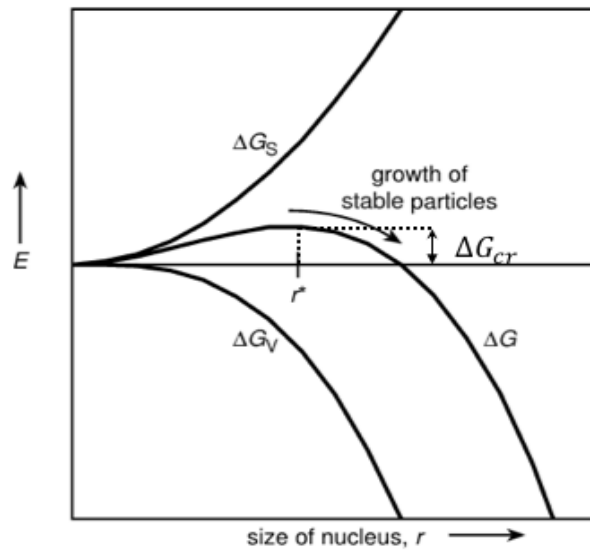
Figure 1.4. Energy diagram of Gibbs free energy [103]

The supersaturation or S is defined as

$$S = \frac{C}{C^*}$$

Equation 1.7

In which C is the particle concentration in the solution and C^* is the equilibrium solubility in the mixture of solvent /anti-solvent. Therefore, higher nucleation rate is governed by lower Gibbs free energy. Based on the equation 1.6, nucleation rate mostly depends on degree of supersaturation (S) and interfacial energy (γ).

The time from mixing of the drug solution with the anti-solvent solution to the appearance of crystals is called the induction time and is described as

$$t_{ind} = kc^{1-p}$$

Equation 1.8

where c is the initial concentration of a supersaturated solution, k is a constant and p is the number of molecules in a critical nucleus. Induction time can range from microsecond to days depending on the degree of supersaturation. The mixing event which is followed by generation of supersaturation is critical in the crystallization process.

After nuclei formation, nuclei will grow by addition of particles on the crystal face. Three physical phenomena occur for crystal growth: i) transport of materials to be crystalized from the bulk solution to the crystal surface boundary layer, ii) transfer of materials from the solution boundary layer to the crystal surface, and iii) diffusion of the growth unit from the impingement site to the growth site and incorporation into the crystal unit. Crystal growth rate depends on temperature and supersaturation. The crystal habit formed can have different shapes and size depend upon the crystallization conditions [104, 105].

1.3.2.2 Sonocrystallization

One approach to modify the rate of nucleation and crystal growth during liquid anti-solvent precipitation involves utilizing power ultrasound. Sonocrystallization is the application of power ultrasound (frequency of 10 – 100 kHz) during the crystallization process. Previous researchers have shown its benefits of providing faster and more uniform nucleation at lower supersaturation ratios, reducing agglomeration and producing more uniform size crystals [105]. By applying ultrasound, alternative cycles of compression and rarefaction within the media, creates tiny water-

28

vapor bubbles [106, 107]. The sudden release of energy as a result of bubble explosion causes extremely rapid and localized temperature reductions that generate rapid nucleation in the solution [106]. Also, the collapse of the bubbles produces intense shock waves which are propagated through the liquid at velocities higher than the speed of sound (in air) leading to uniform micro-mixing of the drug solution and anti-solvent. The sonocrystallization process can be influenced by ultrasound variables such as frequency, intensity, power and duty cycle, as well as by physical variables such as temperature, pressure, time, volume of the vessel and probe diameter [107]. Park et al. [108] investigated the induction time for roxithromycin crystals in the absence and presence of ultrasound in an anti-solvent crystallization process. In the absence of ultrasound, the induction time of roxithromycin crystallization decreased with increasing supersaturation. When ultrasound was employed, the induction time decreased significantly for all levels of supersaturation that were investigated. The authors concluded that it was an acceleration in diffusion in the presence of ultrasound that caused the reduction in induction times. Micronized albuterol powder for pulmonary administration with volume mean diameter of 1.8 µm was produced by optimizing sonocrystallization conditions such as increasing sonication amplitude, lowering temperature and increasing drug concentration in solution [109]. For griseofulvin crystallization, application of ultrasound at 25 W during crystallization significantly reduced the mean particle size of the crystals to 4.87 µm compared to 23.49 µm when no ultrasound was applied during crystallization. However, it was observed that further increasing the ultrasound energy only slightly further reduced the crystal particle size. Also, it has been reported that the probe diameter in relation to the crystallization vessel size was important. Increasing probe diameter was observed to result in production of a smaller crystals by providing more efficient mixing [110]. However, it has also been reported that the flow pattern or mixing of the liquids depends on probe immersion depth,

therefore any change in the flow pattern due to probe immersion may affect the crystallization rate [106].

In a recent technique of spray sonocrystallization, the drug solution was passed into a flow-through ultrasonic probe which was immersed into the anti-solvent with continuous flow. Drug formulation was sprayed into the flow of anti- solvent as fine droplets of solution. The diameter of the spray sonocrystallized particles were 75 -175 nm [111].

In this research, the feasibility of using sonocrystallization technique for producing ciprofloxacin nanocrystals with mean volume diameter of 100 - 200 nm suitable for penetration through mucus and biofilm layers produced by bacteria was assessed.

1.3.2.3   Spray drying

Spray drying is a popular bottom-up approach in the pharmaceutical industry for the production of micrometer and sub-micrometer sized particles [112]. The spray drying technique involves i) atomization of a liquid from feed solution, emulsion, or suspension (in aqueous or organic media) through a nozzle to produce micron-sized liquid droplets; ii) drying of the liquid droplets into powder form using a hot dry gas (usually > 50 °C), and; iii) collection of the particles from the moist gas or air. Particle collection is done using deposition in a cyclone or by electrostatic precipitation. Spray drying of the biological materials is also feasible while maintaining their biological activity as the drying process is very short (in the order of 11ms) and there is reduced temperature in the vicinity of the protein due to evaporative cooling [113, 114]. Control of the drying conditions can be achieved by changing the gas feed rate, solution feed rate and the inlet temperature. The particle size and distribution of the atomized droplets can be controlled by choice of the atomizer, which includes rotary, ultrasonic, twin fluid nozzle designs. The air to liquid ratio

in the atomizer and the feedstock solids concentration define the particle size distribution of the final particle [115, 116]. It is possible to generate nanoparticles in the size range 200 - 400 nm using the spray drying technique. This method usually requires the use of an organic solvent and low solids concentration in the feed stock [117].

Spray drying can be also used for the conversion of nanocrystals (pure drug) or nanosuspensions to a larger sized dry powder formulations suitable for nasal or inhalation drug delivery. Van Eerdenbrug et. al [118] used spray drying to convert nano-suspensions of nine model drugs with no added excipients. Nanoparticle agglomeration was observed visually for all dried powder formulations but change in nanoparticle dry powder formulation dissolution was observed to be specific to the drug compound characteristics (higher log P values was associated with more aggregation). Kumar et al., [119] investigated the effect of low and high molecular weight sugar excipients on indomethacin nano-crystalline suspension powders prepared by spray drying. Small molecular weight sugars such as lactose, mannitol sucrose, maltose and trehalose were able to protect nanosuspension formulations against particle aggregation using a drug:sugar ratio as low as 1:2.5 % w/w, compared to those containing polysaccharides perhaps due to their interaction with the surfactant coated nanoparticles. Additionally, higher powder yields were observed with formulations containing sugars with higher glass transition temperatures during spray drying [119]. In another study, Sham et al. [120] reported a conversion of gelatin and poly isobutyl cyanoacrylate (PIBCA) nanoparticles micro-particles and using lactose as excipient with mass median aerodynamic diameter (MMAD) of as 3.0 ± 0.2 µm. However, the nanoparticle size increased approximately 30% after the spray-drying was statistically different only in case of gelatin nanoparticles.

This project also focuses on the feasibility of using a spray drying technique to convert the

ciprofloxacin nanocrystals into a nanocomposite powder in the size range of 5 - 10 µm suitable for nasal drug delivery. The goal was to produce a powder formulation suitable for use in a nasal dry powder inhaler containing dispersed nanoparticles in a matrix of water soluble excipients. Therefore, after delivery to the nose, the excipients would rapidly dissolve leaving the nanoparticles on the airway surface which would then penetrate through the mucus layer and exert their antimicrobial effects.

CHAPTER 2

HYPOTHESES AND SPECIFIC AIMS

The overall objectives of this research project were i) to develop and evaluate methods of characterizing nasal spray products using realistic nasal airway models as more clinically relevant *in vitro* tools and ii) to develop and evaluate a novel high-efficiency antibiotic nanoparticle dry powder formulation and delivery device for the treatment of the local infections in the nose.

To accomplish these objectives the following hypotheses and specific aims were defined:

Hypothesis 1. Simulated patient-use experimental conditions can influence the *in vitro* regional drug deposition of nasal spray products in realistic nasal models.

Specific Aim 1-1: To develop a realistic *in vitro* testing method for assessing regional nasal drug deposition of a nasal spray product.

Specific Aim 1-2: To assess the effects of patient-use variables on regional nasal deposition of a nasal spray product (Nasonex®) in a realistic geometry of the nasal cavity.

Hypothesis 2. The *in vitro* regional drug deposition of nasal spray products in realistic nasal models is determined by differences in the airway geometry of the nasal model and the formulation / spray device properties.

Specific Aim 2-1: To compare the regional nasal deposition of a nasal spray product (Nasonex®) in a 2nd realistic nasal model with varying geometric features (inter-subject variability).

Specific Aim 2-2: To investigate regional nasal drug deposition of innovator and generic nasal spray products using the developed realistic *in vitro* testing methods.

Specific Aim 2-3: To characterize the regional nasal drug deposition of nasal spray products with varying *in vitro* spray properties.

Hypothesis 3. Enhanced middle passage drug delivery can be accomplished using a novel nanocomposite formulation and nasal powder delivery system.

Specific Aim 3-1: Prepare ciprofloxacin nanoparticles and nanocomposite nasal powder formulations.

Specific Aim 3-2: Develop and evaluate a novel nasal delivery system to target delivery of a nasal nanocomposite dry powder formulation to the nasal middle passages.

Specific Aim 3-3: Characterize the regional nasal drug deposition of the novel nanocomposite formulation and nasal powder delivery system using the developed realistic *in vitro* testing methods.

Specific Aim 3-4: Develop a technique to assess post nasal deposition events such as transepithelial transport of drugs after realistic deposition on human epithelial cell monolayers in a realistic airway geometry.

CHAPTER 3

DEVELOPMENT OF A REALISTIC *IN VITRO* TESTING METHOD TO ASSESS REGIONAL NASAL DRUG DEPOSITION OF NASAL SPRAY PRODUCTS USING SIMULATED PATIENT-USE EXPERIMENTAL CONDITIONS

3.1   Introduction

A large number of *in vitro* studies have employed realistic hollow nasal models to identify the influence of nasal formulation properties, spray pump design and patient variables on regional nasal drug deposition of spray products. These studies have investigated and optimized various parameters including formulation characteristics such as viscosity or surface tension, administration technique including positioning of the nasal spray product and nasal model to optimize nasal drug delivery [19, 38]. Other studies have focused on the effects of simulated patient use experimental conditions such as use of inhalation air flow profiles, nasal wall coating, nasal spray actuation conditions, in attempts to reduce the variability observed during *in vitro* testing and to simulate realistic patient use [34-37, 42]. The conclusions reached regarding the importance of these formulation and spray variables to influence nasal deposition are sometimes contradictory which may be due to the differing experimental conditions used to perform the studies. However, it has been clearly demonstrated that the use of an automated nasal actuator is of critical importance to control parameters such as actuation force and velocity, stroke length, rise time, hold time and to ensure reproducible performance of the nasal spray product during *in vitro* testing. It is also recognized that for meaningful *in vitro* testing of nasal spray products, these actuation conditions should be derived from human performance data (adults and pediatrics, as appropriate). Doughty et al. [121] described the use of hand force actuation monitors to determine

35

in use actuation conditions in appropriate patient populations that can be translated to *in vitro* test conditions. Similarly, it is recognized that coating of the internal walls of the nasal model, especially if powder delivery devices are investigated, should be considered. A number of different materials including mixtures of detergent and acetone, PEGs (400/6000 mixture), propylene glycol - isopropanol and glycerol - Brij-35 have been used to change the surface properties and mimic the mucus lining in the nasal model [34-36, 122]. The selection of coating material is often dependent upon the test drug and extraction solvent, together with compatibility with the drug assay method.

In order to evaluate the importance of other patient related *in vitro* testing variables and move towards a standardization of realistic *in vitro* testing methods for assessing regional nasal drug deposition of nasal spray products, a marketed nasal spray product, Nasonex® nasal spray product, was identified for testing. The instructions described in the Nasonex® patient information leaflet have been incorporated into an *in vitro* test method designed to mimic the recommended patient administration technique and examine the effect of varying these parameters. In the patient information leaflet, the patient is advised to use nasal spray with the following steps: hold the nasal spray in the upright position, insert the nasal spray in one nostril and block the other nostril, tilt head forward, actuate the nasal spray, breathe gently in through one nostril and breathe out through mouth. Therefore, the patient administration related variables that were defined for investigation during the realistic *in vitro* testing were the nasal spray position within the nostril of the nasal airway model, the head angle of the nasal airway model, the actuation force used to deliver the nasal spray formulation to the nasal airway model, the presence or absence of an inhalation airflow during nasal spray administration to the nasal airway model. The effects of each of these patient

administration related variables on the regional drug deposition of Nasonex® nasal spray product was investigated.

This chapter describes the analytical method developed to selectively extract and quantify the administered drug (mometasone furoate) from the *in vitro* nasal airway model, together with preliminary studies that were performed to identify patient use factors that influence the regional nasal deposition of the Nasonex® nasal spray product. Finally, a full factorial design of experiment was constructed to determine the significant main factors or interactions between the patient use study variables on the regional drug deposition of the nasal spray product.

3.2 Material and Methods

3.2.1 *In vitro* experimental setup to assess the regional drug deposition of Nasonex® nasal spray product

Nasonex® nasal spray (Merck & Co. Inc., Whitehouse Station, NJ) delivering 50 mcg mometasone furoate (anhydrous) per dose as mometasone furoate monohydrate was selected to be tested. The experimental setup shown in Figure 3.1 was constructed to allow an *in vitro* simulation of the realistic use of Nasonex®. The test components consisted of the eNSP automated actuation station (MightyRunt, InnovaSystems, Moorestown, NJ), the realistic physical model of the nasal cavity (VCU nasal model 1) and a programmable breathing simulator (ASL 5000-XL, IngMar Medical, Pittsburgh, PA). The nasal spray was placed in nasal spray actuator in the vertical position. A low resistance respiratory filter (PulmoGuard II, Quest Diagnostics, Brockton, MA) was attached at the end of throat to capture drug that passed through the nasal airways. For these studies, the nasal spray was administered to the left nostril and the right nostril blocked. A three-way solenoid valve was positioned between the respiratory filter and the breath simulator such that

the patient exhalation was directed to the atmosphere and not through the nasal model simulating an oral exhalation. The insertion depth of the nasal spray in the model was kept constant at 1 cm. A glass fiber filter (81 mm, New Star Environmental, Inc, Rosewell, GA) with a central hole for the nasal spray nozzle was placed around the nasal spray applicator and positioned at the exit of the nostril to collect the formulation dripping from the nose as shown in Figure 3.2.

Before each experiment, the nasal spray was shaken by hand for 15 sec. Based on instructions provided in the prescribing information the nasal spray was primed as follows: the first ten sprays were fired to waste prior to initial use or if the nasal spray was not used for one week [123]. One or two doses were administered in the left nostril of the model. The weight of nasal spray was recorded before and after each experiment to determine the shot weight.
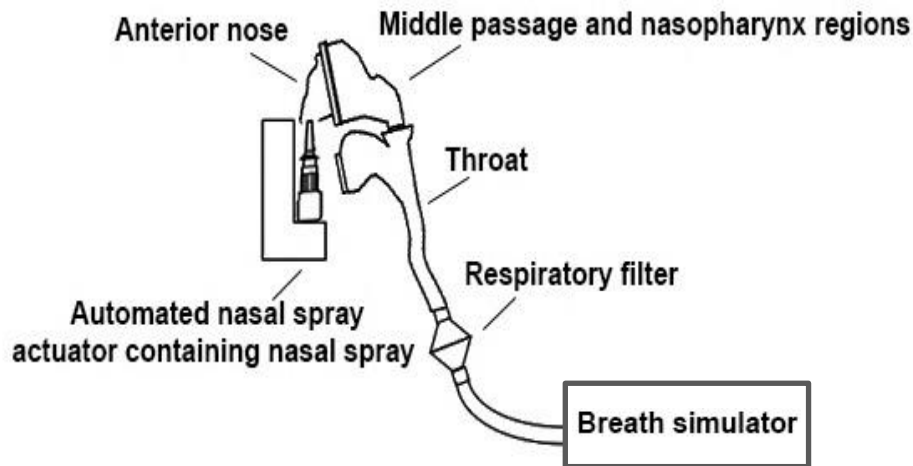
Figure 3.1. Experimental setup for realistic testing of regional nasal deposition of the Nasonex® nasal spray product. The setup consists of an automated nasal spray actuator, realistic nasal airway model, a respiratory filter at the end of throat and a breathing simulator
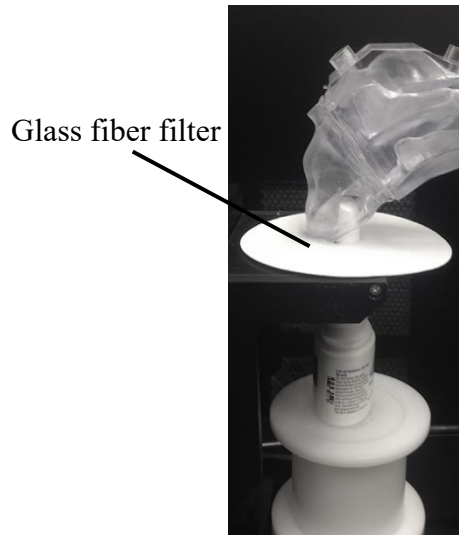
Figure 3.2. A glass fiber filter placed around the nasal spray applicator to collect formulation dripped from the nostril when using the Nasonex® nasal spray product

3.2.2   Nasal mouth throat geometry – VCU nasal model 1

The realistic airway model consisted of the nasal passages and nasopharynx. The dataset used for this model was first introduced by Guilmette [124] and was derived from magnetic resonance imaging (MRI) of a 53-year-old adult male. This model has been used in a number of *in vitro* and *in silico* studies [29, 43, 125-127]. The MRI multi-slice images were segmented in MIMICS (Materialize, Ann Arbor, MI) according to the tissue-air contrast and were converted into a set of coronal polylines that defined the nasal airway. Based on these contours, an internal nasal surface geometry was constructed in Gambit 2.3 (ANSYS Inc., Canonsburg, PA). The nasal data set was smoothed to produce a physiologically realistic 3D structure. The hollow model was built using rapid prototyping, with a Viper SLA machine (3D Systems, Valencia, CA). The nasal airway model was constructed using Accura ClearVue resin (3D Systems, Valencia, CA). The model is

segmented in two parts of i) the anterior nasal vestibule ii) combined middle passages and nasopharynx. As shown in Figure 3.3, the model was connected to the mouth-throat geometry that was previously developed by Xi and Longest which was derived from a CT scan dataset of an adult male [128].
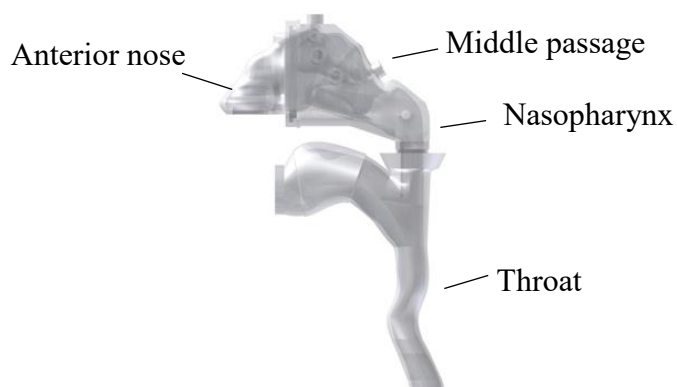
Figure 3.3. Nasal airway geometry (VCU nasal model 1)

3.2.3 Development of methods to extract and assay mometasone furoate following deposition in the nasal airway model using the Nasonex® nasal spray product

The aim of this task was to develop extraction procedures and assay methods suitable for the quantitative analysis of mometasone furoate (anhydrous) following deposition of drug in the realistic nasal model during the in vitro deposition studies. The High-Performance Liquid Chromatography (HPLC) method employed a Waters 2690 separation module, a 2996 PDA detector using the wavelength of 230 nm and mobile phase of acetonitrile and water (60:40 % v/v) at flow rate of 1.3 mL/min modified based on the European Pharmacopoeia monograph for

mometasone furoate [129]. The volume of injection was 100 µL. The Hypersil Gold column (150 mm x 4.6 mm, 5 µm) temperature was kept as ambient temperature (21-23°C).

Different ratios of potential wash solutions containing acetonitrile - water, methanol – water and dimethyl sulfoxide – water with capability of dissolving mometasone furoate were assessed for their compatibility with the realistic physical model plastic resin, both from an interfering extractable perspective and the long-term effects on the integrity of the airway model. This was achieved by separately applying the wash solution and drug spiked wash solutions containing mometasone furoate into VCU nasal model 1 and performing HPLC analysis on the solution following recovery from the model. Wash solutions that did not produce interfering extractables and altered the physical integrity of the airway model were advanced to the next stage of testing.

If appropriate, the next step for the wash solution was to extract and recover mometasone furoate from the nasal model following delivery of the Nasonex® nasal spray suspension formulation. For this study, two actuations of the nasal spray were administered to the left nostril of the nasal model which was then washed with 100 mL of the wash solution. Studies were performed using both an uncoated realistic nasal model and with the model coated with artificial mucus (pH 5.7) containing of 8 %w/v mucin type II [130]. The model parts soaked in the wash solution were sonicated for 30 minutes. The expected concentration of mometasone furoate in the wash solution was 1 µg/mL, assuming 100 µg dose dissolved in 100 mL of wash solution. For HPLC method validation and system suitability assessment, mometasone furoate standard solutions were prepared in the final selected wash solution.

Parallel to this task, it was determined that the wash solution following drug extraction would require a filtration step to remove undissolved suspended excipients prior to HPLC injection

of the samples for drug content quantitation. A series of filters were assessed to examine the removal of suspended excipients without adsorption / absorption losses of mometasone furoate on the filter. The filters evaluated were a nylon filter (Fisherbrand, pore size 0.2 µm, diam. 25 mm, Fisher Scientific, Hampton, NH), a PVDF (polyvinylidene fluoride) membrane filter (Whatman GD/X syringe filters, pore size 0.2 µm, diam. 25 mm, Sigma-Aldrich, St. Louis, MO), and an Anotop® filter (Whatman, 0.2 µm, 25mm, Sigma-Aldrich, St. Louis, MO). The assessment was performed by comparing the measured concentration following filtration of mometasone furoate standard solutions with the concentration of the unfiltered solution by quantified using the previously described HPLC methods. Standard solutions were prepared in wash solution in the range of 0.04 – 10.2 µg/mL for passage through the test filters. The first milliliter of the filtrate solution was discarded.

3.2.4 Determination of shot weight, single drug actuation content and formulation content uniformity of Nasonex® nasal spray

To assess shot weight and single actuation content, after priming the Nasonex® nasal spray product, one dose of the product was sprayed into a 50 mL Erlenmeyer flask. The nasal spray weight was recorded before and after actuation. Actuation was performed manually by operator or using the MightyRunt automated actuator at two actuation forces of 5.8 and 4.5 kg. The actuation profile was defined as force rise time of 0.1 sec, hold time of 0.3 sec and force fall time of 0.1 sec [131]. Following the actuation, drug was recovered from the flask using a known volume of wash solution to produce a target drug concentration of 1 µg/mL. The nasal spray nozzle was washed with 30 mL of wash solution to recover drug remaining on the device. The wash solutions were sonicated for 30 min followed by filtration using the previously developed method.

Formulation content uniformity was also assessed. The pump assembly of the Nasonex®
nasal spray was opened and 100 µL aliquots of the suspension formulation were sampled using a
volumetric pipette. Samples dissolved in wash solution to produce a target concentration of 1
µg/mL. 10 samples were taken to calculate the formulation drug content uniformity from a single
batch of the drug nasal spray product.

3.2.5 Preliminary assessment of the effect of patient use variables on *in vitro* regional nasal deposition of Nasonex® nasal spray

Preliminary experiments were performed to evaluate the importance of a series of patient
use variables (described below) on the *in vitro* regional nasal deposition of Nasonex® nasal spray.
The following general method was employed after deposition of the nasal spray in the nasal model.

Following each experiment, the nasal model was dissembled into its constituent parts of
the anterior nose, combined middle passage and nasopharynx and throat sections. Know volumes
of wash solution (methanol – water 50:50 %v/v) were used to extract drug deposited on i) the nasal
spray device, ii) from the filter positioned to collect formulation dripping from the nose, iii)
individually from the nasal model parts (anterior nose, combined middle passage and nasopharynx
and throat sections) and iv) the respiratory filter at the end of throat. Wash solutions together with
the nasal model parts were sonicated for 30 min followed by filtration using Anotop® filter.
Samples were analyzed by HPLC to quantify mometasone furoate. The total drug mass recovered
was calculated based on the label claim dose. For each of the study variables described below,
mean data for regional nasal drug deposition were expressed as the percent of the recovered dose
together with the calculated standard deviation (SD).

One-way analysis of variance (one-way ANOVA) followed by post hoc Tukey HSD using JMP Pro 12 software (SAS Institute Inc., Cary, NC) was employed to identify the statistically significant differences in anterior + drip deposition and the extent of drug delivery to the combined middle passage and nasopharynx. The significance level was 0.05. The ANOVA assumptions of the normality of data and residuals were assessed by normal quantile plot and residual versus predicted response plot, respectively.

3.2.5.1 Effect of number of administered actuations on regional drug deposition of Nasonex® nasal spray

Based on the information provided by manufacturer for dosage and use, Nasonex® can be administered as one or two sprays per nostril. To assess the effect of number of actuations on regional drug deposition of Nasonex® one or two sprays were actuated into a single nostril. The model head angle for testing was defined as 30° forward from horizontal. The studies were performed using two actuation forces of 4.5 and 5.8 kg. The actuation profiles were defined with a force rise time of 0.1 sec, hold time of 0.3 sec and force fall time of 0.1 sec. The nasal spray positioning was defined with an insertion depth of 1 cm and the distance between the leading edge of the spray and the front of the nostril was 9 mm while maintaining a constant distance from the medial and lateral walls of the nostril (Figure 3.5). Two doses were administered to the left nostril of VCU nasal model 1 in the absence of any inhalation flow.

3.2.5.2 Effect of head angle on the regional drug deposition of Nasonex® nasal spray

For assessing the effect of head tilt angle, the regional drug deposition of the Nasonex® was quantified when model head angle was varied from 30° forward from horizontal to 40° and 50° as demonstrated in Figure 3.4. The nasal spray positioning was defined as an insertion depth

of 1 cm and the distance between the leading edge of the spray and the front of the nostril was 9 mm while maintaining a constant distance from the medial and lateral walls of the nostril. An actuation force of 4.5 kg was used to actuate the product. The actuation profile was defined by a force rise time of 0.1 sec, hold time of 0.3 sec and force fall time of 0.1 sec. Two doses were administered to the left nostril of VCU nasal model 1 in the absence of any inhalation flow.

| (a) | (b) | (c) |
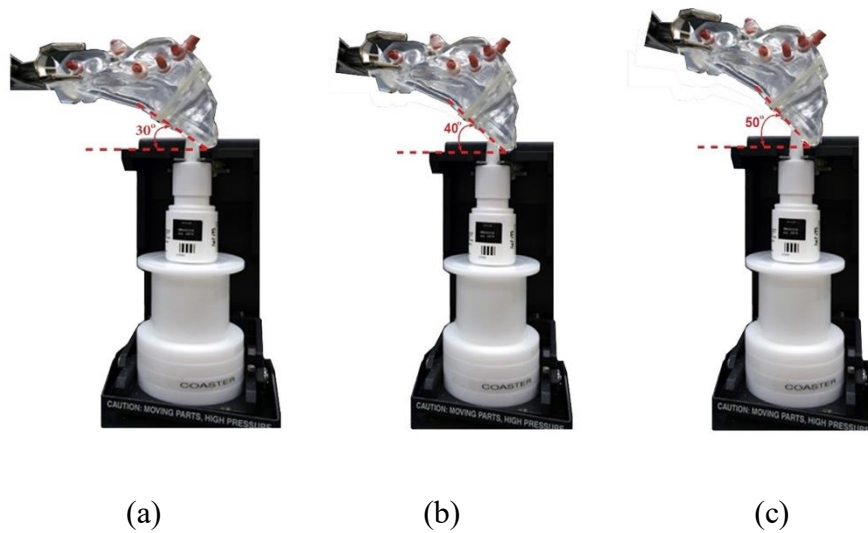
Figure 3.4. Nasal model head angles of (a) 30° (b) 40° and (c) 50° forward from horizontal used to assess regional drug deposition of Nasonex® in VCU nasal model 1

3.2.5.3 Effect of actuation force on the regional drug deposition of Nasonex® nasal spray

To assess the effect of actuation force, Nasonex® was administered using three actuation forces of 4.5, 5.8 and 7.5 kg. The other actuation profile parameters were kept constant with a force rise time of 0.1 sec, hold time of 0.3 sec and force fall time of 0.1 sec. The head angle was 30° forward from horizontal. The nasal spray positioning was defined as insertion depth of 1 cm

and the distance between the leading edge of the spray and the front of the nostril was 9 mm while maintaining a constant distance from the medial and lateral walls of the nostril. Doses were administered to the left nostril of VCU nasal model 1 in the absence of any inhalation flow.

3.2.5.4 Effect of nasal spray position in the nostril on the regional drug deposition of Nasonex® nasal spray

Three different positions were investigated with the distance between the leading edge of the spray and the front of the nostril being varied from 5, 9 and 11 mm, while maintaining a constant distance from the medial and lateral walls of the nostril to provide a series of potential positions that may be employed by the patient (Figure 3.5). Then, the nasal model head angle tilted 30° forward from horizontal. The nasal spray insertion depth was held constant at 1 cm. The actuation parameters for the force-controlled actuator defined as actuation force of 4.5 kg, force rise and fall time of 0.1 sec and force hold time of 0.3 sec. Two doses were administered to the left nostril of VCU nasal model 1 in the absence of any inhalation flow.

(a)   (b)   (c)
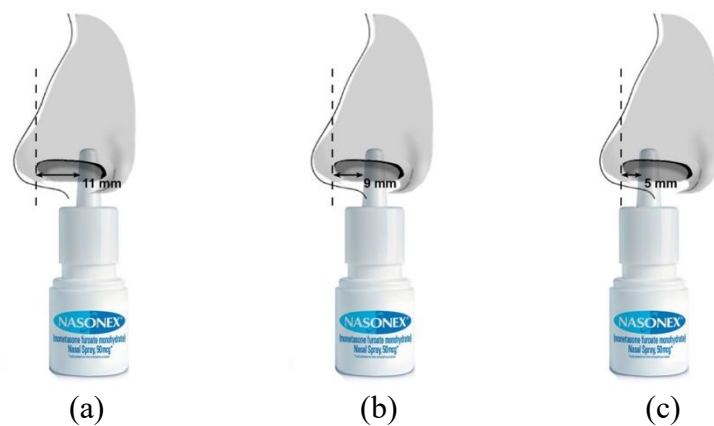
Figure 3.5. Three nasal spray positions of (a) 11mm (b) 9mm and (c) 5mm distance between the leading edge of the spray and the front of the nostril while maintaining a constant distance from the medial and lateral walls of the nostril used to assess regional drug deposition of Nasonex® in VCU nasal model 1

3.2.5.5 Effect of inhalation airflow on regional drug deposition of Nasonex® nasal spray

For assessing the effect of presence of inhalation airflow and its rate, regional nasal deposition of the Nasonex® was assessed in the absence of inhalation airflow (NI) and in the presence of slow (SI) and fast inhalation (FI) airflow. Realistic nasal breathing profiles were adapted from Guo et al., [36] in which nasal breathing parameters for nine healthy adults recorded while they were asked to breathe gently or vigorously from one nostril while the other nostril was closed. The slow breathing profile was defined as peak inspiratory flow rate (PIFR) of 20.2 Lmin^{-1}, time to reach the peak of 0.4 sec, for total duration of 1.9 sec and tidal volume of 560 mL whereas the fast breathing profile had a PIFR of 35.8 Lmin^{-1}, time to reach the peak of 0.3 sec, for total duration of 1.2 sec and tidal volume of 619 mL. The breathing profiles were simulated using breath simulator ASL XL-5000 (Ingmar Medical LLC, Pittsburg, PA). The ASL breath simulator allows coordination of the inhalation with the nasal spray actuation by connecting with the MightyRunt nasal spray actuator. At the beginning of inhalation, a 5mV pulse from the breath simulator triggers the nasal spray actuator via a solid-state relay (Crouzet 84134750, Newark Electronics, Chicago, IL) which results in the actuation of the nasal spray. Following the start of inhalation, there is a 1 sec delay prior to actuation of the nasal spray to ensure that delivery occurs during the nasal inhalation. The nasal spray positioning was defined as insertion depth of 1 cm and the distance between the leading edge of the spray and the front of the nostril was 9 mm while maintaining a constant distance from the medial and lateral walls of the nostril. The model head angle tilted 30° forward from horizontal and actuated using an actuation force of 4.5 kg. The actuation parameters for the force-controlled actuator defined as force rise and fall time of 0.1 sec and force hold time of 0.3 sec. Two doses were administered into the left nostril of VCU nasal model 1.

3.2.5.6 Effect of surface coating on the regional drug deposition of Nasonex® nasal spray

To assess the effect of a simulated nasal mucus lining on regional nasal drug deposition, prior to the deposition experiment, the inner surface of the model was coated with an artificial nasal mucus fluid, drained, and allowed to air-dry. The simulated mucus lining was prepared by dispersing 8% w/v mucin (porcine stomach, type II, Sigma-Aldrich, St. Louis, MO) and 7.45 mg/mL NaCl, 1.29 mg/mL KCl and 0.32 mg/mL $CaCl_2$. $2H_2O$ in water adjusted to pH 5.7 [130]. The regional deposition was assessed in the presence of the fast inhalation profile. The nasal spray positioning was defined as insertion depth of 1 cm and the distance between the leading edge of the spray and the front of the nostril was 9 mm while maintaining a constant distance from the medial and lateral walls of the nostril. The model head angle tilted 30° forward from horizontal and actuated using an actuation force of 4.5 kg. The actuation parameters for the force-controlled actuator defined as force rise and fall time of 0.1 sec and force hold time of 0.3 sec. Two doses were administered into the left nostril of VCU nasal model 1.

3.2.6 CFD simulation for prediction of regional nasal drug deposition of Nasonex® nasal spray product

The computational fluid dynamic (CFD) simulations was performed by Dr. Longest and Dr. Rygg at VCU Department of Mechanical and Nuclear Engineering. Simulation of aerosol particle transport in a gas-phase jet was used to assess the spray characteristics at the nasal spray tip. The effects of aerosol momentum on the gas phase was determined by using a separate air jet velocity at the nozzle orifice to account for momentum exchange between the aerosol and gas phases. The air velocity induced by droplets exiting the spray pump at distance of 1cm downstream of the nozzle tip was considered as 15 m/s. The initial aerosol injection velocity of 7 m/s was specified for the nasal spray with a plume angle of 52º. The nasal spray regional deposition was

predicted i) in the absence of the air flow, ii) with slow inhalation (20.2 $Lmin^{-1}$), and iii) with fast inhalation (35.8 $Lmin^{-1}$). Simulations were run using ANSYS Fluent 15 (ANSYS Inc., Canonsburg, PA) [132].

3.2.7 Full factorial design of experiment (DOE) to assess the effect of patient use variables on the regional drug deposition of Nasonex® nasal spray.

The preliminary studies described above were designed to identify the major factors that affect the regional nasal deposition pattern of Nasonex® nasal spray product. The experimental design was based on changing one variable at a time and did not consider interactions between variables. A full factorial DOE for 4 factors with 2 experimental levels was conducted with a total of 64 experiments to further explore the factors influencing the regional nasal deposition as well as interaction among the factors. Based on the preliminary studies, four factors each with 2 levels were identified as follows: (1) position of nasal spray in the nostril (9 and 5 mm, as the distance between the leading edge of the spray and the front of the nostril while maintaining a constant distance from the medial and lateral walls of the nostril), (2) nasal model head angle (30° and 50° forward from horizontal), (3) actuation force (4.5 and 7.5 kg), and (4) inhalation – actuation timing (nasal spray actuation during nasal inhalation (D) and nasal inhalation started at the end of nasal spray actuation (E)). The fast nasal breathing profile with the PIFR of 35.8 $Lmin^{-1}$, time to reach the peak of 0.3 sec, for total duration of 1.2 sec was used. As previously described the nasal spray actuator was triggered by the breath simulator during inhalation (Section 3.2.5.5). A schematic view of the profiles and timings are shown in Figure 3.6. The nasal spray positioning was defined as insertion depth of 1 cm. The actuation parameters for the force-controlled actuator defined as force rise and fall time of 0.1 sec and force hold time of 0.3 sec. Two doses were administered into the left nostril of VCU nasal model 1. Drug deposited on the device, nasal model

parts and on the filter, was extracted and quantified similarly as performed and described in Sections 3.2.3 and 3.2.5.
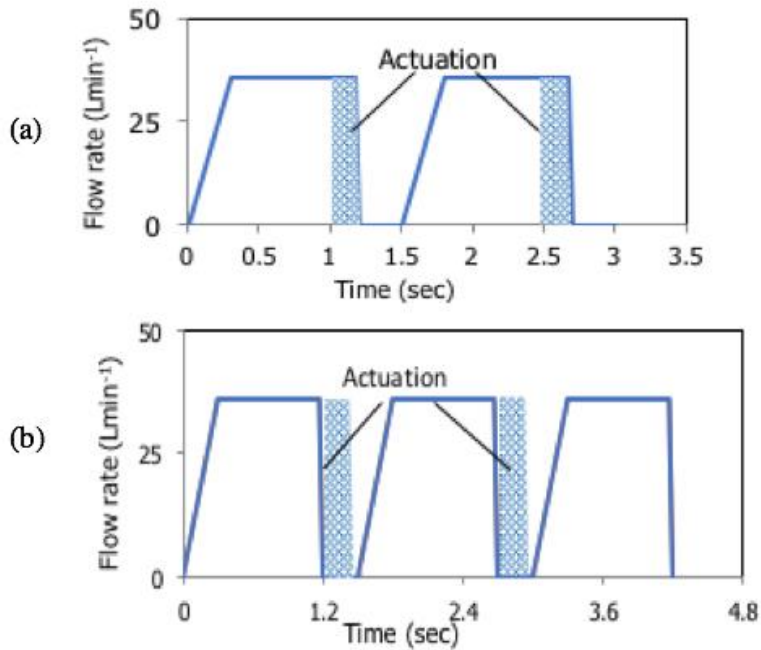
Figure 3.6. Inhalation timing with respect to nasal spray actuation, (a) nasal spray actuation during nasal inhalation (D), (b) nasal spray actuation followed by nasal inhalation (E). The breathing profile (shown by blue line) has a peak inspiratory flow rate of 35.8 Lmin^{-1} and time to reach the peak of 0.3 sec, for total duration of 1.2 sec and tidal volume of 619 mL.

3.2.8 Statistical analysis for full factorial design of experiment (DOE)

The response for the DOE analysis was assessed based on the drug deposited in the combined middle passage and nasopharynx region as the site of action for Nasonex®. The % deposition (deposition fraction) in this region was calculated and expressed as percent of the total recovered dose. The assessment of ANOVA assumption of normality of data was assessed using a probability plot (normal quantile plot). The model assumptions of normality for residuals and homogeneity of variances for the ANOVA test were tested using residual plot. Brown-Forsythe test was used to check the equality of variances where a p-value greater than 0.05 demonstrated equality of variances among groups.

Variables of inhalation-actuation timing and nasal spray position were defined as categorical variables whereas actuation force and head angle were defined as continuous. The influence of each factor and two factor interactions on the response were analyzed using full factorial ANOVA and significant effects were recognized by p-value < 0.05. A linear regression equation describes the model as follow:

$$Y=b_0+b_1x_1+b_2x_2+b_3x_3+b_4x_4+b_5x_1x_2+b_6x_1x_3+b_7x_1x_4+b_8x_2x_3+b_9x_2x_4+b_{10}x_3x_4$$

Equation 3.1

where, b_0 is intercept, and Y is the measured response associated with the factors (x_1, x_2, x_3, and x_4) and the interaction terms (x_1x_2, x_1x_3, x_1x_4, x_2x_3, x_2x_4, x_3x_4). The p-values related to the regression coefficients indicate the significance of the factors on the response. All the analysis performed using JMP Pro 12 software (SAS Institute Inc., Cary, NC).

3.3   Results and Discussion

3.3.1   Development of methods to extract and assay mometasone furoate following deposition in the nasal airway model using the Nasonex® nasal spray product

There were a number of challenges to be addressed when developing assay methods including dissolution of a low aqueous solubility steroid, extraction or dissolution of excipients in the formulation and the compatibility of organic solvents with the plastic resin used to fabricate the realistic physical model. The chemical structure of mometasone furoate is presented in Figure 3.7. It is highly lipophilic with a log P value of 3.5, poorly soluble in water (0.02 mg/mL), and slightly soluble (4 - 8 mg/mL) in methanol [133, 134].

Figure 3.7. Mometasone furoate chemical structure [135]

Ideally, the drug would be dissolved and extracted using an organic solvent, and then filtered to remove insoluble excipients. As an example, for a potential wash solution that was evaluated, Figure 3.8 shows a HPLC chromatogram for a 3 µg/mL mometasone furoate standard solution in the acetonitrile – water (30:70 %v/v) potential wash solution with a drug retention time of 3.4 min. Figure 3.9 shows a HPLC chromatogram of the same standard solution following washing on the realistic nasal model. As demonstrated in Figure 3.9, the drug retention was 3.4 mins, however, significant interfering extractable peaks were observed to co-elute with the

mometasone furoate peak following washing on the airway model using this potential wash solution.

Following extensive studies, methanol – water (50:50 %v/v) was identified as a suitable wash solution, capable of dissolving mometasone furoate when used in combination with sonication for 30 minutes. This solvent mixture was shown to be capable of extracting mometasone furoate deposited on the uncoated realistic nasal model and on the model surface when coated with an artificial mucus. Figure 3.10 demonstrates the absence of co-eluting peaks with the mometasone furoate peak. The mean (SD) peak area for the mometasone furoate (3 μg/mL) peak before and after washing in the nasal airway model was 370143 (358) and 369370 (968), respectively and was not significantly different. HPLC analysis of wash solutions applied to the un-coated and artificial mucus (pH 5.7) coated nasal model revealed peaks that were below the mometasone furoate detection limit confirming the absence of any interfering peak. The ability of the selected wash solvent was validated by determination of the drug content from two sprays of the Nasonex® formulation deposited into the nasal model and subsequently extracted using the wash solution. The mean (SD) drug recovery (% of nominal dose) from the uncoated and artificial mucus coated nasal model was 100.6 (3.2) % and 101.2 (2.8), respectively. Therefore, future studies would employ appropriate volumes of the 50:50 % (v/v) of methanol – water wash solution to recover drug during the *in vitro* deposition experiments.
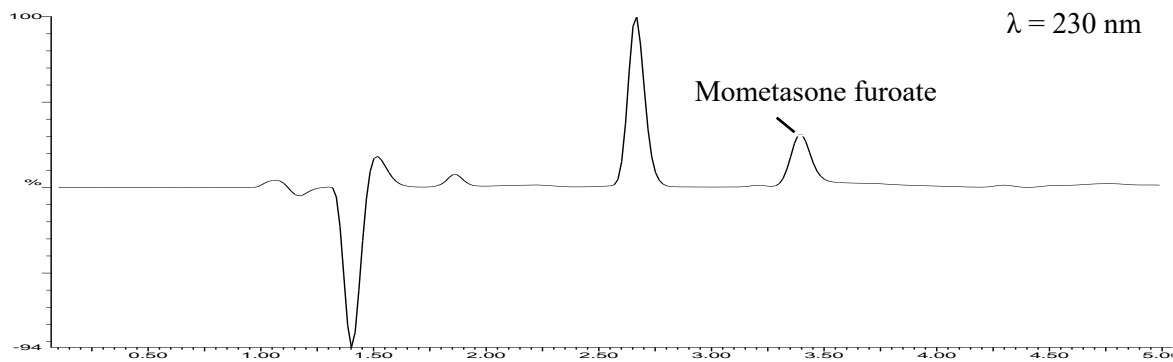
Figure 3.8. Chromatogram of 3 µg/mL mometasone furoate standard solution in acetonitrile – water (30:70 %v/v)
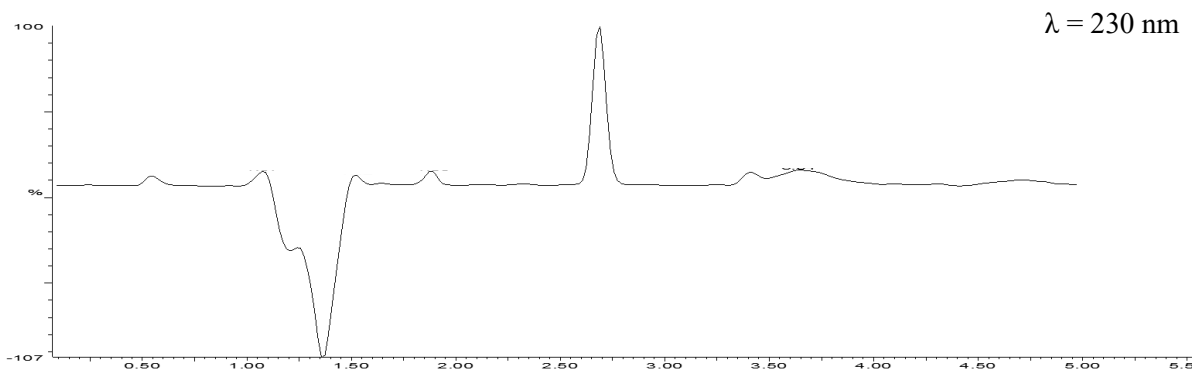
Figure 3.9. Chromatogram of 3 µg/mL mometasone furoate standard solution in acetonitrile – water (30:70 %v/v) following washing on the nasal airway model
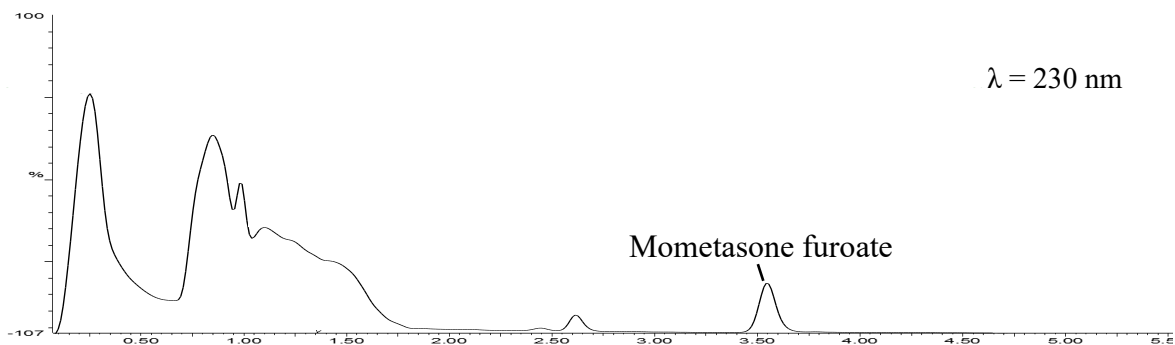
Figure 3.10. Chromatogram of 3 µg/mL mometasone furoate standard solution in methanol – water (50:50 %v/v) following washing on the nasal airway model

For assay method validation, standard solutions in the range of 0.04 – 10.57 µg/mL were prepared in methanol – water (50:50 %v/v) and used to test the linearity of the HPLC assay method (Figure 3.11). The precision of the method was assessed by calculation of % relative standard deviation (RSD) of the mometasone furoate peak area following 6 replicate injections of 0.04 µg/mL mometasone furoate standard solution. The same solution was used to assess the accuracy using 6 replicate injections and calculation of the concentration of mometasone furoate relative to the nominal concentration. The limit of detection (LOD) and quantitation (LOQ) were calculated based on the following equations of 3.2 and 3.3. The method validation results are summarized in Table 3.1.

$$LOD = \frac{3.3 \times SD\ of\ calibration\ curve\ intercep}{Slope\ of\ the\ calibration\ curve} \qquad\qquad \text{Equation 3.2}$$

$$LOQ = \frac{10 \times SD\ of\ calibration\ curve\ intercep}{Slope\ of\ the\ calibration\ curve} \qquad\qquad \text{Equation 3.3}$$

Table 3.1. System suitability parameters for the mometasone furoate HPLC method

System suitability parameter	Value
Linearity range tested	0.040 – 10.570 µg/mL, (r^2>0.9999)
Precision	0.8 %
Accuracy	99.7 %
LOD	0.01 µg/mL
LOQ	0.03 µg/mL
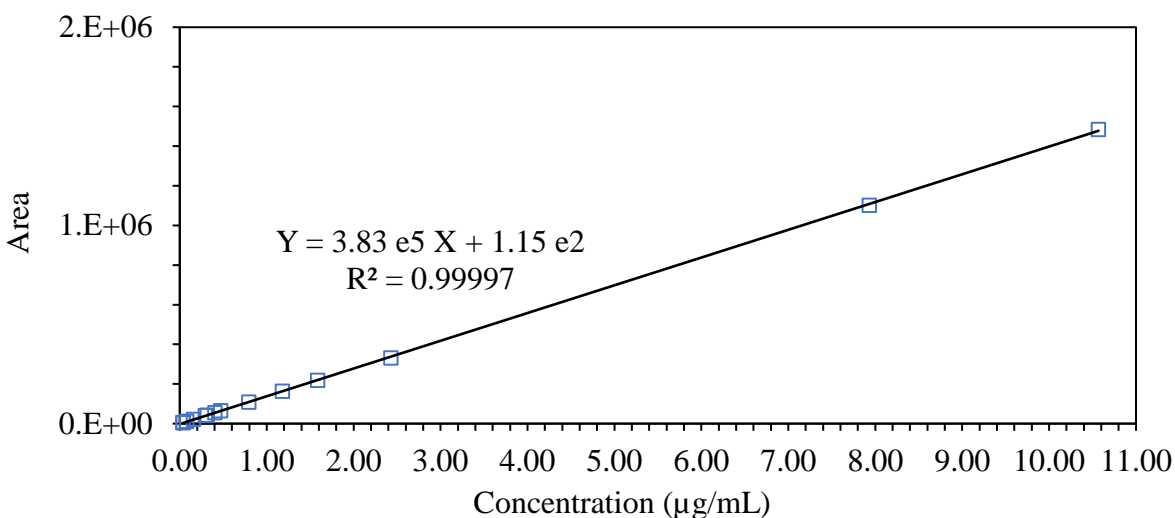
Figure 3.11. Plot of response (area) versus concentration for mometasone furoate in the range of 0.040 -10.570 (µg/mL) measured at 230 nm. The R^2 fitted by linear least square calculated as 0.99997.

Preliminary studies identified the need for sample filtration prior to HPLC of Nasonex[®] formulation derived samples. Filtration was necessary to remove undissolved suspended excipients prior to HPLC injection of the samples for drug content quantitation. Table 3.2 summarizes the mean (SD) mometasone furoate concentration in the filtered standard solutions in methanol – water (50:50 %v/v) following passage through the test filters (expressed as a percentage of the unfiltered solution concentration). For the nylon and PVDF filter, with the low concentration standard solution only, there were significant losses of drug following filtration. There was no significant change in drug concentration relative to the starting concentration for the standard solutions filtered through the Anotop[®] filters.

Table 3.2. Mean (SD) mometasone furoate concentration in the filtered standard solutions in methanol – water (50:50 %v/v) following passage through the test filters (expressed as a percentage of the unfiltered solution concentration) (n=3)

Mometasone furoate conc. (µg/mL)	Nylon Filter (%)	PVDF Filter (%)	Anotop® Filter (%)
0.04	84.8 (3.2)	93.2 (1.0)	100.2 (2.4)
0.25	78.1 (2.8)	98.6 (0.8)	103.3 (0.9)
0.6	84.8 (0.4)	97.9 (1.4)	100.7 (1.7)
10.2	82.1 (0.8)	98.6 (1.6)	99.8 (2.1)

Based on these results, the Anotop® filters used in combination with a wash solution methanol – water (50:50 %v/v) appeared to meet all requirements, with complete dissolution of drug, removal of suspended excipients without altering the concentration of mometasone furoate and the absence of interfering peaks when used to extract drug from the uncoated or artificial mucus (pH 5.7) coated realistic nasal model.

3.3.2 Determination of shot weight, single actuation drug content and formulation content uniformity of Nasonex® nasal spray product

Table 3.3 represent the corresponding results for the mean (SD) shot weight, single actuation drug content and formulation content uniformity. When using the automated nasal spray actuator to generate two different actuation forces of 4.5 and 5.8 kg and following manual actuation, there was no significant difference in the total amount of drug recovered with respect to the actuation technique or applied force in the tested range. Similarly, there was no difference in the measured shot weight, which ranged from 98.8 to 100.4 mg. The corresponding drug content for a single actuation ranged from 98.8 % to 103.0 % of the label claim. The content uniformity of the formulation was also assessed for a single nasal spray product. The mean (SD) formulation drug content for a single nasal spray device was 100.8 (2.1) % of the label claim concentration.

Table 3.3. Mean (SD) single actuation dose content and shot weight of Nasonex® nasal spray product

Experiment	Spray nozzle deposition (% label claim)	Drug recovery (% label claim)	Shot weight (mg)
Single actuation content – actuation force of 4.5 kg	0.6 (0.1)	98.8 (1.3)	98.8 (2.2)
Single actuation content – actuation force of 5.8 kg	0.3 (0.1)	100.5 (2.5)	99.3 (0.8)
Single actuation content – hand actuation	0.7 (0.5)	103.0 (1.0)	100.4 (2.8)

3.3.3 Preliminary assessment of the effect of patient use variables on *in vitro* regional nasal deposition of Nasonex® nasal spray

The results for the preliminary assessment of the effect of patient use variables on *in vitro* regional nasal deposition of Nasonex® nasal spray are summarized in Table 3.4. The mean total drug recovery in deposition studies performed, ranged from 87.7 % to 101.8 % of the labeled dose. For all the deposition studies performed, nasal spray device deposition was low, with less than 2.5 % of the drug deposited on the device. Based on the data presented in Table 3.4, the majority of drug was deposited on the anterior nose region (89.9 % – 70.2 %) with little drug penetration to the combined middle passage and nasopharynx region (7.8 % – 32.1%). The amount of drug recovered from the respiratory filter at the end of the throat for most cases was below 1.0 % and indicated that very low amounts of drug was able to reach the respiratory filter. These results were similar deposition patterns observed for nasal sprays in previous *in vivo*, *in vitro* and CFD studies [16, 17, 31, 136, 137]. These studies also observed that the majority of drug deposited in the anterior nose and there was no drug penetration to the lungs.

3.3.3.1 Effect of number of actuation administered on regional drug deposition of Nasonex® nasal spray

Based on the information provided by manufacturer for dosage and use [123], for the treatment of nasal polyps, congestion and allergic rhinitis, adults and adolescents (above 12 years of age) are recommended to use 2 sprays (100 microgram dose) in each nostril once daily. For children 2-11 years of age the recommendation is one spray (50 microgram dose) in each nostril daily. The effect of number of actuations on the regional nasal drug deposition was assessed using the two actuation forces of 4.5 and 5.8 kg. As demonstrated in Figure 3.12 and Table 3.4 (Exp. 1,2,3 and 8) there was no differences in regional drug deposition for Nasonex® tested in the VCU nasal model 1 when 1 or 2 sprays were administered in a single nostril which was corresponded to administration of 100 µL or 200 µL of the formulation. This indicated that the administration of the second dose did not change the initial regional deposition of the drug formulation within the nasal cavity. Subsequent deposition studies were performed by administering two doses of the Nasonex® to aid analytical quantification.
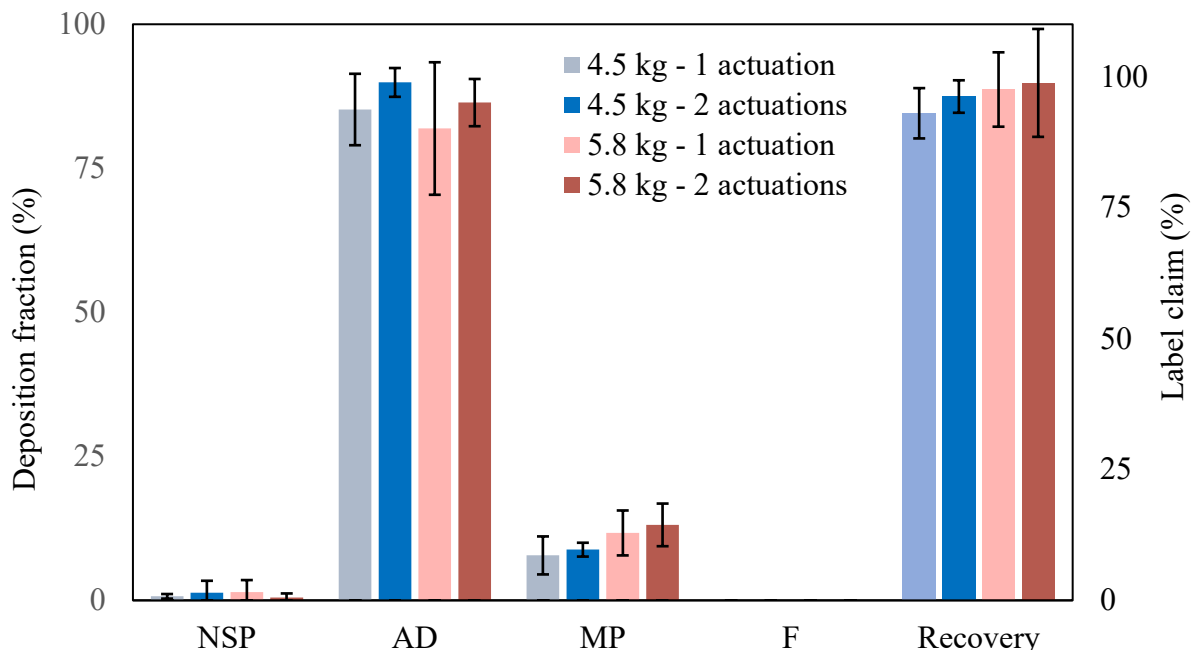
Figure 3.12. Effect of number of actuations administered for Nasonex® nasal spray product on the regional drug deposition in VCU nasal model 1. NSP: nasal spray device, AD: Anterior + drip, MP: Combined middle passage and nasopharynx region, F: Filter. Recovery is presented as % of label claim. Deposition is presented as % of recovered dose (n=4)

3.3.3.2 Effect of head angle on the regional drug deposition of Nasonex® nasal spray

Reviewing packaging insert for Nasonex®, patients are advised to tilt their head forward slightly but there is no quantitative data about the degree of the tilt to be used by the patient. During clinical use, it is likely that various head angles are used. In this study, the nasal model angle was varied by tilting the model 30°, 40°, or 50° forward from horizontal while the distance between the leading edge of the spray and the front of the nostril was 9 mm while maintaining a constant distance from the medial and lateral walls of the nostril (Figure 3.4). The experimental conditions and results for these studies are summarized in Table 3.4 by comparing Exp. 2, 4 and 5. The results from the *in vitro* studies were compared with CFD simulations. Figure 3.13 compares the *in vitro* and CFD deposition results for the effect of head angle. Both *in vitro* (mean (SD)) and CFD simulations showed the highest anterior nose deposition of 89.9 (2.5) % and 89.7 %, respectively,

and lowest combined middle passage and nasopharynx deposition of 8.8 (1.2) % and 8.9 %, respectively, for the head angle of 30°. It appears that there may be a trend of increasing middle passage deposition if the head angle is increased from 30° to 50° forward from horizontal which was shown in both CFD simulations and *in vitro* deposition results. However, due to experimental variability, statistical analysis indicated there was no significant differences in the mean (SD) delivery of the drug to the middle passages (8.8 (1.2) %, 11.6 (6.1) % and 14.4 % (2.3) %) when the model tilt angle increased from 30° to 40° and 50°. CFD simulation (Figure 3.13) results showed reduced anterior drug deposition of 78.5 % and 76.2 %, respectively, when the head angle tilted to 40º and 50º with increased middle passage drug deposition to 21.1 % and 23.6 %, respectively, which suggests the importance of head angle in determining nasal spray deposition.

Reviewing directions and illustrations provided in packaging inserts for a series of corticosteroid nasal spray products, patients are mostly advised to tilt their head forward and this angle varies between 30° to 50° [138]. For example, in directions for use of Nasonex®, Flonase® and Beconase® subjects are advised to tilt their head forward. However, in case of Nasacort®, the patient is directed to tilt the head backward [139]. Foo et al. [42] changed the nasal spray angle and defined an "administration angle" based on a triangle that has one side parallel to the coronal plane of the head and a horizontal plane perpendicular to it (Figure 3.14). They showed that tilting the nasal spray at lower "administration angle" of 30° provided increased middle turbinate deposition compared to 40° and 50° angles. However, based on their definition, it can be observed that increasing the "administration angle" is equivalent to decreasing the head angle in our studies. It is important to note that the studies by Foo et a. contradict the prescribing information for Nasonex®, which state that the nasal spray product needs to be kept in the upright position to deliver the label claim [138]. Kundoor et al. [37] showed that greater deposition in the middle

passages can be achieved by tilting the model 30° back from horizontal compared to 30° forward.

Tilting the nasal model back from horizontal can also significantly reduce the amount of formulation that drips from the nose following actuation.
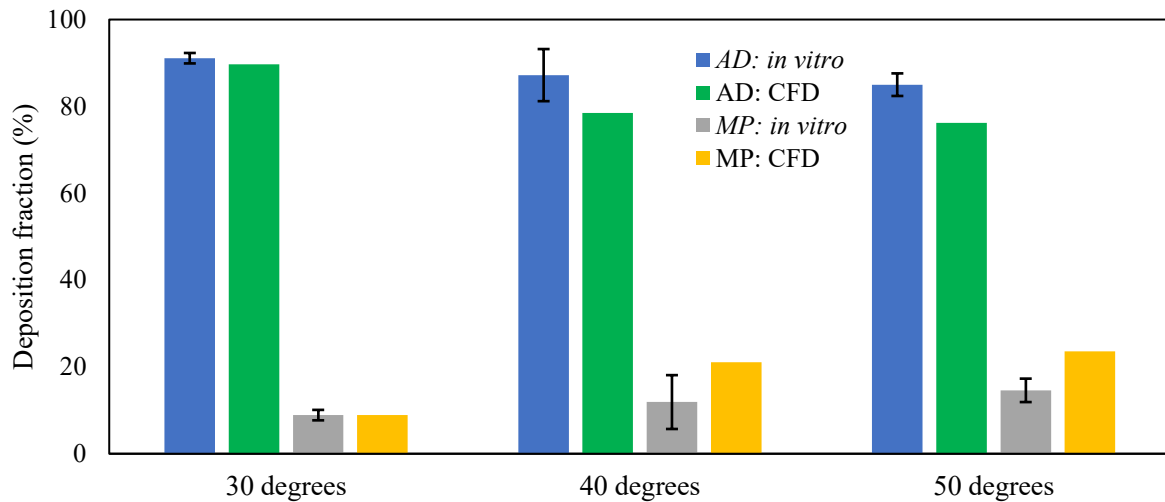
Figure 3.13. Comparison of *in vitro* (mean (error bars are SD)) regional nasal deposition for Nasonex® nasal spray product in the VCU model 1 obtained from experimental data and CFD simulation. AD: Anterior + drip, MP: Combined middle passage and nasopharynx region. The nasal spray is positioned at 9 mm distance from the tip of the nose at the head angle of 30º forward and in the absence of the airflow

(a)   (b)
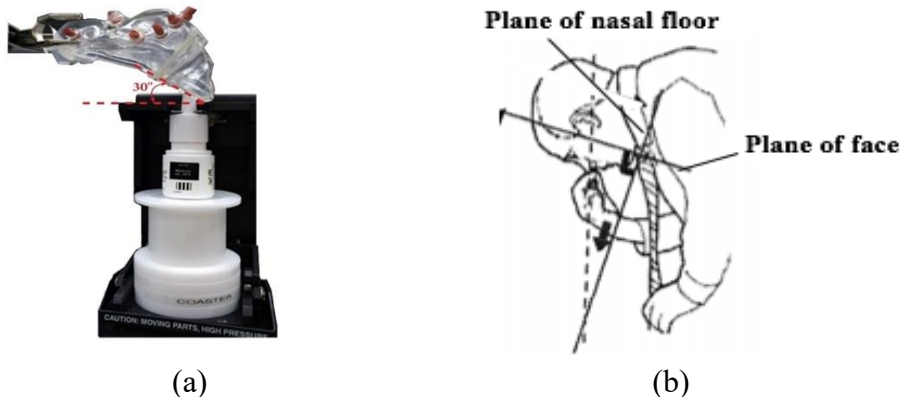
Figure 3.14. Nasal model head angle representations (a) 30º forward from horizontal defined in present study, (b) administration angle defined by Foo et al. [138]

Table 3.4. Mean (SD) *in vitro* regional nasal deposition of mometasone furoate (expressed as a percentage of recovered dose) and total recovery (expressed as percentage of the label claim) for the Nasonex® nasal spray following actuation into the left nostril of VCU nasal model 1 (n=4 – 10)

Exp.	Number of actuation	Actuation force (kg)	Head angle (º)	Flow Profile †	Position# (mm)	NSP (%)	AD (%)	MP (%)	F (%)	Recovery (%)
1	1	4.5	30	NI	9	0.7 (0.4)	85.2 (6.2)	7.8 (3.3)	0.0 (0.0)	93.0 (4.8)
2	2	4.5	30	NI	9	1.3 (2.1)	89.9 (2.5)	8.8 (1.2)	0.0 (0.0)	96.2 (3.1)
3	1	5.8	30	NI	9	1.4 (2.1)	81.9 (11.5)	11.7 (3.9)	0.0 (0.0)	97.5 (7.1)
4	2	4.5	40	NI	9	2.5 (1.2)	85.0 (5.7)	11.6 (6.1)	0.9 (0.5)	93.3 (6.6)
5	2	4.5	50	NI	9	1.5 (2.1)	83.8 (4.3)	14.4 (2.3)	0.3 (0.1)	90.8 (3.1)
6	2	4.5	30	NI	5	0.2 (0.4)	80.9 (4.3)*	18.9 (4.1)*	0.0 (0.0)	101.8 (17.1)
7	2	4.5	30	NI	11	1.3 (0.6)	90.1 (0.8)	8.6 (1.2)	0.0 (0.0)	95.8 (4.0)
8	2	5.8	30	NI	9	0.5 (0.7)	86.4 (4.1)	13.1 (3.7)	0.0 (0.0)	98.8 (10.3)
9	2	7.5	30	NI	9	1.4 (1.9)	85.6 (3.3)	13.0 (4.3)	0.0 (0.0)	87.7 (3.4)
10	2	4.5	30	SI	9	0.8 (1.1)	70.2 (10.6)**	28.9 (10.9)**	0.1 (0.4)	92.8 (7.3)
11	2	4.5	30	FI	9	0.6 (0.9)	67.3 (7.4)**	32.1 (8.0)**	0.0 (0.0)	91.5 (7.3)
12	2	4.5	30	FI-Coated	9	0.4 (0.5)	71.9 (6.5)**	27.3 (4.3)**	0.5 (0.0)	97.4 (4.3)

NSP: Nasal spray, AD: Anterior + drip, MP: Combined middle passage and nasopharynx region, F: Filter, NI: No Inhalation, SI: Slow Inhalation, FI: Fast Inhalation

# $P < 0.05$, significant effect of position (one-way ANOVA); *: $P < 0.05$, Significant difference compared to positioned at 11 and 9 mm, no inhalation airflow (Tukey's HSD)

† $P < 0.05$, significant effect of flow profile (ANOVA); **: $P < 0.05$, Significant difference compared to no inhalation airflow, positioned at 9 mm (Tukey's HSD)

3.3.3.3 Effect of nasal spray positioning on the regional nasal deposition of the Nasonex® in the VCU nasal model 1

The release point position of the nasal spray product in the airway model is considered to be one of the greatest sources of experimental variability that can have significant effects on the observed nasal spray deposition [15]. The release point position of the spray is defined by a combination of the model position and the nasal spray position in the nostril, all of which can be defined by the operator. However, in previous *in vitro* studies a fixed nasal position in the nostril (using nozzle locator) was used or only the information about the insertion depth provided [31, 42, 140]. Variables which can be controlled include nasal model angle, the geometric position of the nasal spray tip within the nostril, the insertion depth and the coronal and sagittal insertion angles. Insertion depth is not usually defined in the patient information leaflet; however, a commonly used value of 10 mm has been widely studied using *in vivo*, *in vitro* and computational fluid dynamic (CFD) models and shown to produce effective delivery to the nose [15, 16, 37, 136].

Three nasal spray positions were defined in our studies which were feasible based upon the nostril hydraulic diameter of VCU nasal model 1 and the geometry of Nasonex® nasal spray nozzle. Considering the results summarized in Table 3.4, small changes of 2-6 mm, (by changing the nasal spray position from 11 mm to 9 mm and 5 mm) in the spray release point were observed to significantly alter deposition, with the middle passage deposition increasing when the spray release point was closer to the front of the nostril. Positioning the nasal spray closer to the front of the nostril at the 5mm distance resulted in more than 2-fold increase in middle passages drug delivery compared to other positions (9 and 11 mm) (mean (SD) = 18.9 (4.1) % (Exp. 6) versus 8.8 (1.2) % (Exp. 2) and 8.6 (1.2) % (Exp. 7) (*p-value* = 0.0004 and 0.0003, respectively)). Correspondingly there was lower anterior nose deposition for the 5 mm position compared to the 9 and 11 mm positions (mean (SD) = 80.9 (4.3) % (Exp. 6) versus 89.9 (2.5) % (Exp. 2) and 90.1 (0.8) % (Exp.

7) (p–value = 0.0030 and 0.0024, respectively)) when tested in the absence of inhalation airflow. It appears that at a position closer to the tip of the nostril of the VCU nasal model 1, spray droplets can be release and develop from the spray pump producing less impaction on the walls of the anterior nose before reaching to the middle passages.

3.3.3.4   Effect of actuation force on the regional drug deposition of Nasonex® nasal spray

Nasal spray generation is dependent on a combination of actuation force, pump design, viscosity and rheological properties of nasal spray formulation. Doughty et al. [141] investigated the effect of variability in actuation force and the force profile observed in adults and children during hand spraying of Flonase® with an instrumented nasal spray. They observed a significant difference in spray weight (especially in pediatrics) and spray plume properties such as droplet size diameter with respect to the manual spray condition applied. In our studies, increasing actuation force from 4.5 kg to 7.5 kg was associated with reducing the mean volume droplet size of Nasonex® nasal spray from 57.2 µm to 47.0 µm measured using Malvern Spraytec. The droplet size measurements are described in details in Section 4.2.7.1. However, despite changes in droplet size, the *in vitro* realistic nasal deposition profiles remained similar (Exp. 2, 8, and 9) when tested using actuation forces of 4.5, 5.8 and 7.5 kg with the nasal spray positioned at 9 mm distance from the front of the nostril. Deposition in the middle passage region was around 10 % of the recovered dose in all cases. Perhaps, the magnitude of change in droplet size distribution of Nasonex® was not large enough to change the regional deposition profile of the formulation due to the initial high velocity of the spray plume and the presence of the nasal valve region in the anterior nose.

3.3.3.5 Effect of inhalation airflow on regional drug deposition of Nasonex® nasal spray

Previous studies have shown that in the absence of an inhalation airflow, the majority of the delivered dose (80 - 90%) was deposited on the anterior nose region and less than 10 - 15% of the formulation penetrated to the posterior part of the nasal cavity. However, employing nasal inhalation in combination with nasal spray administration significantly increased the combined middle passage and nasopharynx deposition and decreased anterior nose losses. The slow and fast breathing profiles investigated (PIFR of 20.2 Lmin^{-1} and 35.8 Lmin^{-1}, respectively) produced mean (SD) anterior nose depositions which were reduced significantly from 89.9 (2.5) % (Exp. 2) to 70.2 (10.6) % (Exp. 10) and 67.3 (7.4) % (Exp. 11), respectively (p-value = 0.0083 and 0.0044, respectively). As a result, the mean (SD) middle passage drug deposition was observed to be significantly higher (almost 4-fold) when an inhalation flow was used (28.9 (10.9) % and 32.1 (8.0) % for slow and fast, respectively) compared to the same experiment performed with the absence of the airflow (8.8 (1.2) %) (p-value = 0.0009 and 0.0010, respectively). The flow rate employed during inhalation in the range of 20 - 35 Lmin^{-1} did not significantly affect the regional nasal deposition. Possible explanations for this improved delivery include that an increased fraction of small sized droplets is entertained by air flow and that travel further distance inside the nasal passages or that spray formulation deposited in the anterior nose is moved as liquid on the surface of the airway into the middle passage region with the inhalation flow. These results appear to demonstrate the significance of inhalation airflow during nasal spray administration to improve delivery to the middle passages. The *in vitro* results were compared to CFD simulations (Figure 3.15) where the flow rate was also shown to significantly increase the middle passage drug deposition. It was also noted that there was no difference observed in the nasal deposition patterns for the slow and fast inhalation flow rates in the CFD results. The use of an inhalation during nasal

spray administration is not clearly stated in patient information leaflet. However, the experimental and CFD results show the importance of the nasal inhalation for improved drug delivery to the middle passages.

These results for middle passage drug deposition in the presence of the airflow are similar to those obtained by Shah et al. [34] using a nasal spray formulation and the Bespak *in vitro* nasal model. They reported middle passage deposition of 28.5% using a post actuation flow of 16 Lmin^{-1} for 12 sec. Also, they observed that there was no change in middle turbinate drug deposition when changing the flow rate from 8 Lmin^{-1} to 16 Lmin^{-1}. Trows et al. [35] employed the Boehringer Ingelheim *in vitro* nasal model and also reported higher deposition in the nasal vestibule, middle and upper turbinates employing 15 and 30 Lmin^{-1} constant air flow compared to no air flow. Kimbell et al. [15] used a CFD simulation model to report a significant increase in number of particles that pass the nasal valve region when employing a nasal flow of 15 Lmin^{-1} for a nasal spray with spray velocity of 1m/sec. No change in formulation penetration through and beyond the valve region was observed when the flow increased from 15 Lmin^{-1} to 30 Lmin^{-1} similar to our observations in the present study. In contrast, there are also a number of other *in vitro* studies that have failed to show any change in *in vitro* deposition using both constant air flow and realistic inhalation profiles [36, 38, 42]. Possible reasons for these discrepancies maybe related to the experimental protocols employed.

3.3.3.6   Effect of surface coating on the regional drug deposition of Nasonex® nasal spray

The presence of the lining fluid did not result in any significant change in either the mean (SD) middle passage (27.3 (4.3) % (Exp. 12) vs 32.1 (8.0) % (Exp.11)) or mean (SD) anterior nose drug deposition (71.9 (6.5) % vs 67.3 (7.4) %) for Nasonex® compared to studies performed in the

absence of a mucus lining fluid. The results demonstrated that coating the nasal model will not change the distribution pattern of Nasonex® formulation in the nasal model cavity. Hence, in order to simplify studies, future studies did not employ surface coating.
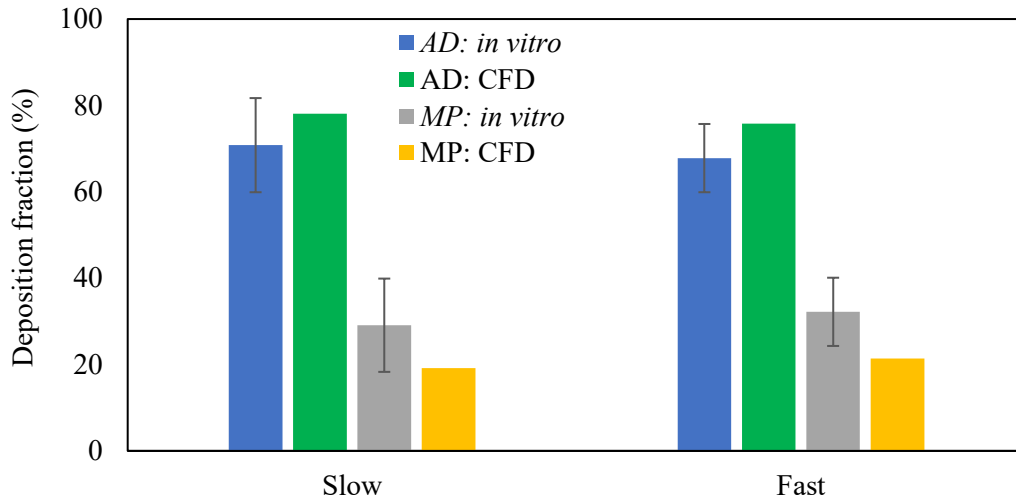
Figure 3.15. Comparison of *in vitro* regional nasal deposition for Nasonex® nasal spray product in the VCU model 1 obtained from experimental data and CFD simulation. AD: Anterior + drip, MP: Combined middle passage and nasopharynx region. The nasal spray is positioned at 9 mm distance from the tip of the nose at the head angle of 30º forward and in the presence of the slow inhalation (20.5 Lmin^{-1}) and fast inhalation (35.8 Lmin^{-1}) airflow

3.3.4 Full factorial design of experiment (DOE) to assess the effect of patient use variables on the regional drug deposition of Nasonex® nasal spray

The four variables of actuation force, head angle, inhalation and actuation timing and nasal spray position at two levels were selected to be investigated for their effects on regional nasal drug deposition of the Nasonex® nasal spray product. Our preliminary studies demonstrated that changing actuation force can result in the generation of a spray plume with small differences in droplet size distributions (described in Section 4.2.7.1) however, these differences resulted in no change in middle passage drug delivery. Varying the nasal head angle from 30º to 50º forward from horizontal and nasal spray position from 11 to 5 mm from the tip of the nostril were both

associated with changes in drug deposition in VCU nasal model 1. Lastly, we observed a significant effect for the presence of inhalation airflow which increased drug delivery beyond the nasal valve region. Therefore, the presence of inhalation airflow seemed to be necessary for the further assessment. Based on literature data and our preliminary studies, timing of nasal inhalation with respect to nasal spray actuation also seemed to be important and was considered for investigation.

The preliminary studies considered each variable in isolation and did not consider the effect that one variable may change as the level of other variables are change. Therefore, a full factorial DOE was performed including two-way interactions which could identify the most important variables influencing regional nasal drug deposition of the Nasonex® nasal spray. Table 3.5 shows the mean (SD) drug deposition for the Nasonex® nasal spray on the nasal spray device (NSP), anterior + drip (AD), combined middle passages and nasopharynx area (MP) and filter (F) as well as the total recovery for the 4-factor full factorial design of experiment performed at two levels (high and low). As demonstrated in Table 3.5, total recovery was similar to previous studies and ranged from 87.3 % - 100.6% of the label claim. Overall, drug deposition on the nasal spray was low, ranging from 0.0 - 5.2 % of the recovered dose. The drug recovery from the respiratory filter at the end of the throat was less than 0.5 % of the label claim for each of the experiments. Depending on the experimental conditions, the mean anterior passage + drip deposition ranged from 42.3 to 81.8 % of the recovered dose. Similarly, the combined middle passage and nasopharynx deposition ranged from 16.6 % to 57.1 %. A combination of an optimal position for spray plume release with the nasal spray positioned close to the nostril tip (5 mm), head angle of 50º and nasal inhalation during nasal spray actuation showed the highest middle passage drug delivery for Nasonex® with 57.1 % of the dose. Figure 3.16 show the results of drug deposition

for 16 different experimental conditions. It appears that coordination of nasal inhalation with nasal spray actuation (D) consistently will result in higher middle passage drug delivery and lower anterior nose deposition. In contrast, lower middle passage deposition was observed when nasal inhalation began at the end of nasal spray actuation (E). Kimbell et al. [15] using CFD simulations also showed that penetration of 20 µm particles from a nasal spray using a 1 sec delay between nasal spray actuation and the start of inhalation was equivalent to no inhalation flow, suggesting that coordination of inhalation and actuation is critical for delivery of drug to the middle passages.

Tables 3.6. and 3.7 show the results of the ANOVA statistical analysis, the estimates for coefficients (the values of the regression coefficient for each variable) and their significance level. The Prob > F gives the *p*-value for the ANOVA effect test where *p*-value of 0.05 or less and indicates that there is at least one variable that has significant effect on middle passage drug deposition. Coefficients (Figure 3.7) with more than one factor term represent the interaction terms which demonstrate how the response (combined middle passage and nasopharynx drug deposition) changes when the two factors were simultaneously changed. A positive value of coefficient indicates an effect that helps to enhance the response value; conversely a negative sign value represents an inverse relationship between the response and the factor. The higher the absolute value the greater the effect of that factor on the response.

Table 3.5. Mean (SD) *in vitro* regional nasal deposition of mometasone furoate (expressed as a percentage of recovered dose) and total recovery (expressed as percentage of the label claim) for the Nasonex® nasal spray following actuation of 2 sprays into the left nostril of VCU nasal model 1 in the full factorial design of experiments (n=4)

Actuation Force (kg) (X1)	Head Angle (X2)	Inhalation-actuation Timing (X3)	Nasal Spray Position (X4)	NSP	AD	MP	F	Recovery (%)
4.5	30	D	9	0.6 (0.9)	67.3 (7.4)	32.1 (8.0)	0.0 (0.0)	91.5 (7.3)
4.5	30	E	9	1.2 (0.9)	73.3 (9.2)	25.1 (9.4)	0.0 (0.0)	87.3 (1.7)
4.5	30	D	5	0.5 (0.7)	58.1 (3.3)	40.9 (2.8)	0.0 (0.0)	89.2 (8.5)
4.5	30	E	5	1.9 (2.1)	68.2 (8.5)	29.9 (7.5)	0.0 (0.0)	92.7 (5.4)
7.5	30	D	9	0.0 (0.0)	55.4 (7.6)	44.6 (7.6)	0.0 (0.0)	88.9 (3.2)
7.5	30	E	9	1.3 (0.7)	78.8 (5.1)	19.8 (4.7)	0.3 (0.6)	92.4 (3.6)
7.5	30	D	5	2.5 (2.6)	63.5 (5.5)	34.1 (3.1)	0.0 (0.0)	100.5 (4.7)
7.5	30	E	5	0.1 (0.2)	70.2 (10.8)	29.7 (10.6)	0.0 (0.0)	95.6 (4.2)
4.5	50	D	9	2.7 (1.7)	51.3 (8.2)	45.8 (7.3)	0.2 (0.3)	92.4 (5.3)
4.5	50	E	9	5.2 (5.7)	76.4 (4.8)	18.4 (3.8)	0.0 (0.0)	89.7 (12.4)
4.5	50	D	5	1.7 (1.5)	48.8 (7.3)	49.1 (6.6)	0.4 (0.8)	95.2 (6.7)
4.5	50	E	5	3.1 (4.4)	76.3 (3.5)	20.6 (4.4)	0.0 (0.0)	90.7 (7.3)
7.5	50	D	9	1.5 (0.8)	48.7 (5.9)	49.8 (5.2)	0.0 (0.0)	93.1 (5.6)
7.5	50	E	9	1.2 (1.1)	81.8 (1.7)	16.6 (2.5)	0.4 (0.7)	100.6 (5.8)
7.5	50	D	5	0.6 (0.7)	42.3 (8.9)	57.1 (9.5)	0.0 (0.0)	95.1 (4.5)
7.5	50	E	5	2.0 (1.2)	68.9 (4.5)	29.2 (3.4)	0.0 (0.0)	93.6 (5.7)

NSP: Nasal spray, AD: Anterior + drip, MP: Combined middle passage and nasopharynx region, F: Filter
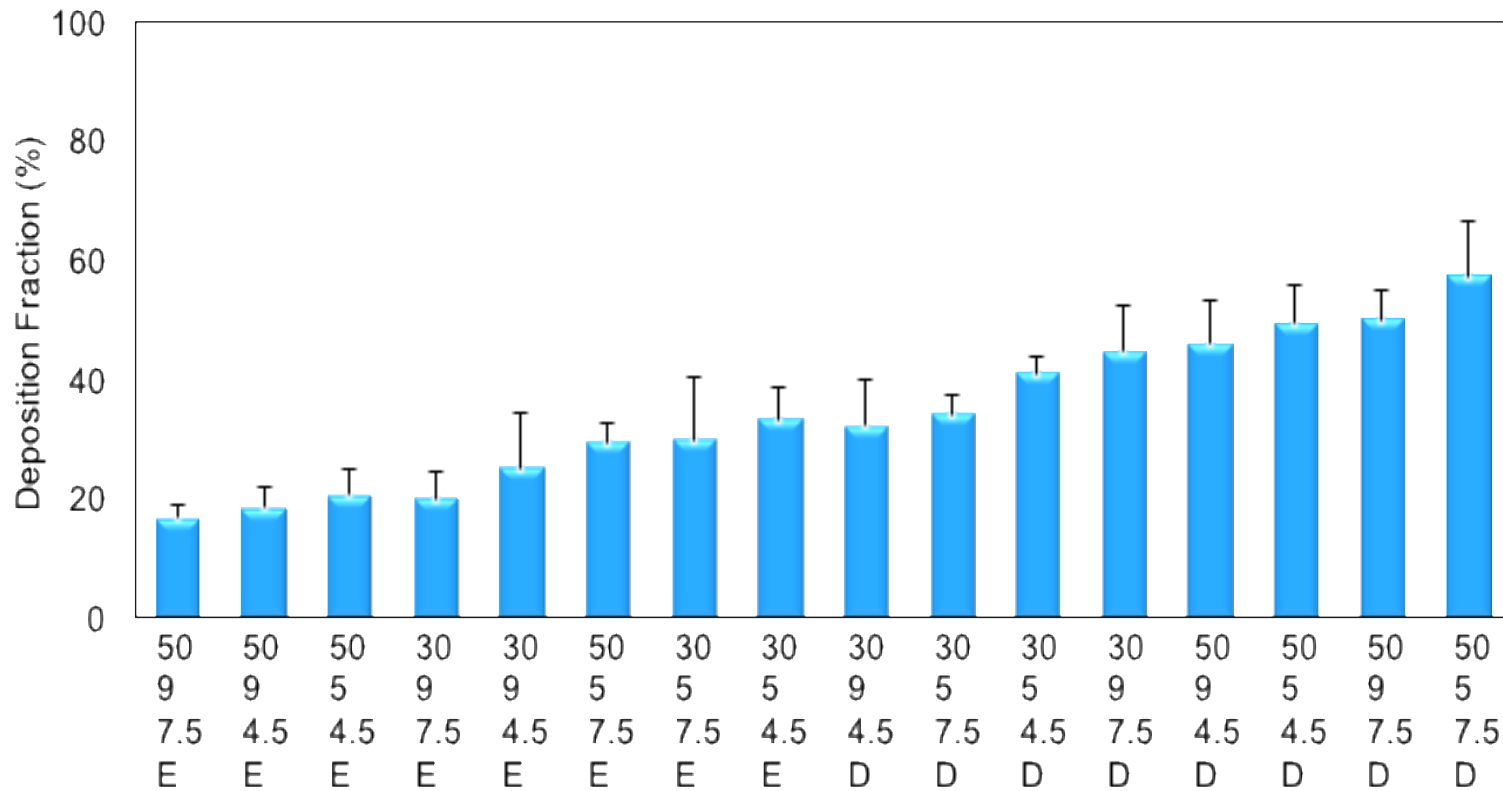
Figure 3.16. Mean (error bars are SD) combined middle passage and nasopharynx regions drug deposition (expressed as % of recovered dose) for Nasonex® nasal spray in the VCU model 1. X-axis represents the combined experimental conditions of head angle (30 ° or 50º), nasal spray position (9 or 5 mm), actuation force (4.5 or 7.5 kg) and nasal inhalation – nasal spray actuation timing (D: Nasal inhalation during nasal spray actuation, E: nasal inhalation at the end of nasal spray actuation, inhalation rate of 35.8 Lmin^{-1}, (n=4)

Table 3.6. Summary of ANOVA parameters for full factorial design of experiment

	DF	Sum of Square	Mean Square	F Ratio	Prob> F
Model	10	8870.3	8870.0	17.8	<0.0001
Error	53	2646	49.9		

Table 3.7. Estimates of coefficients for the predicted model and the significance of each variable and two variables interaction

Source	Estimate of Coefficient	t Ratio	Prob>|t|
Intercept	34.12	38.62	<0.0001*
Inhalation timing (D)	10.06	11.39	<0.0001*
Inhalation timing (E)	-10.06	-11.39	<0.0001*
Angle*Inhalation timing (D)	4.56	5.17	<0.0001*
Angle*Inhalation timing (E)	-4.56	-5.17	<0.0001*
Position (5)	2.60	2.94	0.0048*
Position (9)	-2.60	-2.94	0.0048*
Angle (30, 50)	1.69	1.91	0.0618
Inhalation timing (E)*Position (5)	1.50	1.70	0.0949
Inhalation timing (D)*Position (9)	1.50	1.70	0.0949
Inhalation timing (E)*Position (9)	-1.50	-1.70	0.0949
Inhalation timing (D)*Position (5)	-1.50	-1.70	0.0949
Force*Angle	1.39	1.57	0.1213
Force*Inhalation timing (D)	1.22	1.38	0.1726
Force*Inhalation timing (E)	-1.22	-1.38	0.1726
Force (4.5, 7.5)	0.97	1.10	0.2749
Angle*Position (5)	0.58	0.65	0.5164
Angle*Position (9)	-0.58	-0.65	0.5164
Force*Position (5)	-0.18	-0.20	0.8389
Force*Position (9)	0.18	0.20	0.8389

* $P < 0.05$
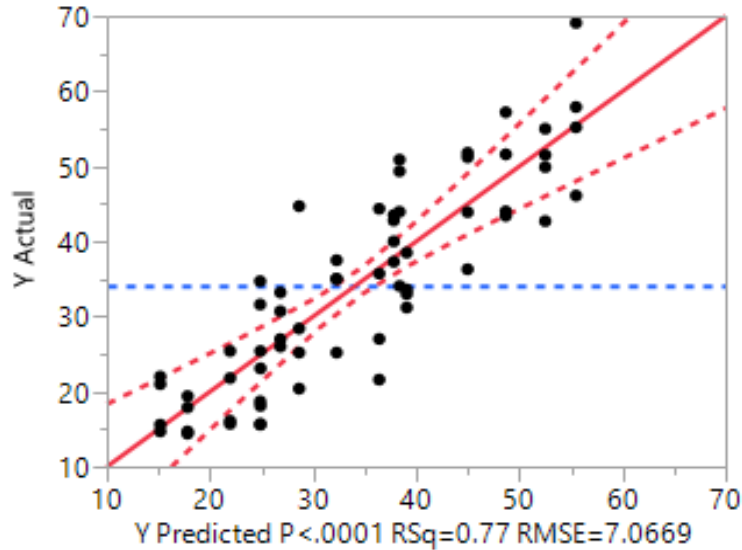
Figure 3.17. Plot of actual (observed) values versus predicted values for combined middle passage and nasopharynx regions deposition. The horizontal broken line shows the mean velocity, the solid line is the line of fit, and the two broken curve lines describe the 95% confident region relative to the line of fit. RSq: correlation coefficient; RMSE: root mean square error

As shown in Table 3.6, analysis of variance of the overall model reports a significant model with p-value < 0.0001. Based on the p-value reported for the variables in Table 3.7, inhalation – actuation timing and nasal spray position have significant effects on middle passage drug deposition with inhalation timing being the more influential factor as shown by larger estimated coefficient. Coordination of inhalation and nasal spray actuation (D) was shown to produce higher middle passage drug deposition (increased by 10.1 %, holding all variables constant, equation 3.6), while conversely, nasal inhalation after nasal spray actuation (E) results in lower drug delivery to the middle passages (decreased by 10.1%, assuming all variables are constant). In addition, positioning the nasal spray closer to the nostril tip (5 mm compared to 9 mm) also resulted in greater delivery efficiency to the middle passages.

In addition to these individual significant variables, there was a significant interaction between the effect of inhalation timing and the head angle of the nasal airway model (p-value <

0.0001). This interaction reveals that the effects of individual variables are not independent and have a combined effect on middle passage drug deposition. The higher head angle of 50º when combined with coordination of nasal inhalation and nasal spray actuation increases middle passage drug delivery. However, nasal inhalation following spray actuation combined with a head angle of 50º lowers middle passage drug deposition.

Based on the experimental data for regional drug deposition of Nasonex® in the DOE study, the following model including the four patient use variables and their interaction (two-way) was developed to predict middle passage drug deposition. It was of interest to observe the effects of individual variables and two variable interactions, therefore all variables were included in the model. JMP uses scaled factor values for the continuous variables (angle and force) to develop an equation that predict responses based on the input parameters. A scaled factor is mean-centered and scaled by range/2.

$$\text{Scaled factor} = \frac{2\,(X - Xcenter)}{Xmax - Xmin} \qquad\qquad \text{Equation 3.5}$$

Scaled factor for angle was calculated as: 2*(input value of angle - 40)/20
Scaled factor for actuation force was calculated as: 2*(input value of force- 6)/3

The built model equation is presented below and Y represents the response factor (middle passage deposition):

$Y = 34.1 + (0.97 * (\frac{force-6}{1.5})) + (1.69 * (\frac{angle-40}{10}))$ + (Match inhalation if "D" then 10.1 or E - 10.1) + (Match position if 5 then 2.60 or 9 then -2.6) + $((1.39 * (\frac{force-6}{1.5}) * (\frac{angle-40}{10})) + ((\frac{force-6}{1.5}) * (\text{Match inhalation if "D" then 1.2 or E -1.2}))* + ((\frac{force-6}{1.5}) * ($ Match position if 5 then -0.2 or 9 then 0.2)) + $((\frac{angle-40}{10}) * ($ Match inhalation if "D" then 4.6 or E -

4.6))+(($\frac{angle-40}{10}$)*(Match position if 5 then 0.58 or 9 then -0.58))+(Match timing if D then (Match position if 5 then -1.5 or 9 then -1.5), if timing E (Match position if 5 then 1.5 or 9 -1.5))
Equation 3.6

Using this model, predicted and observed response values were in the good agreement (R^2= 0.77) (Figure 3.17). The R^2 of 0.77 means that 77% of variability in the response can be explained with the model which was relatively high. The model assumptions of normality for residuals and homogeneity of variances for the ANOVA test were also tested and demonstrated in Figures 3.18, 3.19 and 3.20. Looking at normal quantile plot presented in Figure 3.18 it seems data are normally distributed. For residual plot, graphically shown in Figures 3.19 and 3.20, the equal amount of spread above and below the line is desirable meaning that there is no heteroscedasticity observed (no change in variance of the error term across the observations). Brown-Forsythe among with three other tests were used to check the equality of variances and the result is shown in Table 3.8. The p-value greater than 0.05 demonstrated equality of variances among groups. The p-value for the Brown-Forsythe test was 0.2418.

Table 3.8. Results of statistical analysis for testing unequal variances

Test	F Ratio	DF Num	DF Den	Prob > F
O'Brien	1.0979	15	48	0.3834
Brown-Forsythe	1.2957	15	48	0.2418
Levene	1.7689	15	48	0.0685
Bartlett	1.1093	15	.	0.3408

DF NUM: degrees of freedom in the numerator for each test
DF Den: the degrees of freedom used in the denominator for each test.
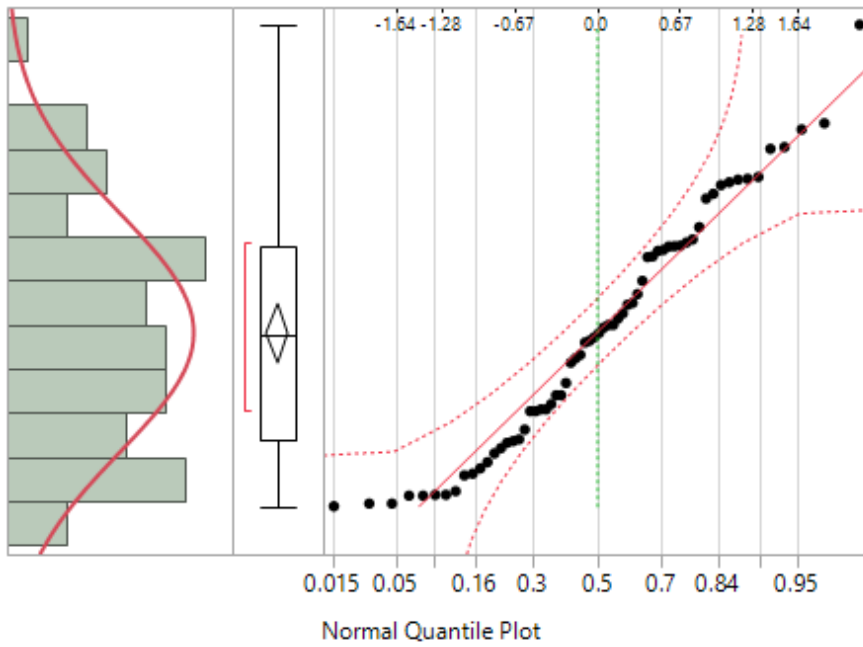
Figure 3.18. Normal quantile plot used to assess the normality of the data for the linear model
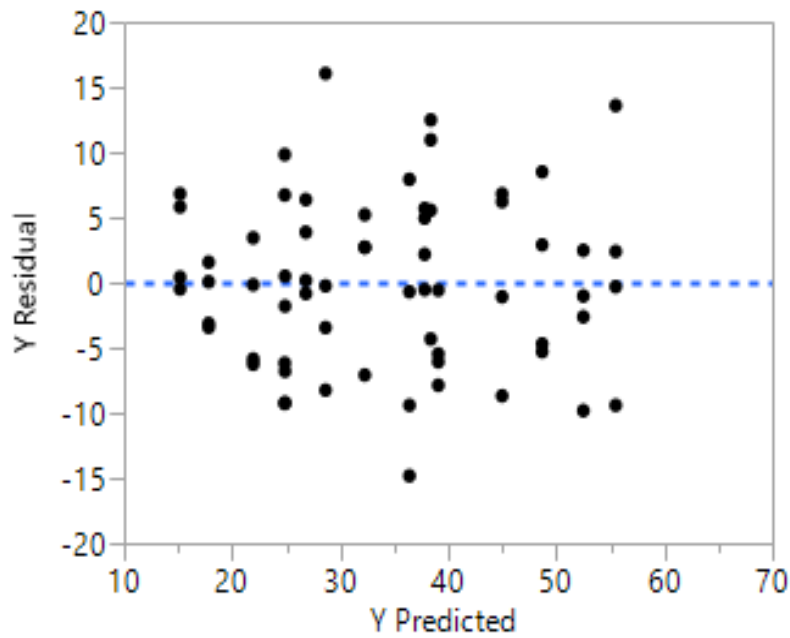
Figure 3.19. Plot of residuals used to assess the normality for the linear model
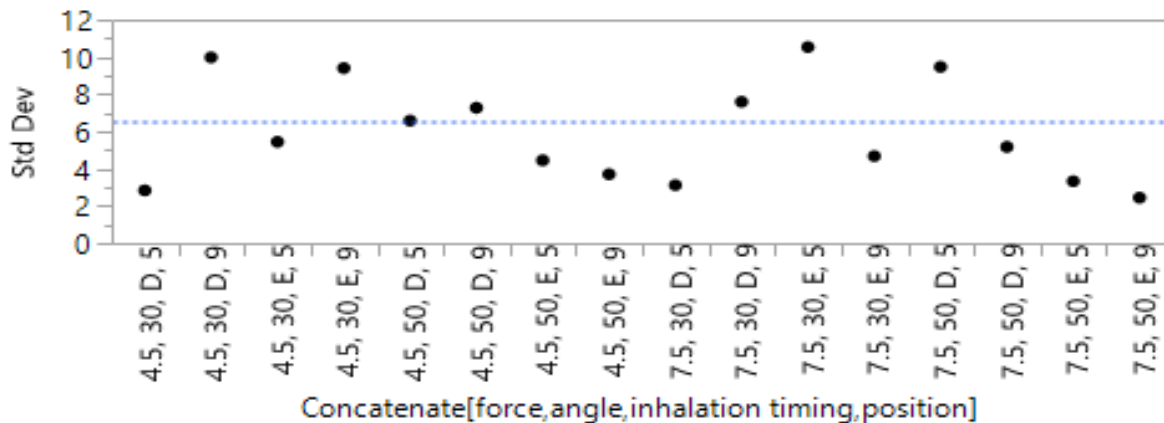
Figure 3.20. Plot of standard deviation for each group constructed by actuation force, head angle, timing and nasal spray position

This study has illustrated the use of *in vitro* realistic testing methods to simulate patient use parameters and their effects on the regional nasal deposition of the Nasonex® nasal spray product. *In vivo* deposition studies with Nasonex® have shown that the mean anterior nose and middle passage deposition healthy volunteers was 26.0 % and 60.1 % [137]. In another *in vivo* study in patients with allergic rhinitis, different results of approximately 65% and 35%, respectively, were reported [18]. Unfortunately, details regarding the controlled administration of the nasal spray and associated patients use variables were not reported. This prevents a direct comparison with similar administration conditions using the developed *in vitro* realistic deposition test method. These *in vivo* results were in line with the results that we observed for Nasonex® in our developed realistic testing condition. Without this *in vitro* – *in vivo* correlation, the conclusions of this *in vitro* study and their significance with respect to optimizing delivery remain to be confirmed. If these developed *in vitro* methods are capable of simulating *in vivo* deposition, then this approach offers

a powerful technique of rapidly screening both formulation and administration variables and their effects on regional nasal deposition.

The results of this study demonstrated that the way the patient administers the nasal spray can result in high drug deposition in the anterior nose which is a non-ciliated region where no drug absorption can take place with corresponding poor drug delivery to the site of action in middle passages. Conversely, there are patient use conditions that can be recommended that appear to significantly increase middle passage drug delivery for this nasal spray product. It should be noted that the conclusions regarding patient use parameters have only been tested using one spray device and formulation (Nasonex®) and may not be applicable to other nasal spray products.

3.4   Conclusions

In this chapter, a realistic *in vitro* deposition testing method was developed for the Nasonex® nasal spray product based on realistic patient use conditions (Specific Aim1-1). The effects of patient use factors on regional nasal deposition of the Nasonex® nasal spray product was investigated (Specific Aim 1-2). The overall deposition pattern within the nasal cavity and the potential for the lung deposition were found to be similar to previous *in vivo* studies which indicated that the developed method may be used as a tool for estimating the initial sites of regional nasal drug deposition, although a prospective *in vitro* and *in vivo* study with identical patient use conditions would be desirable.

The results suggest that the presence of the nasal inhalation and its timing with respect to the nasal spray actuation is crucial for enhanced nasal valve penetration of the formulation. The effect of head angle was also found to be significant. Significant drug losses in anterior nose region can be observed under certain patient use conditions. Based on the DOE studies, nasal drug

delivery to the middle passages could be increased up to 3-fold by a combination of patient use parameters in a single nasal geometry. Realistic nasal airway models can be used to identify the key administration technique factors required to maximize drug delivery to the site of action.

This study has demonstrated that when comparing *in vitro* nasal deposition studies, it is important to control and report the spray administration experimental variables used to simulate patient use conditions if comparable results are to be obtained. It should also be observed that the conclusions made in the chapter are specific to the Nasonex® nasal spray tested in a single airway nasal geometry. Studies should also consider comparisons between a series of innovator and generic nasal spray products, rather than a single test product if this method is to be utilized to accelerate regulatory reviews of nasal sprays. It is also important to evaluate the role of inter-subject nasal geometry on the regional deposition of nasal sprays if these methods are to be used to simulate variability observed in the population.

CHAPTER 4

ASSESSMENT OF THE EFFECTS OF PATIENT-USE VARIABLES, NASAL GEOMETRY AND FORMULATION / DEVICE COMBINATION ON REGIONAL DEPOSITION OF NASAL SPRAY PRODUCTS IN THE REALISTIC NASAL GEOMETRIES

4.1 Introduction

Drug delivery to the posterior part of nasal cavity from a nasal spray product is dependent upon a number of factors including patient use factors, the geometry of nose and nasal cavity, and the formulation/device characteristics [2, 9]. Investigations of drug delivery efficiency and assessments of bioequivalence of nasal spray products may be aided by the use of physically realistic nasal airway models in combination with simulated patient use to determine *in vitro* spray deposition patterns within the nose as described in the previous chapter. These realistic *in vitro* tests may provide an improved means of comparing innovator and generic nasal spray products compared to traditional droplet size and plume geometry tests. In this chapter, we have investigated the effects of inter-subject variability in nasal geometry on the *in vitro* regional drug deposition of Nasonex® nasal spray product by comparing its regional nasal deposition in two nasal airway geometries. In addition, this chapter also describes studies assessing the utility of the developed realistic deposition test methods to discriminate between products when changing the formulation-device combination and comparing innovator and generic nasal spray products. This capability of the developed realistic test methods to discriminate between nasal spray products was also assessed by comparing the regional nasal deposition of nasal spray formulations with different spray plume characteristics.

4.2   Material and Methods

4.2.1   VCU nasal model 2

The VCU nasal model 2 was previously developed by Walenga [48]. The computerized tomography (CT) scan data of a 20-year old female was segmented using the commercial software package Mimics 16.0 (Materialise, Belgium). The 3D file was then converted to an .stl file and imported to a CAD software package, SolidWorks 2011 (Dassault Systèmes Solidworks Corp., Waltham, MA). Finally, the file was converted into a volumetric file type (.igs) using the mesh development software 3-Matic (Materialise, Belgium).

The VCU nasal model 2, shown in Figure 4.1, was characterized by a nasal cavity with a surface area to volume ratio (SA/V) of 0.75 mm^{-1} in the anatomical left side of the posterior part of the nasal cavity and 1.33 mm^{-1} on the right side, indicating that significant nasal cycling was present, a phenomenon described in more detail by Gungor et al. [142]. However, in this study drug deposition was investigated using the right side of the nasal cavity and the left side was blocked. Table 4.1 describes the geometric characteristics of the VCU nasal model 2 and compares with the corresponding features in VCU nasal model 1. For these studies VCU nasal model 2 was incorporated to the experimental setup in the similar fashion as VCU nasal model 1 as depicted in Figure 4.2.
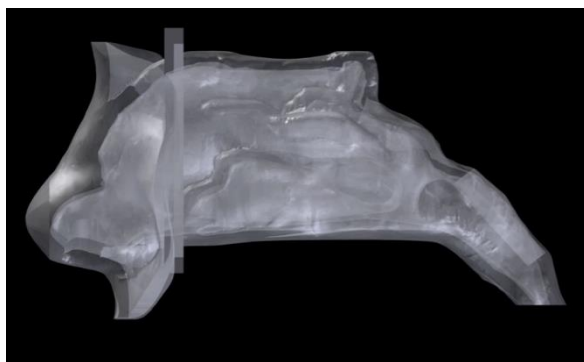
Figure 4.1. Realistic nasal model (VCU nasal model 2) developed at Virginia Commonwealth University
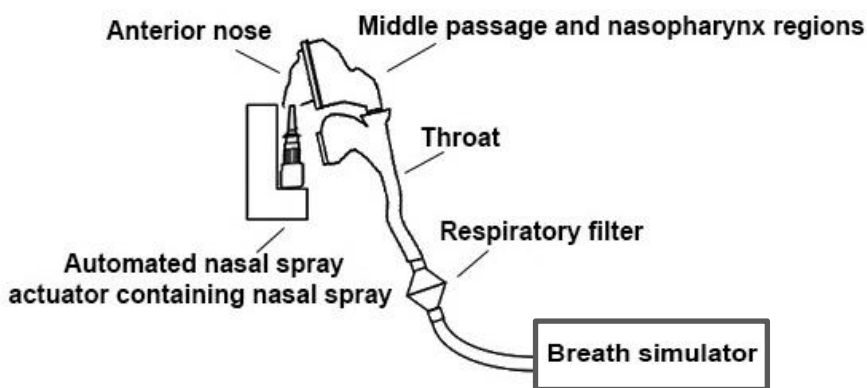
Figure 4.2. Experimental setup for realistic testing of regional nasal deposition of the Nasonex® nasal spray product in VCU nasal model 2

Table 4.1. Geometric measurements of the nasal cavity for the left side of VCU nasal model 1 and right side of VCU nasal model 2. The dimensions tabulated are the posterior surface area-to-volume ratio (SA/V), the average nostril hydraulic diameter (dh, nostril), the nasopharynx exit hydraulic diameter (dh, nasopharynx), anterior nose volume, and surface area of the nasal vestibule (SA).

VCU nasal model	SA/V (mm^{-1})	$D_{h, nostril}$ (mm)	$D_{h, nasopharynx}$ (mm)	Anterior nose volume (mL)	SA of the anterior nose (mm^2)
1	0.74	12.1	5.9	3.2	1153
2	1.33	10.6	4.5	2.2	1493

4.2.2   Selection of inhalation flow rate to be employed using VCU nasal model 2

The resistance of VCU nasal models 1 and 2 against the incoming airflow was determined by measuring the pressure drop across the models at a series of flow rates in the range of 5 to 50 Lmin^{-1}. The assembled nasal models were sealed air-tight completely with only one nostril open to air flow. Pressure drop across the model was measured using a digital manometer (Air - Neotronics Ltd., Oxford, England). Air flow was drawn through the nasal model via the throat which was connected to the vacuum pump capable of pulling constant flows of between 5 and 50 Lmin^{-1} through the model. Air flow rate was varied and plotted against the measured square root of the pressure drop to calculate the air flow resistance through the nasal model. Assuming frictionless flow through the nasal models, the relationship between the volumetric flow and pressure drop is based on the following equation [143]:

$$\sqrt{\Delta P_D} = \sqrt{P_a - P_1} = R_D Q \qquad \text{Equation 4.1}$$

In which P_a is the ambient pressure, P_1 is the pressure measured at the nasal airway model tracheal pressure tap at the entrance of nasal airway model, and Q is the volumetric flow. Therefore, R_D or model related resistance can be calculated form the slope of the linear line.

Following calculation of resistance of VCU nasal models 1 and 2, flow rates with equivalent pressure drops were evaluated in the *in vitro* test setup.
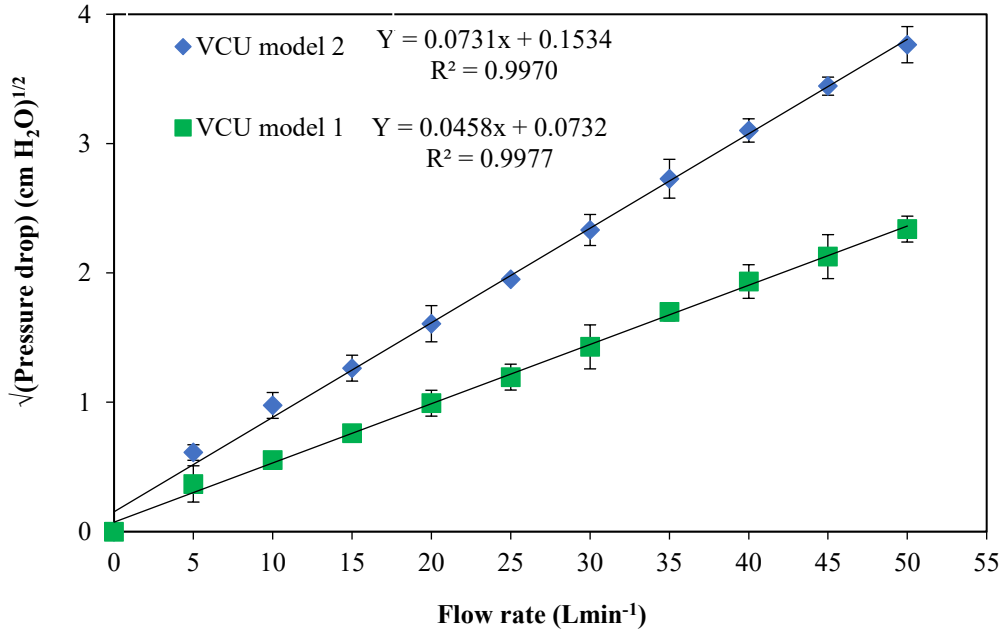
Figure 4.3. √(Pressure drop) - flow rate relationship in VCU nasal models 1 and 2. The line equation and correlation coefficient (R^2) were calculated for each nasal model. The resistance was calculated as 0.046 ($cmH_2O^{1/2}$/($Lmin^{-1}$)) for VCU nasal model 1 and 0.073 ($cmH_2O^{1/2}$/($Lmin^{-1}$)) for VCU nasal model 2

The resistance calculated for VCU nasal model 2 was compared to that of determined for VCU nasal model 1. As demonstrated in Figure 4.3, VCU nasal model 2 has a higher airflow resistance of 0.073 ($cmH_2O^{1/2}$/($Lmin^{-1}$)) compared to VCU nasal model 1 with 0.046 ($cmH_2O^{1/2}$/($Lmin^{-1}$)). This difference in resistance can be explained by variability in the model geometries with VCU nasal model 2 being more constricted in the right side of the nasal cavity as shown previously by large SA/ V ratio in the middle passage region (1.33 mm^{-1}) compared to the left side of VCU nasal model 1 (0.74 mm^{-1}) (Table 4.1).

It was important to test the two nasal models at equivalent realistic flows if flow rates are important in determining the regional drug deposition. Initial studies examined the regional drug

deposition of Nasonex® in VCU nasal model 1 at two flow rates of 20.5 Lmin^{-1} (equivalent to a square root of pressure drop of 1.01 cmH$_2$O$^{1/2}$) and 35.8 Lmin^{-1} (equivalent to a square root of pressure drop of 1.65 cmH$_2$O$^{1/2}$). However, those studies indicated that there was no difference in the regional nasal deposition at those two flow rates. The higher flow rate (35.8 Lmin^{-1}) was therefore selected for comparison in VCU nasal model 2. This flow in VCU nasal model 1 generated a pressure drop of 1.65 cmH$_2$O$^{1/2}$. The equivalent flow at this pressure drop in VCU nasal model 2 was determined as 20.5 Lmin^{-1}. Studies in VCU nasal model 2 were then performed i) using an identical flow rate of 35.8 Lmin^{-1} compared to VCU nasal model 1 (with a higher resulting pressure drop) and with an identical pressure drop of 1.65 cmH$_2$O$^{1/2}$ to VCU nasal model 1 (with a lower resulting flow rate of 20.5 Lmin^{-1}). The mean (SD) total drug recovery was similar for both experiments with 88.2 (1.8) % recovered at 35.8 Lmin^{-1} and 90.7 (2.5) % recovered at 20.5 Lmin^{-1} as shown in Figure 4.4. It is evident that there is no significant difference between the amount of the drug deposited on the nasal spray device and in the regional nasal drug deposition for Nasonex® when using the different flow conditions in VCU nasal model 2. The experimental conditions used an actuation force of 4.5 kg, nasal spray position at 5 mm from the front of the nasal tip and nasal spray actuation during nasal inhalation (D).

This indicated that changing flow rates from 20.5 Lmin^{-1} to 35.8 Lmin^{-1} did not affect the regional drug deposition of Nasonex® in VCU nasal model 2. We observed similar findings of no change in the regional drug deposition of the Nasonex® in VCU nasal model 1 with respect to the flow rates used despite differences in model airway resistance.
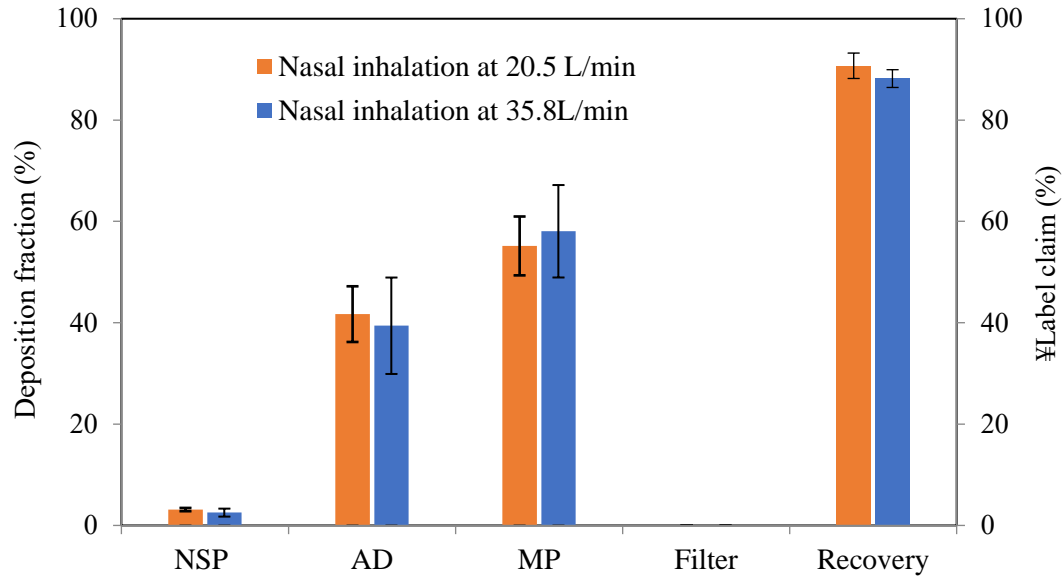
Figure 4.4. Regional nasal drug deposition of Nasonex® in the VCU nasal model 2 tested at flow rates of 20.5 Lmin[-1] and 35.8 Lmin[-1]. Data presented as mean (error bars are SD) (n=4). NSP: nasal spray device, AD: Anterior + drip, MP: Combined middle passage and nasopharynx region, F: Filter. Recovery is presented based on the label claim. Device deposition and regional drug deposition data are presented based on the recovered dose.

4.2.3 Assessing the effects of patient use variables on the regional drug deposition of Nasonex® in VCU nasal model 2 using a full factorial design of experiment

A full factorial DOE for 3 factors at 2 experimental levels was conducted (for a total of 32 experiments) to explore the influence of patient use factors and the interactions among the factors in the VCU nasal model 2. Similar to the variables that were tested in the VCU nasal model 1, three independent variables of actuation force, head angle and inhalation timing at two levels were selected to perform the regional nasal deposition studies in VCU nasal model 2. The smaller hydraulic diameter of the nostril for VCU nasal model 2 compared to VCU nasal model 1 allowed defining only one nasal spray position within in the nostril as 5 mm distance from the tip of the nostril. Nasal spray insertion depth of 1 cm was kept constant. The previously defined nasal

breathing profile with the PIFR of 35.8 Lmin^{-1} was used. Two doses of the Nasonex® nasal spray were administered in the right nostril while the other nostril was blocked. The amount of drug deposited on the i) the nasal spray device (NSP), ii) amount that dripped from the nose + anterior nose (AD), iii) combined middle passage and nasopharynx (MP), iv) respiratory filter + throat (F) were quantified. Samples were assayed for mometasone furoate content by a validated HPLC method and using methanol and water (50:50 %v/v) as the wash solution (Sections 3.1.3 and 3.2.1).

In order to compare, the inter-subject variability between the two nasal airway models, the regional nasal drug deposition of Nasonex® nasal spray product obtained from VCU nasal model 1 (Section 3.2.4) and 2 were compared under identical experimental conditions.

4.2.4   Statistical analysis for full factorial design of experiment

Results were processed as a percentage of the recovered dose. The ANOVA assumption of normality of data was assessed using normal quantile plot. The model assumptions of normality for residuals and homogeneity of variances for the ANOVA test were tested using residual plot. Brown-Forsythe test was used to check the equality of variances where a p-value greater than 0.05 demonstrated equality of variances among groups. Variables of inhalation-actuation timing and nasal spray position were defined as categorical variables whereas actuation force was defined as continuous. The response for the DOE analysis was defined as the combined middle passage and nasopharynx deposition. The influence of each factor and two factor interactions on the response was analyzed using full factorial ANOVA and significant main effects or any interactions between these effects was recognized by p-value<0.05. The linear regression equation employed was:

$$Y = b_0 + b_1x_1 + b_2x_2 + b_3x_3 + b_4x_1x_2 + b_5x_1x_3 + b_6x_2x_3 \qquad \text{Equation 4.2}$$

where, b0 is the line intercept, and Y is the measured response (combined middle passage and nasopharynx deposition) associated with the factors (x1, x2, and x3) and their interactions (x1x2, x1x3, and x2x3). The *p*-values related to the regression coefficients indicated the significance of each factor on the response.

Student t-test was used to compare the regional drug deposition obtained using VCU nasal models 1 and 2 using identical experimental conditions and significance was assessed using a *p*-value < 0.05 (JMP Pro 12 software). Finally, a linear equation model was built to include the independent variables of nasal model geometry, nasal model head angle, nasal spray position and inhalation-actuation timing to predict the regional nasal drug deposition of Nasonex® nasal spray product. The model was evaluated based on the goodness of fit criteria (Akaike information criterion (AIC), Bayesian information criterion (BIC) and Root Mean Square Error (RMSE)).

4.2.5 Evaluating the developed realistic *in vitro* test method using innovator and generic nasal spray products

To test the utility and reproducibility of the developed realistic test methods for evaluation of regional nasal drug deposition of nasal spray products, the regional nasal drug deposition of formulations designed to be 'generic' copies were compared to their innovator products.

4.2.5.1 Mometasone furoate nasal spray products

Commercially sourced Nasonex® (Merck & Co. Inc., Whitehouse Station, NJ) nasal spray product was identified as the innovator product for mometasone furoate nasal sprays. "In house" mometasone furoate formulations were manufactured by the University of Bath (Bath, UK) to be generic copies of the Nasonex® product and contained 50 µg of mometasone furoate in each metered spray. Two batches of the "in house" mometasone furoate nasal sprays (batch #s

MFM11TF5 and MFM13F2) were characterized and compared to the innovator product, in VCU nasal models 1 and 2 using the previously described methods. The "in house" nasal spray formulations were developed to be qualitatively (Q1) and quantitatively (Q2) equivalent to the innovator product [144]. The batches differed only in the particle size of the drug product included in the formulation. Batch MFM11TF5 had a mean diameter of 1.9 µm and MFM13F2 had a diameter of 1.07 µm, however this change did not affect the spray characteristics of the nasal spray. The container closure system for the "in house" generic was different from Nasonex® and included a bottle and nasal pump (Figure 4.5). The nasal spray pump was an Aptar VP3/93 pump (AptarGroup, Inc., Le Vaudreuil, France) with 404E/A4 internal gasket, 908 EVA neck gasket and 40 mm visible dip tube. This nasal pump was not crimped onto the bottle and employed a screw on mechanism. The bottle was a standard HDPE container which was sourced from Gerresheimer (Chalon-sur-Saône, France) (Figure 4.5).

| (a) | (b) | (c) | (d) |
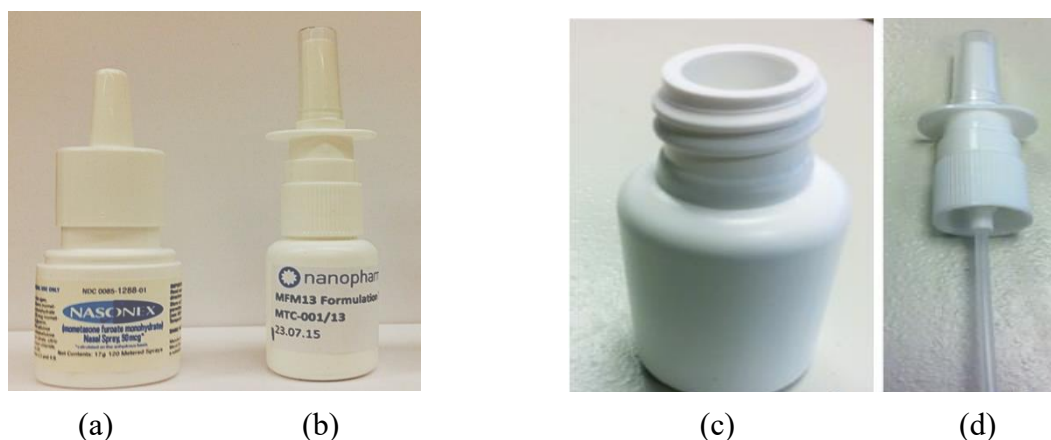
Figure 4.5. Images of (a) Nasonex® nasal spray product (Merck & Co. Inc., Whitehouse Station, NJ) and the "in house" mometasone furoate nasal spray (b) (University of Bath, Bath, UK). Also, shown here container closure system for the "in house" mometasone furoate nasal spray products (c) bottle and (d) pump

4.2.5.2 Fluticasone propionate nasal spray products

Commercially sourced Flonase® (GlaxoSmithKline, Research Triangle Park, NC) nasal spray product was identified as the innovator product for fluticasone propionate nasal sprays. A previously FDA approved and commercially available generic fluticasone propionate (Roxane Laboratory, Columbus, OH) was obtained as the generic comparator (Figure 4.6). Based on FDA guidance for the development of the generic fluticasone propionate nasal sprays, the generic formulation should have both qualitatively quantitatively within ± 5% similar ingredients compared to the innovator product [56]. The device should deliver the same number of doses as the reference listed product, and should be similar in shape, size, and external operating principles. In addition patients should not need to retrain or take more steps to use the generic product compared to the innovator product [144].

(a)   (b)
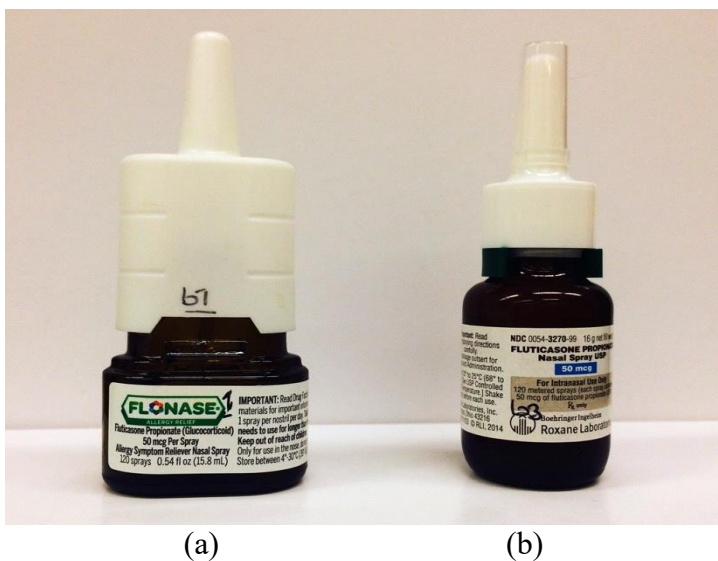
Figure 4.6. Images of (a) Flonase® nasal spray product (GlaxoSmithKline, Research Triangle Park, NC) and (b) the generic fluticasone propionate nasal spray (Roxane Laboratory, Columbus, OH)

4.2.5.3 *In vitro* realistic deposition test conditions

The experimental conditions for the *in vitro* regional drug deposition tests using the two airway models were designed to reflect the possible *in vivo* variability that can be associated with patient use factors. The design of experiment approach described previously revealed the influence of patient use factors when implemented *in vitro* on nasal deposition within the middle passage region. An attempt was made to select a manageable series of *in vitro* experiments that reflect the potential inter-subject and patient use factors that could affect the deposition of the test nasal spray products. The approach sought to identify *in vitro* test conditions from the DOE experiments that produce low, intermediate and high drug deposition in combined middle passage and nasopharynx regions in each of the two airway models as shown in Table 4.2.

For Flonase® nasal spray, an "in use" measurement of actuation force was obtained from the literature [121] and therefore only one actuation force of 5.8 kg was employed in those studies. The remaining test conditions for "low", "medium" and "high" deposition experiments were based upon the Nasonex® DOE experimental conditions. The previously described HPLC quantitative analysis method for mometasone furoate (Sections 3.1.3 and 3.2.1) was also used for fluticasone propionate and validated to ensure drug mass balance and recovery from the nasal models in the *in vitro* experiments.

For each of the test nasal spray products, the droplet size distribution was characterized using the method described in Section 4.2.7.1.

4.2.5.4 Statistical analysis for innovator and generic comparison

Student t-test was used to compare the regional drug deposition of the "in house" mometasone furoate nasal spray with Nasonex® nasal spray product and the generic fluticasone propionate with Flonase® nasal spray product across the range of experimental conditions in the two nasal models (JMP Pro 12 software; *p*-value < 0.05).

Table 4.2. Experimental conditions for testing of innovator and generic nasal spray products using VCU nasal models 1 and 2

Expected combined middle passage and nasopharynx regions drug deposition	Actuation force (kg)[3]	Nasal spray position (mm)[1]	Head angle	Inhalation and actuation timing[2]
VCU Model 1				
Level 1 - Low (~ 20 %)	7.5	9	50°	E
Level 2 - Intermediate (~ 40 %)	7.5	5	30°	D
Level 3 - High (~ 60 %)	7.5	5	50°	D
VCU Model 2				
Level 1 - Low (~ 50 %)	7.5	5	30°	E
Level 2 - Intermediate (~60 %)	4.5	5	30°	D
Level 3 - High (~77 %)	4.5	5	50°	D

[1]Distance between nasal spray applicator and the tip of the nose
[2]E: inhalation followed by actuation, D: actuation during inhalation
[3]Fluticasone propionate products were tested using only an actuation force of 5.8 kg

4.2.6 Evaluating the developed realistic *in vitro* test method using nasal spray products with varying spray plume properties

A series of nasal spray products with differing *in vitro* spray properties were tested to assess their regional drug deposition in VCU nasal model 1. Four products were considered, two custom-made mometasone furoate nasal sprays (Batches No: A and B), and two commercial Nasonex® nasal sprays with expiration dates of Feb 2007 (expired) and Oct 2015 (in-date), respectively.

The regional nasal drug deposition of the custom-made mometasone furoate nasal sprays and Nasonex® nasal sprays were tested using the VCU nasal model 1. The experimental conditions used to test the *in vitro* nasal sprays are nasal spray position of 9 mm from front of the nostril, head angle of 30° forward from horizontal, and nasal spray actuation during nasal inhalation (D). The regional drug deposition tests were performed at two actuation forces of 4.5 and 7.5 kg. The *in vitro* spray plume properties of these products was also characterized by examining the droplet size distribution and spray pattern and plume geometry tests (as described in Section 4.2.7) based on FDA recommended *in vitro* tests for establishing BE for nasal spray products [131].

4.2.7 *In vitro* nasal spray characterization methods

4.2.7.1 Droplet size distribution measurements (DSD)

Droplet size distribution (DSD) measurement for nasal spray products was conducted by laser diffraction technique using a Malvern Spraytec (Malvern Instruments Ltd, Worcestershire, UK) equipped with 100 mm focal lens. The spray nozzle was positioned below the laser beam, aligned vertically at the specified distance (2 cm mostly based on FDA guidance below the center of laser sensing zone [144]. The distance between nasal spray and detector was 9 cm. Data collection was initiated when the percent laser light transmittance falls below 99.0% and acquisition continued for 2000 ms. Data analysis of the droplet size distribution was performed on the average of all scans collected in the fully developed phase of the nasal spray, that is indicated by the entire plateau region for the transmittance plot. The data were reported as volume diameters at the 10th, 50th and 90th percentile as Dv10, Dv50, and Dv90, respectively, together with the span which is defined as below:

$$\text{Span} = \frac{(Dv90 - Dv10)}{Dv50} \qquad\qquad \text{Equation 4.3}$$

4.2.7.2 Spray pattern measurement

Spray pattern tests were performed from the analysis of a two-dimensional image of the emitted plume using a SprayVIEW™ NSP system (Proveris Scientific Corporation, Sudbury, MA). This system includes a laser light sheet, high-speed digital camera, and SprayVIEW™ NSx automated actuation force system. For spray pattern measurements, the distance of nasal spray nozzle to the laser beam was 30 mm. The laser light illuminates the spray horizontally and images are taken from the above. The automated actuator is a velocity control actuator and actuation parameters for the nasal sprays were defined as velocity 70 (mm/sec), acceleration of 5000 (mm/s²), initial and final delay of 200 (ms) and hold time of 300 (ms) generating an actuation force of 7.5 kg. Stroke length (displacement of the nasal spray pump (mm)) for each nasal spray bottle was automatically characterized. The SprayVIEW™ NSP software determines the outlines of the spray pattern and reports Dmax, Dmin, ovality, and area for spray pattern measurements. Dmax and Dmin are defined as the longest and shortest diameter that can be measured for the spray pattern image and the ratio of the two diameters is used to calculate the ovality ratio. The area is also calculated after defining the perimeter of the resulted spray pattern image.

4.2.7.3 Plume geometry measurement

Plume geometry measurements were also carried out using SprayVIEW™ NSP system (Proveris Scientific Corporation, Sudbury, MA). For plume geometry measurements, the laser sheet was positioned vertically, and the spray plume was imaged from the right side, directly above the device tip. Plume geometry measurement was performed at distance of 30 mm from spray orifice. Similar actuation settings as spray pattern test were employed for the nasal spray actuator. By monitoring the intensity profile during the spray life, a single frame from the fully developed

phase with the highest intensity was selected and the spray angle defined as the angle of the emitted plume measured from the vertex of the spray cone and spray nozzle and plume width as the width of the plume at a given distance from the spray nozzle.

4.2.8   Statistical analysis for spray plume characterization tests

Data for DSD, spray pattern test and plume geometry test results are expressed as mean (SD) and subjected to statistical analysis of variance (ANOVA) followed by Tukey's HSD test using JMP software version 12.0. The analyses were done at 95% confidence limits for two-tailed tests. Probability values of <0.05 were considered statistically significant.

4.3   Results and Discussion

4.3.1   Assessing the effects of patient use variables on the regional drug deposition of Nasonex® in VCU nasal model 2 using a full factorial design of experiment

Table 4.3 shows the drug deposition results of the 2- level, 3- factor full factorial design of experiment for the Nasonex® nasal spray tested in VCU nasal model 2. Total drug recovery along with the drug deposition on the nasal spray device (NSP), anterior +drip (AD), combined middle passages and nasopharynx area (MP) and filter (F) are reported. As demonstrated in Table 4.3, mean (SD) drug recovery from VCU nasal model 2 and nasal spray device ranged from 90.9 (2.4) % to 94.3 (7.5) % of the label claim. Drug deposition on the nasal spray device was less than 1.9 % of the recovered dose and no formulation was observed to reach the respiratory filter at the end of the throat. Changing patient use related variables in 8 different combinations of actuation force, head angle and inhalation - actuation timing relative to actuation for Nasonex® nasal spray product in VCU nasal model 2 resulted in mean (SD) anterior passage + drip deposition that varied from

21.5 (9.0) % to 53.3 (10.2) % and mean (SD) combined middle passage and nasopharynx region ranged 46.6 (10.0) % to 77.4 (8.5) %.

A linear model including three variables and the two-way interactions was constructed and analysis of variance (ANOVA) performed to evaluate the model significance. The model was statistically significant as shown by p-value <0.004 in Table 4.4. The summary of the ANOVA analysis is presented in Table 4.4. As demonstrated in Figure 4.7 and Table 4.5 the developed model did not predict a strong correlation between predicted and observed data shown by the R^2 of 0.3861 and adjusted R^2 of 0.2387 meaning that there are other factors controlling the regional drug deposition in VCU nasal model 2 that are not considered in the predicted model.

Table 4.6 illustrated the estimates (the values of the regression coefficients), t-ratio and their significance for the constructed model. Using VCU nasal model 2, patient related parameters of inhalation timing and angle had significant effects on middle passage drug delivery of Nasonex® (p-value = 0.0150 and 0.0215, respectively). A positive value of estimate (4.86) for inhalation timing (D), indicated that this effect helps to enhance middle passage drug delivery; conversely, a negative sign value for inhalation (E) represents an inverse relationship between the response and the factor. This is also evident by comparing the data in Table 4.3 for all the study sets that differ only with respect to the inhalation – actuation timing condition. Experiments with coordination between actuation and inhalation (D) had higher middle passage drug delivery and lower anterior nose deposition compared to the studies in which there was a delay between actuating the nasal spray and then commencing inhalation (E). In VCU nasal model 2, tilting the model to the head angle of 50° while nasal spray is actuated during nasal inhalation, using actuation force of 4.5 kg or 7.5 kg, resulted in drug delivery to the middle passages that ranged from 72.2 % - 77.4 % of the recovered dose. However, nasal inhalation after nasal spray actuation at the head angle of 30° and

actuation force of 7.5 kg resulted in the lowest middle passage drug deposition of 46.6 % which demonstrates the significant effects of the head angle and inhalation timing. These results were similar to the trends observed with the deposition studies using VCU model 1 (Chapter 3). As we observed previously, actuation of nasal spray during nasal inhalation did increase middle passage drug delivery as the larger fraction of the droplets were entrained in the airflow, perhaps traveling deeper into the posterior region through the nasal valve from the initial release point in the nostril. However, we did not see any significant interaction between the two variables of inhalation timing and head angle as previously observed for VCU nasal model 1.

In addition, the extent of deposition variability that was observed due to the patient variables differed between the two models. Middle passage drug deposition in VCU nasal model 2 varied by 1.7-fold with respect to the tested patient use parameters (46.6 % – 77.4 %). However, varying the corresponding patient use parameters produced a 3.4-fold change in middle passage drug delivery using VCU nasal model 1 (16.6 % - 57.1 %). This suggested that the regional nasal drug deposition in VCU nasal model 2 was influenced more by the nasal airway geometry than by the employed patient use variables.

Table 4.3. Mean (SD) *in vitro* regional nasal deposition of mometasone furoate (expressed as a percentage of recovered dose) and total recovery (expressed as percentage of the label claim) for the Nasonex® nasal spray following actuation of 2 sprays into the right nostril of VCU nasal model 2 for the full factorial design of experiments (n=4)

Actuation Force (kg) (x1)	Head Angle (x2)	Timing (x3)	NSP	AD	MP	F	Recovery (%)
4.5	30	D	0.2 (0.2)	38.2 (9.4)	61.6 (9.6)	0.0 (0.0)	91.3 (5.6)
7.5	30	E	0.1 (0.1)	53.3 (10.2)	46.6 (10.0)	0.0 (0.0)	92.5 (11.2)
7.5	30	D	0.3 (0.6)	31.8 (3.8)	68.0 (4.2)	0.0 (0.0)	93.1 (6.3)
4.5	50	E	1.9 (2.8)	44.7 (8.2)	53.4 (9.4)	0.0 (0.0)	92.3 (5.1)
7.5	50	D	0.9 (1.4)	26.9 (4.6)	72.2 (4.7)	0.0 (0.0)	90.9 (2.4)
4.5	30	E	1.1 (1.1)	33.9 (10.4)	65.0 (9.5)	0.0 (0.0)	93.1 (10.1)
4.5	50	D	1.1 (1.1)	21.5 (9.0)	77.4 (8.5)	0.0 (0.0)	94.3 (7.5)
7.5	50	E	0.2 (0.5)	25.9 (8.7)	73.9 (8.5)	0.0 (0.0)	93.1 (9.8)

Timing; D: Nasal spray actuation during nasal inhalation, E: Nasal spray actuation followed by nasal inhalation
NSP: Nasal spray, AD: Anterior + drip, MP: Combined middle passage and nasopharynx region, F: Filter

Table 4.4. Summary of ANOVA analysis for full factorial design of experiment including actuation force, head angle and inhalation timing in VCU nasal model 2

	DF	Sum of Square	Mean Square	F Ratio	Prob> F
Model	6	1802.9	300.5	2.6	<0.0400
Error	26	2976.7	114.5		

DF: degree of freedom
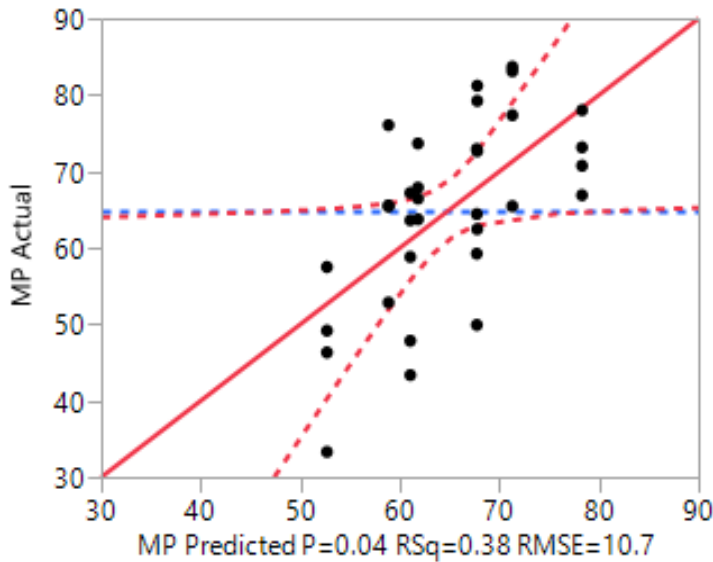
Figure 4.7. Plot of actual (observed) value versus predicted values of Nasonex® middle passage deposition in VCU model 2. The horizontal broken line shows the mean velocity, the solid line is the line of fit, and the two broken curve lines describe the 95 % confident region relative to the line of fit.

Table 4.5. Summary of fit for regional nasal drug deposition of Nasonex® in VCU nasal model 2 including three variables of actuation force, head angle, and timing

	R^2	R^2 Adj	Root Mean Square Error (RMSE)	Mean of Response	Observations
Model	0.3861	0.2387	10.83	64.75	32

R^2 Adj: Adjusted R

Table 4.6. Estimates of coefficients for the model predicting the combined middle passage and nasopharynx drug deposition of Nasonex® nasal spray product in VCU nasal model 2 along with the significance of each variable and two variables interaction

Term	Estimate	t Ratio	Prob>|t|
Intercept	45.46	4.18	0.0003*
Inhalation Timing (D)	4.86	2.60	0.0150*
Inhalation Timing (E)	-4.86	-2.60	0.0150*
(Force-6.0) * (Angle-40)	0.22	1.73	0.0955
Angle	0.46	2.45	0.0215*
Force	0.20	0.16	0.8718
(Force-6.0) * Inhalation Timing (D)	0.05	0.04	0.9708
(Force-6.0) * Inhalation Timing (E)	-0.05	-0.04	0.9708
(Angle-40) * Inhalation Timing (D)	0.03	0.18	0.8556
(Angle-40) * Inhalation Timing (E)	-0.03	-0.18	0.8556

* $P<0.05$, significant effect

Timing; D: Nasal spray actuation during nasal inhalation, E: Nasal spray actuation followed by nasal inhalation

4.3.2   Evaluating the developed realistic *in vitro* test method using nasal spray products with varying spray plume properties

The results for Nasonex® drug deposition in the two nasal geometries were compared and shown in Table 4.7. These studies compare experiments performed using identical experimental conditions with a nasal spray position of 5 mm from the nasal tip. Comparing the anterior nose deposition in VCU nasal model 1 and 2, in general, there was higher drug deposition observed in VCU nasal model 1. The extent of drug deposition in the anterior nose + drip for VCU nasal model 1 was 1.3-fold to 2.7-fold higher compared to what was observed in the VCU nasal model 2, depending on the experimental conditions. This resulted in consistently lower middle passage delivery to VCU nasal model 1 (1.3-fold to 2.6-fold) compared to VCU nasal model 2. The most pronounced difference (2.7-fold increase) in the anterior nose deposition was observed when the nasal model tilted 50º forward with a delay in nasal inhalation timing with respect to nasal spray actuation (E). Differences in the geometry of nasal valve region between the two models may play a significant role as VCU nasal model 2 has a wider nasal valve region compared to VCU nasal model 1. Therefore, a larger fraction of the exiting plume can penetrate through the nasal valve region regardless of head angle, nasal spray position and inhalation time.

In summary, it has been observed that patient use variables have less impact on the regional nasal drug deposition pattern in the VCU nasal model 2. Differences in the regional deposition between the two airway geometries indicated the potential effects of inter-subject nasal geometry variability on the regional drug deposition of Nasonex® nasal spray product. Significantly higher drug formulation was able to penetrate into the middle passages of VCU model 2 under almost all test conditions compared to VCU model 1 (Table 4.7). Differences in the geometry of nasal valve region between the two models may play a significant role as VCU nasal model 2 has a wider nasal

valve region compared to VCU nasal model 1. These differences may even occur in the left and right side of the nasal cavity of a subject. Previous studies using CFD simulations have shown changes in the drug deposition pattern for 22 μm particles in the right and the left sides of a realistic nasal cavity geometry and concluded that geometry is an important parameter for deposition of the micron size particles [30]. Similar results may be found for regional nasal drug deposition of nasal sprays when tested in different sides of the nasal cavity.

Table 4.7. Mean (SD) *in vitro* regional drug deposition (standard deviation (SD)) (expressed as a percentage of recovered dose) of Nasonex® nasal spray product in VCU models 1 and 2. Results are ranked based on increasing deposition for Nasonex® in the VCU nasal model 1 (n=4)

Actuation force (kg)	Head angle (°)	Timing	VCU model 1	VCU model 2	*p*-value	change
			Anterior + drip deposition			
7.5	50	D	42.3 (8.9)	26.9 (4.6)	0.0318*	1.6-fold
4.5	50	D	48.8 (7.3)	21.5 (9.4)	0.0037*	2.3-fold
4.5	30	D	58.1 (3.3)	38.2 (9.4)	0.0187*	1.5-fold
7.5	30	D	63.5 (5.5)	31.8 (3.8)	0.0002*	2.0-fold
4.5	30	E	68.2 (8.5)	33.9 (10.4)	0.0022*	2.0-fold
7.5	50	E	68.9 (4.5)	25.9 (8.7)	0.0005*	2.7-fold
7.5	30	E	70.2 (10.8)	53.3 (10.2)	Not significant	1.3-fold
4.5	50	E	76.3 (3.5)	44.7 (8.2)	0.0020*	1.7-fold
			Combined middle passage and nasopharynx deposition			
4.5	50	E	20.5 (4.4)	53.4 (9.4)	0.0025*	2.6-fold
7.5	50	E	29.2 (3.4)	73.9 (8.5)	0.0007*	2.5-fold
7.5	30	E	29.7 (10.6)	46.6 (10.1)	Not significant	1.6-fold
4.5	30	E	29.9 (7.5)	65.0 (9.5)	0.0014*	2.2-fold
7.5	30	D	34.1 (3.1)	68.0 (4.2)	<0.001*	2.0-fold
4.5	30	D	40.9 (2.8)	61.6 (9.6)	0.0188*	1.5-fold
4.5	50	D	49.1 (6.6)	77.4 (8.5)	0.0022*	1.6-fold
7.5	50	D	57.1 (9.5)	72.2 (4.7)	0.0411*	1.3-fold

Timing; D: actuation during inhalation, E - inhalation followed by actuation
* P<0.05 (Student t-test)

4.3.2.1 Combined geometry and patient variable statistical analysis

It was also of interest to develop a mathematical model to predict the *in vitro* middle passage drug deposition using the data generated for Nasonex® in VCU nasal models 1 and 2 combined with the different patient use variables. The continuous predictors considered were actuation force (4.5 kg and 7.5 kg), head angle (30º and 50º) and VCU nasal model geometry (1 with SA/V ratio of 0.75 mm^{-1} and 2 with SA/V ratio of 1.33 mm^{-1}), and nasal spray position (9 mm and 5 mm), and timing (D and E) were defined as categorical variables. Using JMP software, a multiple regression approach was used to identify the significant predictors and the most informative subset among all the combinations that could be used to estimate the middle passage drug deposition. All the possible combinations were considered starting with addition of one parameter at a time to the model and assessing the correlation coefficient and goodness of fit criteria between the built models. The goodness of fit criteria included the Akaike information criterion (AIC), Bayesian information criterion (BIC) and Root Mean Square Error (RMSE) and can be found in the multiple regression results (Table 4.9). Both BIC and AIC attempt to resolve this problem by introducing a penalty term for the number of parameters in the model; the penalty term is larger in BIC than in AIC. RMSE is a measure of the difference between the predicted values (sample and population) by the model and the observed data. The model with the lowest AIC, BIC and RMSE is preferred. However, the predictors first assessed if there is any co-linearity between them. If the predictors that are correlated are used in a model, the overall regression model and the effect of individual predictors are influenced. The performed multivariate analysis from JMP is presented in Table 4.8.. The highest correlation coefficient was found between combined middle passage and nasopharynx drug deposition and VCU nasal model geometry, meaning that this variable is the most impactful variable. Table 4.9 represents the goodness of fit criteria for the

models built in this study. The numbers of variables are added one at the time and the results are only presented for the models showing the best goodness of fit among its subset. As shown, when including only the VCU nasal model as a predictor, the model is able to explain 55 % ($R^2 = 0.5513$) of the variability around the predicted mean middle passage drug deposition. Adding the timing variable to the model, the R^2 and predictability of the model increased to 0.7294. However, adding the variables of angle and position further increased R^2 to 0.7673 (shown in Table 4.9 and Figure 4.8). Using this model with R^2 of 0.7673, almost 77% variability around the mean response data can be explained. In this case, each of the goodness of fit criteria (RMSE, AIC, and BIC) showed the lowest values. Including the two variables interaction between the predictor did not increase the model predictability. The ANOVA summary of the model is shown in Table 4.10. All the variables included in the model showed significant effect on combined middle passage and nasopharynx deposition for Nasonex[®] (Table 4.9, $p < 0.05$). Based on the estimate of coefficients for the final model presented in Table 4.11, nasal airway geometry with the absolute largest coefficient was the most influential factor in determining the extent of drug delivery to the middle passages for the Nasonex[®] nasal spray product. The second important factor was the coordination of nasal inhalation and spray actuation as it was consistently observed previously in the results of deposition assessments using the individual models 1 and 2.

Table 4.8. Correlations of predictors with response (middle passage drug deposition) and between predictors of force, angle, VCU nasal model, timing and nasal spray position

	Response	Angle	VCU nasal model	Timing	Position	Force
VCU nasal model	0.7425	-0.0000	1.0000	-0.0000	-0.4980	-0.0000
Position	0.4658	-0.0000	-0.4980	-0.0000	1.0000	-0.0000
Timing	0.4312	-0.0000	-0.0000	1.0000	-0.0000	-0.0000
Angle	0.1345	1.0000	-0.0000	-0.0000	-0.0000	-0.0000
Force	0.0402	-0.0000	-0.0000	-0.0000	-0.0000	1.0000

Table 4.9. Goodness of fit criteria for models built to predict the regional nasal drug deposition for Nasonex® nasal spray product using patient use parameters of timing, nasal spray position, actuation force and head angle together with the VCU nasal model predictor. The variables are added one at the time and the results are only presented for the models showing the best goodness of fit among its subset

Model	Number	R^2	RMSE	AIC	BIC
VCU nasal model	1	0.5513	13.2	771	780
VCU nasal model, Timing	2	0.7372	10.1	722	732
VCU nasal model, Timing, Angle	3	0.7553	9.8	717	729
VCU nasal model, Timing, Angle, Position	**4**	**0.7673**	**9.7**	**715**	**729**
VCU nasal model, Timing, Angle, Position, Actuation force	5	0.7689	9.7	716	733
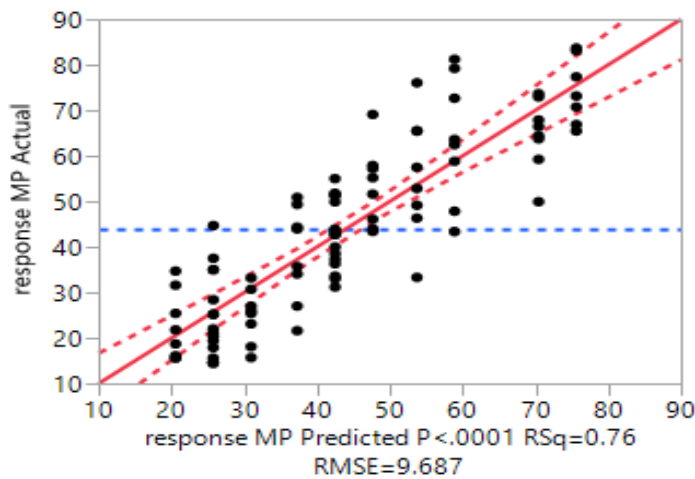
Figure 4.8. Plot of actual (observed) value versus predicted values of middle passage deposition for the model built using four predictors of VCU nasal model geometry, timing, angle and nasal spray position. The horizontal broken line shows the mean velocity, the solid line is the line of fit, and the two broken curve lines describe the 95% confident region relative to the line of fit.

Table 4.10. Analysis of Variance (ANOVA) results for the model including four variables of VCU nasal model geometry, inhalation timing, angle and position to predict middle passage drug deposition of the Nasonex® nasal spray product

Source	DF	Sum of Squares	Mean Square	F Ratio	Prob > F
Model	4	27858.7	6964.7	75.0	<.0001*
Error	91	8450.8	92.9		
C. Total	95	36309.4			

DF: degree of freedom
* P<0.05

Table 4.11. Estimates of coefficients and the significance of each variables for the model including four variables of VCU nasal model geometry, inhalation timing, angle and position to predict middle passage drug deposition of the Nasonex® nasal spray product

Term	Estimate	Standard Error	t Ratio	Prob>|t|
Intercept	-12.6	5.5	-0.45	<.0001*
VCU nasal model	48.3	1.2	11.6	<.0001*
Timing[D]	8.4	1.0	8.5	<.0001*
Timing[E]	-8.4	1.0	-8.5	<.0001*
Position	-2.6	1.2	-2.15	0.0344*
Angle	0.3	0.1	2.7	0.0093*

* P<0.05

In the developed model, based on the estimated coefficient presented in Table 4.11, all the variables have significant effects on middle passage drug deposition with the VCU nasal model geometry having the largest effect followed by inhalation timing.

The prediction expression for middle passage drug deposition (Y) is shown below:

Y = - 12.5 + (48.3 * VCU nasal model) + (0.3 * angle) + (Match inhalation,

if D then 8.3, or E then -8.6) – (Match position,

if 5 mm then 2.6, or 9 mm then – 2.6)   Equation 4.4

Based on the above equation, having a geometry similar to the VCU nasal model 2 with coordination of nasal inhalation and spray actuation, nasal spray positioning closer to the tip of the nostril and higher head angle of 50º forward from horizontal results in higher drug delivery to the middle passages for the Nasonex® nasal spray product.

The model assumptions of normality of residuals and homogeneity of variances for the ANOVA test were also tested and presented in Figures 4.9, 4.10 and 4.11 as well as Table 4.12. Looking at the normal quantile plot presented in Figure 4.9, it appears that the data are normally distributed. For the residual plot, graphically shown in Figures 4.10 and 4.11, equal amount of spread above and below the line is observed with no sign of heteroscedasticity. Tabulated in Table 4.12, the Brown-Forsythe test was used to check the equality of variances with a *p*-value of less than 0.05 indicating statistical significance. Table 4.12. shows that a *p*-value of 0.4758 and confirms the equality of variances among the groups that were studied.

In summary, using realistic *in vitro* developed method, it seems the geometry of the nasal cavity and patient use parameters such as head angle and nasal spray position in the nostril are

influential in the delivery efficiency of the Nasonex® nasal spray product and the developed

mathematical model can predict the range of variability for the drug delivery beyond the nasal

valve region. The actuation force for the nasal spray in the tested range for this nasal spray did not

result in change in drug delivery due to the presence of the nasal value and large droplet size of

the spray plume. It seems the positioning of the nasal spray with respect to the nasal valve and the

nasal valve geometry determine the extent of the penetration for the exiting plume into the

posterior region of the nasal cavity. This can be effected by patient use technique including head

angle and nasal spray position in the nostril. These results show the utility of the nasal airway

models in the development and screening of the nasal spray products.
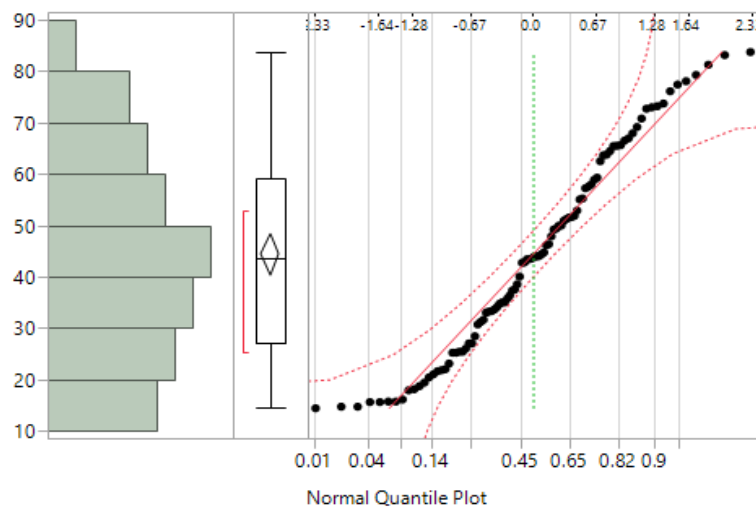
Figure 4.9. Normal quantile plot used to assess the normality of the data for the linear model
built using the predictors of VCU nasal model geometry, timing, angle and nasal spray position
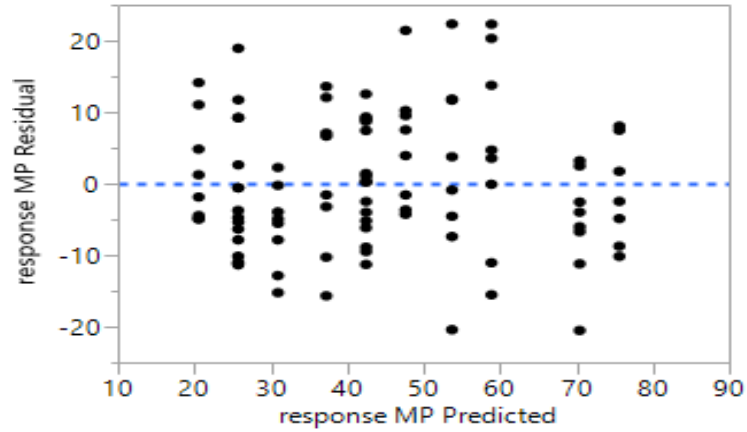
Figure 4.10. Plot of residual used to assess the normality of the residual for the linear model built using the predictors of VCU nasal model geometry, timing, angle and nasal spray position
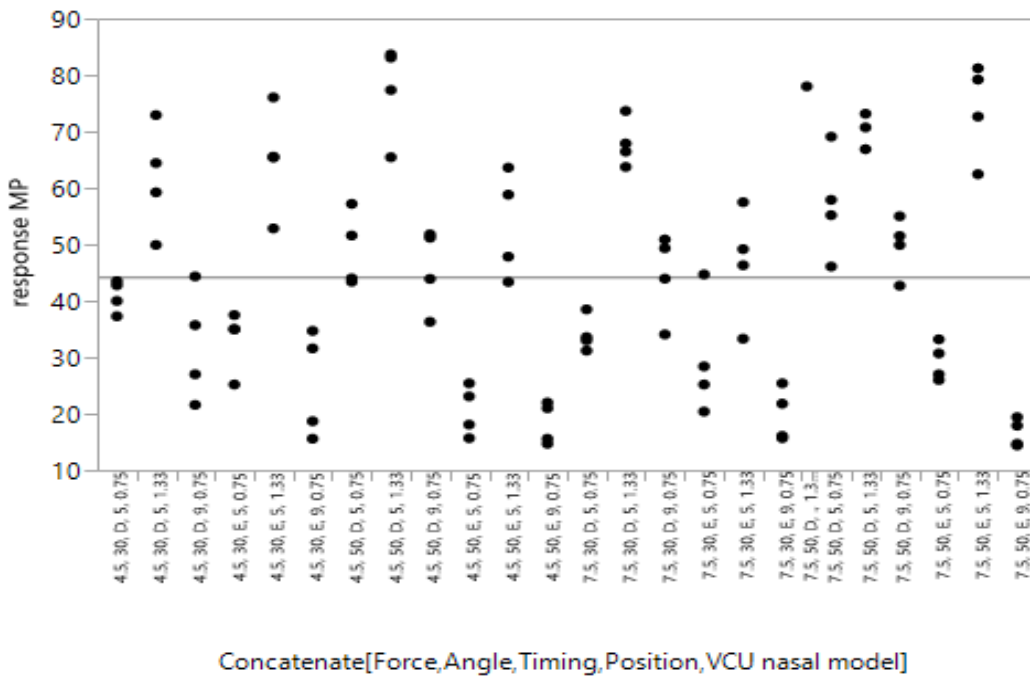
Figure 4.11. Plot of standard deviation for each of the group constructed using the variables of actuation force, head angle, timing and VCU nasal model geometry

Table 4.12. Results of statistical analysis for testing equality of variances among groups

Test	F Ratio	DFNum[1]	DFDen[2]	Prob > F
Brown-Forsythe	1.0009	23	71	0.4758

[1]Degrees of freedom in the numerator
[2]Degrees of freedom in the denominator

4.3.3 Evaluating the developed realistic *in vitro* test method using innovator and generic nasal spray products

To assess the utility of the developed *in vitro* test method for characterizing regional nasal drug deposition of nasal spray products, innovator and generic nasal spray products were characterized and compared. Two innovator products, Flonase® and Nasonex® were tested alongside their respective generic or "in house" nasal spray products, respectively. Specifically, the capability and reproducibility of the developed *in vitro* deposition test method in characterizing equivalent formulations and products was assessed. Generic nasal spray products are formulated to have an equivalent *in vitro* and *in vivo* performance compared to the innovator product. Therefore, it was expected that using this new *in vitro* realistic test method, the regional nasal drug deposition for the generic nasal spray will not be statistically different from the innovator product when tested under identical conditions in VCU nasal models 1 and 2. Based on previous studies performed for the Nasonex® nasal spray product, test conditions for VCU nasal model 1 and 2 were selected by varying patient use parameters to produce low, intermediate and high combined middle passage and nasopharynx drug deposition (Table 4.2). For VCU model 2, only one nasal spray position was identified for testing due to its smaller nostril hydraulic diameter.

4.3.3.1   Mometasone furoate nasal spray products

Conventionally, to develop generic solution or suspension nasal spray products, the establishment of the equivalent *in vitro* performance between test and innovator is one of the requirements. The droplet size distribution (DSD) measurement is one of the *in vitro* spray plume characteristic tests that needs to be conducted. Similarity in DSD between products is evaluated using the population bioequivalence approach.

The DSD for Nasonex® and the mometasone furoate "in house" formulations used in this study was determined using two actuation forces of 4.5 kg and 7.5 kg. The results are shown in Figure 4.12. At an actuation force of 4.5 kg and a distance of 2 cm between the nasal spray orifice and the laser sensing zone, the mean (SD) of Dv10 for Nasonex® and "in house" formulation batch #s of MFM11TF5 and MFM13F2 were measured as 19.4 (0.4) µm, 17.9 (0.3) µm and 17.2 (0.4) µm, respectively. The Dv10 was significantly different for the two "in house" mometasone furoate formulations compared to the Nasonex® nasal spray product (*p*-value = 0.008 <0.0001, respectively) and there was also a significant difference observed in Dv10 between the two "in house" formulations (*p*-value = 0.0261).

For Dv50, the mean (SD) measured values were 57.2 (1.4) µm, 54.0 (1.3) µm and 49.0 (1.3) µm for the Nasonex® and "in house" formulation batch #s of MFM11TF5 and MFM13F2, respectively. Similar to the Dv10, the mean Dv50 was smaller for the two "in house" formulations compared to Nasonex® (*p*-value = 0.0018 and <0.0001, respectively) and they were significantly different from each other (*p*-value = 0.0290). Similar observations made for Dv90 with corresponding mean (SD) values for the nasal spray products of 126.7 (4.0) µm, 96.4 (1.9) µm and

90.7 (1.3) μm, respectively ($p < 0.0001$, < 0.0001 and 0.0116, respectively). The mean (SD) span for these products were 1.9 (0.1), 1.5 (0.1) and 1.5 (0.1), respectively.

The two "in house" generic formulations were developed to have identical spray characteristics with only the drug particle size differing, however there did appear to be some statistically significant differences in the droplet size distributions both between the "in house" generic formulations and with the Nasonex® product. This demonstrates the difficultly generic manufacturers currently encounter when attempting to produce statistically equivalent formulations with respect to their *in vitro* droplet / spray characteristics. The experimental significance of these small, but statistically significant droplet size differences were evaluated using the realistic *in vitro* deposition test method.

Increasing the actuation force from 4.5 kg to 7.5 kg resulted in a reduction in the DSD for all three nasal sprays, with the more pronounced effect being on the Dv50 and Dv90 parameters. For Nasonex® the mean (SD) Dv50 and 90 were reduced from 57.2 (1.4) μm to 47.0 (1.0) μm and 126.7 (4.0) μm to 109.8 (1.7) μm, respectively. For the "in house" generic formulation (MFM11TF5) at 7.5 kg it showed a similar mean (SD) Dv50 of 47.2 (1.7) μm but smaller Dv90 of 91.2(1.7) μm ($p < 0.001$) compared to Nasonex®. The other "in house" formulation (MFM13F2) tested at 7.5 kg was observed to have even smaller mean (SD) values for Dv50 and Dv90 of 36.7 (0.5) μm and 80.3 (1.5) μm ($p < 0.001$, < 0.001, respectively, compared to Nasonex®).

The results for comparison of *in vitro* regional nasal drug deposition of Nasonex® nasal spray and the "in house" generic mometasone formulations are shown in Tables 4.13 and 4.14 in VCU nasal models 1 and 2, respectively. In these studies, the recovery of the "in house" mometasone furoate formulation from VCU nasal models 1 and 2 was in the acceptable range of

86.5 (3.5) % to 102 (11.9) % with no difference in the drug recovery between the two "in house" formulations.

As shown in Table 4.13, the mean (SD) % drug delivery to the middle passages of VCU nasal model 1 for the two "in house" generic mometasone furoate formulations varied from 20.2 (3.2) % to 59.1 (6.8) % for batch # MFM11TF5 and 19.5 (2.2) % to 47.9 (8.7) % for batch # MFM13F2 which was similar to the results obtained for the Nasonex® nasal spray product (16.6 (2.4) % to 57.1 (9.4) %). Comparing the regional drug deposition for the two "in house" mometasone furoate nasal formulations and the innovator product, there was no significant differences in drug deposited in the anterior nose region and combined middle passage and nasopharynx regions, when they were compared at three levels of low, intermediate and high middle passage drug delivery in the VCU nasal model 1.

Similarly, using VCU nasal model 2, the *in vitro* regional nasal drug deposition of "in house" generic mometasone furoate formulation (batch #MFM11TF5) was compared with Nasonex® nasal spray product in Table 4.14 (insufficient product was available to test batch # MFM13F2). The mean (SD) middle passage drug deposition for the "in house" mometasone furoate formulation varied from 49.6 (10.7) % to 70.9 (6.5) % with the change in the experimental conditions which was comparable with the observations for Nasonex® of 46.6 (10.0) % to 77.4 (8.5) %. It was concluded that there were no statistical differences in *in vitro* regional drug deposition for the "in house" mometasone furoate formulation of MFM11TF5 and Nasonex® measured in VCU nasal model 2 and across the three different experimental conditions.

With respect to the comparison between the conventional spray characterization methods and the realistic deposition method for comparing nasal spray products, it appears that marginal

but statistically significant differences in DSD were not important with respect to the regional deposition profile in the *in vitro* nasal airway models. Similar results were observed by Suman et al. [52]. They compared the regional nasal deposition, rate and extent of absorption for nicotine administered to 9 healthy subjects by two nasal spray pumps producing statistically different droplet size (Dv50 of 37.3 vs 48.2 μm measured at distance of 2.5 cm) and spray plume characteristic. However, they reported these *in vitro* differences did not alter the site of drug deposition or the rate and extent of nicotine absorption. The *in vitro* characterization tests for nasal sprays products such as DSD and spray plume characterizations are appropriate as quality control tests but a more realistic and clinically relevant test may be necessary if an assessment of clinical equivalence is to be made for comparison generic and innovator suspension nasal spray products using *in vitro* testing.
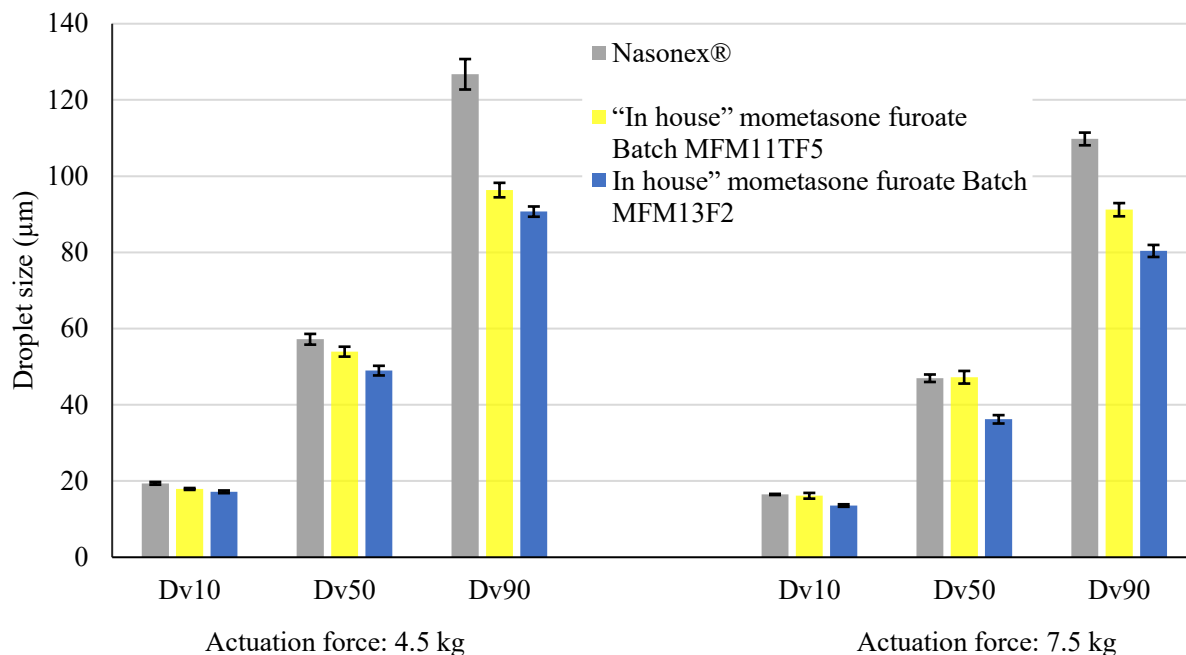
Figure 4.12. Mean (error bars are SD) droplet size distribution results for a single actuation of the Nasonex® and "in house" mometasone furoate nasal spray products at actuation force of and 7.5 kg and 4.5 kg at 2 cm distance between the tip of the nasal spray and laser sensing zone. These measurements performed in the beginning of the nasal spray life. Data represent mean (SD) (n = 4)

Table 4.13. Mean (SD*) in vitro* regional nasal drug deposition (expressed as a percentage of recovered dose) and total recovery (expressed as percentage of the label claim) for the "in house" generic mometasone furoate (batches #MFM11TF5 and MFM13F2) and Nasonex® nasal spray products in VCU nasal model 1 at three different experimental conditions (n=4).

Expected combined middle passage and nasopharynx deposition	NSP	AD	MP	F	Total recovery (%)
"In house" mometasone furoate #MFM11TF5					
Level 1 - Low (~ 20 %)	1.5 (1.7)	78.3 (12.6)	20.2 (3.2)	0.0 (0.0)	97.3 (7.4)
Level 2 - Intermediate (~ 40 %)	1.7 (0.9)	62.4 (11.5)	37.0 (9.9)	0.0 (0.0)	102.0 (3.4)
Level 3 - High (~ 60 %)	0.8 (1.3)	40.0 (5.5)	59.1 (6.8)	0.0 (0.0)	86.5 (3.5)
"In house" mometasone furoate #MFM13F2					
Level 1 - Low (~ 20 %)	1.8 (1.3)	78.7 (2.0)	19.5 (2.2)	0.0 (0.0)	92.5 (1.8)
Level 2 - Intermediate (~ 40 %)	1.1 (1.4)	70.4 (3.7)	28.5 (3.6)	0.0 (0.0)	96.2 (7.0)
Level 3 - High (~ 60 %)	0.4 (0.6)	51.6 (8.7)	47.9 (8.7)	0.0 (0.0)	100.2 (11.9)
Nasonex®					
Level 1 - Low (~ 20 %)	1.2 (1.1)	81.8 (1.7)	16.6 (2.4)	0.0 (0.0)	100.6 (5.8)
Level 2 - Intermediate (~ 40 %)	2.5 (2.6)	63.5 (5.5)	34.1 (3.1)	0.0 (0.0)	100.5 (4.7)
Level 3 - High (~ 60 %)	0.6 (0.7)	42.3 (8.9)	57.1 (9.4)	0.0 (0.0)	95.1 (4.1)

NSP: Nasal spray, AD: Anterior + drip, MP: Combined middle passage and nasopharynx region, F: Filter NSP: Nasal spray, AD: Anterior + drip, MP: Combined middle passage and nasopharynx region, F: Filter

Table 4.14. Mean (SD) *in vitro* regional nasal drug deposition (expressed as a percentage of recovered dose) and total recovery (expressed as percentage of the label claim) for the "in house" generic mometasone furoate (batch# MFM11TF5) nasal spray formulation and Nasonex® nasal spray product in VCU nasal model 2 at three different experimental conditions (n=4)

Expected combined middle passage and nasopharynx deposition	NSP	AD	MP	F	Total recovery (%)
"In house" mometasone furoate #MFM11TF5					
Level 1- Low (~ 50 %)	1.2 (1.3)	49.2 (9.5)	49.6 (10.7)	0.0 (0.0)	98.2 (7.9)
Level 2- Intermediate (~ 60 %)	2.4 (1.0)	35.5 (13.4)	62.1 (13.8)	0.0 (0.0)	88.7 (3.2)
Level 3- High (~77 %)	1.2 (0.7)	28.0 (5.8)	70.9 (6.5)	0.0 (0.0)	86.8 (4.1)
Nasonex®					
Level 1- Low (~ 50 %)	0.1 (0.1)	53.3 (10.2)	46.6 (10.0)	0.0 (0.0)	92.5 (11.2)
Level 2- Intermediate (~ 60 %)	0.2 (0.2)	38.2 (9.4)	61.6 (9.6)	0.0 (0.0)	91.3 (5.6)
Level 3- High (~ 77 %)	1.1 (1.1)	21.5 (9.0)	77.4 (8.5)	0.0 (0.0)	94.3 (7.5)

NSP: Nasal spray, AD: Anterior + drip, MP: Combined middle passage and nasopharynx region, F: Filter

4.3.3.2 Fluticasone propionate nasal spray products

For the Flonase® nasal spray product, as shown in Figure 4.13, the mean (SD) Dv10, Dv50 and Dv90 using an actuation force of 5.8 kg was measured as 20.9 (1.1) μm, 72.0 (1.7) μm and 120.4 (0.6) μm, respectively. Similar results were observed for the generic fluticasone propionate spray product with mean (SD) values of 21.9 (0.2) μm, 69.4 (2.1) μm and 118.6 (2.8) μm, respectively. Increasing the actuation force for the fluticasone products from 5.8 kg to 7.5 kg, did not product the same magnitude of changes in DSD that was observed for the mometasone furoate nasal spray products. The values of Dv50 were 67.2 (1.7) μm and 65.6 (1.1) μm and DV90 of 115.4 (1.1) μm and 114 (1.3) μm for Flonase® and the generic product, respectively using an actuation force of 7.5 kg. Similar results were observed by Doughty et al. [141] when increasing actuation force from 5.8 kg to 7.5 kg did not result in any change in DSD for Flonase® nasal spray product. However, it was noted that reducing the actuation force to 3 kg (pediatric force) resulted in a significant increase in DSD. This suggests that at higher actuation forces, formulation properties (such as viscosity) are not significantly affected for the fluticasone propionate nasal spray product.

The *in vitro* regional nasal drug deposition was investigated for the Flonase® (innovator product) and a marketed generic fluticasone propionate nasal spray product. The results are presented in Table 4.15 when performed using VCU nasal model 1 and in Table 4.16 for VCU nasal model 2. For experiments performed using VCU nasal model 1, mean (SD) drug recovery ranged from 97.4 (8.5) % to 99.9 (6.2) % for the generic formulation and 92.6 (5.9) % to 100.3 (10.7) % for Flonase® nasal spray product. Similar results in VCU nasal model 2 were 88.8 (3.6) % to 102.2 (6.3) % and 90.5 (10.0) % to 94.4 (2.4) %, respectively.

Table 4.15 shows that the mean (SD) amount of drug deposited on the device and the regional drug deposition in the anterior nose and combined middle passages were similar for Flonase® and the generic fluticasone propionate nasal spray product. There were no statistical differences when comparing the two formulations at three different levels of low, intermediate and high expected middle passage drug delivery. The mean (SD) combined middle passage and nasopharynx deposition ranged from 17.5 (1.0) % to 39.5 (5.9) % for generic fluticasone formulation and 21.0 (3.8) % to 47. 2 (10.4) % for the Flonase® in the VCU nasal model 1. It was noted that the drug deposition in middle passages at level 3 appeared to be lower (40 - 50%) compared to the deposition observed with the Nasonex® and mometasone furoate formulations (50 - 60%). It appeared that the level 3 - "high" conditions that were derived from the Nasonex® DOE experiments may not have translated to "high" deposition for the fluticasone propionate products due to differences in the spray characteristics of the different drug formulations and nasal sprays. It would be ideal to investigate using a DOE type approach the effect of patient use variables in the *in vitro* testing specifically for the individual test drug product (in this case fluticasone propionate) in any future application of these methods. This would allow identification of study conditions for the particular test nasal spray that produce the range of low, intermediate and high deposition.

For the fluticasone products tested in VCU nasal model 2, there was no significant differences in the deposition pattern for the two formulations inspected at three different experimental conditions (Table 4.16). Using the VCU nasal model 2 and three experimental conditions, for these formulations we observed a similar trend in the mean (SD) middle passage drug deposition ranging from 64.6 (4.8) % to 78.6 (5.6) % for the generic fluticasone propionate and 55.6 (7.3) % to 79.6 (0.3) % for the Flonase® nasal spray product.
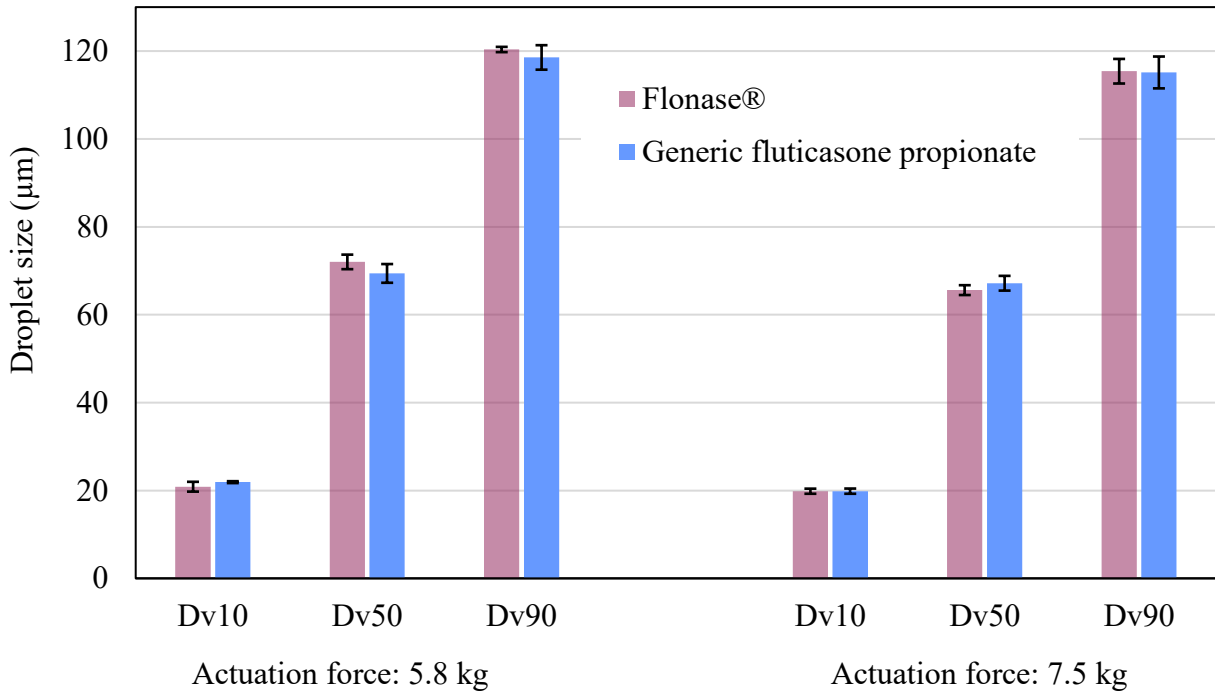
Figure 4.13. Mean (SD) droplet size distribution results for a single actuation of the Flonase[®] and generic fluticasone propionate nasal spray products at actuation force of and 7.5 kg and 5.8 kg at 2 cm distance between the tip of the nasal spray and laser sensing zone. These measurements performed in the beginning of the nasal spray life. Data represent mean (SD), (n = 4)

Table 4.15. Mean (standard deviation) *in vitro* regional nasal drug deposition (expressed as a percentage of recovered dose) and total recovery (expressed as percentage of the label claim) for the fluticasone propionate generic and Flonase® nasal spray products in VCU model 1 at three different experimental conditions (n=4)

Expected combined middle passage and nasopharynx deposition	NSP	AD	MP	F	Total recovery (%)
Generic fluticasone propionate					
Level 1 - Low (~ 20 %)	1.2 (0.8)	81.3 (0.9)	17.5 (1.0)	0.0 (0.0)	99.7 (5.4)
Level 2 - Intermediate (~ 40 %)	1.2 (0.5)	56.0 (3.6)	42.7 (4.1)	0.0 (0.0)	99.9 (6.2)
Level 3 - High (~ 60 %)	1.1 (0.5)	59.4 (5.9)	39.5 (5.9)	0.0 (0.0)	97.4 (8.5)
Flonase®					
Level 1 - Low (~ 20 %)	2.4 (2.5)	78.0 (3.4)	21.0 (3.8)	0.0 (0.0)	97.7 (4.4)
Level 2 - Intermediate (~ 40 %)	1.6 (0.5)	56.6 (8.9)	41.7 (8.4)	0.0 (0.0)	92.6 (5.9)
Level 3 - High (~ 60 %)	1.1 (0.7)	51.7 (10.3)	47.2 (10.4)	0.0 (0.0)	100.3 (10.7)

NSP: Nasal spray, AD: Anterior + drip, MP: Combined middle passage and nasopharynx region, F: Filter

Table 4.16. Mean (standard deviation) *in vitro* regional nasal drug deposition (expressed as a percentage of recovered dose) and total recovery (expressed as percentage of the label claim) for the fluticasone propionate generic and Flonase® nasal spray products in VCU model 2 at three different experimental conditions (n=4)

Expected combined middle passage and nasopharynx deposition	NSP	AD	MP	F	Total recovery (%)
Generic fluticasone propionate					
Level 1 - Low (~ 50 %)	1.4 (1.0)	34.0 (4.1)	64.6 (4.8)	0.0 (0.0)	95.3 (6.2)
Level 2 - Intermediate (~ 60 %)	0.7 (0.5)	24.9 (3.2)	74.5 (3.3)	0.0 (0.0)	102.2 (6.3)
Level 3 - High (~77 %)	0.8 (0.9)	20.6 (6.2)	78.6 (5.6)	0.0 (0.0)	88.8 (3.6)
Flonase®					
Level 1 - Low (~ 50 %)	1.1 (1.3)	43.3 (6.4)	55.6 (7.3)	0.0 (0.0)	93.4 (7.5)
Level 2 - Intermediate (~ 60 %)	1.3 (1.7)	30.6 (11.6)	68.1 (10.8)	0.0 (0.0)	94.4 (2.4)
Level 3 - High (~ 77 %)	2.7 (0.7)	17.8 (0.9)	79.6 (0.3)	0.0 (0.0)	90.5 (10.0)

NSP: Nasal spray, AD: Anterior + drip, MP: Combined middle passage and nasopharynx region, F: Filter

4.3.3.3 Summary of innovator and generic comparison studies and comparison with *in vivo* deposition data

To assess the utility of the developed *in vitro* test methods using VCU nasal models of 1 and 2 for characterization of regional nasal drug deposition of nasal spray products, two innovator spray products (Flonase® and Nasonex®) and their respective generic and "in house" products were characterized. No statistical differences were observed for regional nasal drug deposition of the Flonase® and the generic copy of the product in the VCU nasal model 1 and 2 for three different experimental deconditions. These two formulations had no statistical differences in their spray plume DSD. Similar observation was made for Nasonex® and the "in house" mometasone furoate formulations, despite their small differences in the DSD.

The experimental condition was selected based on the extent of drug delivery to the combined middle passage and nasopharynx regions of Nasonex® nasal spray products. Despite the differences in the DSD of Nasonex® and Flonase® (Dv50 of 57 µm vs 70µm) the range of drug delivery to the posterior nose region almost remained the same for three different experimental conditions reflecting different patient use conditions (Similar trend observed) in the two VCU nasal model 1and 2 (Except level 1 in VCU nasal model 1). It seems the combination of patient use variables of inhalation-actuation timing, head angle and actuation force has similar effects as observed for Nasonex® on regional drug deposition profile of Flonase®. Moreover, the effect of inter-subject variability in the geometry of the nasal cavity was also profound for Flonase® nasal spray product.

An *in vivo* study was performed to characterize the regional nasal drug deposition in 9 human subjects with allergic rhinitis for the Nasonex® and Flonase® nasal spray products [18]. In

this open-label, nonrandomized, crossover study subjects were administered one dose of ^{99m}TC radiolabeled Nasonex® or Flonase® to one nostril using the method described in the patient information package insert. Deposited drug in the nasal cavity were quantified by merging the gamma camera images with magnetic resonance images. Evaluating the 3D data obtained from this study, shown in Figure 4.14, it appears that the mean deposition of the drug in the posterior part of nasal cavity is about 30 % and 35 % (of the administered dose) for Nasonex® and Flonase®, respectively. However, considering the variability the drug deposition could be increased up to 60 % and 70 %, respectively. The mean results are similar to our reported *in vitro* deposition findings for Nasonex® and Flonase® when they tested in VCU nasal model 1 at intermediate or level 2. Also, the range of drug deposition produced in VCU nasal model 1 and 2 can be observed *in vivo*. Similarly, in a separate clinical study the regional drug deposition for Nasonex® nasal spray product was tested in 12 healthy subjects. Based on scintigraphy results, the author reported that 60 (9.1) % of the formulation deposited into the posterior part of the nasal cavity which is almost twice as the result for the previous observation. In both studies drug was administered based on information provided in the packaging insert [140]. The effect of different patient use technique and geometry of the nasal cavity may be the reason for the observed different extent of drug delivery to the middle passages. In addition, failure to accurately define the separation line between anterior and middle passages for MRI image of subjects may result in inaccurate segmentation of the nasal cavity which might be another source of observed high middle passage drug deposition in the later *in vivo* study [145]. Overall, this range of variability was also seen with our developed technique in the two nasal airway models.
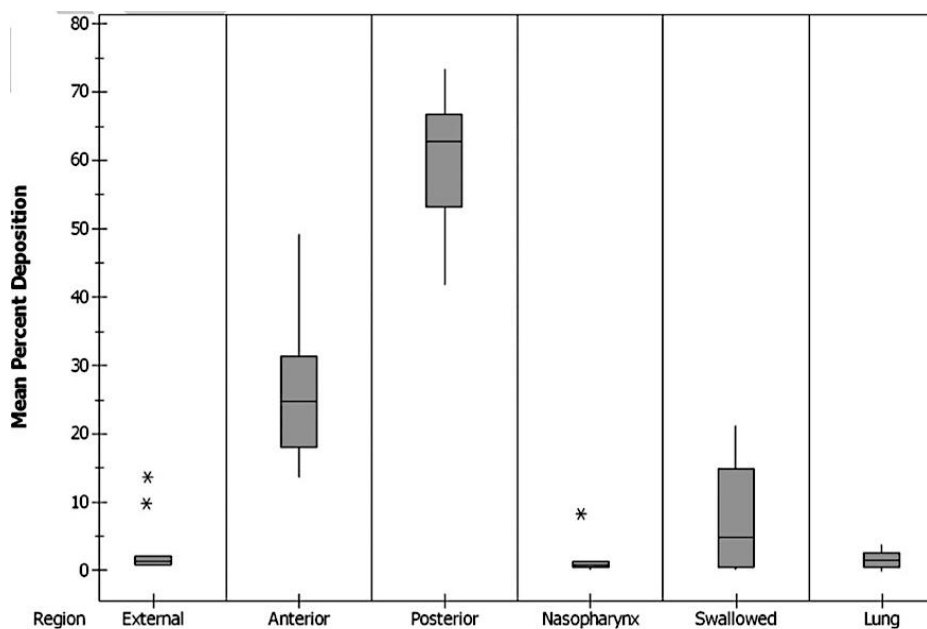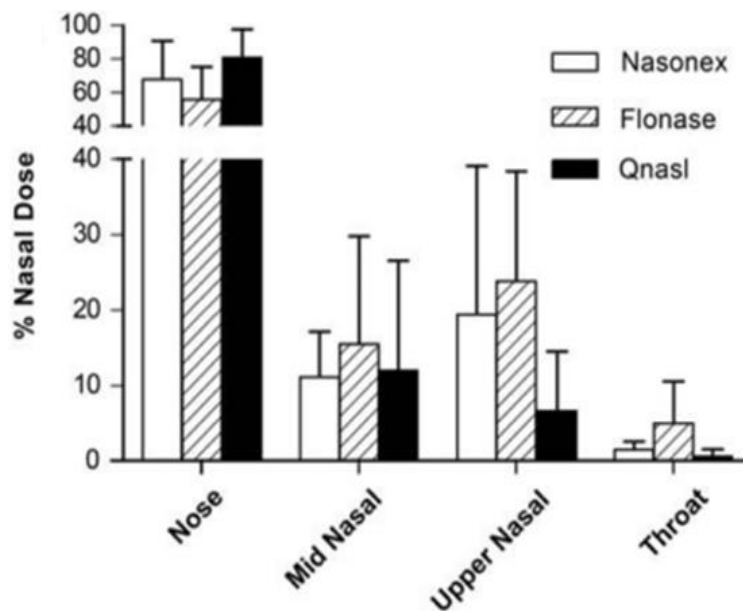
Figure 4.14. Image of the 3D SPECT data for the regional nasal drug deposition of Nasonex[®] and Flonase[®] nasal spray products administered to 9 subjects with allergic Rhinitis [18] (top), box and whisker diagram showing deposition fraction of mometasone furoate in the nasal cavity based on the percentage of the label claim administered to 12 healthy volunteers (bottom) [140]

A series of nasal spray products with differing *in vitro* spray properties were tested to assess their regional drug deposition in VCU nasal model 1 and to characterize their differing spray plume properties. Four products were considered, two custom-made mometasone furoate nasal sprays (Batch: A and B), and 2 commercial Nasonex® nasal sprays with expiration dates of Feb 2007 (expired) and Oct 2015 (in-date), respectively.

A summary of spray pattern test characteristics (Dmin, Dmax, Ovality ratio, and area) is presented in Table 4.17 using an actuation force of 7.5 kg. For the illustration purposes, Figure 4.15 shows the images obtained from spray pattern tests for the four nasal spray products. Nasonex® 2015, the reference product that was in-date when tested appeared to have the smallest Dmin, Dmax, area and a more circular shape as shown by its ovality ratio of 1.1 compared to the other formulations. The custom-made mometasone furoate formulation batch A showed a significantly larger Dmin, Dmax, ovality ratio and area compared to the other formulations. Its area of 755.9 mm^2 was almost double the area measured for Nasonex® 2015 with area of 363.4 mm^2 (p-value<0.0001). The expired Nasonex® 2007 showed a larger Dmin, Dmax and area compared to the in-date formulation (p-value<0.0001). It is unclear as to the reasons for these changes, possible reasons include alteration in the formulation rheology and viscosity. However, a previous *in vitro* study showed changes in spray dimensions and properties depended on the type of viscosity enhancer polymer. For example, addition of Avicel FMC (microcrystalline cellulose and sodium carboxymethylcellulose) increased formulation viscosity without a pronounced change in spray plume characteristics. Spray dimensions for a formulation without a viscosity enhancer polymer revealed that increasing the percentage of the polymer reduced the spray dimensions. It has been suggested that modification of these characteristics can be used to enhance the retention of the formulation in the nasal cavity and reduce drainage from anterior nose [19].

Table 4.17. Mean (SD) spray pattern data for a single actuation of Nasonex® 2015 and 2007 nasal spray products and custom-made mometasone furoate nasal spray formulations (batches A and B) measured using an actuation force of 7.5 kg, (n = 3)

Device	$^{\#}D_{min}$ (mm)	$^{\dagger}D_{max}$ (mm)	Ovality	*Area (mm^2)
Nasonex® 2015	20.5 (0.2)	22.9 (0.3)	1.1 (0.0)	363.4 (7.6)
Nasonex® 2007	23.8 (0.5)[a,b,c]	28.7 (0.3)[a,b]	1.2 (0.1)	531.3 (11.2)[a]
Custom-made mometasone furoate, batch B	21.3 (0.2)[b]	26.4 (1.3)[a,b]	1.2 (0.1)	462.4 (25.3)[a,b]
Custom-made mometasone furoate, batch A	28.3 (0.6)[a]	34.6 (2.2)[a]	1.2 (0.0)	755.9 (35.2)[a,c]

Statistical analysis of variance (ANOVA), followed by Tukey's HSD

[#]$P<0.05$, significant difference in D_{min}; [†]$P<0.05$, significant difference in D_{max} [*]$P<0.05$, significant difference in Area

[a]compared to Nasonex 2015

[b]compared to custom-made mometasone furoate batch A

[c]compared to custom-made mometasone furoate batch B

(a) (b) (c) (d)
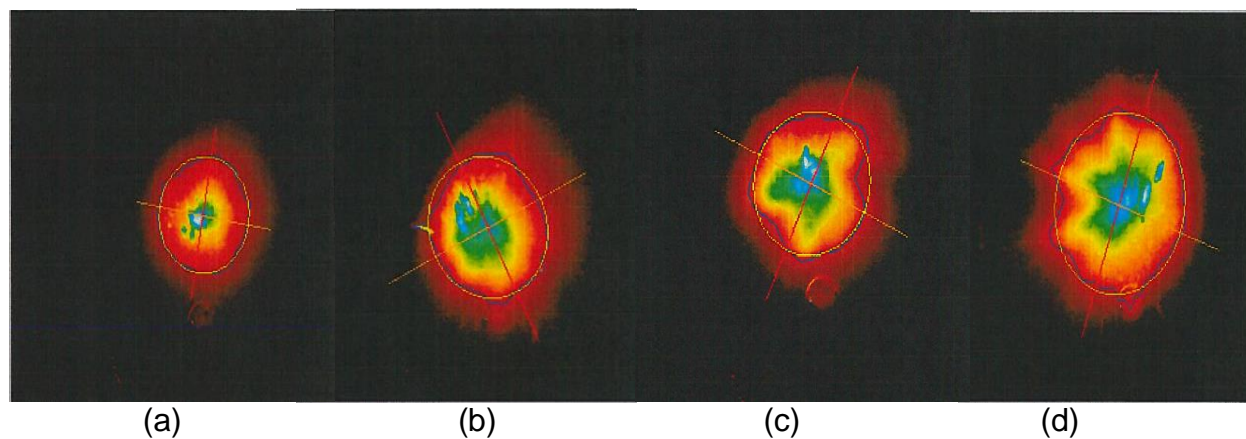
Figure 4.15. Spray pattern images of (a) Nasonex 2015, (b) Nasonex 2007, and custom-made mometasone nasal spray formulation batches (c) B and (d) A obtained using SprayVIEWTM NSP system using an actuation force of 7.5 kg (Proveris Scientific, Corporation, Sudbury, MA)

Results for plume angle measurements and width measured using an actuation force of 7.5 kg are shown in Table 4.18 and Figure 4.16. Compared to Nasonex® 2015, the expired Nasonex® 2007 product and the two custom-made mometasone furoate formulations had significantly larger plume angles and widths. The custom-made mometasone furoate batch A had the largest plume angle 60.5º compared to the in-date Nasonex® 2015 product with the smallest plume angle of 47.7º. The respective plume width was 33.1 mm for batch A and 27.2 mm for the in-date Nasonex® 2015 nasal spray product. Again, the expired Nasonex® 2007 nasal spray product showed a larger plume geometry compared to the in-date formulation.

Table 4.18. Mean (SD) plume geometry data for a single actuation of the Oct 2015 and Feb 2007 expiry Nasonex® nasal spray products and custom made mometasone nasal spray measured using an actuation force of 7.5 kg (n=3)

Device	[+]Angle	*Width (mm)
Nasonex® 2015	47.7 (1.1)	27.7 (2.1)
Nasonex® 2007	55.4 (1.2)[a, b]	31.5 (0.8)
Custom-made mometasone furoate, batch B	54.4 (1.8)[a, b]	30.8 (1.2)
Custom-made mometasone furoate, batch A	60.5 (1.3)[a]	33.1 (2.6)[a]

Statistical analysis of variance (ANOVA), followed by Tukey's HSD

[+] $P<0.05$, significant difference in plume angle; * $P<0.05$, significant difference in plume width,

[a]compared to Nasonex®2015

[b] compared to custom-made mometasone furoate batch A
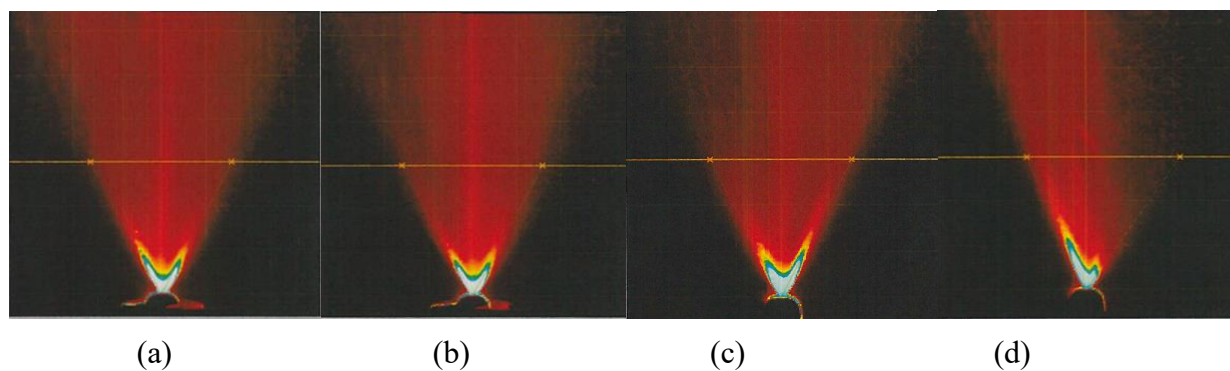
Figure 4.16. Spray pattern images of (a) Nasonex® 2015, (b) Nasonex® 2007 nasal spray products and custom-made mometasone nasal spray formulation batches (c) B and (d) A obtained by SprayVIEW™ NSP system using an actuation force of 7.5 kg (Proveris Scientific, Corporation, Sudbury, MA)

The DSD for the studied nasal sprays were also measured at two actuation forces of 4.5 and 7.5 kg and are summarized in Tables 4.19 and 4.20. At actuation force of 4.5 kg, the DSD of the expired Nasonex® 2007 nasal spray product was significantly smaller than the in-date Nasonex® 2015 with a mean (SD) Dv50 of 48.8 (0.1) μm compared to 57.2 (1.5) μm, respectively (*p*-value=0.0112). Using the same actuation force, the custom-made mometasone furoate batch A had the smallest DSD with a mean (SD) Dv50 of 43.1 (3.6) μm, however, batch B was observed to have a mean (SD) Dv50 of 50.9 (3.6) μm which was comparable to expired Nasonex® 2007 product. Increasing the actuation force to 7.5 kg resulted in smaller droplet size distribution for all nasal spray products. Compared to in-date Nasonex® 2015, each of the nasal spray products had a significantly smaller droplet size distribution.

There was a negative linear relationship between the area obtained from the spray pattern results and the Dv50 obtained from the DSD measurements at 4.5 kg as shown in Figure 4.17. Previous studies also showed a negative linear relationship between spray pattern data and DSD

as formulation viscosity was reduced which was correlated with a larger spray area [131]. These studies also showed that for nasal formulations containing carboxymethyl cellulose as viscosity enhancer, which is present in Nasonex® formulation, the formulation behaved as Newtonian fluid and the DSD was reduced by increasing the actuation force.

Table 4.19. Mean (SD) droplet size distribution results for a single actuation of the study nasal sprays using an actuation force of 4.5 kg (n=4)

Device	#Dv 10 (µm)	†Dv50 (µm)	*Dv90 (µm)	Span
Nasonex® 2015	19.4 (0.4)	57.2 (1.5)	126.7 (4.0)	1.9 (0.1)
Nasonex® 2007	17.8 (0.1)[a]	48.8 (0.1)[b]	106.9 (2.0)[a]	1.8 (0.0)
Custom-made mometasone furoate, batch B	20.3 (1.1)	50.9 (3.6)[b]	118.6 (10.5)	1.9 (0.1)
Custom-made mometasone furoate, batch A	16.9 (0.6)[a, b]	43.1 (0.2)a[a, b]	99.1 (3.7)[a ,b]	1.9 (0.0)

Statistical analysis of variance (ANOVA), followed by Tukey's HSD

# $P<0.05$, significant difference in DV_{10}

† $P<0.05$, significant difference in DV_{50}

* $P<0.05$, significant difference in Dv_{90}

[a]compared to custom-made mometasone furoate, batch B

[b]compared to Nasonex® 2015

Table 4.20. Mean (SD) droplet size distribution results for a single actuation of the study nasal sprays using an actuation force of 7.5 kg (n=4)

Device	#Dv 10 (μm)	†Dv50 (μm)	*Dv90 (μm)	Span
Nasonex® 2015	16.5 (0.2)	47.0 (1.0)	109.8 (1.7)	2.0 (0.1)
Nasonex® 2007	14.3 (0.1)[a, b]	36.3 (0.8)[a]	88.8 (0.8)[a, b]	2.1 (0.0)
Custom-made mometasone furoate, batch B	16.1 (0.9)	38.7 (3.0)[a]	100.9 (8.5)	2.2 (0.1)
Custom-made mometasone furoate, batch A	14.3 (0.2)[a, b]	35.6 (0.5)[a]	91.1 (1.0)[a]	2.2 (0.0)

Statistical analysis of variance (ANOVA), followed by Tukey's HSD

\# $P<0.05$, significant difference in DV_{10}

† $P<0.05$, significant difference in DV_{50}

* $P<0.05$, significant difference in Dv_{90}

[a]compared to Nasonex® 2015

[b]compared to custom-made mometasone furoate, batch B

y = -27.735x + 1915
R² = 0.9386
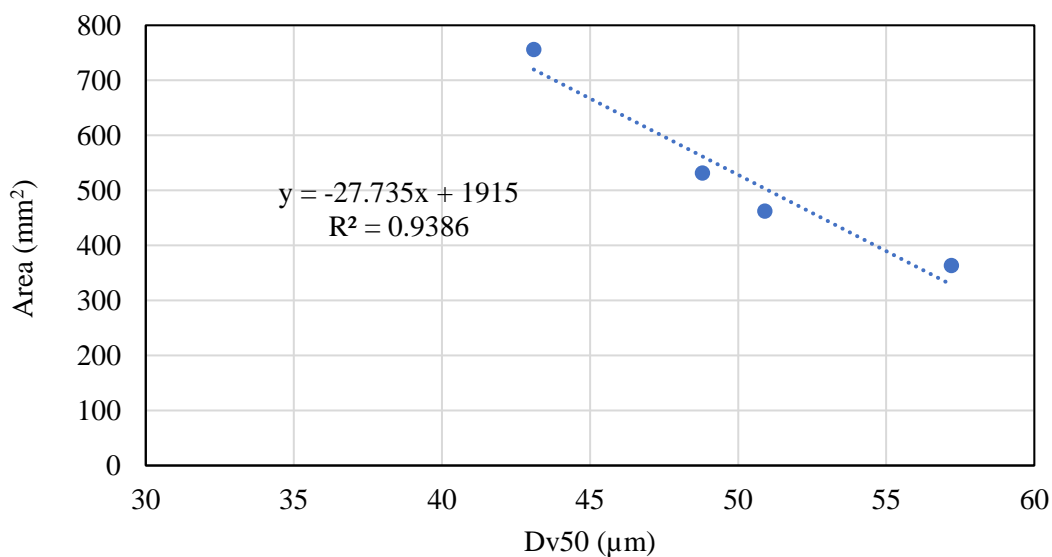
Figure 4.17. Linear relationship between spray pattern area and Dv50 measured using 4.5 kg actuation force for four study nasal sprays

The results of *in vitro* regional drug deposition for nasal spray products with varying plume characteristics, are summarized in Tables 4.21 and 4.22. The measurements were performed at two actuation forces of 4.5 kg and 7.5 kg, with the nasal model angled 30˚ forward from horizontal and the nasal spray positioned at 9 mm from front of the nasal spray tip with synchronized nasal spray actuation and inhalation (D). The mean total recovery for these experiments ranged from 88.9 % to 103.1 %. Comparing the regional drug deposition of Nasonex® 2007 with the in-date Nasonex® 2015, there was no statistical differences between the mean (SD) amount of drug delivered to the anterior part of the nose + drip of 65.9 (13.6) % vs 67.3 (7.4) % of recovered dose, respectively, and middle passages of 33.9 (13.8) % vs 32.1 (8.0) % of recovered dose, respectively, when nasal sprays were actuated using a force of 4.5 kg. For the two custom-made nasal spray products, mean (SD) anterior + drip deposition was 63.4 (6.3) % and 54.0 (2.8) % for nasal formulation batches B and A, respectively. The corresponding mean (SD) middle passage depositions were 34.1 (6.7) % and 43.2 (6.5) %. When comparing the regional nasal drug deposition across the 4 nasal spray products at actuation force of 4.5 kg, there was no statistically significant differences in anterior + drip or middle passage drug deposition for these nasal spray products evaluated by ANOVA.

When tested using a 7.5 kg actuation force, the results shown in Table 4.22 reveal that the anterior nose + drip deposition of batch A was significantly greater than in-date Nasonex® 2015 (*p*-value = 0.0430) with mean (SD) values of 67.1 (8.3) % versus 55.4 (7.6) %. The anterior nose + drip deposition of the two custom-made mometasone furoate nasal spray products was also significantly different (*p*-value = 0.0017). Batch B produced a significantly lower mean (SD) anterior + drip drug deposition (48.4 (9.2) %) compared to batch A (67.1 (8.3) %). Correspondingly, the mean (SD) middle passage drug delivery of batch A (31.0 (8.5) %) was significantly lower than batch B (49.6 (8.8) %) and also lower than the in-date Nasonex® 2015

nasal spray product (44.6 (7.6) %) (p-value = 0.0008 and 0.0126, respectively). Finally, the Nasonex® 2007 had significantly lower mean (SD) middle passage deposition of 38.8 (3.8) % when compared with custom batch B (p-value = 0.0374).

When considering all four nasal sprays, with the data available from actuation using a 7.5 kg force, the greatest differences in droplet size and spray plume characteristics were observed between Nasonex 2015 (large droplet size and small plume angle and area) and the custom made batch A formulation (small droplet size and large plume angle and area), with Nasonex 2007 and custom made batch B formulations appearing to have similar spray properties which were between the extremes of the other two formulations. This was translated into the highest anterior nose deposition observed with batch A corresponding with the large plume angle and spray area. Cheng et.al [31] also showed increased anterior nose deposition with increasing spray angle. However, it should be noted that in their study increasing in the plume angle was accompanied with larger spray plume droplet size, which is in contrast to the observations for batch A which had the smallest droplet size of the study nasal sprays. Newman et al. [16] using gamma scintigraphy, reported that deposition of a spray with a 35° plume angle gave improved posterior (turbinate) deposition compared to a spray with a similar droplet size (70 µm) but with a 60° plume angle. In contrast, Guo and colleagues [146] compared two cellulose-containing formulations; they observed an improved turbinate-region deposition from the spray with the wider plume angle (67° vs. 32°), and the CFD predictions of Kimbell et al.[15] failed to show any effect based on plume angle.

The two custom made nasal spray products, tested at an actuation force of 7.5 kg using identical spray pump containers were found to have significant differences in the spray plume properties while they droplet size distributions were found to be similar (mean Dv50 = 35.6 µm

and 38.7 µm for batch A and B, respectively). For these products, there were significant differences in the regional drug deposition when tested at 7.5 kg. With batch A having high anterior nose deposition (67.1%) and low middle passage drug delivery (31%), compared to almost 50% deposition in the middle passage for batch B. Further evidence the limited effect of droplet size in determining the nasal deposition profile can be found when comparing Nasonex 2015 actuated at 4.5 kg, which had a mean Dv50 of 57.2 µm and Batch A actuated at 7.5 kg, which had a mean Dv50 of 35.6 µm. Despite, large differences in the measured particle size of these sprays, the regional nasal deposition in the anterior nose was nearly identical with 67.3% vs 67.1 % deposition for Nasonex 2015 and batch A, respectively. Similarly values for middle passage deposition were 32.1 % and 31.0 %, respectively. From these results, it appears that for nasal spray plumes with high initial plume velocities, due to the presence of the nasal valve, droplet size in the range of 35 – 60 µm was less important with respect to penetration through the nasal valve and deposition fraction to the middle passages compared to the spray plume properties.

Table 4.21. Mean (SD) *in vitro* regional nasal drug deposition (expressed as a percentage of recovered dose) and total recovery (expressed as percentage of the label claim) for the Nasonex® nasal spray product and custom-made mometasone furoate formulations in VCU model 1, when the nasal spray is located at position of 9 mm from front of the nose, nasal model head angle of 30°forward from horizontal, nasal spray actuation during nasal inhalation (D) using actuation force of 4.5 kg (n=4)

Nasal spray product	NSP	AD	MP	F	Total recovery (%)
Nasonex 2015	0.6 (0.9)	67.3 (7.4)	32.1 (8.0)	0.0 (0.0)	91.5 (7.3)
Nasonex 2007	0.2 (0.3)	65.9 (13.6)	33.9 (13.8)	0.0 (0.0)	92.2 (4.3)
Custom-made mometasone furoate, batch B	2.0 (1.1)	63.4 (6.3)	34.1 (6.7)	0.0 (0.0)	90.4 (5.7)
Custom-made mometasone furoate, batch A	2.8 (3.7)	54.0 (2.8)	43.2 (6.5)	0.0 (0.0)	89.7 (6.2)

NSP: Nasal spray, AD: Anterior + drip, MP: Combined middle passage and nasopharynx region, F: Filter

Table 4.22. Mean (SD) *in vitro* regional nasal drug deposition (expressed as a percentage of recovered dose) and total recovery (expressed as percentage of the label claim) for the Nasonex® nasal spray product and custom-made mometasone furoate formulations in VCU model 1, when the nasal spray is located at position of 9 mm from front of the nose, nasal model head angle of 30°forward from horizontal nasal spray actuation during nasal inhalation (D) using actuation force of 7.5 kg (n=4)

Nasal spray product	NSP	*AD	#MP	F	Total recovery (%)
Nasonex 2015	0.0 (0.0)	55.4 (7.6)	44.6 (7.6)	0.0 (0.0)	88.9 (3.2)
Nasonex 2007	3.6 (2.8)	56.8 (7.5)	38.8 (3.8)[b]	0.9 (1.8)	90.5 (8.0)
Custom-made mometasone furoate, batch B	2.0 (0.9)	48.4 (9.2)	49.6 (8.8)	0.0 (0.0)	103.1(19.9)
Custom-made mometasone furoate, batch A	1.9 (1.9)	67.1 (8.3)[a, b]	31.0 (8.5)[a, b]	0.0 (0.0)	97.7(10.8)

NSP: Nasal spray, AD: Anterior + drip, MP: Combined middle passage and nasopharynx region, F: Filter
*P<0.05, significant difference in AD,
#P<0.05, significant difference in MP
[a]compared to Nasonex® 2015
[b]compared to batch B

The aim of this work was to identify the effect of changes in spray plume characteristics and droplet size distributions on *in vitro* regional drug deposition for these nasal spray products. Despite statistically significant differences in the droplet size characteristics of the nasal sprays tested at 4.5 kg actuation force, these did not translate into statistically significant changes in the *in vitro* regional nasal deposition for these sprays. Combining the data from *in vitro* characterization tests of droplet sizing, plume geometry and spray pattern tests with the regional nasal drug deposition test performed at actuation force of 7.5 kg, it appears the custom mometasone furoate batch A with larger spray plume area, Dmin, Dmax, plume angle and width and smaller DSD produced a lower middle passage drug deposition. In order to see investigate the relationship between the *in vitro* plume characterization results and *in vitro* regional nasal drug deposition, the correlation of these factors was studied using JMP 12.0 software. The response, Y, was selected as combined middle passage and nasopharynx drug deposition measured at actuation force of 7.5 kg, nasal head angle of 30º, nasal spray position of 9 mm and nasal spray actuation occurred during nasal inhalation (D). The predictors, Xs, were considered as Dmin, Dmax, ovality, area, plume angle, width, Dv10, Dv50 and Dv90.

Firstly, the correlation between each predictors and response was evaluated by assessing the correlation coefficient. As demonstrated in Table 4.23, the strongest correlation was observed between the middle passage drug deposition and Dmin measured in spray pattern test with a negative correlation of -0.5982 and with $R^2 = 0.3579$, the line intercept of 90.5 and the slope of - 2.1 (SE = 0.87) which was significantly different from zero (t ratio = -2.36, *p* value = 0.0399) signifying the importance of the Dmin in determining middle passage drug delivery. The negative correlation between these variables implies that increasing Dmin will produce a decrease in drug delivery to the middle passages. Among the tested nasal sprays, the custom mometasone furoate

formulatinon batch A with the largest Dmin exhibited the lowest middle passage drug delivery. Negative correlation between the predictors and response were also found for Dmax, area, plume angle and width. The remaining predictors had a positive correlation with middle passage drug deposition. However, with regards to DSD, it is important to recognized the relatively small range of droplet sizes that were considered using the actuation force of 7.5 kg (Dv50 36 μm - 47 μm) which perhaps limits extrapolation of the effects of Dv50 on middle passage drug deposition.

The next step in the analysis was to identify the predictors and the most informative subset among all the combinations that can be used to estimate combined middle passage drug deposition in VCU nasal model 1 using a multiple regression approach. The previous approach of adding one variable at a time and judging the models based on goodness of fit was employed. The co-linearity between predictors was assessed and reported in Table 4.24. The lowest correlation was observed between the two variables of Dmin and ovality as shown in Table 4.24.

In JMP using multiple regression platform, all possible models were constructed by adding predictors one at a time and the models with best results for R^2 and lower AIC, BIC and RMSE for each subset are summarized in Table 4.25. The best model using only including one predictor was the model using Dmin, which had the highest correlation with middle passage drug deposition resulted in a R^2 of 0.3579, AIC value of 94.1, BIC of 92.5 and RMSE of 9.2. The model which included two predictors, Dmin and Ovality, was able to generate an $R^2 = 0.77$, which indicates that 77 % of the variability of the response data around mean can be explained by the built model (Figure 4.18). The analysis of variance for this model reports a p-value = 0.0014. The derived model expression for predicting middle passage drug deposition (Y) was:

Y= -18.4 – (2.8*Dmin) + (105.4*ovality)   Equation 4.5

The parameter estimates and the *p*-values of the predictors for this model are listed in Table 4.26. The ANOVA assumptions of normality of the data (Figure 4.19) and equal variance (*p*-value of 0.9583 for Brown-Forsythe test) were also assessed. Considering the middle passage residual versus predicted middle passage plot (Figure 4.20) for the model, no heteroscedasticity was observed, meaning that there was no change in variance with change in the fitted value of the response, for the model including the two predictors of Dmin and Ovality.

Table 4.23. Correlation between *in vitro* middle passage drug deposition and spray plume properties and their reported levels of statistical significance

	Dmin	Dmax	Ovality	Area	Plume angle	Width	Dv10	Dv50	Dv90
Correlation	-0.5982	-0.3428	0.4191	-0.4379	-0.3498	-0.1529	0.4934	0.2814	0.4793
Line intercept	90.5	65.2	-36.1	58.9	86.1	62.3	-26.7	17.2	-12.0
Estimate (SE)	-2.1 (0.9)	-0.8 (0.7)	65.5 (44.8)	0.0(0.0)	-0.8(0.7)	-0.6(1.3)	4.5(2.5)	0.6(0.7)	0.6(0.3)
t ratio	-2.4	-1.2	1.5	-1.5	-1.2	-0.5	1.8	0.9	1.7
p-value	0.0399	0.2754	0.1750	0.1545	0.2506	0.6352	0.1031	0.3762	0.1149

Table 4.24. Correlation matrix for *in vitro* spray plume properties measured for mometasone furoate nasal formulations with varying spray plume characteristics

	D min	D max	Ovality	Angle	Width	Area	Dv 10	Dv 90	Dv 50
Dmin	1.00	0.94	**0.31**	0.87	0.67	0.98	-0.80	-0.77	-0.75
Dmax	0.94	1.00	0.61	0.89	0.80	0.99	-0.82	-0.80	-0.83
Ovality	**0.31**	0.61	1.00	0.52	0.67	0.50	-0.43	-0.48	-0.65
Angle	0.87	0.89	0.52	1.00	0.78	0.91	-0.69	-0.76	-0.89
Width	0.67	0.80	0.67	0.78	1.00	0.74	-0.62	-0.70	-0.75
Area	0.98	0.99	0.50	0.91	0.74	1.00	-0.79	-0.77	-0.81
Dv10	-0.80	-0.82	-0.43	-0.69	-0.62	-0.79	1.00	0.96	0.83
Dv90	-0.77	-0.80	-0.48	-0.76	-0.70	-0.77	0.96	1.00	0.91
Dv50	-0.75	-0.83	-0.65	-0.89	-0.75	-0.81	0.83	0.91	1.00

Table 4.25. Possible linear models built to predict *in vitro* middle passage drug deposition of mometasone furoate nasal spray products with spray plume characteristic data as predictors

Model	Number	R^2	RMSE	AIC	BIC
Dmin	1	0.3579	9.2	94.1	92.5
Dmin, Ovality	2	0.7677	5.8	86.5	82.8
Ovality, Area, Dv90	3	0.8617	4.8	86.6	79.1
Dmax, Area, Dv90, Dv50	4	0.9050	4.2	90.9	77.0
Dmax, Area, Dv10, Dv90, Dv50	5	0.9283	4.0	100.8	76.2
Dmin, Ovality, Angle, Area, Dv10, Dv90	6	0.9814	2.2	106.5	62.4
Dmin, Ovality, Angle, Area, Dv10, Dv90, Dv50	7	0.9914	1.7	141.2	55.6
Dmin, Dmax, Ovality, Angle, Area, Dv10, Dv90, Dv50	8	0.9939	1.6	269.1	53.9

Table 4.26. Parameter estimates and significance of the model that includes Dmin and ovality as predictors of middle passage drug deposition of mometasone furoate nasal spray formulations with varying spray characteristics

Term	Estimate	Std Error	t Ratio	Prob>|t|
Intercept	-18.4	30.3	7.13	<.0001*
Dmin	-2.7	2.3	-5.27	0.0005*
Ovality	105.4	0.05	4.50	0.0015*
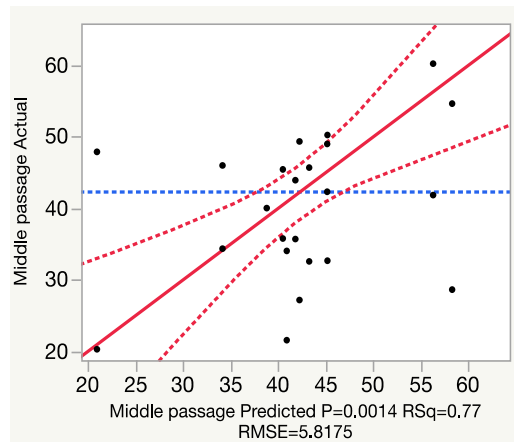
Figure 4.18. Plot of middle passage deposition for mometasone furoate predicted versus observed data using a model including Dmin and ovality as two predictors
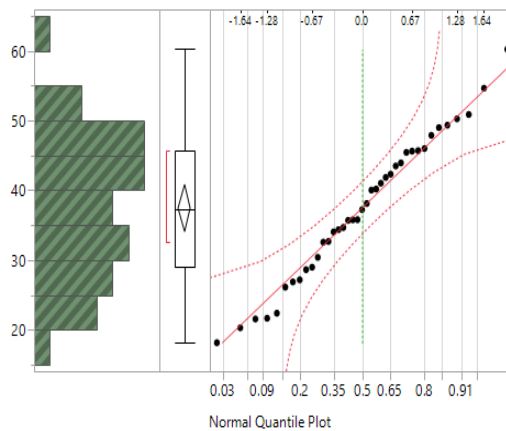
Figure 4.19. Normal quantile plot for middle passage drug deposition of mometasone furoate nasal spray formulations with varying spray properties
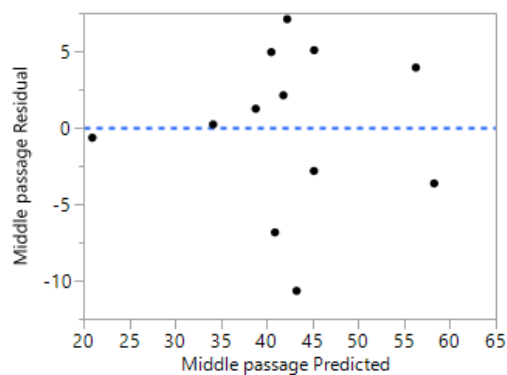
Figure 4.20. Residual plot for residual versus predicted middle passage deposition for mometasone furoate nasal spray formulations with varying spray properties using a model that includes two predictors of Dmin and ovality

4.4 Conclusion

In this chapter, the importance of nasal geometry on regional nasal drug deposition of nasal spray products was demonstrated. In addition, it was observed that the effects of patient use variables can vary with respect to the nasal cavity geometry employed for *in vitro* testing (Specific Aim 2-1). The regional nasal drug deposition in VCU nasal model 2 appeared to be less sensitive with respect to changes in patient use parameters. However, the previously identified critical patient use variables that affect deposition in VCU nasal model 1 were observed to be similarly important for determining deposition in VCU nasal model 2. Deposition testing using VCU nasal model 2 confirmed that nasal inhalation during nasal spray actuation and head angle were important patient use factors. The developed *in vitro* test methods were able to reliably produce similar regional nasal deposition profiles for the nasal spray products with similar spray plume characteristics (Specific Aim 2-2). These methods were also capable of detecting differences in the regional nasal drug deposition of the nasal spray products with different plume geometries which appeared to be more critical than droplet size in determining the deposition fate of the nasal

spray (Specific Aim 2-2). Future studies should consider performing measurements of regional nasal drug deposition for a series of nasal spray products with differing spray plume properties in a series of nasal models with different nasal valve region geometries to further investigate the importance of spray plume properties on regional nasal drug deposition in combination with inter-subject variability.

It is important to recognize that the results and observations described in this chapter will require further *in vivo* validation. The *in vitro* deposition data obtained in this study for the Nasonex® and Flonase® nasal spray products was observed to agree with previous literature *in vivo* deposition studies. However, due to the variability observed in the *in vivo* literature data, it would be desirable to investigate *in vivo* deposition performed under controlled conditions alongside simultaneous *in vitro* deposition studies with the same nasal spray used in the same manner and possibly using models of the airway geometries of the *in vivo* test subjects. Only then can meaningful *in vitro - in vivo* correlations be made to assess these nasal spray products and validate the proposed approach. However, to date, it was only possible to examine retrospectively the literature to identify an *in vivo* deposition study using the nasal sprays employed in this project and observe that the *in vivo* regional drug deposition was comparable with the results obtained *in vitro* using VCU nasal models 1 and 2.

Chapter 5

DEVELOPMENT AND EVALUATION OF A NOVEL CIPROFLOXACIN NANOCRYSTAL FORMULATION FOR NASAL DRUG DELIVERY

5.1   Introduction

Chronic rhinosinusitis (CRS) is a common chronic disease of the nasal airways and paranasal sinuses affecting approximately 10 -15% of the US population [62, 63]. The etiology of CRS is not completely clear, but it is believed that one or more factors, such as anatomical obstruction due to high mucus secretion, accumulation of bacterial or fungal infection in the sinuses, or allergies results in a chronic inflammation of the nasal airways. The main organisms in CRS include *Staphylococcus aureus, Enterobacteriaceae spp*., and *Pseudomonas spp*., and less commonly *Streptococcus pneumoniae, Haemophilus influenza*, and beta hemolytic streptococci [64, 65]. The high rate of endoscopic sinus surgery demonstrates that current therapeutics are not sufficiently effective [62]. One potential therapeutic option is the short-term administration of oral or topical antibiotics.

Ciprofloxacin, a fluoroquinolone, is a broad-spectrum antibiotic which has been used widely used to treat *Pseudomonas aeruginosa* infection [147, 148]. *Pseudomonas aeruginosa* is cultured in patients with chronic rhinosinusitis, especially in patients with previous sinus surgery [149]. Systemic or nebulized delivery of ciprofloxacin has been administered in patients with chronic rhinosinusitis [70, 71]. Local administration of antibiotics is the preferred mode of delivery, as it ensures direct deposition of the medication to the site of infection, resulting in high local concentrations and lower systemic levels and associated systemic toxicity. To date, topical

antibiotics, administered in patients who have not undergone surgical intervention, in the form of nebulizers or sprays have failed to demonstrate any clinical benefit due to limited mucosal distribution from nasal sprays as well as off-target delivery to the lungs in case of using nebulizers. Therefore, there is a need to develop a formulation with high-efficiency drug delivery to the posterior part of the nasal cavity [59] if antibiotic therapy is to become a viable therapeutic option.

Among the challenges of local nasal delivery, hyper-viscoelastic mucus in CRS patients (because of high mucin, DNA and actin content from degenerated neutrophils) serves as a barrier for drug penetration reaching the nasal epithelial. Lai et al. [76] estimated the average pore size of mucus obtained from CRS patients was about 150 ± 50 nm measured based on the mobility of PEGylated nanoparticles. The first aim of this chapter was to evaluate the feasibility of using a sonocrystallization technique to produce ciprofloxacin nanoparticles which may better penetrate the mucus barrier. The process variables related to the crystallization technique were assessed to investigate the effects on particle size and to produce nanocrystals in the size range of 100 – 200 nm.

The second aim was to develop an aerosolizable nasal formulation incorporating the ciprofloxacin nanoparticles into nanocomposite particles suitable for delivery to the middle passages and paranasal sinuses. A spray drying technique was employed for this task to formulate a water-soluble excipient powder composite containing ciprofloxacin nanoparticles in the target particle size range of 5 – 10 μm. The nanocomposites should have the ability to release the ciprofloxacin nanoparticles after dissolution of excipients in the nasal fluid lining. The particle size distribution and dissolution profile of the optimized ciprofloxacin nanoparticles were evaluated following their release from the nanocomposite formulation to determine their release properties.

The third aim was to characterize the delivery of the nanocomposite formulation using a novel powder delivery system developed to enhance the nasal delivery to the middle passages using the development realistic nasal airway geometry (VCU nasal model 1). The novel powder delivery system utilizes the VCU low volume DPI (2.3-343) modified to deliver aerosol to the nasal cavity and used in combination with a novel breathing maneuver. The method allowed aerosol to be delivered to the nasal cavity at a low flow rate ($10 - 15$ Lmin^{-1}) during a simultaneous nasal exhalation [150].

The fourth aim was to develop a technique to assess post nasal deposition events such as transepithelial transport of drugs after realistic deposition on human epithelial cell monolayers in a realistic airway geometry. Previous attempts have been made to study the transport of fractionate inhalation aerosols that have deposited drug on Transwell® based cell monolayers which have been inserted into cascade impactors [151]. Deposition using these methods often produced focused areas of drug deposition corresponding to the position of the Transwell® under an individual impactor jet and would not be considered realistic mimics of airway deposition. In this study, we have inserted three Transwell® inserts into the nasal cavity walls such that a cell monolayer is exposed to the airflow through the middle passages of a realistic nasal airway model. Drug depositing on the monolayer may enable a more clinically relevant sampling of the aerosol and be used to study the transepithelial transport of the drug.

5.2   Materials

Ciprofloxacin (base, anhydrous) and Polysorbate 80 (Tween™ 80) were purchased from Sigma - Aldrich, St. Louis, MO. Pearlitol® PF-Mannitol was donated from Roquette Pharma, Lestrem, France. Polyvinylpyrrolidone (PVP K30) was purchased from TCI Chemicals, Japan.

Hydroxypropylmethyl cellulose (HPMC) capsules (size 3) were donated by Capsugel, NJ. HPLC grade isopropyl alcohol, methanol, acetonitrile, phosphoric acid, and trimethylamine were purchased from Fischer Scientific, Pittsburgh, PA.

5.3 Methods

5.3.1 Nanoparticle preparation

5.3.1.1 Preparation of ciprofloxacin solution

Aqueous solutions of ciprofloxacin base (CPF) were prepared by dissolving 37.5 mg of drug in 1 mL of 0.1N hydrochloric acid with the aid of water bath sonication (Branson® 5510 Sonicator, Fischer Scientific, Pittsburgh, PA) for 30 min at room temperature (25 ºC). 37.5 mg of drug was the highest mass that could be dissolved in 1 mL of 0.1N hydrochloric acid with the aid of sonication. The ciprofloxacin solution was then filtered using an Anotop® syringe filter (0.2 μm, 25mm, Whatman, Sigma-Aldrich, St. Louis, MO) to remove any particulate matter.

5.3.1.2 Sonocrystallization of ciprofloxacin nanoparticles using liquid anti-solvent precipitation with sonication

Ciprofloxacin crystallization was achieved by introducing 3 mL of ciprofloxacin in 0.1N hydrochloric acid solution (37.5 mg / mL) at 25 ºC into 50 - 300 mL of phosphate buffer pH 7 (U.S. Pharmacopeial Convention, 29) as the anti-solvent solution. Ciprofloxacin has a solubility of 70 µg/mL at pH 7 [152]. The drug solution was delivered through a PTFE tube with an internal diameter of 0.12 inch which was maintained 2 cm above the anti-solvent. The aqueous solution of CPF was pumped into the anti-solvent via a syringe pump (PHD 2000 Infusion, Harvard Apparatus, Holliston, MA) at a constant infusion rate of 1.25 mL/sec using a 3-mL syringe (BD Medical, VWR, Bridgeport, NJ). The experimental setup is shown in Figure 5.1. A solid ultrasound probe (tip diameter = 0.5 inches; Qsonica, Newtown, CT) which is suitable for processing 20-250

mL volumes of organic solvents or low surface tension liquids was used. The anti-solvent was cooled to 6 °C prior to each experiment in the refrigerator. The probe was immersed in the anti-solvent solution at a depth of 2 cm below the anti-solvent surface. The sonication was started immediately prior the addition of the drug solution to the anti-solvent and was continued for 10 min at 100% amplitude (20 kHz, Q700, Qsonica, Newtown, CT). The volume of the jacketed vessel containing the anti-solvent was either 100 mL (for 50 mL anti-solvent volume) or 600 mL (for > 50 mL anti-solvent volumes). The temperature of the anti-solvent solution was monitored during the process and cooled water was circulated through the jacketed vessel to control the temperature when required. The final suspension containing the crystallized nanoparticles was centrifuged (5.3 rotor, Sorvall ST 16R, Thermo Scientific, Waltham, MA) at 3000 rpm for 3 min to separate large titanium residue contamination released from the probe. Particle size analysis and zeta potential characterization were performed on the suspended nanoparticles. CPF nanoparticles in solid form were collected immediately after centrifugation by vacuum filtration using PVDF membrane filters (0.1µm, Durapore™ Membrane filters, Merck Millipore Ltd, Billerica, MA) and allowed to dry overnight at room temperature (25 °C).

Using the general method described above, the particle size distribution of the CPF nanoparticles was optimized to produce particles in the size range of below 150 nm by assessing the effect of the following experimental variables known to influence crystallization:

- Anti-solvent temperature
- Mixing during crystallization
- Addition of excipient stabilizer to the anti-solvent solution
- Solvent:anti-solvent volume ratio

- Anti-solvent composition
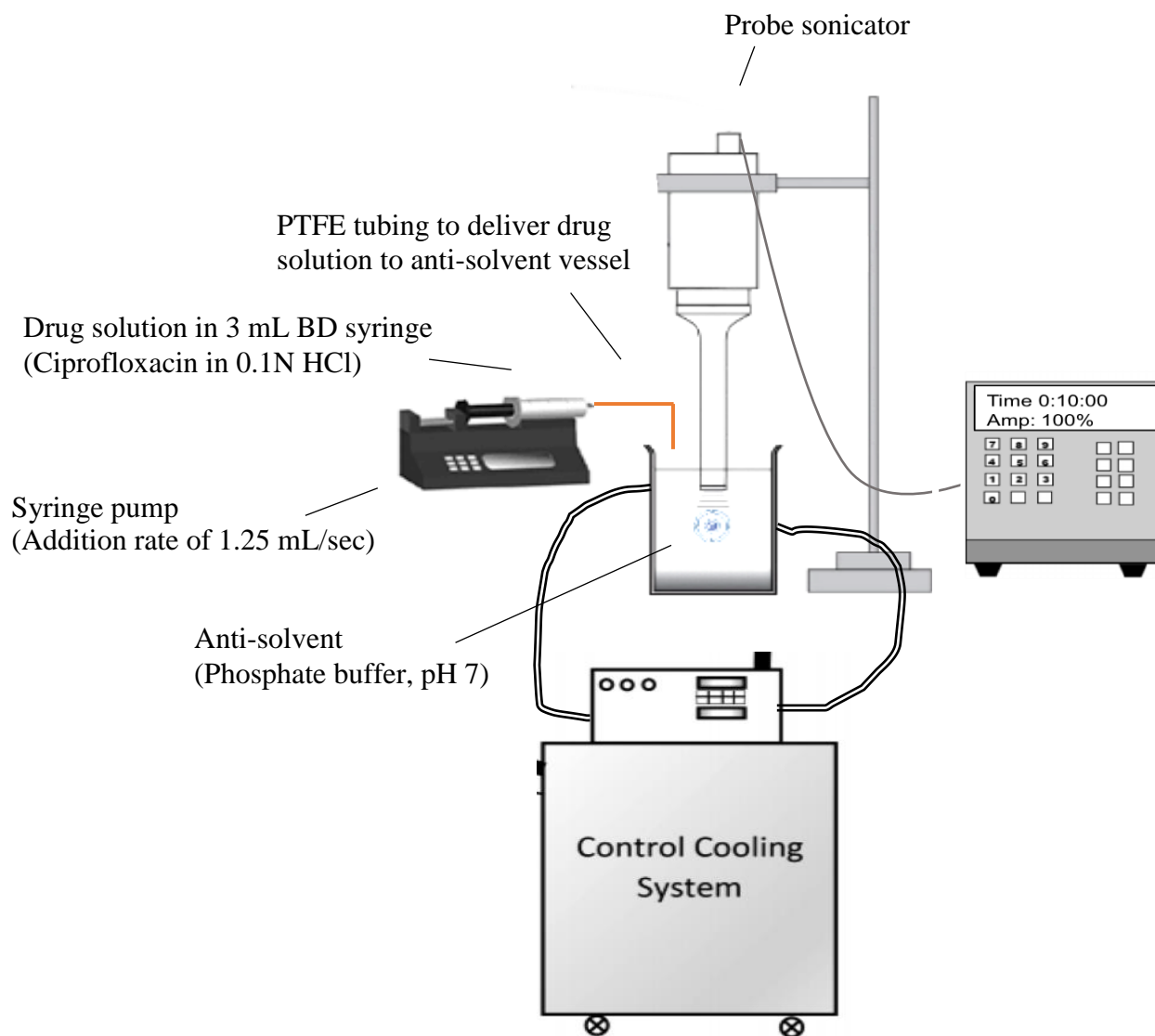
Figure 5.1. Schematic representation of the experimental setup for the liquid anti-solvent crystallization with sonication for ciprofloxacin (sonocrystallization technique)

5.3.1.3 Particle size optimization of ciprofloxacin nanoparticles

The experimental conditions are summarized in Table 5.1. After each experiment, the crystallized particles were characterized to determine their particle size distribution and zeta potential. In addition, the particles were characterized by differential scanning calorimetry (DSC) and thermogravimetric analysis (TGA) as described in Section 5.3.3.3. The goal of this study was to identify conditions that produced a stable nanoparticle suspension with particles in the size range of 100-200 nm.

5.3.1.3.1 Effect of anti-solvent temperature

The effect of anti-solvent temperature was assessed in the presence of probe sonication (Qsonica, Newtown, CT). Prior to each experiment, the anti-solvent was cooled to 6°C. The sonication process generates significant thermal energy that heats the anti-solvent during the crystallization. Without additional cooling, the temperature of the anti-solvent during sonication for 10 min increases to about 55 °C (Exp. 1). In order to assess the effect of anti-solvent temperature, a cooling water recirculating bath (Fisher Scientific, Asheville, NC) was used to maintain the anti-solvent temperature at 12°C throughout the crystallization process (Exp. 2). The temperature of the anti-solvent was monitored at defined intervals using thermocouples inserted into the reaction vessel (Easy View 10, Extech Instruments, Nashua, NH). In both studies, 3 mL of CPF solution (37.5 mg/mL) was introduced into 100 mL phosphate buffer pH 7 (Exp. 1 and Exp. 2). The solvent:anti-solvent ratio was 0.03. Characterization of CPF nanoparticles was assessed using the methods described in Section 5.3.3.

5.3.1.3.2 Effect of mixing during crystallization

Mixing during crystallization is important to ensure homogenous particle formation. In this study, mixing using the ultrasonic probe or a single blade paddle stirrer was compared. Mixing of drug solution with an anti-solvent solution was achieved by means of a paddle stirrer (Caframo stirrer type RZR 50, Wiarton, ON, Canda) (Exp. 3) and compared with probe sonication (Exp. 2). In the case of stirrer, a single blade paddle with the dimension of 5.1 x 2.5 x 1.5 cm was used with the stirring rate of 1000 rpm. Similar to the sonication approach, the stirring was initiated just before the addition of the drug solution and was carried out for 10 min. The anti-solvent temperature was maintained at 12°C and all other conditions were held constant.

5.3.1.3.3 Effect of the addition of excipient stabilizer to the anti-solvent solution

The effect of the addition of an excipient surfactant stabilizer was assessed by adding 0.01%w/v Tween™80 to the anti-solvent solution (Exp. 4). The crystallization conditions were as described in Table 5.1 with probe sonication and the anti-solvent temperature of 12°C.

5.3.1.3.4 Effect of solvent:anti-solvent volume ratio

The effect of solvent:anti-solvent ratio was assessed by increasing the volume of the anti-solvent. For this study, 3mL of solvent drug solution (37.5 mg/mL) was added to 250 mL of anti-solvent containing 0.01%w/v Tween 80 (Exp. 5), to produce a ratio of 0.012 and was compared to results obtained using a ratio of 0.03 (Exp. 4). The crystallization conditions were as described in Table 5.1 with probe sonication and the anti-solvent temperature of 12°C.

5.3.1.3.5 Effect of anti-solvent composition

Changing the anti-solvent composition was investigated by adding 20%v/v isopropanol to the phosphate buffer pH 7 anti-solvent. For these studies, as shown in Table 5.1, 3 mL of the CPF solution (37 mg/mL) was introduced to 3 volumes of the phosphate buffer pH 7 – isopropanol

153

(80:20 % v/v) anti-solvent mixture, 50, 100, and 250 mL (Exp. 6, 7 and 8), producing solvent –
anti-solvent ratios of 0.06, 0.03 and 0.012, respectively. Crystallization was performed using probe
sonication with an anti-solvent temperature and 12°C as shown in Table 5.1.

Table 5.1. Experimental conditions for the particle size optimization of ciprofloxacin nanoparticles.

Exp.	Solvent /Anti-solvent ratio (mL)	Anti-solvent temp. (°C)	Stabilizer	Mixing tool	Anti-solvent
1	3/100	55	-	Probe sonicator	Phosphate buffer pH7
2	3/100	12	-	Probe sonicator	Phosphate buffer pH7
3	3/100	12	-	Paddle stirrer	Phosphate buffer pH7
4	3/100	12	Tween™ 80 (0.01%w/v)	Probe sonicator	Phosphate buffer pH7
5	3/250	12	Tween™ 80 (0.01%w/v)	Probe sonicator	Phosphate buffer pH7
6	3/100	12	Tween™ 80 (0.01%w/v)	Probe sonicator	Phosphate buffer pH7: isopropanol (80:20%v/v)
7	3/250	12	Tween™ 80 (0.01%w/v)	Probe sonicator	Phosphate buffer pH7: isopropanol (80:20%v/v)
8	3/50	12	Tween™ 80 (0.01%w/v)	Probe sonicator	Phosphate buffer pH7: isopropanol (80:20%v/v)

In all experiments the drug concentration was 112.5 mg/ 3mL in 0.1N of HCl solution

5.3.2 Preparation of ciprofloxacin nanocomposites using spray drying

To prepare a powder for nasal administration containing ciprofloxacin nanoparticles, the Büchi Nano Spray Dryer B-90 (Büchi Laboratory Techniques, Flawil, Switzerland) was used to incorporate the nanoparticles into a 5-10 μm–sized nanocomposite powders with water soluble excipients. Studies were performed to develop a powder formulation suitable for nasal inhalation. The formulation variables that were investigated included the % solids concentration of the spray drying stock mixture, the drug:excipient ratios and the composition of excipients employed. The goal of this optimization was to produce a nanocomposite dry powder formulation which is easily dispersed and contains primary particles in the size range of 5 – 10 μm. The general procedure included initially suspending known masses of the optimized CPF nanoparticles (Section 5.3.1.3.5, Exp. 6) in water with the aid of stirring for 3 minutes using a magnetic stirrer. A solution containing the study excipients was then prepared in a water – ethanol solution. The nanosuspension and solution were then combined to produce a spray drying feed stock mixture in water and ethanol (80:20 %v/v). The final total solid concentration in this mixture was varied in the range of 0.4 – 4 %w/v, depending upon the individual experiment (Table 5.2). The following water soluble excipients were employed PVP K30, or mannitol, together with leucine as a dispersion enhancer and Tween™80 as the surfactant as components of the nanocomposite powder. The formulations tested are tabulated in Table 5.2 showing the spray drying stock mixture solids concentration and the nominal % composition of drug and excipient in the final powder formulation. The spray drying stock mixture was placed on a magnetic stirrer at 6 rpm (Corning®, Steuben County, NY) and the mixture was spray dried while continuously stirring. The following spray drying process conditions were used: drying airflow = 120 Lmin^{-1}, liquid feed rate = 50%, spray nozzle diameter (vibrating mesh) = 7μm, dryer length = 90 cm and inlet temperature = 80°C. The outlet temperature

was recorded as 45°C. The spray dried powders were collected from the spray drier electrostatic precipitator and placed in sealed capped vials and stored in a desiccator (approximately RH <10%) at room temperature.

Drug yield (%) was calculated using gravimetric analysis using the following equation of 5.1.

$$\% \text{ Yield} = \frac{\textit{Mass of dried ciprofloxacin spray dried formulation collected}}{\textit{Mass of drug in the stock mixture}} \times 100 \qquad \text{Equation 5.1}$$

The drug content of the spray dried powder was assessed by dissolving approximately 1.5 mg of powder (mass corrected for moisture content) in 50 mL of phosphate buffer pH 3. HPLC quantification was performed to determine the concentration of CPF in the solution and was used to calculate the mass of CPF per mg of spray dried powder (Section 5.3.3.4). The geometric particle size distribution of the spray dried powder was characterized using the HELOS/RODOS (Sympatec, GmbH, Clausthal-Zellerfeld, Germany) using the method described in Section 5.3.3.5.

Table 5.2. Spray drying feed composition and drug:excipient ratios in powder formulations

Exp.	Solid Conc. (%w/v)	Formulation composition (% w/w)				
		Drug	Leucine	Mannitol	PVP K30	Tween™80
1SD	0.4	22	22	54	-	2
2SD	0.7	22	22	54	-	2
3SD	1.0	22	22	54	-	2
4SD	4.0	20	20	58	-	2
5SD	2.0	20	20	-	58	2
6SD	3.0	21	21	-	56	2
7SD	4.0	22	22	-	54	2

5.3.3 Characterization of ciprofloxacin nanoparticle suspensions and spray dried formulations

5.3.3.1 Suspension nanoparticle sizing

The size distribution of the CPF suspensions following crystallization were assessed directly (without dilution) using the Malvern Mastersizer 2000 with the size measurement range of 0.02 μm to 2000 μm (Malvern Instruments, Ltd., Worcestershire, UK). The Hydro 2000G was used as liquid dispersion unit allowing characterization of wet samples. The corresponding anti-solvent was used as a dispersant for background measurements in each experiment. The suspension was added dropwise to the sample cell until an obscuration of ~10 – 30% was obtained. The optimized particle size measurement conditions to ensure particle deagglomeration without attrition employed sonication at 20% and a pump speed of 1000 rpm prior the measurement. Three measurements were performed for each formulation. Volume frequency versus particle size distribution plots, D10, 50 and 90 as well as Span were reported. Span is calculated as follow:

$$\text{Span} = \frac{D90 - D10}{D50}$$

Equation 5.2

5.3.3.2 Suspension nanoparticle zeta potential measurement

The Nanosizer NanoS (Malvern Instruments, UK) was used to characterize the zeta potential of the suspensions produced following crystallization. Suspensions were diluted to the final concentration of 0.01 %w/v using deionized water. A disposable folded capillary cell was used for the measurement.

5.3.3.3 Differential scanning calorimetry (DSC) and thermogravimetric analysis (TGA) of solid nanoparticles

Differential scanning calorimetry (DSC) thermograms were measured using a DSC Model 7 (Perkin-Elmer Inc., Waltham, MA) equipped with a data station Thermal Analysis Controller 7/DX and Pyris Software for Windows (version 3.81). Dry nitrogen gas was used as the purge gas through the DSC cell at a flow rate of 20 mL/min. Approximately 2 mg of nanoparticle powder samples were weighed into aluminum pans which were hermetically sealed. Each sample was allowed to equilibrate for 1 min at 30°C and then heated at a rate of 10°C /min to 350°C. Figure 5.2 shows a representative temperature program. Thermogravimetric analysis (TGA) was conducted using a Pyris 1 system (Perkin-Elmer Inc., Waltham, MA) to assess the residual moisture content in the CPF nanoparticles and in the spray dried formulations. Weight loss from 2 mg samples (dried ciprofloxacin precipitates or spray dried formulations) during heating at a rate of 10°C /min from 30°C to 350°C under nitrogen purge 40 mL/min was recorded.
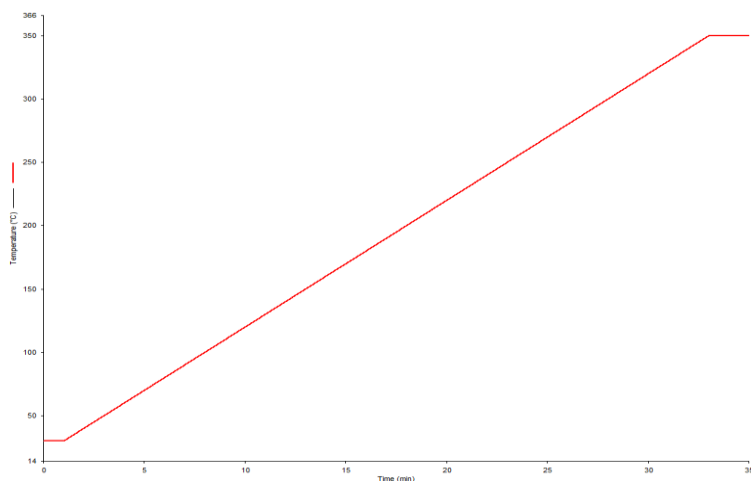
Figure 5.2. Temperature program used for DSC characterization of ciprofloxacin nanoparticles

5.3.3.4 Drug content measurement using high-performance liquid chromatography (HPLC) of spray dried nanocomposite formulations

Ciprofloxacin drug content was quantified using the USP 29 HPLC assay method for ciprofloxacin. The mobile phase contained a mixture of 0.025 M phosphoric acid previously adjusted with trimethylamine to pH 3.0 ± 0.1 and acetonitrile (87:13 %v/v). The HPLC method employed a Waters 2690 separation module, a 2996 PDA detector using the wavelength of 274 nm and the column used was a Hypersil Gold (4.6-mmx 15-cm, 5 μm pore size) maintained at a temperature of 27°C ± 2. The flow rate was 1.8 mL/min. Standard solutions in the range of 0.026 – 10.400 μg/mL were prepared in phosphate buffer pH 3 and used to test the linearity of the HPLC assay method (Table 5.3 and Figure 5.3). The precision of the method was assessed by calculation of % relative standard deviation (RSD) of the ciprofloxacin peak area following 6 replicate injections of 0.104 μg/mL ciprofloxacin standard solution. The same solution was used to assess the accuracy using 6 replicate injections and calculation of the concentration of ciprofloxacin relative to the nominal concentration. The limit of detection (LOD) and quantitation (LOQ) were calculated based on the equations of 3.1 and 3.2. The method validation results are summarized in Table 5.3. A representative HPLC chromatogram for 1.04 μg/mL ciprofloxacin standard solution is presented in Figure 5.4.

Table 5.3. System suitability parameters for the ciprofloxacin HPLC method

System suitability parameter	Value
Linearity range tested	0.026 – 10.400 (μg/mL), (r^2>0.9999)
Precision	0.9 %
Accuracy	99.7 %
LOD	0.02 (μg/mL)
LOQ	0.06 (μg/mL)
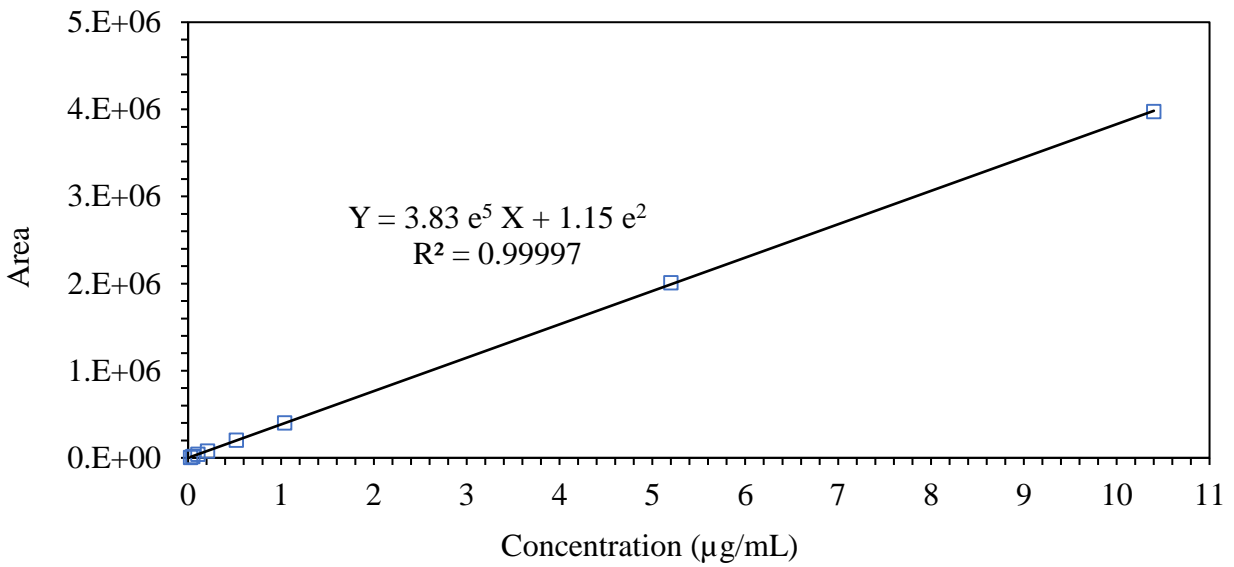
Figure 5.3. Plot of response (area) versus concentration for ciprofloxacin in the range of 0.026 - 10.400 (µg/mL) measured at 274 nm. The R^2 fitted by linear least square calculated as 0.99997.

The equation on the plot reads:

$$Y = 3.83\,e^5\,X + 1.15\,e^2$$
$$R^2 = 0.99997$$
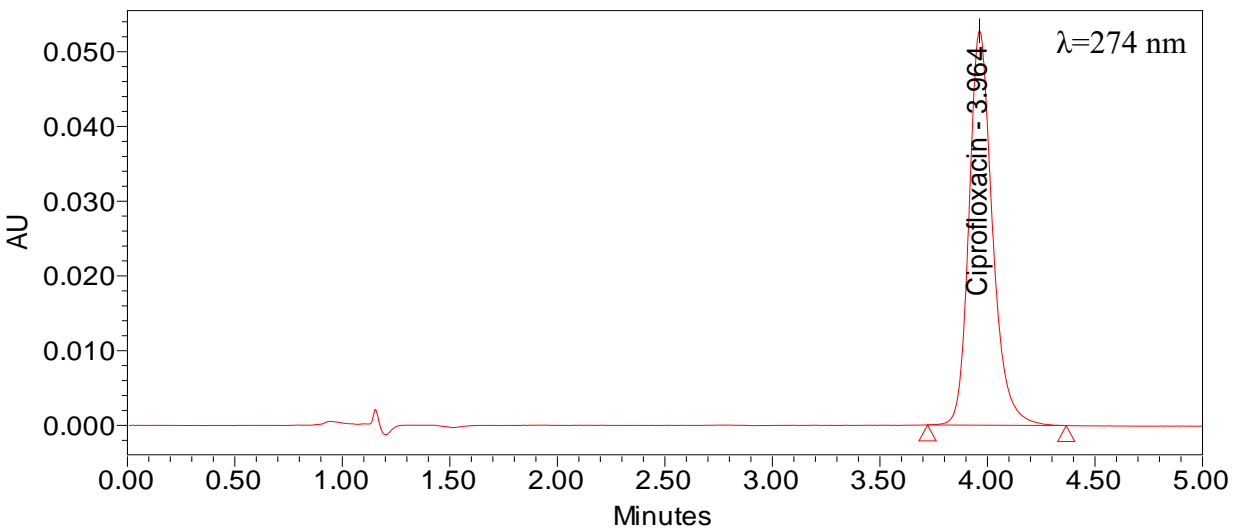
Figure 5.4. HPLC chromatogram of 1.04 µg/mL ciprofloxacin standard solution in phosphate buffer pH 3

161

5.3.3.5 Particle size analysis measurement using Sympatec HELOS/RODOS

The primary particle size of spray dried powder (ciprofloxacin nanocomposite formulations and unprocessed ciprofloxacin powder) was characterized using the HELOS laser diffraction technique (Sympatec GmbH, Clausthal-Zellerfeld, Germany) equipped with the RODOS/ASPIRO/L dispersion system. A small amount of test powder (about 3 mg) was filled in sample vials, sealed and placed in ASPIROS/L dosing device. A feed velocity of 60 mm/s and pressure of between 2 - 4.5 bar was used to disperse the powder sample into the measuring zone. The measurement was set to trigger when the optical concentration (Copt) exceeded 2.1%. The laser beam with measuring zone of 0.1- 35 μm were selected for these powder samples.

5.3.4 Development and evaluation of a nasal aerosol delivery method

5.3.4.1 Aerodynamic particle size characterization and emitted dose optimization for the nanocomposite formulation

The optimized spray dried nanocomposite powder was evaluated for their aerosolization characteristics in a series of dry powder inhalers (DPIs). A Next Generation Impactor (NGI; MSP Co., Shoreview, MN) was used to determine aerodynamic particle size characteristics of the CPF spray dried nanocomposite formulation. For each of the experiments, the impactor collection stages and pre-separator were coated with Molykore®316 silicone spray to minimize particle re-entrainment. About 3 mg of the spray dried nanocomposite formulation was filled into HPMC capsules (size 3). The dry powder inhalers evaluated were the Aerolizer® (Novartis AG), Handihaler® (Boehringer Ingelheim) and a VCU DPI designed to operate at low flow rates. The VCU DPI was previously described by Longest et al., 2015 and has a 2.3 mm flow orifice and a 3D rod array for powder dispersion in an orientation of 3 rods – 4 rods – 3 rods. The inhaler is denoted as the VCU DPI 2.3 – 343 and is shown in Figure 5.5 [126]. The DPI incorporates a flow control orifice, capsule chamber and flow passage containing the 3D rod array that for these studies

are attached to a streamlined nasal cannula with a single nasal exit prong. The nasal prong angle for the initial design of the device was 60º to the vertical plane of the nasal airway. Additional studies were also performed using a device in which the nasal prong angle was 90º to the vertical plane of the nasal airway. For the VCU DPI, the capsule was pierced twice using a 0.5 mm needle, as shown by the aperture location in Figure 5.5. The location was optimized previously by Behara et al [153]. For the other inhalers, the capsule was pierced using the in-built device mechanisms.

To perform the aerodynamic particle size analysis, the inhalers were actuated into the NGI through a pre-separator. For the Aerolizer®, it was operated at 80 Lmin⁻¹ for 3 sec (producing an approximate pressure drop of 2 kPa, [154]). For the Handhaler®, it was operated at 45 Lmin⁻¹ for 5.3 sec (producing a pressure drop of 4 kPa, [155]). For the VCU 2.3-343 DPI, an air flow rate through the device of 15 Lmin⁻¹ for 10 sec was supplied to the device. In each case, the inhaler was positioned such that the emitted aerosol was delivered to the NGI pre-separator. Following aerosolization, the CPF mass remaining in the device (including the capsule), deposited on the pre-separator, and on each of the impactor collection stages was collected by washing each item with 10 mL of phosphate buffer pH 3. Wash solutions were analyzed using a validated HPLC method to quantify the concentration of ciprofloxacin and calculate the deposited drug mass (Section 5.3.3.4). The emitted dose exiting the DPI was determined by subtracting the amount of CPF remaining in the DPI (including capsule) from the nominal loaded drug dose. The emitted dose was expressed as a % of the nominal dose. The initial dose of the drug loaded in the DPI was calculated from the weight of spray dried nanocomposite formulation (based on the dried mass after correcting for TGA determined water content) and the measured % CPF content in the nanocomposite formulation. The aerosol fine particle fraction (FPF<5µm$_{ED}$) and submicrometer particle fraction (FPF<1µm$_{ED}$), defined as the fraction of the emitted CPF dose with aerodynamic

diameters smaller than 5 μm and 1 μm, respectively. These were calculated using a linear interpolation method using a plot of the cumulative % drug mass less than the stated size versus aerodynamic diameter. Each measurement was repeated three times.
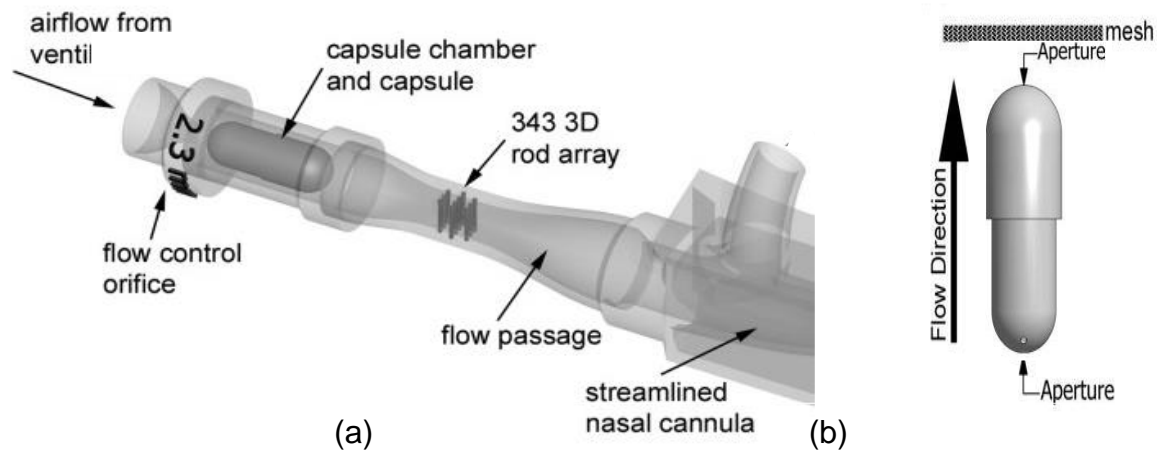
Figure 5.5. (a) Illustration of the VCU DPI 2.3 – 343 connected to a streamlined nasal cannula and (b) the site capsule piercing with a 0.5 mm needle

Similarly, the mass median aerodynamic diameter (MMAD) was determined at the 50th percentile on the cumulative % drug mass less than the stated size (probability scale) versus logarithmic aerodynamic diameter plot.

Cut off diameter for stages at each flow rate were calculated from the following equation based on USP (U.S. Pharmacopeial Convention, 2013):

$$D_{50,Q} = D_{50,Qn} \left(\frac{Qn}{Q}\right)^x$$

Equation 5.3

Based on USP equation, $D_{50,Q}$ is the cut-off diameter at the flow rate, Q that is employed. $D_{50,Qn}$ is the nominal value of cut-off diameter at a flow rate of 60Lmin^{-1} and the value of the exponent x is an emprical constant calculated for the archival NGI [156]. Table 5.4 shows the calculated cut-off diameters employed at the three study flow rates and we used to calculate the aerodynamic particle size distribution of the aerosols.

Table 5.4. Calculated NGI cut-off diameters for flow rates of 80 Lmin^{-1}, 45 Lmin^{-1}, and 15 Lmin^{-1} and used for the Aerolizer®, Handihaler® and VCU 2.3-343 DPIs respectively

	80 Lmin^{-1}	45 Lmin^{-1}	15 Lmin^{-1*}
Pre-separator	11.4	13.85	
Stage 1	6.9	9.41	14.1
Stage 2	3.84	5.18	8.61
Stage 3	2.44	3.26	5.39
Stage 4	1.45	1.90	3.30
Stage 5	0.81	1.09	2.08
Stage 6	0.46	0.65	1.36
Stage 7	0.28	0.41	0.98

*Calibration performed without including pre-separator [156]

In order to improve the emitted dose from the VCU 2.3-343 DPI, a series of modifications were investigated including, varying the needle size for capsule piercing, coating the DPI using a polytetrafluoroethylene (PTFE) suspension spray (LU™708, Sprayon™ Products, Cleveland, OH) [153] and removing the 3D-rod array from within the flow passage. For needle size, the larger needles from the Handihaler® were employed to increase the capsule hole size. The piercing orientation was kept constant as described above (Figure 5.5). In an attempt to reduce powder adhesion to the DPI, the inner surfaces of the DPI were coated using a PTFE suspension spray. The capsule chamber, flow passage and nasal cannula were coated. Following coating, compressed air was blown through the device until the surface appeared dry and then left at room temperature

for 30 min before use. The device was coated prior to each experiment to ensure reproducible surface coverage with PTFE. Finally, the 3D-rod array was removed from the flow passage to further reduce device retention (Figure 5.6). This device was originally developed by Dr. Longest's group for the dispersion of submicrometer powder aerosols with the 3D-rod array providing additional deagglomeration of submicrometer particles following initial dispersion in the capsule [126].

Emitted drug dose determination from the nasal prong of the VCU DPI 2.3 was performed by placing the prong in the center of the USP DUSA (dosage unit sampling apparatus). There was no seal between the DUSA and the nasal prong. The emitted aerosol was entrained in air flowing at 20 Lmin^{-1} for 10 sec drawn through the sampling apparatus. The DUSA and filter were washed with an appropriate volume of phosphate buffer pH 3 and the drug was quantified using the HPLC method for ciprofloxacin (Section 5.3.3.4).
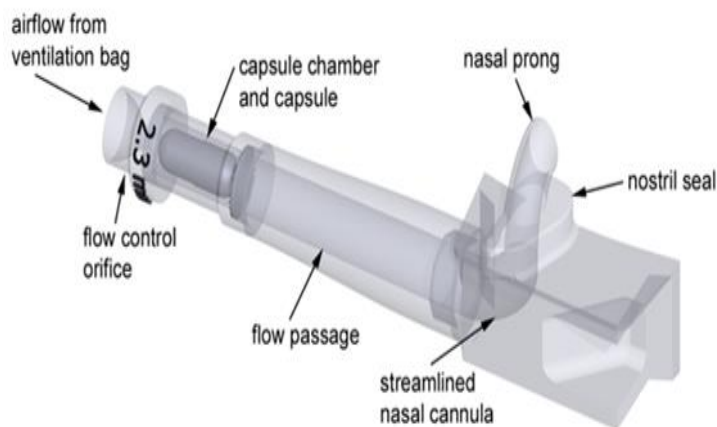
Figure 5.6. Illustration of the VCU DPI 2.3 connected to a streamlined nasal cannula. The 343 3D-rod array in the flow passage part is removed

5.3.4.2 Particle size characterization of the nanocomposite formulation emitted from the optimized VCU DPI 2.3 using the Malvern Spraytec®

The geometric particle size distribution (PSD) of ciprofloxacin nanocomposite aersols exiting from the VCU DPI 2.3-343 and VCU DPI 2.3 were also determined using a laser diffraction technique (Spraytec, Malvern Instruments Ltd, Worcestershire, UK). To assess the geometric diameter in an open environment, the device was mounted on a holder such that the nasal cannula prong was orientated perpendicular to the laser beam. A distance of 2.5 cm was maintained between the prong and the laser sensing zone. A respiratory filter (PulmoGuard II, Quest Diagnostics, Brockton, MA) was attached to a vacuum line operating at 30 Lmin^{-1} and placed under the nasal prong (at the distance of 10 cm) to capture the emitted dose after passage through the laser sensing zone. The loaded dose of ciprofloxacin nanocomposites was approximately 5 mg. As described previously, aerosols were generated using a flow rate of 15 Lmin^{-1} for 15 secs through the DPI. Particle size measurement begins when laser transmission is below 99%. Drug deposition on the filter was quantified by washing with an appropriate volume of phosphate buffer pH 3. HPLC analysis was performed to quantify the ciprofloxacin concentration and used to calculate the emitted dose from the device (Section 5.3.3.4).

5.3.4.3 Characterization of the dissolution and diffusion properties of the ciprofloxacin nanoparticles and nanocomposite formulations

A commercial Transwell® system was used to assess and compare the dissolution and diffusion properties of the ciprofloxacin nanoparticles and nanocomposite powder formulations. The Transwell® insert used was a polyester membrane (6.5 mm diameter and 0.4μm pore size; Corning®, Steuben County, NY). For this study, known amounts of CPF, as unprocessed ciprofloxacin (mean (SD) = 12.7 (0.5) μg), ciprofloxacin nanoparticles (mean (SD) = 14.0 (1.3) μg) and optimized nanocomposite (spray dried formulation) (mean (SD) = 9.0 (4.0) μg) were placed on the outer surface of the membrane (apical side, A-side) (Figure 5.7). 200 μL of phosphate

buffer pH7 (US Pharmacopeia 29) was added to the receiver compartment (B-side) and 800 µL of the same media was added to the 24 well plate (donor compartment), (Corning®, Steuben County, NY) containing a magnetic stirring bar (0.02 inches x 0.3 inches). These volumes of media were selected to have equal levels of buffer inside and outside of the Transwell® inserts to avoid any hydrostatic pressure and liquid transfer between chambers. The transport of ciprofloxacin solution through the Transwell® membrane was also assessed using a 0.625 µg/mL ciprofloxacin solution in phosphate buffer pH 3. For this study, 250 µL of this solution was diluted using 10 mL phosphate buffer pH 7 to have the final concentration of 15.6 µg/mL of ciprofloxacin. 800 µL of this solution was added to the donor compartment to produce 12.5 µg of ciprofloxacin in donor compartment. The rpm of the magnetic stir plate was set to 6 (Corning ®, Steuben County, NY). An addition experiment was performed to investigate the transport of unprocessed ciprofloxacin with the addition of 0.01% w/v Tween™ 80 in phosphate buffer pH7. The dissolution test was started by placing the insert inside the well plates. Samples of 200 µL were taken at 5, 10, 20, 30, 45, 60, 90,120, 180, 240, 270 and 300 min from the B-side and replenished with fresh dissolution media. After the final sample was taken, the membrane was washed with phosphate buffer pH 3 to analyze the amount of undissolved drug. Three replicates were performed for each experiment. The amount of dissolved drug dissolved at each time point (V x Ct) was determined by quantification of the drug concentration at each sample time point (C_t) using validated HPLC method for ciprofloxacin (Section 5.3.3.4) in the known volume (V) of 200 µL. This amount was added to the previous amounts dissolved (Q_{t-1}) to calculate cumulative amount of dissolved and transported drug over the 5-hour experimental period (Equation 5.4). This amount (Q_t) was divided by initial drug mass to calculate the cumulative percentage of drug dissolved and transported.

$$Q_t = Q_{t-1} + (V \times C_t) \hspace{4cm} \text{Equation 5.4}$$
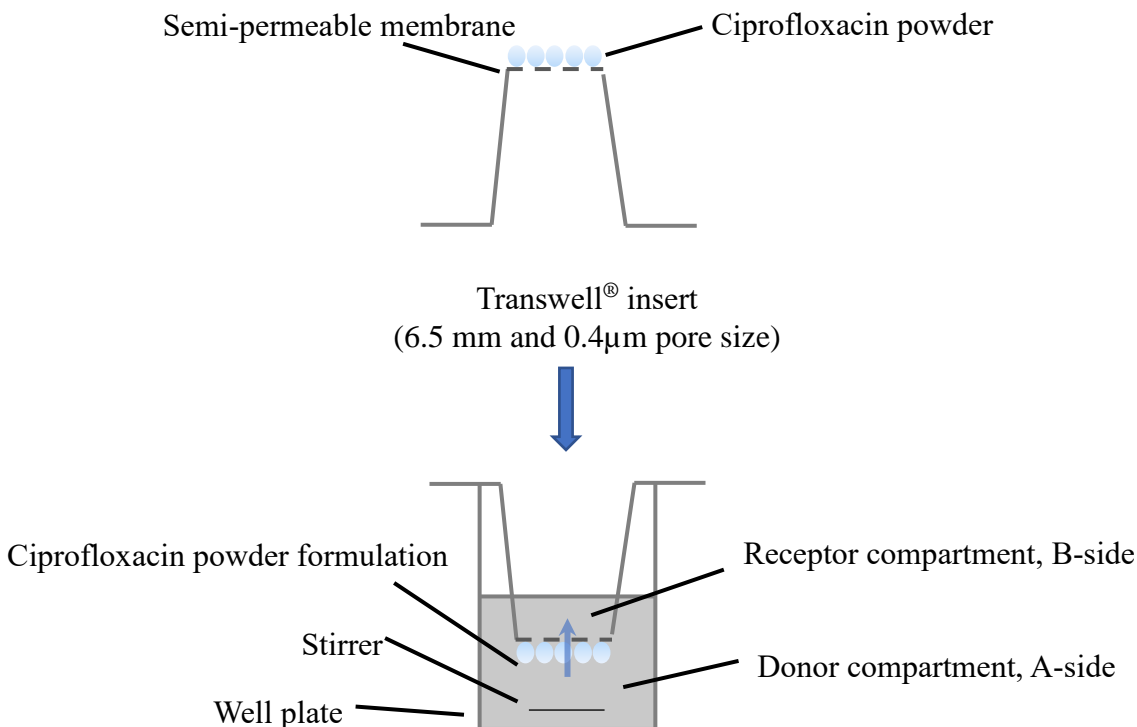
Figure 5.7. Schematic view of dissolution and transport setup for ciprofloxacin nanoparticle and nanocomposite formulations using a Transwell® system

5.3.4.4 Evaluation of the regional nasal deposition of ciprofloxacin nanocomposite formulations administered using the VCU DPI and a novel delivery method

In order to maximize nasal deposition of the CPF nanocomposite formulation, a novel delivery method was employed. The technique was developed by Dr. Longest (VCU School of Engineering) and optimized using computational fluid dynamic simulations. The method employs bolus aerosol delivery (via a soft mist spray, nebulizer or dry powder) in a fixed volume of air (vol = 0.1 - 1.25 L) at a low flow rate (1-15 Lmin^{-1}). The aerosol is delivered via a streamlined cannula with the nasal prong sealed in a single nostril of the nasal model. Using a low, but fixed volume of air allows the aerosol to penetrate into the nasal cavity and down to the pharynx and trachea. Simultaneously, the patient employs a rapid nasal exhalation that will facilitate the nasal deposition

in the nasal cavity as the aerosol is redirected through the other side of the nasal cavity and exiting via the open nostril.

The optimized ciprofloxacin nanocomposite formulation with a mean particle size of about 5 – 10 μm was evaluated for nasal drug delivery. The regional nasal drug deposition of formulation delivered using the VCU DPI in combination with the novel delivery method was evaluated a realistic airway geometry (VCU nasal model 1; Chapter 3). The experimental setup is shown in Figure 5.8. To enable the required simulated patient nasal exhalation and fixed volume aerosol delivery, a compressed air source was connected to a mass flow meter and a timer controlled three-way solenoid valve. The compressed air source was split to provide air to the VCU DPI and for the simulated patient exhalation. Flow control valves were used to control the flow rates and simultaneous delivery and exhalation were achieved by opening the timer controlled 3-way solenoid valve for the required duration. Two low pressure-drop flow meters (Sensirion SFM3000, Sensirion AG, Stafa, Switzerland) positioned before the DPI device and a respiratory filter was used to monitor flow rates. A respiratory filter was placed in the trachea region to collect drug that would have been delivered to the lungs. Finally, to collect the drug that was exhaled and not deposited in the realistic airway geometry, a respiratory filter was placed adjacent to the open nostril (right nostril) and was attached to a vacuum pump drawing air at the flow rate of 60 – 90 Lmin^{-1}.

The regional nasal drug deposition was evaluated using combinations of DPI actuation flow rates of 15 and 10 Lmin^{-1} provided to the VCU DPI with simulated patient exhalation flow rates of 60 and 90 Lmin^{-1}. The DPI actuation flow and expiratory flow were administered simultaneously for 15 sec. For some experiments, the nasal model was coated with Brij mixture in ethanol and glycerol (1mL of Brij 35 dissolved in 10 mL ethanol and diluted with 50 g glycerol)

to simulate nasal fluid lining and investigate potential powder bounce on the nasal model surface [157]. For this purpose, the nasal model was filled with the Brij 35 ethanol – glycerol mixture, then drained and left at room temperature to dry for 30 min.

In all experiments, approximately 5.0 mg of nanocomposite powder formulation was filled in a size 3 HPMC capsule and manually pierced as described in section 5.3.4.1. The experimental conditions for each study are summarized in Table 5.5. The nasal cannula prong was sealed in the left nostril of VCU nasal model 1. Following aerosol delivery, the DPI, capsule, nasal model parts and respiratory filters were washed using the appropriate volume of phosphate buffer pH 3 to extract the drug which was then quantified using the HPLC method to determine the regional distribution of the drug powder mass.

Table 5.5. Experimental conditions used for optimization of regional drug deposition of the ciprofloxacin nanocomposite powder formulation tested in VCU nasal model 1

Exp.	DPI actuation airflow (Lmin⁻¹)	Exhalation airflow (Lmin⁻¹)	Nasal cannula (º)	Nasal model coated	VCU DPI
1NASAL	15	60	60	N	2.3-343
2NASAL	15	60	60	Y	2.3-343
3NASAL	15	90	60	Y	2.3-343
4NASAL	15	90	90	Y	2.3-343
5NASAL	10	90	90	Y	2.3-343
6NASAL	10	90	90	Y	2.3-coated
7NASAL	10	90	90	Y	2.3-FormLabs clear resin-coated
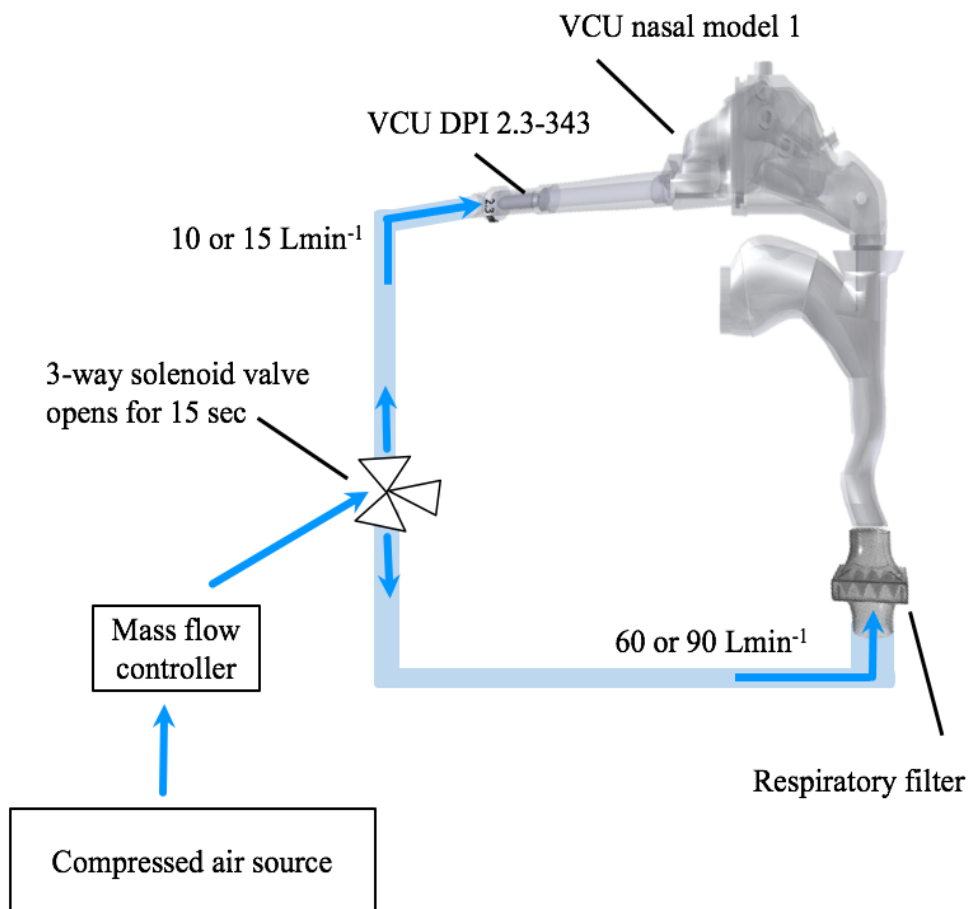
Figure 5.8. Experimental setup for nasal administration of ciprofloxacin nanocomposite formulation using the VCU DPI in VCU nasal model 1

5.3.5 Development of a realistic nasal airway model incorporating cell monolayers into the airway passage walls to investigate transepithelial transport after realistic nasal deposition

5.3.5.1 Modification of VCU nasal model 1 to incorporate cell monolayer Transwell® inserts into the nasal airway passage walls

The physically realistic nasal model used in previous studies was modified to allow assessment of post nasal deposition events (e.g. transepithelial transport) on cell monolayers positioned in the nasal airway passage walls. The ability to deposit drug particles on cell monolayers realistically following nasal inhalation would be desirable compared to current approaches. The physically realistic VCU nasal model 1 was modified to accommodate two Transwell® inserts (TW) in its middle (TW1 and TW2) meatus region) and one insert in the superior (TW3) meatus region as shown in Figure 5.9. The TWs were inserted in sampling ports such that the outer membrane surface was aligned with the nasal airway surface wall allowing for realistic deposition of nasally administered drugs.
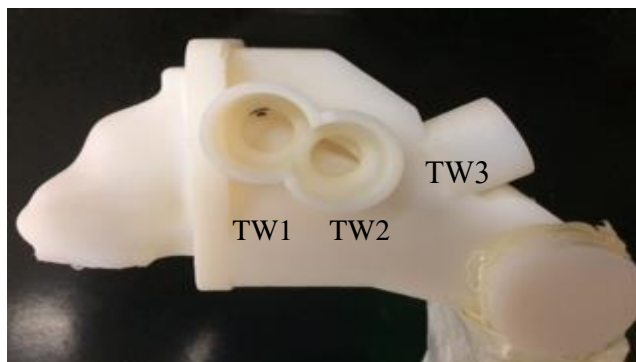
(a)   (b)

Figure 5.9. (a) VCU nasal model 1 modified to accommodate three Transwell® inserts in middle passages. Two Transwell® inserts in its middle (TW1 and TW2) meatus and one insert in the superior (TW3) meatus region (b). Transwell® insert membrane is polyester (PET) with diameter of 6.5 mm and surface area of 0.33 cm^2

Initial studies were performed by placing the Transwell® inserts in the modified VCU nasal model 1 in the absence of cells to determine the mass deposition following administration of the ciprofloxacin nanocomposite formulation delivered using the VCU DPI. An additional unprocessed ciprofloxacin powder was also aerosolized using the same method. The internal surfaces of the realistic airway model (modified VCU nasal model 1) were pre-coated with Brij 35. Known masses (approximately 6 mg) of the ciprofloxacin nanocomposite spray dried formulation (drug content = 20. 8%w/w) or ciprofloxacin un-processed powder (CPF) were filled into size 3 HPMC capsules and placed in the VCU DPI 2.3. The DPI was coated with PTFE and the nasal cannula prong angle was 90º. The nasal prong was sealed in the left nostril of VCU nasal model 1 and aerosol was delivered using a flow of 10 Lmin^{-1} through the DPI with a simultaneous nasal exhalation at 90 Lmin^{-1} for 5 sec. After nasal administration of the powders, the Transwell® inserts were removed and the amount of drug deposited on each Transwell® inserts, together with the remaining drug deposited on the DPI, on nasal model walls, and the lung and exhalation filters were determined by collecting the drug from each deposition site using appropriate volumes of phosphate buffer pH 3 wash solution. The concentration of drug in each solution was determined using the previously described HPLC method (Section 5.3.3.4) and then used to determine the regional mass distribution of the delivered dose (for comparison with previous studies). In addition, replicate experiments were performed to investigate the reproducibility of drug deposition on the three TW surfaces.

5.3.5.2 Preparation of Calu-3 cell monolayers on apical surface of Transwell® inserts

Human bronchial epithelial cells, Calu-3 cell line, was received from ATCC® HTB-55 at passage numbers between 18 and 25. The cells were thawed based on the manufacturer protocol. Next, the cells were seeded at the density of 0.1×10^6 cells/cm^2 in a 25 cm^3 culture flask (Corning® polystyrene, VWR, Radnor, PA), and grown using Eagle's minimum essential medium (EMEM, Lonza, Walkersville, MD) (pH = 7 - 7.4) which was supplemented with 10% fetal bovine serum albumin (FBS; VWR, Radnor, PA) and 1% penicillin-streptomycin (PS; potassium penicillin (10,000 U/mL) and streptomycin sulfate (10,000 µg/mL) in 0.85% saline, Lonza, Walkersville, MD) in the incubator (Symphony 5.3 A, VWR, Radnor, PA) providing 5 % CO_2, 95 % CO_2 at 37°C. The culture media was changed every other day until the monolayer reached to 70 – 80 % confluency at days 5 – 7. At this point, cells were sub-cultured to a 75 cm^3 culture flask based on ATCC protocol using EDTA-Trypsin (Trypsin 0.25% and EDTA 0.02%, Quality Biological, Inc., Gaithersburg, MD) or seeded on the inverted surface of the Transwell® insert membrane (Polyester, 6.5 mm, 0.4µm) (Corning®, Steuben County, NY). Communication with the Transwell® inserts manufacturer indicated that the surface characteristics of the inverted surface (coating, pore size) should be identical to the conventional surface that is normally employed to grow the cell monolayer.

For seeding the cells on the Transwell® insert membrane, inverted inserts were placed in a 150mm culture dish (Corning®, Steuben County NY) and appropriate volume of cell suspension in the growth media, (EMEM, 10% FBS and 1% PS) was added to the outer surface of the inverted Transwell® inserts to have a cell density of 0.1×10^6 cells/cm^2. The lid was placed on the culture dish containing the inverted transwell® inserts and they were kept in the incubator overnight.

The next day, the Transwell® inserts were inserted into a 24-well plate and 600 µL and 100 µL of the growth media was introduced to the apical (A-side, cells are present) and basolateral (B-side) sides, respectively, to grow the cells under liquid-covered culture (LCC) conditions. The media on both sides was replaced every day.

5.3.5.3 Calu-3 epithelial cell integrity

The integrity of Calu-3 cell monolayer was assessed visually on days 12- 16 using an inverted microscope and by measuring the transepithelial electrical resistance (TEER) using an epithelial voltammeter equipped with chopstick electrodes, EVOM2 (World Precision Instrument (WPI), Sarasota, FL). Before the measurements, the cells were equilibrated with fresh culture media in both A and B sides for 15 minutes in the incubator (5 % CO_2, 95 % CO_2 at 37°C). The measured TEER was corrected first by measuring the TEER for a blank insert (no cells) and then the surface area considered. The TEER was reported as Ω cm^2. Cell monolayers with a TEER value in the range of 750-900 Ω cm^2 were considered confluent and suitable for use in the transepithelial transport study. The TEER measurement was repeated 1hr at the end of transport study and 12 hours later.

5.3.5.4 Transepithelial transport across the Calu-3 cell line after realistic nasal deposition

Prior to the deposition experiment, 300 µL fresh growth media (or HBSS; Hank's Balanced Salt Solution) was added to the B-side, then three Transwell® inserts with cell monolayers were inserted in the three sampling ports in the modified VCU nasal model 1. In order to maintain the integrity of the cell monolayer, nasal powder delivery was performed within 10 minutes using the method described previously (Section 5.3.4.4). The inserts were immediately removed from airway model and placed cell monolayer faced down in a 24-well plate. Fresh growth media or

HBSS (40 µL) was placed in the 24-well plate covering the cell monolayer surface with a thin layer of media to prevent cell shrinkage during the transport studies (Figure 5.10).

The transport studies carried out over 5 hours and the media on the B-side was removed every hour and replenished with the fresh media. After 5 hours, the A-side was washed three times with the 600 µL of fresh media, acidified with 200 µL of phosphoric acid (85%) (Fisher Chemicals, Asheville, NC) and sonicated for 30 minutes. Collected samples were analyzed by the HPLC method described in section 5.3.3.4 to determine the concentration of ciprofloxacin in each sample and the mass of drug transported. The percent cumulative mass transported across the Calu-3 cell monolayers was calculated based on the mass transported (measured concentration x B-side volume) at each time point and expressed as a percentage of the initial deposited dose. The initial deposited dose was estimated as the sum of the cumulative mass transported over the 5 hours plus the mass recovered from the A-side after 5 hours.

The cumulative ciprofloxacin mass transport – time profile was determined for each Transwell® insert and plotted to calculate the Flux value:

$$J = (\frac{dM}{dt})/A \hspace{6cm} \text{Equation 5. 5}$$

In which J is the flux (the cumulative mass flow rate through the unit area of the surface) and dM/dt is the linear slope for steady-state transport of ciprofloxacin in the plot (calculated between 1 to 5 hours) and A is the surface area of the Transwell® used (0.33 cm^2).
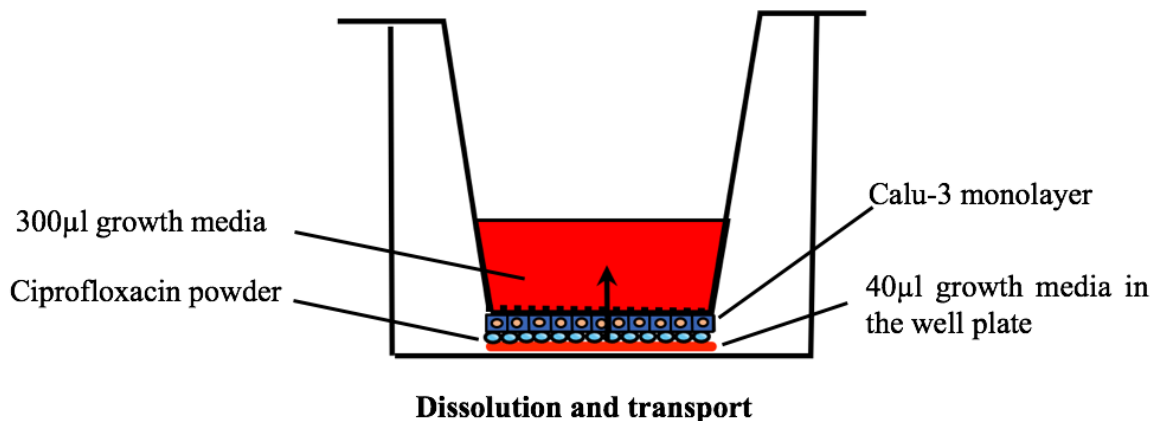
Figure 5.10. Schematic representation of the transepithelial transport study following realistic deposition of the ciprofloxacin nasal powder formulation

5.4 Results and Discussion

5.4.1 Nanoparticle preparation

5.4.1.1 Particle size optimization of ciprofloxacin nanoparticles

The primary parameter used to evaluate the nanoparticles was geometric particle distribution in the suspension mixture following crystallization. The particle size distribution results for each of the process optimization studies are summarized in Table 5.6 and discussed below. For each of the experiments, the time for visual appearance of the particulate precipitate was also recorded and summarized in Table 5.6 as the induction time.

5.4.1.2 Effect of anti-solvent temperature

As demonstrated in Figure 5.11, using the 100mL precooled anti-solvent at 6°C in combination with sonication at 100 % amplitude, the anti-solvent temperature was observed to rise to 55°C during the process. To control the temperature during the crystallization process, a

179

recirculating cooler system was employed to minimize the change in anti-solvent temperature. Using the cooler system at a temperature of 6 °C during 10 min sonication at amplitude of 100% produced an anti-solvent temperature of about 12°C. The particle size distribution of the precipitates formed under these two anti-solvent temperature conditions are shown in Figure 5.12 and Table 5.6 (Exp. 1 and 2). As demonstrated, crystallization at a controlled temperature of 12 °C using the controlled temperature system produced particles with a small size with the mean (SD) Dv50 of 0.28 (0.12) µm. Crystallization using the un-controlled system, in which the anti-solvent temperature rose to 55°C, resulted in ciprofloxacin precipitates with a larger particle size, the mean (SD) Dv50 was 2.19 (1.24) µm, although there was a narrow distribution around the median diameter with a Span of 1.3.

The pH of the anti-solvent following the addition of 3 mL ciprofloxacin solution to the 100 mL anti-solvent phosphate buffer changed from pH 7 to 6.8. It is expected that at this pH, ciprofloxacin as a zwitterion, will exhibit low solubility. It has been reported that the solubility of ciprofloxacin in water can be increased from 67 µg/mL to 158 µg/mL by increasing the temperature from 20°C to 50°C. Yu et. al [79] reported at pH 6.8 that increasing the temperature from 6°C to 40 °C resulted in a CPF solubility increase from about 60 µg/mL to 240 µg/mL. Therefore, the formation of larger precipitates under the higher temperature conditions can perhaps be explained by increased solubility of ciprofloxacin in the solvent-anti-solvent mixture at that temperature. Controlling the anti-solvent temperature at 12°C reduces the solubility of ciprofloxacin at pH 6.8, producing higher supersaturation leading to an increased nucleation rate. In this case, more nuclei will form and the particle size of the crystallized particles will be smaller. It was also observed that under these conditions, there was a relatively large polydispersity of the nanoparticles, with a Span of 13.9. As demonstrated in Table 5.6 the appearance of the precipitates

is faster when the smaller particles are formed using the controlled lower temperature conditions with the higher nucleation rate (Exp.2).

In addition, increasing the temperature of the anti-solvent can change the interfacial tension and perhaps reduce the viscosity of anti-solvent. This can alter the mixing in the reaction mixture producing an increased molecular transport rate from the solution to the crystal surface by diffusion, convention or a combination of the two processes and increased particle collision frequency. Also, the increased temperature of the anti-solvent can enhance the reaction rate for the incorporation of additional crystals to particle surfaces and result in more particle growth [158, 159]. It has also been reported that Ostwald ripening is reduced at lower temperatures [106]. Ostwald ripening is one of the major mechanisms causing widening of particle size distribution of drug nanoparticles suspensions. Lifshitz et al. [160] reported that smaller particles (with diameters smaller than the critical diameter) dissolve due to their high surface energy and will be transported onto the surface of the larger particles causing particle growth. The main factors which cause growth of particles by Ostwald ripening are reported as the polydispersity of nanoparticles formed, drug solubility in the solvent / anti-solvent systems, and the amount of organic solvent in final suspension [161].

From this study, it was concluded that for future studies using probe sonication the temperature of the anti-solvent should be controlled using recirculating cooler.
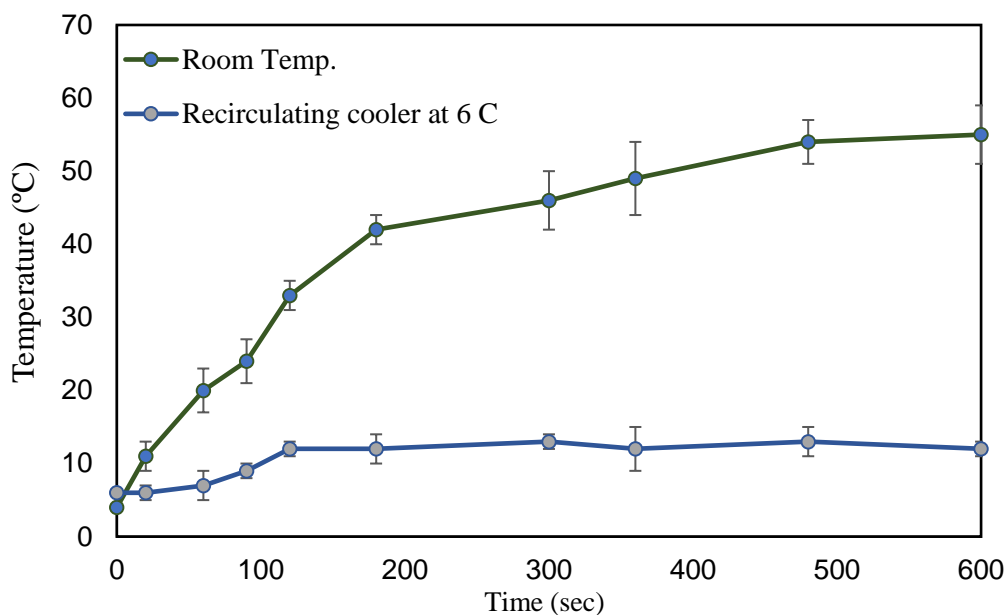
Figure 5.11. Anti-solvent temperature monitored during sonocrystallization of ciprofloxacin. The volume of anti-solvent (phosphate buffer pH=7) was 100 mL. The probe sonication was 100% amplitude for 10 min. Results are presented as mean (error bars are SD), n = 3
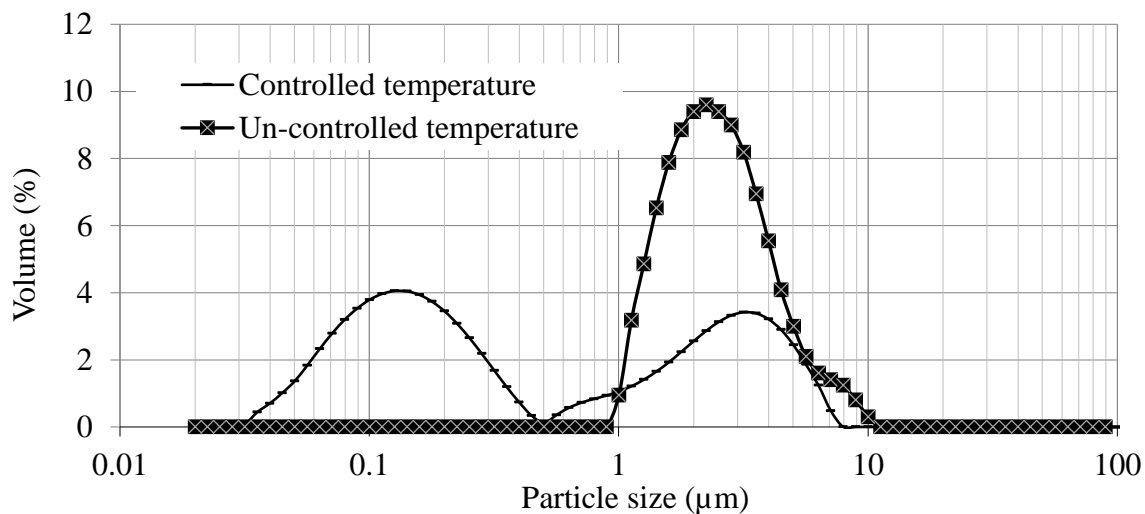
Figure 5.12. Representative volume frequency distribution of ciprofloxacin particles precipitated in phosphate buffer pH 7 under continuous sonication. 3 mL of ciprofloxacin (37.5 mg/mL) solution was added to 100 mL anti-solvent

Table 5.6. Effect of formulation and process variables on the particle size distribution of ciprofloxacin precipitates measured by Malvern Mastersizer. Results are presented as mean (SD) (n =3).

Exp.	Size distribution (µm)			Span	Zeta potential (mv)	Induction time (sec)
	Dv10	Dv50	Dv90			
1	1.41 (0.35)	2.19 (1.24)	4.17 (0.68)	1.3	-7.4 (0.3)	180
2	0.08 (0.01)	0.28 (0.12)	3.96 (0.57)	13.9	-9.2 (2.1)	100
3	2.46 (0.44)	7.84 (2.45)	43.34 (4.35)	5.2	0.1 (0.1)	420
4	0.09 (0.01)	0.19 (0.9)	1.1 (0.24)	5.3	-11.8 (1.1)	100
5	0.09 (0.01)	0.64 (0.21)	1.1 (0.92)	1.6	- 9.3 (0.7)	140
6	0.07 (0.01)	0.12 (0.01)	0.24 (0.01)	1.4	- 12.8 (0.3)	20
7	0.06 (0.01)	0.13 (0.01)	0.95 (0.03)	6.8	-10.6 (1.0)	100
8	0.08 (0.01)	0.23 (0.01)	4.74 (0.85)	20.3	- 8.2 (1.0)	100

Exp. 1 and 2 compares the effect of antisolvent temperature (55°C and 12°C, respectively) at solvent:anti-solvent ratio of 0.03.
Exp. 2 and 3 compares the effect of mixing type (paddle mixing and probe sonication, respectively) at solvent:anti-solvent ratio of 0.03 at 12°C.
Exp. 3 and 4 compares the effect of addition of surfactant stabilizer (Tween™ 80 (0.01%w/v)) at solvent:anti-solvent ratio of 0.03 at 12°C.
Exp. 4 and 5 compares the effect of solvent:anti-solvent ratio in the presence of Tween™ 80 (0.01%w/v) at 12°C.
Exp. 6, 7 and 8 compares the effect of anti-solvent composition and solvent:anti-solvent ratio in the presence of Tween™ 80 (0.01%w/v) at 12°C.

5.4.1.3 Effect of mixing during crystallization

The results presented in Table 5.6 (Exp. 2 and 3) reveal that the use of ultrasonic mixing compared to paddle mixing significantly reduced the particle size distribution of the CPF nanoparticles. There was a lower induction time (appearance of CPF precipitates in anti-solvent vessel) of 100 sec with probe sonication assisted precipitation compared to 420 sec for the paddle mixing conditions. Micrometer-sized CPF precipitates with a mean (SD) median volume diameter of 7.84 (2.45) µm (Dv50 measured by Malvern Mastersizer) were produced by paddle mixing, compared to nanoparticles with a mean (SD) median volume diameter of 280 (120) nm during ultrasonic mixing. However, as shown in Figure 5.13, both mixing conditions produced bimodal particle size distributions using the test experimental conditions. Similar results were reported with respect to the use of ultrasound and paddle mixing for the preparation of griseofulvin particles [106, 162].

It has been reported that the use of ultrasound results in more rapid and uniform mixing of the two liquid streams (reflected in the shorter induction time) which results in the production of cavitation energy together with the generation of supersaturation. This produces a rapid nucleation rate and the precipitation of smaller particles. In addition, ultrasound energy can breakdown the larger particles and agglomerates to a smaller particle size [163, 164]. In case of ciprofloxacin, the use of ultrasound showed the positive effects on the particle size distribution.
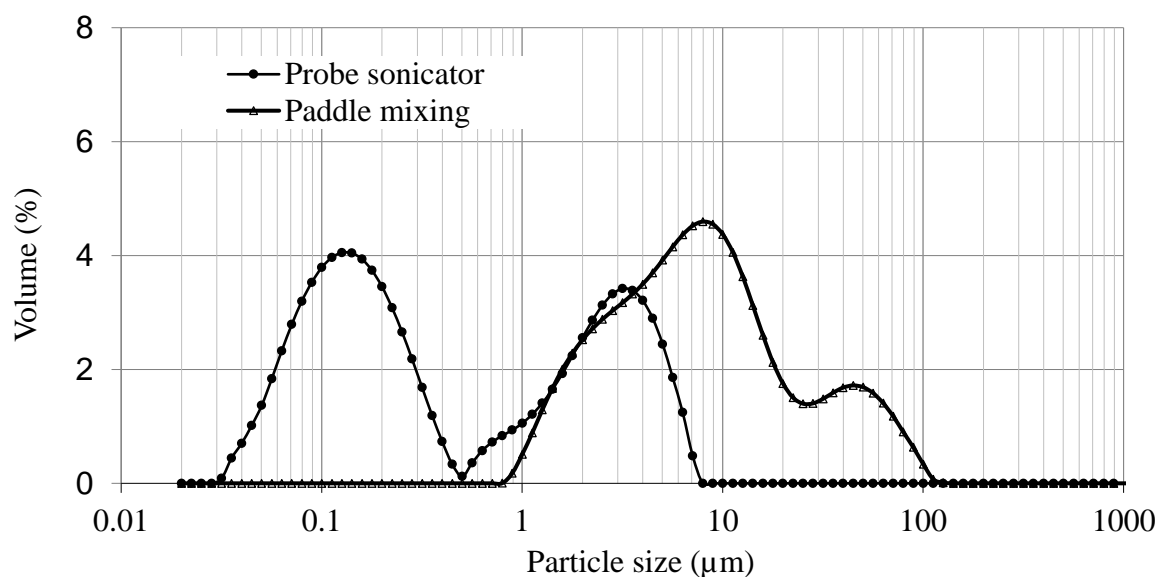
Figure 5.13. Representative volume frequency distribution of ciprofloxacin particles precipitated in phosphate buffer pH 7 under continuous probe sonication using an anti-solvent temperature of 12˚C. 3 mL of ciprofloxacin (37.5 mg/mL) solution was added to 100 mL anti-solvent with or without Tween™ 80 (0.01%w/v)
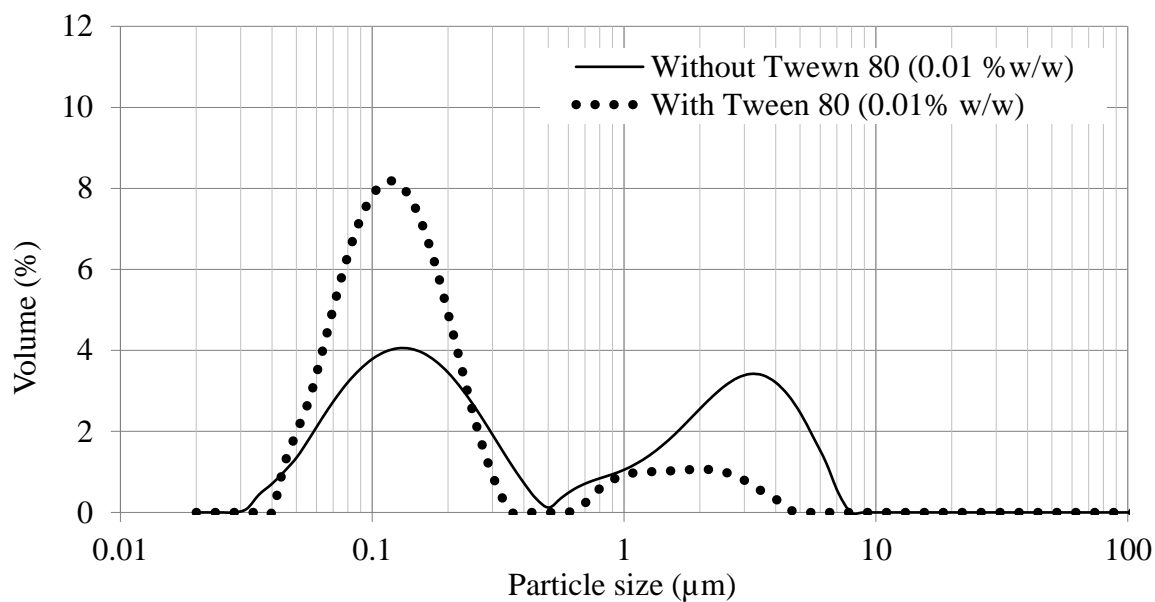
Figure 5.14. Representative volume frequency distribution of ciprofloxacin particles precipitated in phosphate buffer pH 7 under continuous probe sonication using an anti-solvent temperature of 12˚C. 3 ml of ciprofloxacin (37.5 mg/ml) solution was added to 100 ml anti-solvent with or without Tween™ 80 (0.01%w/v)

5.4.1.4   Effect of the addition of excipient stabilizer to the anti-solvent solution

A decrease in particle size to nano-scale is accompanied by an increased surface area to volume ratio. This large increase in surface area potentially creates excessive surface energy, which may be thermodynamically unfavorable and produces un-stable formulations and particle growth [164, 165]. Since crystal growth is a surface phenomenon, impurities (or stabilizers) that adsorb at the crystal surface can potentially affect the crystal growth rate and alter the crystal shape [166]. It is known that the adsorption of ionic and non-ionic surfactants and polymers onto the surface of crystals at the solid – liquid interface is accompanied by a reduction in interfacial tension, blocking the surface from further particle adsorption and an increase in the nucleation rate [106, 164, 166-168]. Examples of surfactants include cetyltrimethylammonium bromide (CTAB) Tween™ 80, Pluronic®127, sodium dodecyl sulfate (SDS). Examples of polymers include HPMC and PVP.

Therefore, to produce a stabilized ciprofloxacin nanoparticle suspension, the effects of the addition of a stabilizer to the anti-solvent was investigated. For this purpose, a nonionic surfactant, Tween™ 80 (Polysorbate 80) at a concentration of 0.01% w/v was added to the 100 mL phosphate buffer pH 7. (Tables 5.1 and 5.6, Exp. 4 and 2). It is hypothesized that Tween™ 80 will compete with ciprofloxacin particles to adsorb to the formed surface and inhibits surface growth. The combined effect of ultrasound and 0.01% w/v Tween™ 80 produced a larger fraction of submicrometer CPF precipitates and reduced the micron sized portion of the distribution, the mean (SD) Dv50 was reported as 0.19 (0.9) µm and the Dv90 was 1.1 (0.24) µm (Table 5.6 and Figure 5.14). It is believed that the amount of surfactant or polymer added to the system should enable complete coverage of the large surface area of the nuclei.

5.4.1.5 Effect of solvent:anti-solvent volume ratio

The solvent:anti-solvent ratio was varied by increasing the anti-solvent volume, from 100 mL to 250 mL in the presence of 0.01%w/v Tween™ 80 (Tables 5.1 and 5.6, Exp. 4 and 5). By increasing the anti-solvent ratio volume and reducing the solvent:anti-solvent ratio, the solvent content in the mixture of solvent – antisolvent reduces, therefore it is expected to reduce the degree of particle growth due to Ostwald ripening and observe smaller and narrower particle size distribution. As the results show in Table 5.6 and Figure 5.15 (Exp. 4 and 5), increasing the anti-solvent volume, and decreasing the solvent:anti-solvent ratio did not result in smaller particle size distribution. This might be due to reducing the effectiveness of the ultrasonic mixing for the larger volume of the antisolvent used. It is hypothesized that mixing was not as effective and slower in the larger volume compared to a smaller volume and there was potentially slower generation of supersaturation, followed by a slower nucleation rate. Dalvi et al., [106] observed a similar effect on the particle size of griseofulvin precipitates when increasing the anti-solvent volume under sonication due lower quality of mixing.
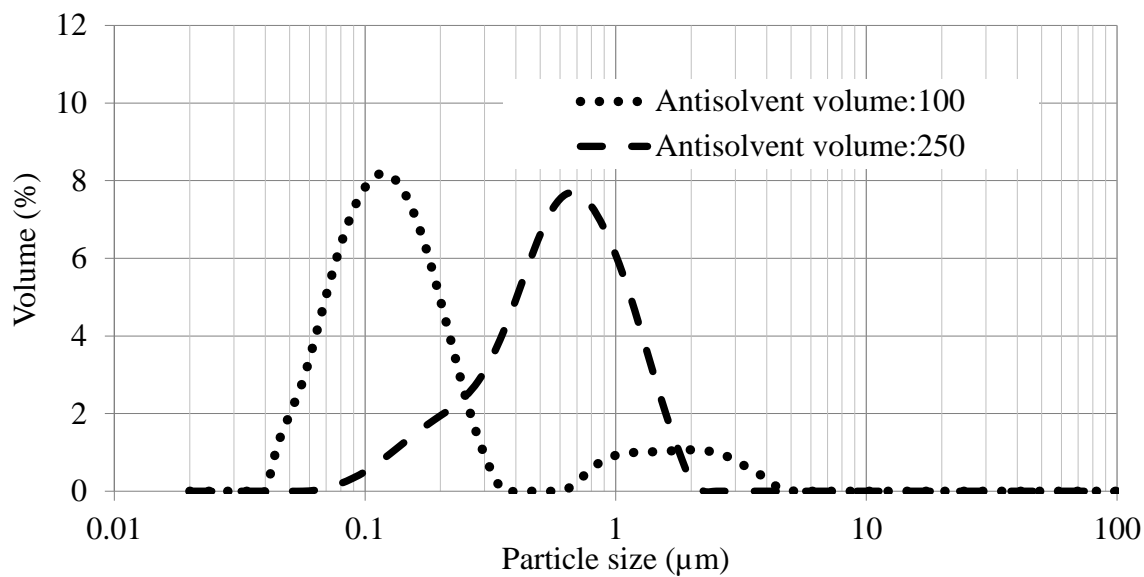
Figure 5.15. Representative volume frequency distribution of ciprofloxacin particles precipitated in phosphate buffer pH 7 under continuous probe sonication using an anti-solvent temperature of 12˚C. 3 mL of ciprofloxacin (37.5 mg/mL solution) was added to 100 or 250 mL anti-solvent in the presence of Tween™ 80

5.4.1.6 Effect of anti-solvent composition

Isopropanol as an organic non-solvent for ciprofloxacin was selected to be added to the anti-solvent phosphate buffer pH 7. The solubility of ciprofloxacin in isopropanol at 20°C is reported as 55 µg/mL compared to its solubility of 67 µg/mL in water [169]. Also, mixing of isopropanol with phosphate buffer pH 7 increased the pH to 7.2. Therefore, considering the reduced solubility of ciprofloxacin in phosphate buffer pH7 – isopropanol (80:20 %v/v), it is expected to increase the supersaturation ratio, nucleation rate and produce a smaller particle size distribution. Based on the results in Table 5.6 comparing Exp. 4 and 6, the addition of isopropanol as expected reduced the particle size with the mean (SD) Dv50 of 0.12 (0.01) µm and a narrower distribution compared to 0.19 (0.9) µm in the absence of isopropanol (Figure 5.16). The induction time or the time between generation of supersaturation and appearance of detectable precipitates is also much lower with isopropanol in the anti-solvent compared to the other studies.

Given that the conditions described above appeared to produce CPF nanoparticles in the target range (100-200 nm), the final optimization step re-assessed the effects of solvent:anti-solvent ratio for the buffer / isopropanol anti-solvent. In this case, ratios of 0.06 (3 m:50 mL; Exp. 8), 0.03 (3mL:100 mL; Exp. 6) and 0.012 (3mL:250 mL; Exp. 7) were compared. Similar to the previous results increasing the anti-solvent volume resulted in a larger and more polydisperse particle size distribution due to inefficient mixing of the two streams of solvent and anti-solvent in the large vessel. However, comparing the Exp. 7 and 5, in which the solvent:anti-solvent is constant (0.012), results indicate the effect of the addition of isopropanol to the anti-solvent. The CPF precipitates in the isopropanol containing anti-solvent had a smaller size distribution with a mean (SD) volume median diameter of 0.13 (0.01) µm compared to 0.64 (0.21) µm without isopropanol. Both methods produced a bimodal distribution at this solvent:anti-solvent ratio as

shown in Figure 5.17 probably due to reduced mixing efficiency of the ultrasound in larger volume. Reducing the anti-solvent volume from 100 to 50 mL (Exp. 6 and 8) resulted in an increased median diameter together with an increased polydispersity. This might be explained by increasing the solubility of ciprofloxacin due to the larger solvent content in smaller volume of anti-solvent, reducing the supersaturation ratio and increasing the possibility of the Ostwald ripening.

Based on the particle size distribution data ciprofloxacin nanoparticles with median volume diameter of 120 nm and narrow distribution can be prepared with the liquid anti-solvent precipitation technique under sonication. Particle size distribution optimization using sonocrystallization technique was performed with the aid of Tween™ 80 as a stabilizer in the anti-solvent mixture of phosphate buffer pH7:isopropanol (80:20 %v/v) with the optimized volume of 100 mL. This condition was identified as the optimal condition (Exp. 6) for successful production of a monodisperse and stable ciprofloxacin nanoparticle suspension.
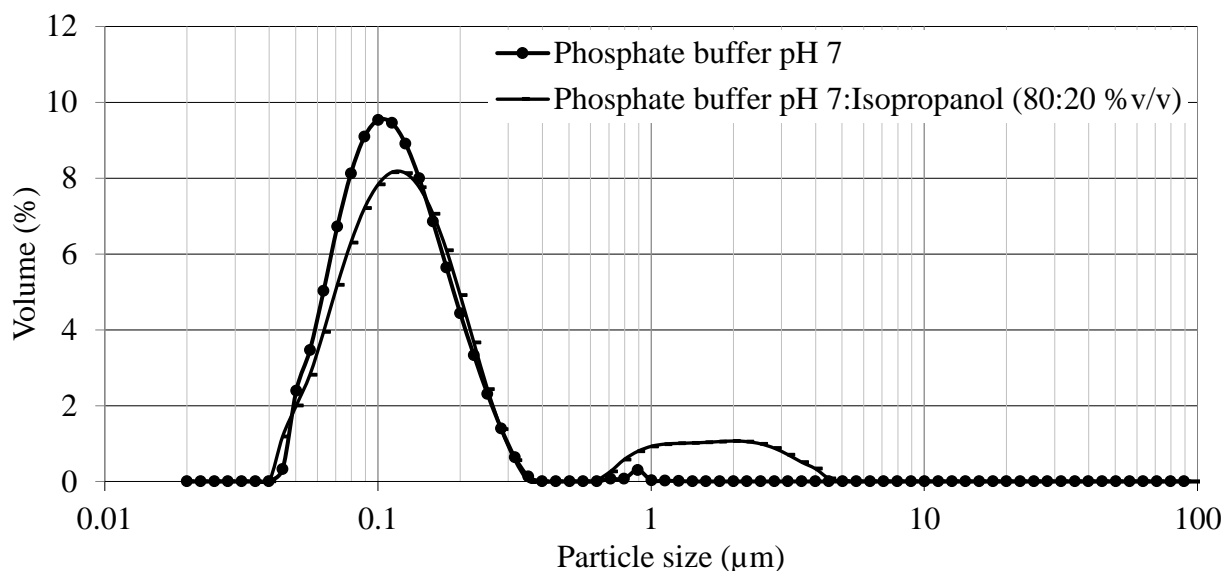
Figure 5.16. Representative volume frequency distribution of ciprofloxacin particles precipitated in phosphate buffer pH 7 and isopropanol containing 0.01%w/v Tween™ 80 under continuous probe sonication using an anti-solvent temperature of 12˚C. 3 mL of ciprofloxacin (37.5 mg/mL solution) was added to 100 mL anti-solvent.
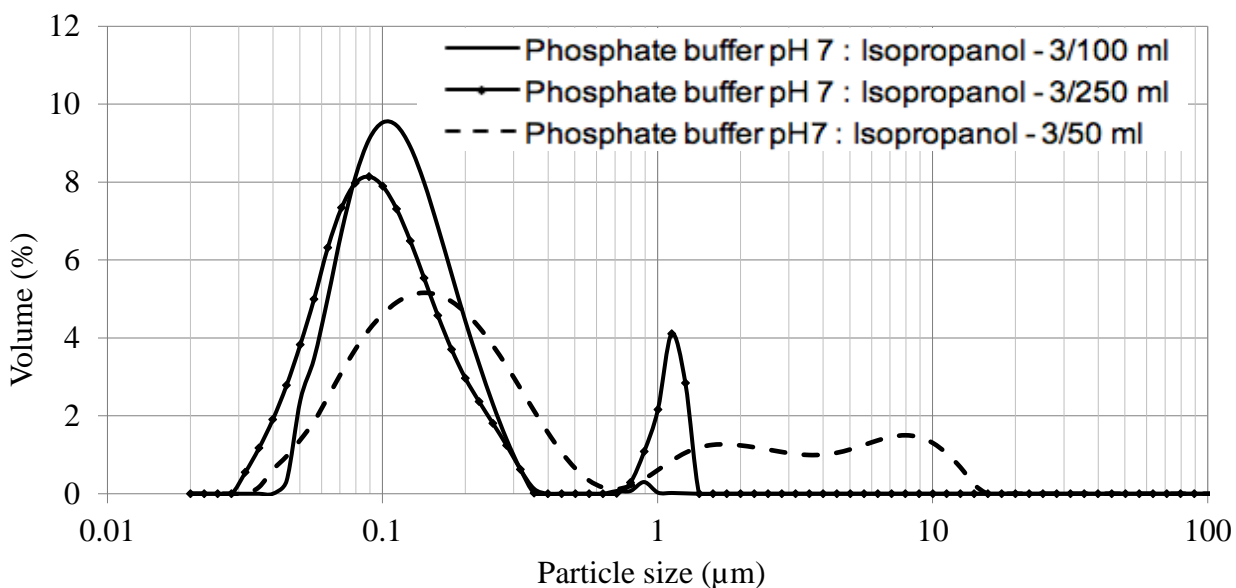
Figure 5.17. Representative volume frequency distribution of ciprofloxacin particles precipitated in phosphate buffer pH 7 and isopropanol containing 0.01%w/v Tween™ 80 under continuous probe sonication using an anti-solvent temperature of 12˚C. 3 mL of ciprofloxacin (37.5 mg/mL solution) was added to 100 mL, 250 mL and 50 mL of anti-solvent.

5.4.1.7 Zeta potential measurement

The zeta potential is related to the surface charge and is an indicative of the stability of suspension. The zeta potential exists as the potential difference between bulk of solution and the outer layer of the electric double layer. Generally, a zeta potential higher than ±30 mV is a sign of good stability of the suspension for long- term storage [164, 168]. The zeta potential values measured for the ciprofloxacin nanosuspensions are summarized in Table 5.6. For all experiments performed with probe sonication, the zeta potential had a negative value ranging from a mean (SD) of -7.4 (0.3) to – 12.8 (0.3) mV. Figure 5.18 shows a representative zeta potential graph for Exp. 6. Mixing using the paddle stirrer resulted in an unstable suspension with a zeta potential of approximately zero. This was visually observed at the end of mixing where all ciprofloxacin particles were settled to the bottom of the vessel. However, after sonocrystallization, the suspensions were stable for at least 3 days stored at 4°C with no particle settling observed. The stability of the nanosuspension is important during the filtration, drying and particle collections process. Unstable suspensions may result in particle growth and Ostwald ripening is possible.

The zeta potential was also measure for ciprofloxacin nanoparticles following recovery as a dried powder. The nanoparticles had a median volume diameter of 120 nm (Table 5.6, Exp. 6) and were re-dispersed in water at a concentration of 0.1%w/v (similar to the concentration in the solvent:anti-solvent mixtures). The mean (SD) zeta potential values for the nanoparticles in the original solvent:anti-solvent mixture and after powder collection with re-dispersion in water were -12.8 (0.3) mV and -11.8 (0.2) mV, respectively. Development of a stable powder which is capable of being re-dispersed to the primary particles is important following removal of the phosphate buffer and isopropanol vehicle. From the zeta potential measurement, it appears that the re-

dispersed suspension in water retained its original characteristics and is suitable for use during the spray drying process.
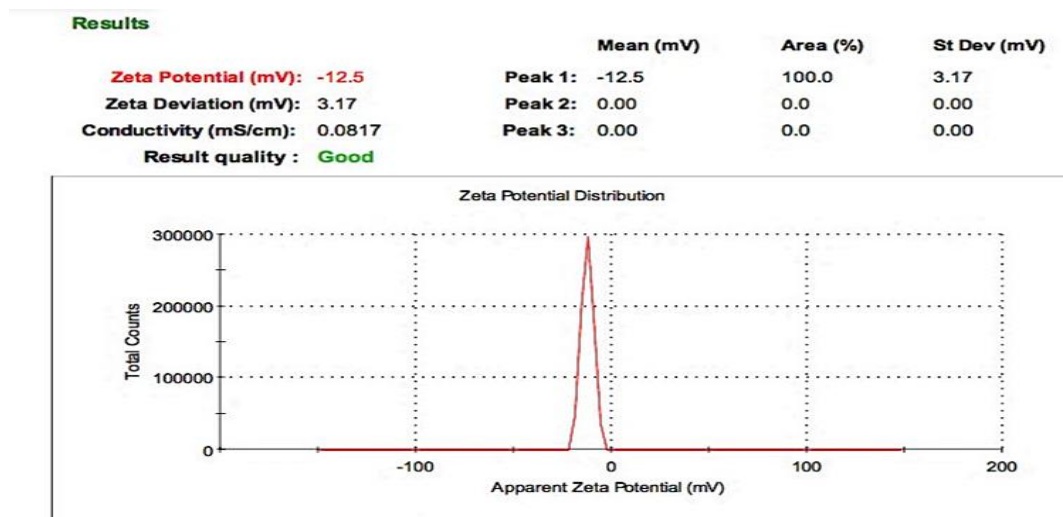
Figure 5.18. Representative zeta potential graph showing negative value of -12.5 mV for ciprofloxacin nano-suspension made by sonocrystallization (Exp. 6)

5.4.2 Preparation of ciprofloxacin nanocomposites using spray drying

The spray drying technique used a water-soluble excipient matrix to prepare ciprofloxacin nanocomposites in the particle size range of 5 -10 μm suitable for targeted nasal delivery.

The spray drying feed stock mixture contained a combination of suspended CPF nanoparticles with a median volume dimeter of 120 nm (Exp. 6) and a water-soluble bulking excipient, a dispersibility enhancer and surfactant dissolved in a water:ethanol mixture. This mixture was spray dried to produce nanocomposite powders using a Büchi Nano spray dryer. As shown, in Table 5.7, a total of 7 spray dried powder formulations were investigated. The geometric diameter of the spray dried powder depends upon the formulation composition and the spray

drying conditions such as inlet temperature, feed rate and spray airflow. The geometric diameter for dry powders can be estimated based on the following equation:

$$d_g = \sqrt[3]{\frac{C_F}{\rho_p}}\, d_D \qquad\qquad \text{Equation 5.6}$$

Where d_g is the geometric diameter for a particle with the density of the ρ_p. From above equation, it can be inferred that the geometric diameter depends on feed stock solution solids concentration (C_F) for the spray drying and primary droplet size after atomization in spray drying system (d_D). The mass median aerodynamic diameter (MMAD or d_a) is defined as:

$$d_a = \sqrt{\frac{\rho_p}{\rho^*}}\, d_D \qquad\qquad \text{Equation 5.7}$$

Combining equations 5.6 and 5.7, the aerodynamic particle size of a spray dried powder can be estimated by knowing the values of particle density and the solids concentration of feed stock solution as below:

$$d_a = \sqrt[6]{\frac{\rho_p}{\rho^*}}\, \sqrt[3]{\frac{C_F}{\rho^*}}\, d_D \qquad\qquad \text{Equation 5.8}$$

Previously, extensive investigations performed in our labs have produced spray dried monodisperse particles with an MMAD of 1.0 - 1.4 μm using a stock solution with a solids concentration of 0.5% w/v and vibrating mesh spray nozzles with diameter of 4 μm [154]. This nozzle size is reported (Büchi Laboratory-Techniques, Flawil, Switzerland) to generate water droplets with the size of 8 μm. A larger vibrating mesh spray nozzle option of 7μm is also available and is reported to generate a mean water droplet size of 21μm.

To achieve particles in the size range of 5 -10 μm, the total solid concentration in feed stock mixture for spray drying and selection of water soluble bulking excipient (mannitol and PVP K30) were varied. All studies were performed with the nozzle size of 7μm. Drying of nanoparticles can creates thermal stress on the particles causing particle aggregation which is undesirable. Sugars such as mannitol have previously been used to protect nanosuspensions from aggregation during spray drying and help re-dispersibility of the nanoparticles in an aqueous media [170].

Table 5.7 shows the measured mean (SD) drug content which ranged from 19.7 (0.5) % to 21.7 (0.4) % and was very close to the nominal values of 20-22 %w/w (Table 5.2). Two-way ANOVA for the two variables of water soluble excipient type and % solids concentration was performed to assess the effects on the particle size of the spray dried powder. There were significant effects of both variables (excipient and % solids) on Dv50 (p-value<0.0001 and p-value<0.0001). Within the mannitol group, it was observed that by changing the % solids concentration of 0.4 to 1 % w/v, the mean (SD) median volume particle size measured by Sympatec only increased from 2.7 (0.3) μm to 3.1 (0.1) μm. The changes in Dv10, 50 and 90 for the mannitol formulations were statistically significant but perhaps the small magnitude of change in particle size would not change nasal airway deposition. In addition, the mannitol formulations were below our target size for the nasal drug delivery application. For the mannitol formulations, increasing the % solids resulted in greater powder yield. Further increasing the % solids to 4.0 % for the mannitol formulation significantly increased the particle size distribution with mean (SD) Dv10, 50 and 90 of 0.9 (0.1) μm, 4.5 (0.2) μm and 9.7 (0.2) μm (Table 5.7 and Figure 5.19).

The effect on the spray dried powder particle size distribution of PVP K30 with % solids of 2-4 % w/v was also assessed. It appears that particle sizes were larger when PVP K30 was used

compared to mannitol (Figures 5.19 and 5.20). At the highest % solids concentration of 4.0%, the mean (SD) Dv50 of the spray dried powder was 6.5 (0.2) μm with mean (SD) Dv10 and Dv90 of 1.7 (0.0) μm and 12.3 (0.1) μm, respectively.

The stability of nanoparticles following spray drying and their ability to produce primary nanoparticles following the dissolution of the excipient matrix was assessed using the powder generated from Exp 6SD. The nanocomposite powder was added to water and the particle size of suspended nanoparticles were characterized (Figure 5.21). The results indicate a similar size distribution of the nanoparticles following spray drying (Exp 6SD) compared to the freshly prepared nanosuspension (Exp. 6, Table 5.6). The mean (SD) Dv10 and 50 were 0.07 (0.01) μm and 0.14 (0.01) μm for the spray dried nanoparticles and not significantly different from the original values of 0.07 (0.01) μm and 0.12 (0.01) μm for freshly made ciprofloxacin nanosuspension (Student t-test, p-value<0.05). Corresponding values for Dv90 were observed to have a small but significant increase (p- value< 0.05; Student t-test, mean (SD) = 0.31 (0.02) μm and 0.24 (0.01) μm), respectively).

The spray dried nanocomposite formulation generated using the conditions described in Exp. 6SD produced a powder within the target size range. In addition, it appeared that it was possible to successfully obtain primary nanoparticles following dissolution of the matrix excipients. Therefore, future nasal aerosol development would use this spray drying protocol to produce nanocomposite powders with a 3% solids concentration in the feed stock mixture. The ratio of solids would be 21 %w/w CPF, 21 %w/w leucine, 56 % w/w PVP K30 and 2 %w/w Tween™ 80.

Table 5.7. Feed stock composition used for spray drying of ciprofloxacin nanocomposite formulations and their measured particle size distributions. Formulations differ in % solids concentration and the type of water soluble excipient. Results are presented as mean (SD) (n = 3).

Exp.	Solid Conc. (%w/v)	Yield (%w/w)	CPF content (%w/w)	Particle size distribution (measured by Sympatec) (µm)		
				$Dv10^{1,2}$	$Dv50^{3,4}$	$Dv90^{5,6}$
1SD	0.4	45	21.7 (0.4)	0.7 (0.4)*	2.7 $(0.3)^{+,++}$	6.1$(0.2)^{\neq\#}$
2SD	0.7	53	21.6 (0.4)	0.7 $(0.1)^{*\#}$	2.4 $(0.1)^{+,++}$	5.6 $(0.1)^{\neq\#}$
3SD	1.0	69	21.0 (1.5)	0.8 (0.0)*	3.1$(0.1)^{+}$	6.6 $(0.1)^{\neq\#}$
4SD	4.0	66	19.7 (0.5)	0.9 (0.1)	4.5 $(0.2)^{\neq}$	9.7 $(0.2)^{\neq\#}$
5SD	2.0	57	20.6 (0.2)	1.3 (0.1)	5.2 $(0.1)^{\neq}$	12.5 (0.3)"
6SD	3.0	60	20.8 (0.5)	1.8 (0.1)**	5.6 $(0.1)^{\neq}$	10.6 (0.1)
7SD	4.0	63	21.8 (0.7)	1.7 (0.0)**	6.5 $(0.1)^{\neq}$	12.3 (0.1)"

All formulations had similar concentrations of leucine and drug (20-22 %w/w) and 2 %w/w Tween™ 80.
Exp. 1 - 4SD contain mannitol (54-58 %w/w) and 5 - 7SD contain PVP K30(54-58 %w/w).

[1] Significant difference in Dv10 for mannitol containing formulation (Exp.1 - 4SD). * P<0.05, significant difference compared to Exp.4SD.[#] P<0.05, significant difference compared to Exp.3SD.
[2] Significant difference in Dv10 for PVPk30 containing formulation (Exp.5 - 7SD). ** P<0.05, significant difference compared to Exp.5SD.
[3] Significant difference in Dv50 for mannitol containing formulation (Exp.1-4SD). [+] P<0.05, significant difference compared to Exp.4SD.[++] P<0.05, significant difference compared to Exp.3SD.
[4] Significant difference in Dv50 for PVPk30 containing formulation (Exp.5-7SD). [≠]P<0.05, significant differences for values compared.
[5] Significant difference in Dv90 for mannitol containing formulation (Exp.1-4SD). [#]P<0.05, significant differences for values compared.
[6] Significant difference in Dv90 for PVPk30 containing formulation (Exp.5-7SD). " P<0.05, significant differences compared to Exp.6SD.
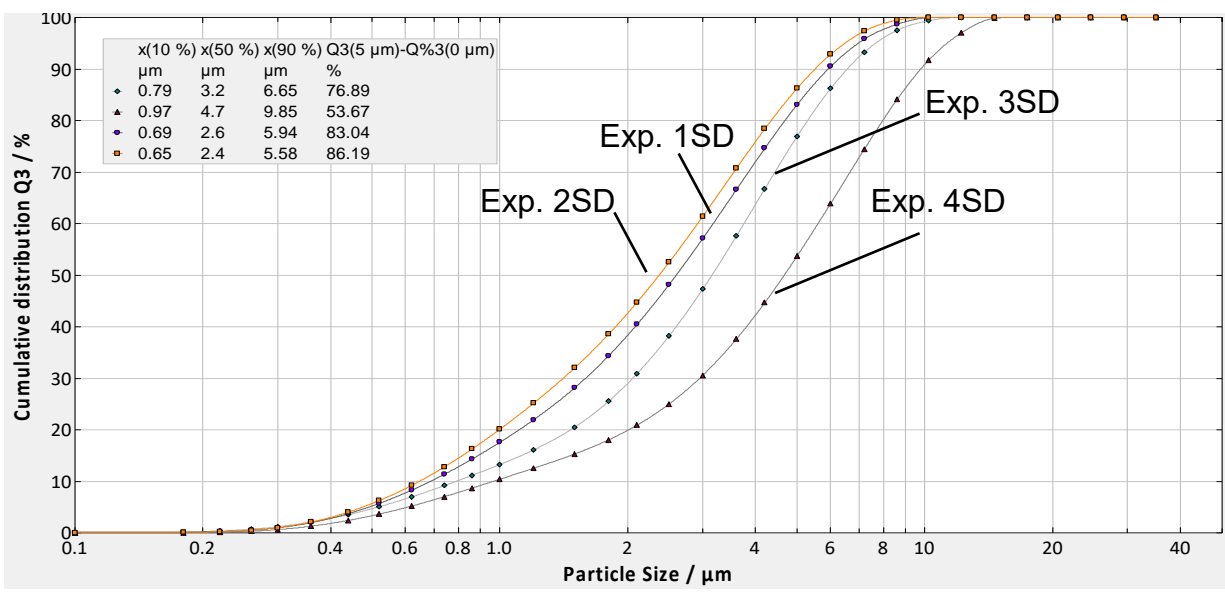
Figure 5.19. Representative cumulative volume distribution plot for ciprofloxacin spray dried nanocomposite formulations measured by Sympatec. For experiments 1 – 4 SD, the % solids concentration of feed stock suspension varied from 0.4 to 4 %w/v (Table 5.7). These formulations contained similar concentration of drug and leucine (20-22 % w/w) and 54-58% mannitol and 2 % Tween™ 80. The legend also show the percentage particles in the size fraction below 5µm.
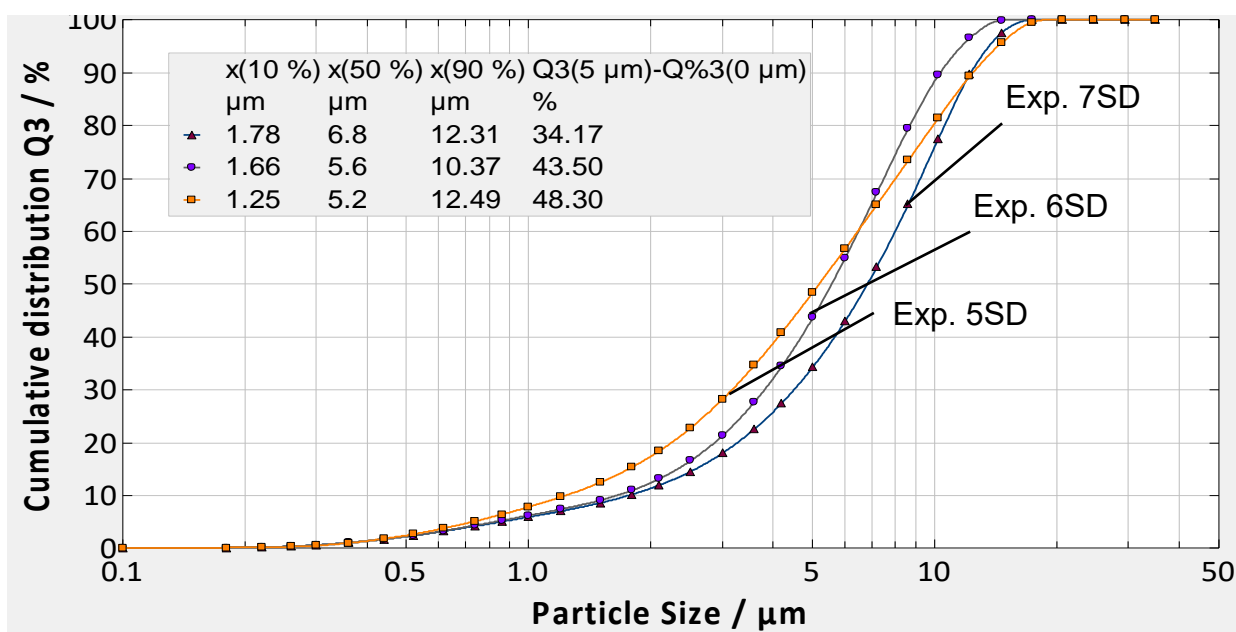
Figure 5.20. Representative cumulative volume distribution plot for ciprofloxacin spray dried nanocomposite formulations measured by Sympatec. For experiments 5 – 7 SD, the % solids concentration of feed stock suspension varied from 2 to 4 %w/v (Table 5.7). These formulations contain similar concentration of drug and leucine (20-22 % w/w) and 54-58% PVPK30 and 2 % Tween™ 80. The legend also show the percentage particles in the size fraction below 5µm.
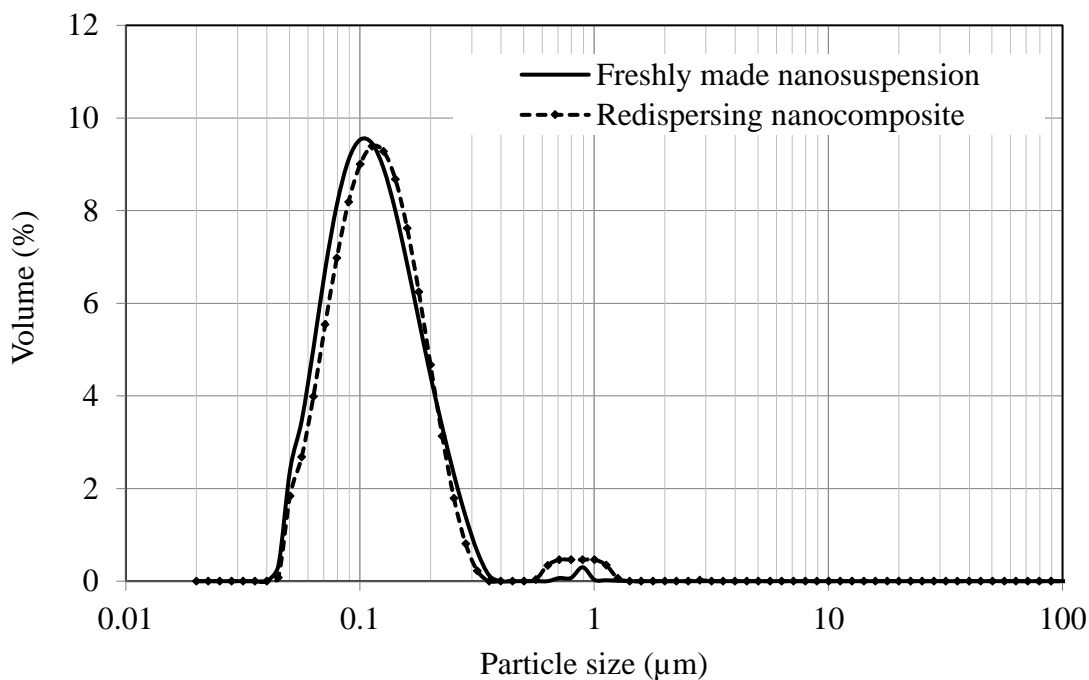
Figure 5.21. Representative volume frequency distribution of ciprofloxacin nanocomposite powder re-dispersed in water following spray drying (Exp. 6SD) and the corresponding freshly made ciprofloxacin nanosuspension (Exp. 6)

5.4.3 Differential scanning calorimetry (DSC) and thermogravimetric analysis (TGA) characterization of CPF nanoparticles and nanocomposite formulations

Figure 5.22 shows the representative thermogram for ciprofloxacin (base, anhydrous) as the source material used for sonocrystallization technique and production of CPF nanoparticles (Section 5.3.1). Figure 5.22 also shows the thermogram for ciprofloxacin hydrochloride. Figure 5.22 demonstrates that the endothermic peaks for the melting of the ciprofloxacin base and hydrochloride forms are at 273.2 °C and 334.4°C respectively. Similar values of 277°C and 326 °C were reported for the melting points of ciprofloxacin base and hydrochloride, respectively [171, 172] other endothermic peak observed at 155°C in the ciprofloxacin hydrochloride sample was related to dehydration of ciprofloxacin hydrochloride and its associated monohydrate form. This

loss of 1 water molecule is further confirmed by TGA thermogram [172]. As demonstrated by the thermograms, DSC could distinguish between the two forms of ciprofloxacin. Figure 5.23 is a representative thermogram for ciprofloxacin nanoparticles produced using the optimized process described previously (Exp. 6). The thermogram reveals a sharp endothermic melting peak corresponding to a mean (SD) temperature of 275 (1.4) °C. This supports the hypothesis that the CPF nanoparticles remain as the base form following crystallization. The endothermic peak with a mean (SD) temperature of 125 (1.1) °C in nanoparticle thermogram represents the loss of 3.5 molecules of water. This was confirmed by TGA analysis (performed using an identical heating rate profile) where a weight loss corresponding to 16.2% was observed for the nanoparticle formulation (Figure 5.24). This weight loss corresponds to 3.5 molecules of water. Weers et al [173] also reported a 3.5 hydrate for ciprofloxacin base (ciprofloxacin betaine) formulated for pulmonary delivery. For the spray dried formulations containing PVP K30, leucine and Tween 80 (Exp 6SD), two endothermic events with mean (SD) temperatures of 132 (1.3) °C and 255 (0.3) °C were observed (Figure 5.23). For the spray dried formulations containing mannitol, leucine and Tween™ 80 (Exp 4SD), two endothermic events of 146 (1.3) °C and 255 (0.3) °C were observed. For both spray dried formulations the first endothermic peak is associated with a mean (SD) weight loss of 9.3 (0.4) % and 12.5 (1.0) %, respectively, measured by TGA (Figure 5.24). It appears that there is a higher content of water for mannitol containing nanocomposite formulation possibly due to the more hygroscopic nature of mannitol.
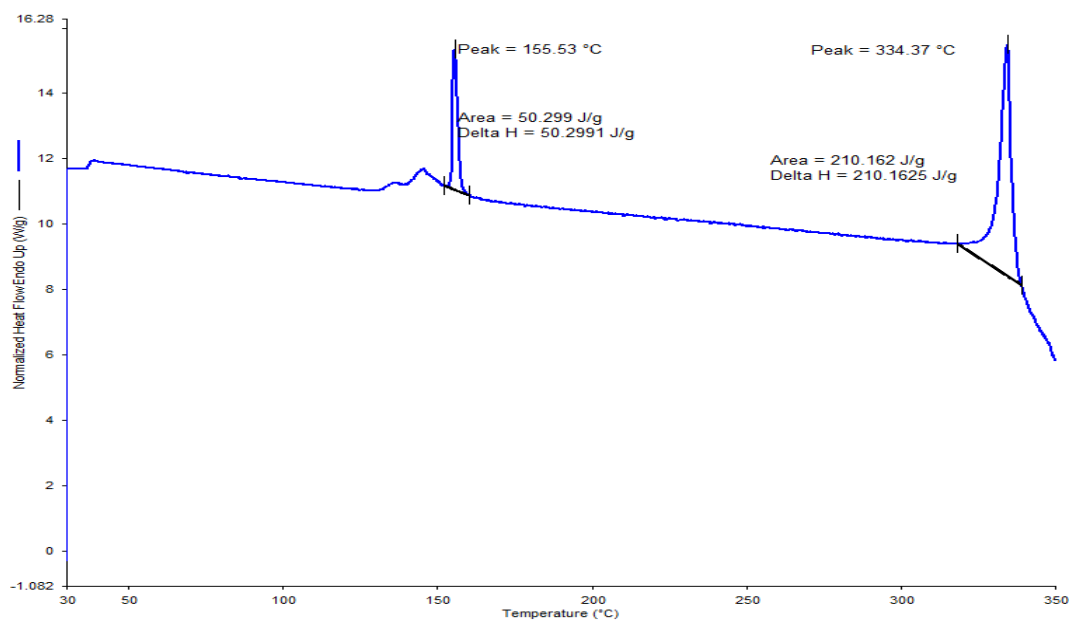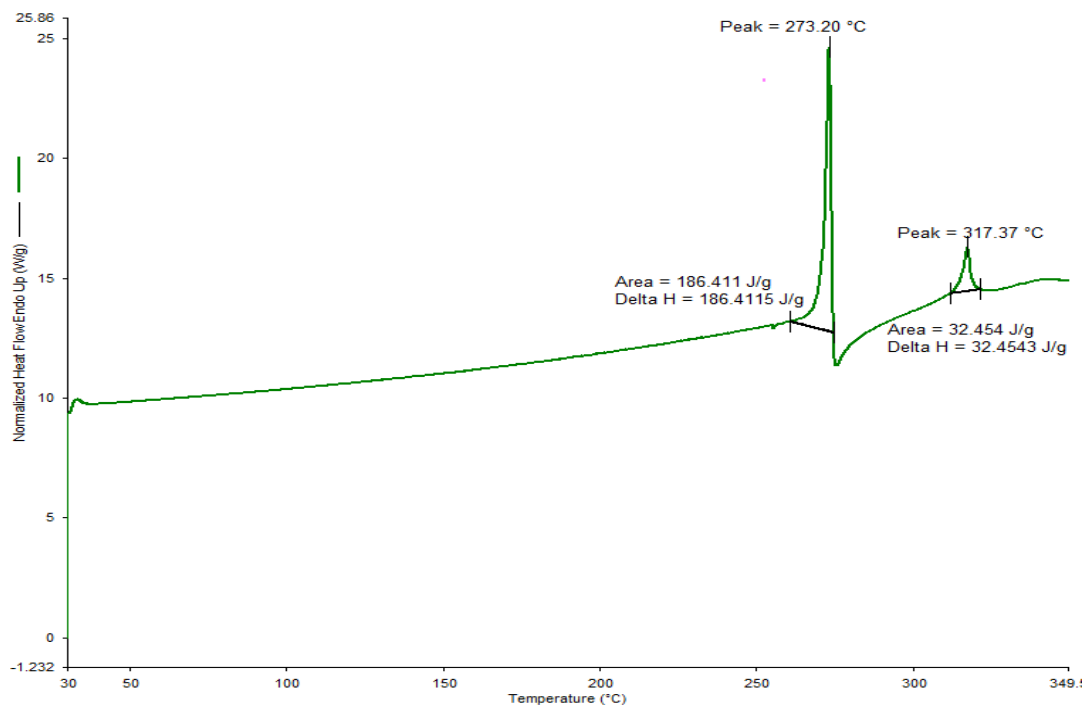
Figure 5.22. Representative DSC thermograms for ciprofloxacin base (top) and ciprofloxacin hydrochloride (bottom) heated at 10°C /min
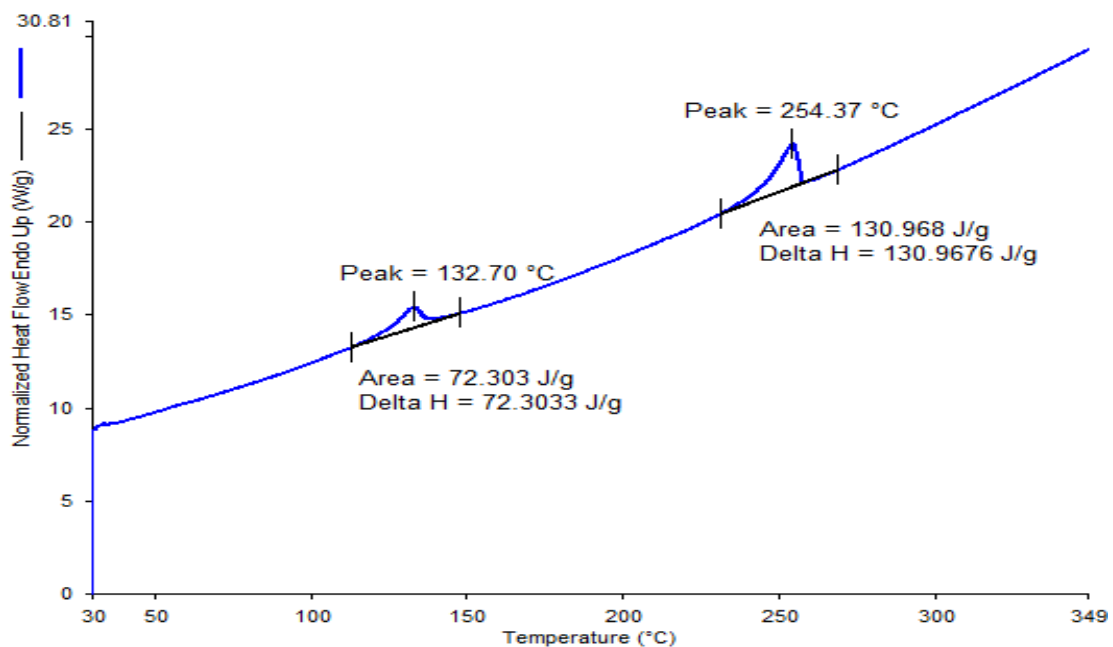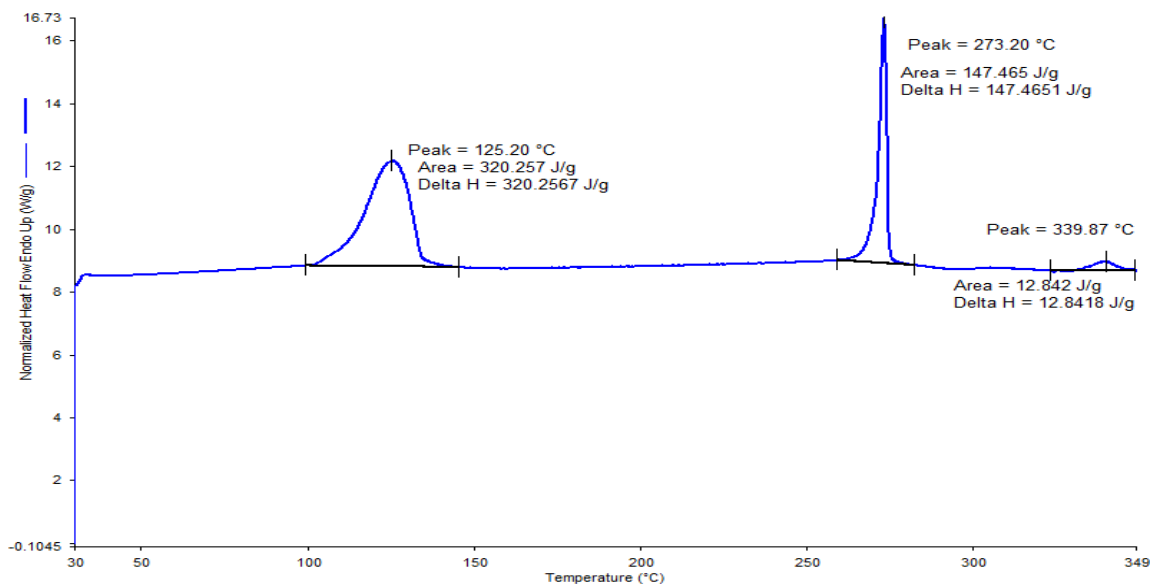
Figure 5.23. Representative DSC thermograms for ciprofloxacin nanoparticles (Exp. 6) (top) and the optimized spray dried nanocomposite formulation containing PVP K30 (Exp. 6SD) (bottom) heated at 10°C /min
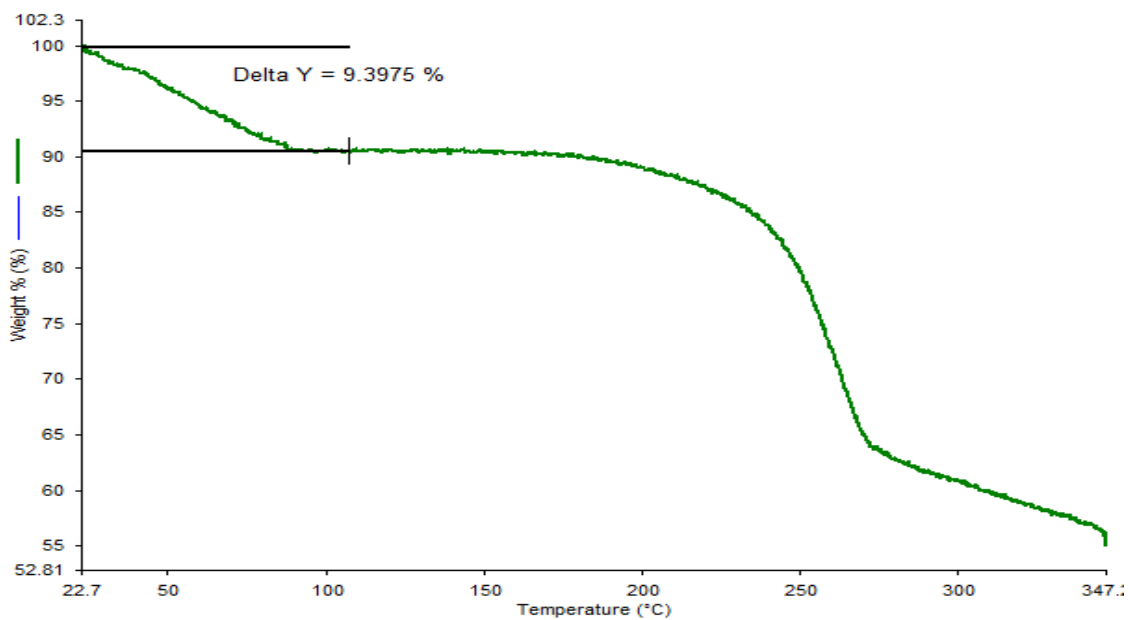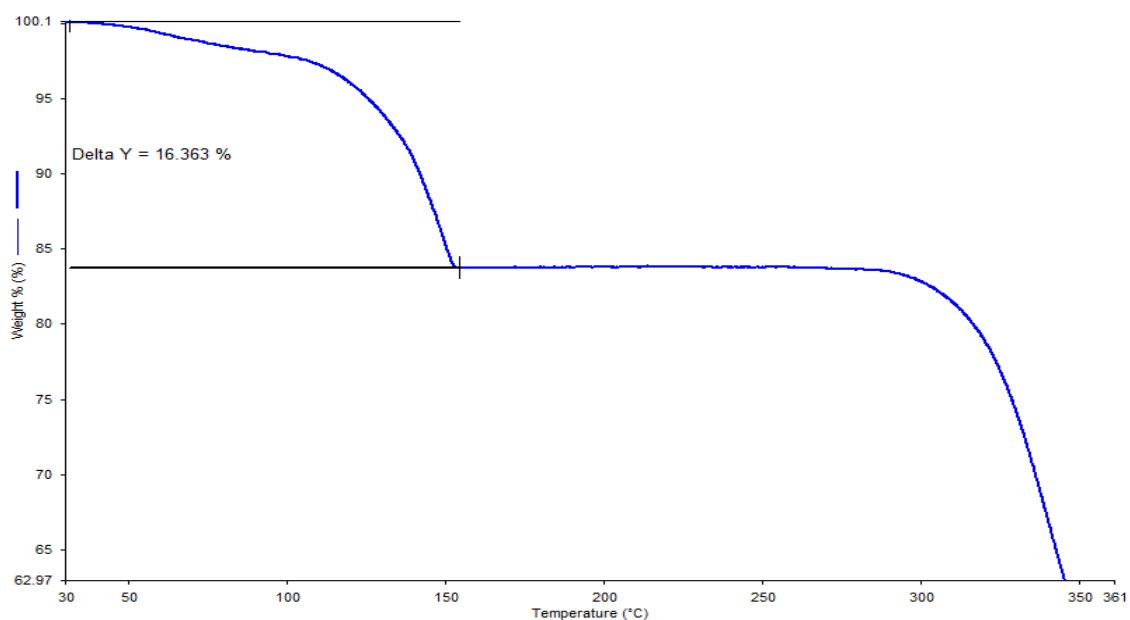
Figure 5.24. Representative TGA thermogram for ciprofloxacin nanoparticles (Exp. 6) (top) and the optimized spray dried formulation containing PVP K30 (Exp. 6SD) (bottom) heated at 10°C /min

5.4.4 Characterization of the dissolution and diffusion properties of the ciprofloxacin nanoparticles and nanocomposite formulations

The result for the dissolution of a series of ciprofloxacin samples in phosphate buffer pH 7 are presented in Figure 5.25. As demonstrated in the Figure, the dissolution method could distinguish between different formulations of ciprofloxacin. For powders to be transported across the semi-permeable membrane, the powder first needs to dissolve in the dissolution media and then diffuse through the membrane. However, for the ciprofloxacin solution the only barrier is the diffusion process across the membrane as the drug is already in solution. For all samples, a zero-order appearance of drug into the receptor compartment was observed. For ciprofloxacin powder (unprocessed raw material), the mean (SD) cumulative percent mass of drug transported into the receptor compartment over the period of 5 hours was 20.1 (2.6) % of the nominal dose. For ciprofloxacin solution, prepared in phosphate buffer pH 3, the mean (SD) cumulative percent mass of drug transported into the receptor compartment was 33.2 (1.5) % and significantly higher than was observed for the unprocessed powder (p-value = 0.0028, Student t-test). From the time profile, it was observed the amount of drug transported was higher at each individual sampling time point for the solution versus the unprocessed powder. However, it was observed that even for the solution transport did not reach 100 % after 5 hours due to slow diffusion through the semi-permeable membrane. The effects of producing nanoparticles and a nanocomposite formulation on the dissolution and diffusion of CPF are also shown in Figure 5.25. The nanoparticle suspension formulation (Exp. 6) and the spray dried nanocomposite powder CPF formulation (Exp. 6SD) exhibited a similar transport rate. The mean (SD) cumulative % mass drug transport for nanoparticle suspension and the spray dried nanocomposite CPF formulation were 31.7 (2.3) and 34.5 (2.4), respectively, and not significantly different from each other. However, they were

significantly higher than the unprocessed ciprofloxacin powder (*p*-value = 0.0029 and 0.0004, respectively, Tukey HSD). This indicated that the rate and extent of dissolution for the nanoparticle formulations was significantly higher compared to the ciprofloxacin unprocessed powder with its median volume diameter of 2 μm. In addition, the spray drying to produce nanocomposite formulations did not appear to result in any changes to the dissolution of the primary nanoparticles. Further studies were performed to investigate the apparent increased dissolution rate of the nanoparticles compared to the unprocessed powder and to exclude the effects of surfactant excipients (Tween™ 80) used in both the crystallization and spray drying process. Figure 5.25 also shows the dissolution rate of unprocessed ciprofloxacin powder in the presence of Tween™ 80 at same molar concentration used in the ciprofloxacin crystallization process. The addition of Tween™ 80 did not result in any increase in the dissolution rate of the unprocessed ciprofloxacin powder. It was concluded that the increased dissolution rate for the CPF nanoparticle suspension and the spray dried CPF nanocomposite formulation was due to reduced particle size of the CPF nanoparticles resulting in an increased surface area of the drug according to the Noyes-Whitney equation:

$$\frac{dQ}{dt} = \frac{D}{h} S(C_s - C)$$
<div align="right">Equation 5.9</div>

where the dissolution rate $\frac{dQ}{dt}$ is directly proportional to the diffusion coefficient of the drug (D), the available surface area (S), and the difference between saturation solubility of the drug in the boundary layer (C_s) and concentration of drug in the bulk fluid (C). Therefore, as particle size decreases, surface area increases which leads to an increased dissolution rate. Any change in the

nanoparticle size following spray drying as nanocomposite would also be reflected by changes in the dissolution rate. If the nanoparticles form fused aggregates, then the overall surface area would decrease and the dissolution rate would be negatively impacted. Such phenomena were not observed for the nanocomposites obtained in this study, indicating that the nanoparticles retained their improved dissolution characteristics after spray drying as nanocomposites and that the dissolution and transport process was not rate limited by the dissolution of other excipients contained in the spray dried nanocomposite formulation or its 5 μm particle size prior to dissolution and release of the CPF nanoparticles.
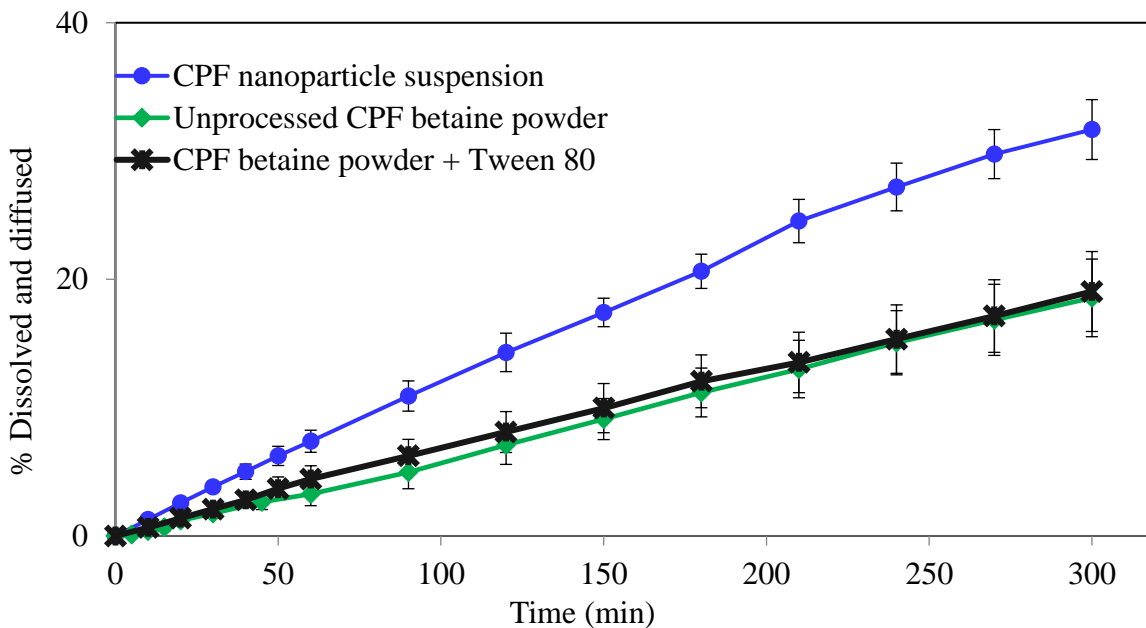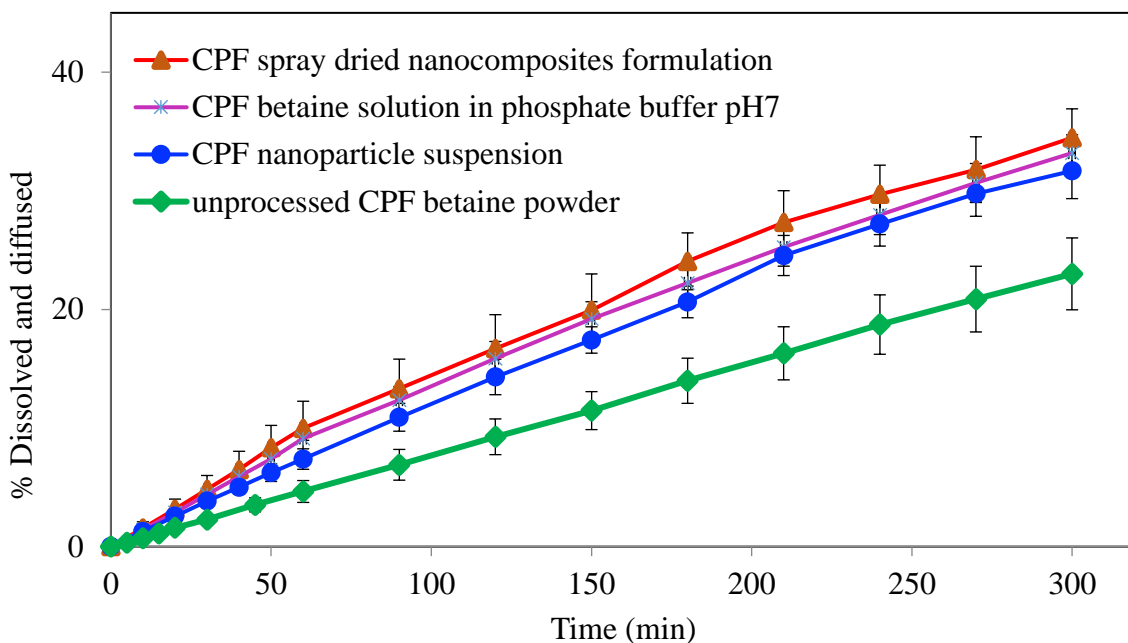
Figure 5.25. Cumulative percent mass of ciprofloxacin transported into the receptor compartment as a function of time in phosphate buffer pH 7. The following mean (SD) masses of CPF were used: solution = 12.5 µg, nanocomposite formulation 9.0 (4.0) µg, nanoparticle suspension = 14.0 (1.3) µg, unprocessed ciprofloxacin base powder =12.7 (0.5) µg. Results are presented as mean (error bars are SD) (n=4)

The dissolution and transport rate of the spray dried formulation and unprocessed powder was also assessed in water (pH = 5). As the results in Figure 5.26 show the mean (SD) cumulative percent mass of drug transported for unprocessed ciprofloxacin powder was slightly increased in water at pH 5 (26.9 (4.1) %), compared to phosphate buffer at pH7 (*p*-value= 0.0291) (Figure 5.25). It is expected that the zwitterion CPF will have increase ionization at the lower pH resulting in increased solubility. However, for the spray dried nanocomposite formulation, in water at pH 5, the mean (SD) cumulative percent mass of drug transported after 5 hours remained same as 34.5 (2.4) %. It appears that phosphate buffer at pH 7 as the dissolution media is better able to distinguish between different ciprofloxacin formulations. The primary purpose of these experiments was to assess if there were any measurable difference in the dissolution rate of ciprofloxacin nanoparticles due to their particle size and using this Transwell system it was possible to detect chances in the dissolution rate comparing unprocessed CPF and nanoparticles.

Finally, these studies provide sham dissolution and transport studies for the transepithelial transports studies of the nanocomposite formulation across the Calu-3 cell monolayer grown on these Transwell membranes. Initial baseline values were obtained for dissolution and diffusion of the nanocomposite CPF formulation through membranes in the absence of cells.
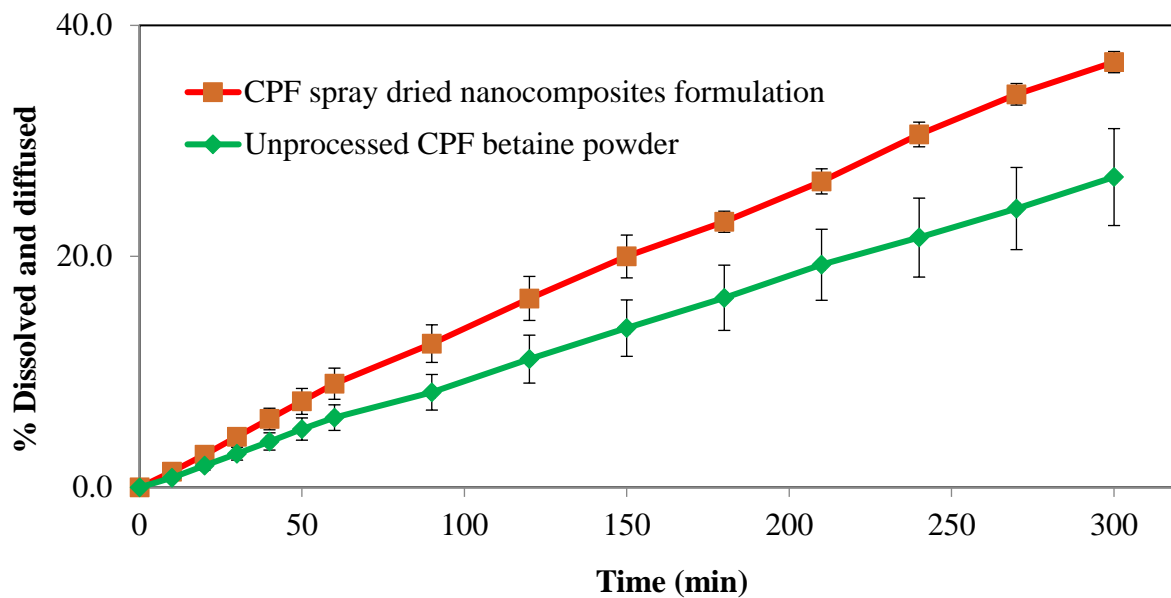
Figure 5.26. Cumulative percent mass of ciprofloxacin transported into the receptor compartment as a function of time in water (pH 5). The following mean (SD) masses of CPF were used: nanocomposite formulation = 11.3 (6) µg, unprocessed ciprofloxacin base powder = 22 (6) µg. Results are presented as mean (error bars are SD) (n=4)

5.4.5 Development and evaluation of a nasal aerosol delivery method

5.4.5.1 Aerodynamic particle size characterization and emitted dose optimization for the nanocomposite formulation

The previously described optimized spray dried ciprofloxacin nanocomposite powder with a median volume diameter of about 6 μm (Exp. 6SD) was further characterized to evaluate its aerosolization properties and suitability for nasal drug delivery. The mean (SD) drug content of this powder was 20.8 (0.5) %w/w (Table 5.7). To investigate the powder aerosolization properties, two commercial dry powder inhalers, the Aerolizer® and Handihaler®, and the VCU low volume DPI were used and the results are shown in Table 5.8. Drug recovery from the impactor and inhaler devices was acceptable in the range of 89.4 % to 100.4 %. Using the Aerolizer® and Handihaler®, the CPF nanocomposite formulation had a good emitted dose of over 82 % (mean (SD) = 82.9 (3.7) % and 82.6 (4.5) %, respectively) of the nominal dose. A significant fraction of the emitted dose was deposited in the pre-separator for both these devices. The mean (SD) dose deposited in the impactor from the Aerolizer® and Handihaler® was 44.8 (6.0) % and 57.8 (6.0) % of the nominal dose, respectively. The MMAD of the aerosol was calculated based on the impactor dose. The calculated mean (SD) MMAD from Aerolizer® and Handihaler® was 8.9 (2.0) μm and 11.5 (3.4), respectively. These results suggest that the aerosolized nanocomposite formulation was not fully dispersed by these commercial devices to the primary particles given that its initial size was about 6 μm. For the VCU 2.3-343 DPI operated at a flow rate of 15 Lmin^{-1}, a mean (SD) dose of 50.7 (2.4) % was emitted from the device which was significantly lower than both the Aerolizer® and Handihaler® (p-value <0.0001). Also, there was lower a mean (SD) FPF<5μm$_{ED}$ of 18.2 (1.6) % with the VCU DPI compared to 31.2 (6.3) % and 35.0 (5.0) % for the Aerolizer® and Handihaler®, respectively (p-value = 0.112, p-value = 0.0349). For nasal drug delivery, it is

important to minimize the fraction of the aerosol that is less than 5 μm to prevent potential inhalation of the nasal powder. For the VCU DPI, the mean (SD) MMAD was 8.7 (1.4) μm which was not significantly different from the other devices. Previous studies using submicrometer spray dried formulations and the VCU DPI reported emitted doses of 66.5 to 71.3 % using a ciprofloxacin EEG (excipient enhanced growth) formulation that had an MMAD of 1.4 – 2.7 μm [126]. Further studies were designed to increase the emitted dose from the VCU DPI with the nanocomposite powder formulations. This was investigated by changing parameters such as the needle size for capsule piercing, coating the device using PTFE spray and removing the 343-rod array within the flow passage.

Table 5.8. Mean (SD) aerosolization properties of the optimized ciprofloxacin nanocomposite formulation measured using the Next Generation Impactor and delivered from three dry powder inhalers (Aerolizer[®], Handihaler[®] and VCU 2.3-343 DPI) (n=3)

	Aerolizer[®]	Handihaler[®]	VCU 2.3-343
Emitted dose (% nominal) [1]	82.9 (3.7) *	82.6 (4.5) *	50.7 (2.4)
FPF <5 μm (% ED) [2]	31.2 (6.3) **	35.0 (5.0) **	18.2 (1.6)
MMAD (μm)	11.5 (3.4)	8.9 (2.0)	8.7 (1.4)
Mass in impactor (% ED)	44.8 (6.0)	57.8 (6.0)	69.0 (4.8)
Recovery (%)	89.4 (3.7)	90.7 (8.1)	100.4 (4.0)

Aerolizer[®] flow rate = 80 Lmin[-1] for 3 sec, Handihaler[®] flow rate = 45 Lmin[-1] for 5.3sec, VCU 2.3-343 flow rate = 15 Lmin[-1] for 10 sec. n=3.
[1]$P < 0.05$, significant difference in emitted dose; *$P < 0.05$, significant difference in emitted dose compared to VCU 2.3-343.
[2]$P < 0.05$, significant difference in FPF< 5 μm; **$P < 0.05$, significant difference in FPF< 5 μm to VCU 2.3-343.

Enhancement of the emitted dose from the VCU DPI device was investigated by changing the needle size for capsule piercing using Handihaler® device needle, coating the device using a commercial PTFE spray and removing the 343-rod array within the flow passage and the results are summarized in Table 5.9. Using the Handihaler® needle to produce a hole size of 2mm diameter did not significantly increase the nanocomposite power aerosol emitted dose compared to the piercing with the 0.5 mm needle (Exp. 1VCU and 2 VCU). There did appear to be improved emptying from the capsule with the larger holes, however this did not result in a significant change in the emitted dose and the drug retention in the device remained unchanged (Student t-test).

Coating the device using PTFE spray significantly increased the emitted dose up to 63.5 (1.1) % compared to 50.7 (2.4) % in the absence of coating as PTFE coating. PTFE coating on the device surface provides smoother surface and reduces the particle adhesion. Finally, removing the 343-3D rod array from the flow passage significantly reduced the device retention. The 3D rod array was designed to increase deagglomeration of submicrometer spray dried particles. However, for the current application using a 6 μm formulation the presence of the rods appeared to prevent compete emptying of the device and the additional deaggregation may not be required for these larger primary nanocomposite particles. We also tested the emitted dose from VCI-DPI 2.3 a device prototyped in Dr. Golshahi's lab in VCU School of Mechanical Engineering. This device was made from a FormLabs clear resin and coated with PTFE. This device had a significantly higher mean (SD) emitted dose of 85.0 (1.9) % compared to the Stratasys VeroWhitePlus resin manufactured devices. This implies that the selection of the plastic resin used to manufacture the 3D printed DPI may play a significant role in determining the adhesion of these ciprofloxacin nanocomposite formulations to the surface of the device either due to the device surface roughness or electrostatic interactions. From these optimization studies a low flow VCU DPI design was

identified that produced an acceptable emitted dose (85.0 %). Additional studies were then required to measure the aerosol performance of the nanocomposite CPF formulation in this modified inhaler.

Table 5.9. Optimization of the mean (SD) device retention and emitted dose from the VCU DPI powder inhaler operated at 15 Lmin^{-1} for 15 sec (n=3-4)

Exp.	Conditions	Capsule (% nominal)	Device (% nominal)	Emitted dose (% nominal)
1VCU	VCU DPI 2.3-343 0.5mm capsule hole size no coating	21.0 (3.2)	28.3 (2.4)	50.7 (2.4)
2VCU	VCU DPI 2.3-343 2mm capsule hole size no coating	12.1 (5.4)	32.6 (3.9)	55.3 (3.6)
3VCU	VCU DPI 2.3-343 0.5mm capsule hole size PTFE coated	10.8 (0.9)	25.7 (1.1)	63.5 (1.1) *
4VCU	VCU DPI 2.3 0.5mm capsule hole size PTFE coated	9.6 (0.5)	18.3 (1.9) **	72.1 (1.9) ***
5VCU	VCU DPI 2.3 FormLabs clear resin 0.5mm capsule hole size PTFE coated	4.9 (2.3)	10.1 (1.9) [#]	85.0 (1.9) [##]

Emitted dose was calculated by subtracting the measured ciprofloxacin mass retained in the capsule, DPI and nasal cannula from the nominal dose, and expressed as a % of the nominal dose.

*P<0.05, significant difference in emitted dose, compared to Exp. 1VCU (Student t-test, *p*-value = 0.0076).

** P<0.05, significant difference in device deposition, compared to Exp. 3VCU (Student t-test, *p*-value = 0.0176).

*** P<0.05, significant difference in emitted dose, compared to Exp. 3VCU (Student t-test, *p*-value= 0.0188).

[#] P<0.05, significant difference in device deposition, compared to Exp. 4VCU (Student t-test, *p*-value= 0.0102).

[##] P<0.05, significant difference in emitted dose, compared to Exp. 4VCU (Student t-test, *p*-value= 0.0016).

5.4.5.2 Particle size characterization of the nanocomposite formulation emitted from the optimized VCU DPI using the Malvern Spraytec®

The geometric particle size distrbution for ciprofloxacin nanocomposite aerosols exiting the VCU DPIs were evaluated using the Malvern Spraytec instrument (Malvern Instruments Ltd, Worcestershire, UK). The aerosol spray emitted from the nasal prong was directed through the laser beam to measure the laser diffraction. The device was mounted on a holder such that the nasal cannula prong was facing prependicular to the laser beam and the emitted dose was collected using a respiratory filter after passage through the laser. The results are presented in Table 5.10. The device containing 343 3D rod array operating at the flow rate of 15 Lmin^{-1} resulted in an aerosol with a mean (SD) median volume dimeter of 9.1 (0.3) μm (Exp. 6VCU). This measured size was slightly larger than that observed for analysis of the bulk formulation sized using the Sympatec HELOS/RODOS indicating that the VCU DPI did not fully disperse the powder to its primary particles. Removing the rod array slightly increased the mean (SD) Dv50 to 10.1 (0.5) μm (Exp. 7VCU). The % cumulative volume versus particle size graph for the VCU DPIs with and without the 3D-rod array and their respective time history plot are presented in Figures 5.27 and 5.28. As the graphs demonstrate in the presence of the 3D-rod array produces an aerosol with a bimodal distribution indicative of primary particles and particle aggregates in the emitted aerosol. When the 3D-rod array was removed, they were less deaggregation to primary particles and a monomodal distribution of aggregates was observed with a median diameter around 10 μm. Time history plots are also presented in Figures 5.27 and 5.28 showing the variation in the Dv10 (green), Dv50 (blue) and Dv90 (red) measured during the emission of the aerosol cloud from the DPI. The transmission (black) relates to the concentration of particles in the measurement zone. The time history plots indicate that for both devices, the particle size distribution of the emitted aerosol were relatively constant throughout the spray duration. The spray duration for capsules loaded with

about 5 mg of formulation was less than 1 sec indicating rapid emptying of powder formulation from the DPI. Finally, the effects of lowering the aerosolization flow rate to 10 Lmin^{-1} on the aerosol particle size distribution was assessed (Exp. 8VCU). As the results in Table 5.10 show reducing the flow rate from 15 to 10 Lmin^{-1} did not result in significant changes in the emitted dose from the device or the aerosol particle size distribution.

Table 5.10. Mean (SD) emitted dose and aerosol size distribution data for ciprofloxacin nanocomposites measured by Malvern Spraytec (n=3)

Exp.	Conditions	Emitted dose (% nominal)	Dv10 (μm)	Dv50 (μm)	Dv90 (μm)	Span
6VCU	VCU DPI 2.3-343 0.5mm capsule hole size PTFE coated 15 Lmin^{-1}	63.0 (2.4)	2.3 (0.4)	9.1 (0.3)	26.1(3.2)	2.1 (0.0)
7VCU	VCU DPI 2.3 0.5mm capsule hole size PTFE coated 15 Lmin^{-1}	75.1 (1.0)	3.2 (0.1)	10.1 (0.5)	24.4 (1.3)	2.6 (0.5)
8VCU	VCU DPI 2.3 0.5mm capsule hole size PTFE coated 10 Lmin^{-1}	73.3 (4.8)	3.1 (0.1)	11.6 (0.3)	25.3 (3.4)	2.8 (0.3)
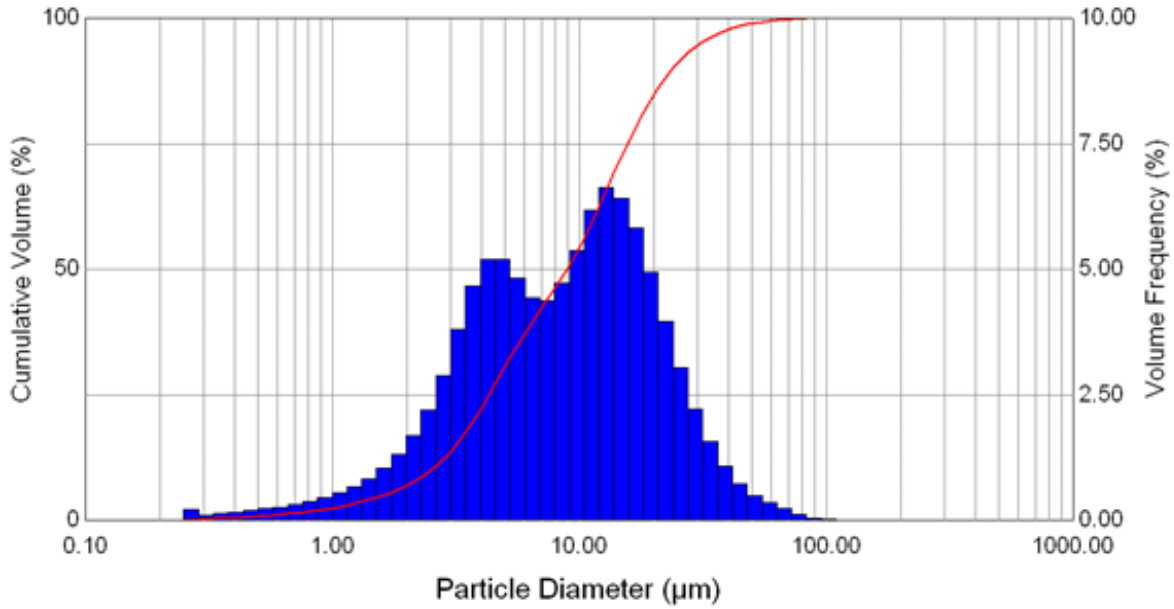
(a)
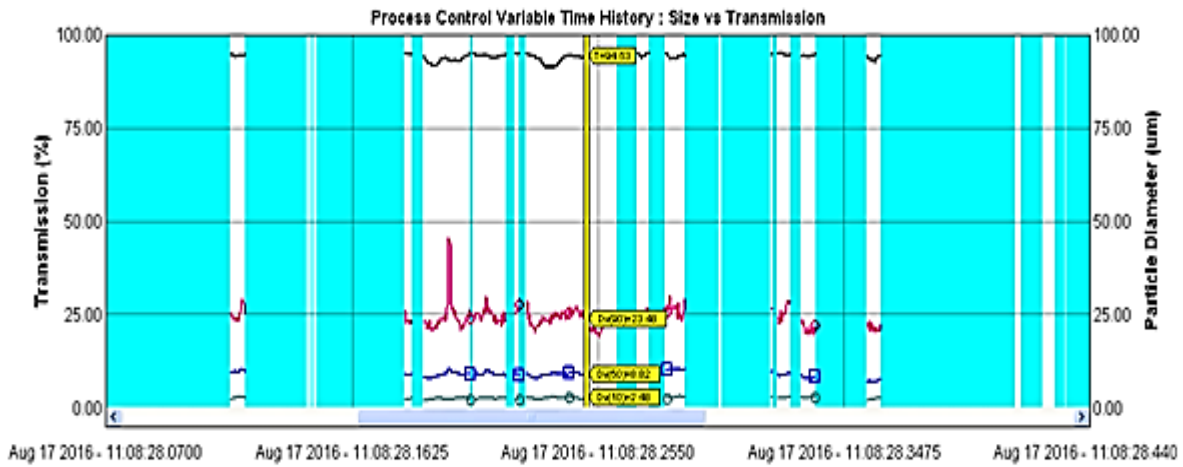
(b)

Figure 5.27. (a) Aerosol size distribution of ciprofloxacin nanocomposites aerosol exiting from VCU DPI 2.3-343 device operated at flow rate of 15 Lmin^{-1} (b) Time course showing Dv10 (green), Dv50 (blue) and Dv90 (red) measured during spray emission. The transmission (black) relates to the concentration of particles in the measurement zone
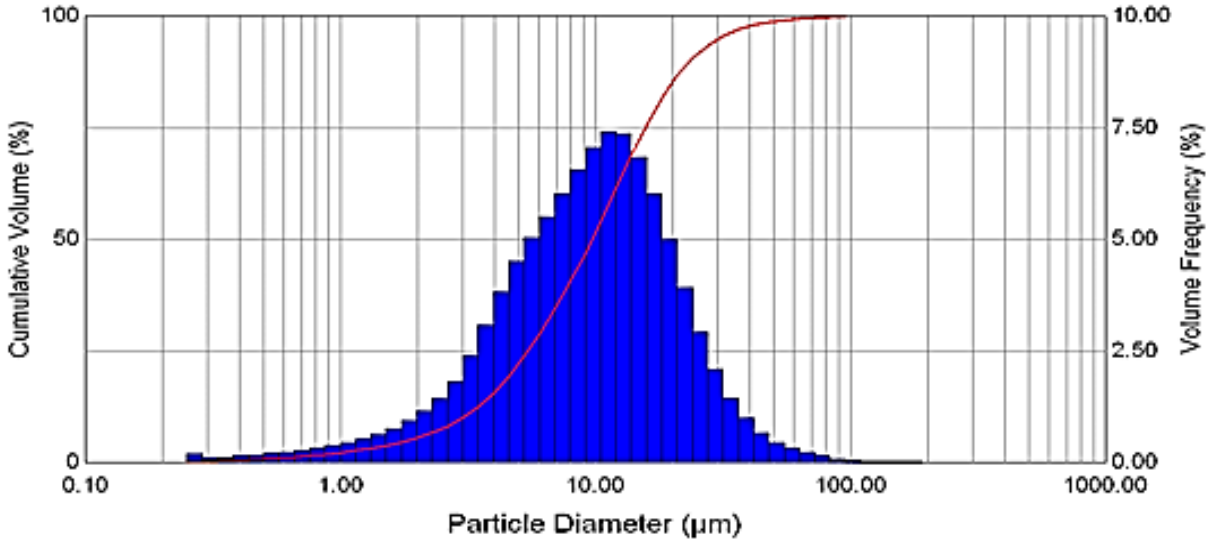
(a)
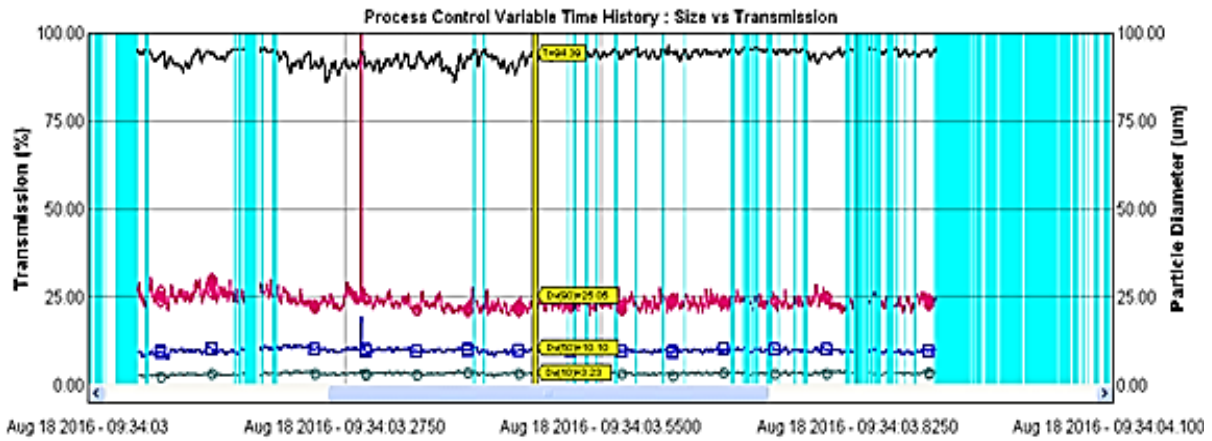
(b)

Figure 5.28. (a) Aerosol size distribution of ciprofloxacin nanocomposites aerosol exiting from VCU DPI 2.3 device operated at flow rate of 15 Lmin^{-1} (b) Time course showing Dv10 (green), Dv50 (blue) and Dv90 (red) measured during spray emission. The transmission (black) relates to the concentration of particles in the measurement zone

5.4.6 Evaluation of the regional nasal deposition of ciprofloxacin nanocomposite formulation administered using the VCU DPI and a novel delivery method

The effectiveness of the developed device-formulation-breathing maneuver combination as a method to improve drug delivery to the nasal middle passages was tested using a realistic nasal airway geometry. Specifically, the deposition of an aerosol generated from the VCU DPIs loaded with the optimized spray dried ciprofloxacin nanocomposite powder formulation with a median particle size of 5.6 µm (Exp. 6SD) was evaluated in combination with the nasal exhalation breathing maneuver. Aerosol is delivered to one nostril with the DPI sealed in place. Deposition is achieved by simultaneously exhaling and directing the aerosol away from the lungs and out of the open nostril. Table 5.11 demonstrates experimental conditions and corresponding emitted dose for VCU DPI device. Figures 5.29 and 5.30 show the regional nasal deposition of CPF when these methods were evaluated using VCU nasal model 1. In preliminary studies to evaluate the novel breathing maneuver, VCU DPI 2.3-343 was used in combination with an aerosolization flow rate of 15 $Lmin^{-1}$ and nasal exhalation flow rate of 60 $Lmin^{-1}$ (Exp. 1NASAL). In this study, emitted dose was 52.2 % of the nominal dose and the mean (SD) total nasal drug deposition was 62.6 (3.8) % of the emitted dose. Despite the low emitted dose, these initial studies with the VCU DPI 2.3-343 device provided useful information to optimize the breathing maneuver and other delivery parameters as described below. The mean (SD) exhaled dose was 37.4 (3.4) % of the emitted dose. The regional nasal distribution indicated that the mean (SD) deposition in the anterior nose was 24.6 (3.5) % and 23.4 (6.1) % in combined middle passage and nasopharynx regions. There was 14.4 (4.9) % of the emitted dose recovered in throat and filter. In order to exclude the possibility of drug bounce and re-entrainment, the nasal model surface was coated with a mucus mimic to simulate the presence of a mucus blanket in the nose and its ability to trap inhaled particles. This approach was resulted in a significant reduction in the mean (SD) % exhaled dose (21.2 (2.3) %,

Exp. 2NASAL) compared to the dose exhaled without mucus coating (p-value = 0.0038). The mean (SD) amount of drug deposited on the anterior nose was 31.0 (3.0) % and 27.0 (1.9) % of the emitted dose was deposited in combined middle passage and nasopharynx regions. It appeared that there was increased deposition in the throat and respiratory filter region (mean (SD) = 20.8 (1.1) %), however, this was not statistically different compared to the model without coating. To reduce the throat and filter drug deposition, the higher exhalation flow rate was increased to 90 Lmin^{-1} (Exp. 3NASAL). This resulted in a reduction in drug deposition in the mean (SD) throat and filter deposition with only 2.4 (0.4) % of the emitted dose being recovered in that region which was statistically significant compared to the 60 Lmin^{-1} study (p-value=0.0004). Using a flow of 90 Lmin^{-1} produced significant increases in the regional nasal drug deposition in the anterior nose, combined middle passage and nasopharynx regions together with the exhaled dose with mean (SD) values of 38.1 (1.4) %, 32.2 (2.6) % and 27.2 (2.2) %, respectively (p-values in comparison to 60 Lmin^{-1} were 0.0372, 0.0266 and 0.0272, respectively).

In order to reduce anterior nose deposition and improve delivery to the middle passage region, the design of the nasal cannula prong was altered. The streamlined nasal cannula prong angle was changed from 60º to 90º to better align the exit part of the nasal cannula prong with the entrance to the middle passages in VCU nasal model 1. This change in angle was also designed to prevent particle impaction on the anterior nasal walls (Exp. 4NASAL). Changing the nasal cannula prong angle resulted in a significant reduction in anterior nose deposition compared to the 60º angle (p-value< 0.0001) and increased drug delivery to the middle passages (p-value= 0.0275). However, the exhaled dose fraction was also increased. Future studies would all employ the 90º angle in the DPI design as it provided the optimal regional drug distribution within the nasal model, with low anterior nose deposition and enhanced delivery to the middle passages.

The nasal drug delivery of ciprofloxacin nanocomposites from VCU DPI 2.3-343 was also tested using an aerosolization flow rate of 10 Lmin^{-1} (Exp. 5NASAL). Deposition efficiency in the nasal airway is the function of impaction parameters of aerodynamic particle size (d_a^2) and flow rate (Q) [174]. However, this magnitude of the reduction in aerosolization flow rate for the ciprofloxacin nanocomposite aerosols using the VCU DPI did not result in any significant changes in regional nasal drug deposition or the amount of exhaled dose compared to aerosolization at 15 Lmin^{-1} (Exp. 4NASAL)

As described previously, the development of the VCU DPI produced a modified version with the 3D-rod array removed and device was PTFE coated to improve the emitted dose. The modified DPI employed a nasal cannula prong angle of 90º. Using the VCU DPI 2.3, the regional nasal deposition was evaluated and was observed to produce similar deposition fractions in the nasal model but less drug loss by exhalation compared to the DPI with the 3D-rod array. Most significantly for the development of a viable DPI, the emitted dose was increased from 46.4 (3.7) % with 3D-rod array (Exp. 5 NASAL) to 79.2 (2.7) % without the 3D-rod array (p-value = 0.0180). It appeared that as the emitted dose increases the relative amount of drug that is lost by exhalation decreases (Exp. 5NASAL, 6NASAL and 7NASAL). The VCU DPI 2.3 manufactured using the FormLabs clear resin (Exp. 7NASAL) produced a mean (SD) emitted dose of 85.0 (1.6) % and had the lowest exhalation drug losses compared to the (p-value = 0.0035 and p-value=0.0134, respectively compared to 32.2% and 18.4%). Using this DPI, the middle passage drug delivery of the ciprofloxacin nanocomposite formulation was increased to 65 % of the emitted dose which was equivalent to approximately 650 μg of drug from a 5 mg powder formulation contains 20.8 w/w% of drug content with an 85.0 % emitted dose. Figure 5.30 shows that these modifications of altering the exhalation flow rate, removal of the 3D-rod array and coating the device, altering the

nasal cannula prong angle to 90º and use of the FormLabs clear resin improved the emitted dose of the formulation from the device and resulting reducing deposition in the anterior nose, throat and filter and increasing the deposition in the target middle passage region.

CFD simulations performed by Dr. Longest and his group using a similar approach in which aerosol was delivered at 15 Lmin^{-1} to one nostril while simultaneously exhaling at 60 Lmin^{-1} through the other nostril. Using a similar sized aerosol (5 – 10 µm), the CFD predicted drug deposition in combined middle passage and nasopharynx area was 77.5 % which was similar to our experimentally determined value of 65 % (Exp. 7NASAL). The CFD predicted a slightly lower anterior nose deposition of 5.1% and an exhaled dose of 4.2 %. The results shown in Figure 5.31, it should be noted that the CFD conditions were not identical to those used for the experiments and simulated delivery via a tubing interface for administration of the aerosol to the nasal cavity.

Table 5.11. Experimental conditions used for optimization of regional drug deposition of the ciprofloxacin nanocomposite powder formulation tested in VCU nasal model 1. The emitted dose is calculated based on (%) nominal dose

Exp.	DPI actuation airflow (Lmin^{-1})	Exhalation airflow (Lmin^{-1})	Nasal cannula (º)	Nasal model coated	VCU DPI	Emitted dose (%nominal)
1NASAL	15	60	60	N	2.3-343	52.2 (3.8)
2NASAL	15	60	60	Y	2.3-343	55.3 (4.1)
3NASAL	15	90	60	Y	2.3-343	53.1 (2.8)
4NASAL	15	90	90	Y	2.3-343	60.1 (9.2)
5NASAL	10	90	90	Y	2.3-343	46.4 (3.7)
6NASAL	10	90	90	Y	2.3-coated	79.2 (2.7)
7NASAL	10	90	90	Y	2.3 FormLabs clear resin-coated	85.0 (1.6)
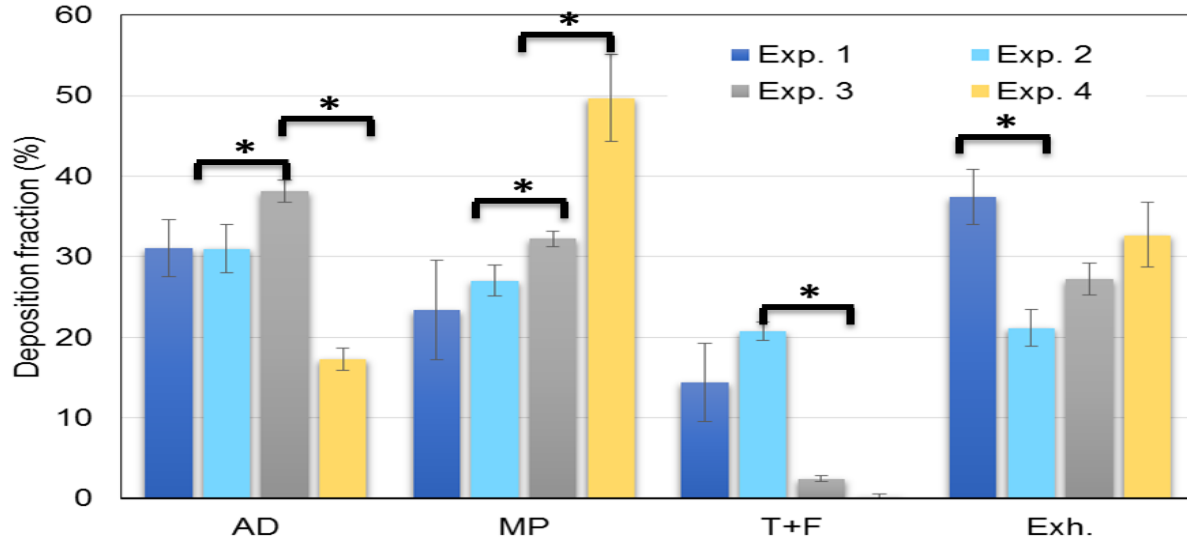
Figure 5.29. Optimization of the regional drug deposition of ciprofloxacin using the nanocomposite formulation delivered from the VCU DPI 2.3-343. Mean (error bars are SD) deposition in the anterior nose (AD), combined middle passage and nasopharynx region (MP), throat and filter T+F and the exhaled dose (Exh) are reported (n = 3). * P < 0.05
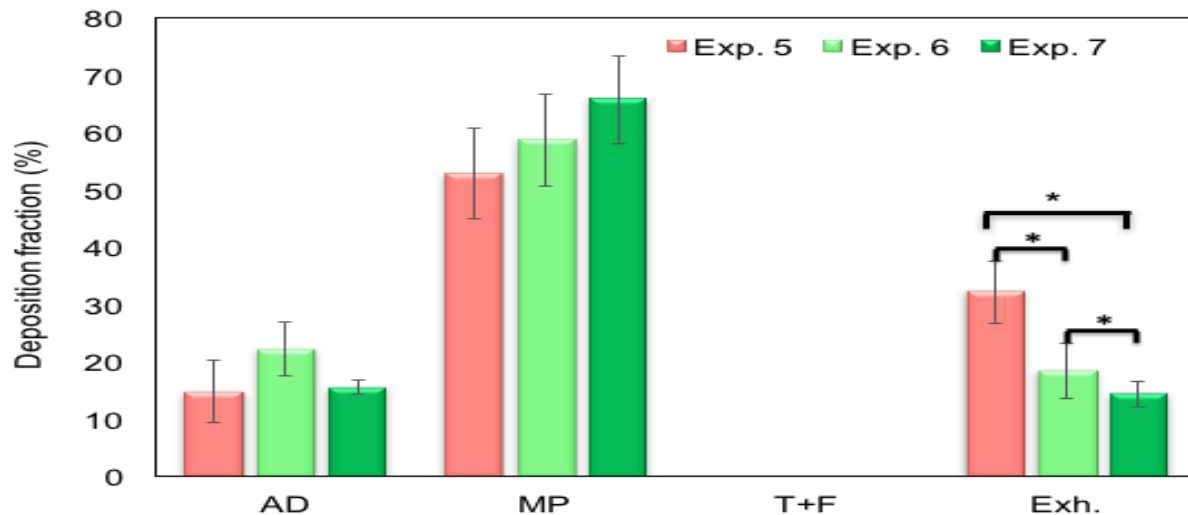
Figure 5.30. Optimization of the regional drug deposition of ciprofloxacin using the nanocomposite formulation delivered from the VCU DPI 2.3-343. Mean (error bars are SD) deposition in the anterior nose (AD), combined middle passage and nasopharynx region (MP), throat and filter T+F and the exhaled dose (Exh) are reported (n = 3-6). * P < 0.05
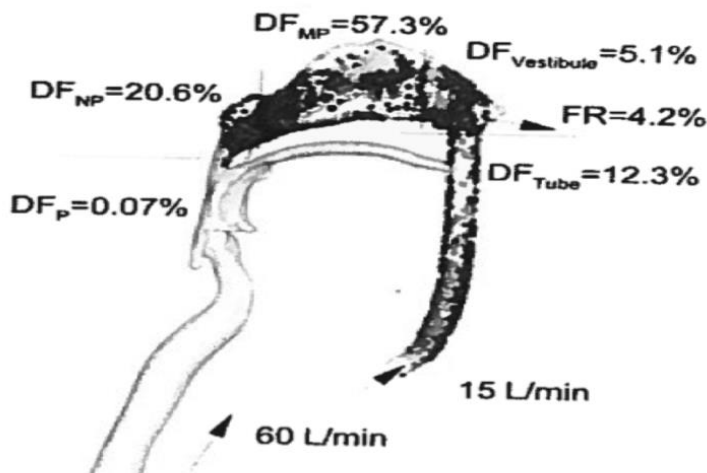
Figure 5.31. CFD simulation of regional nasal deposition of an aerosol delivered using a flow rate of 15 Lmin^{-1} to one nostril while simultaneously exhaling at 60 Lmin^{-1} through the other nostril.

In an effort to increase the drug load in the spray dried formulation, leucine was removed from the spray drying feed stock mixture, the concentration of PVP K30 reduced to 34.8 % w/w with the concentration of Tween 80™ remaining at 2.0 %w/w. This allowed the concentration of ciprofloxacin to be increased to 65 %w/w. This modified feed stock mixture had a solids concentration of 3.0 % w/v in water - ethanol 80:20 %v/v and was spray dried using the conditions described previously (section 5.3.2). The primary particle size distribution of the modified nanocomposite powder was measured using the Sympatec HELOS/RODOS (Section 5.3.3.5). For comparison, the unprocessed ciprofloxacin powder (starting material) was also sized. As shown in Table 5. 12 and Figure 5.32, the particle size distribution of the modified nanocomposite powder formulation was bigger to the previously optimized nanocomposite formulation was a mean (SD) Dv50 of 7.7 (0.1) µm compared to 5.6 (0.1) µm (*p*-value = 0.0080). The un-processed raw material

CPF powder exhibited a broad particle size distribution as shown in Figure 5.32, with mean (SD) Dv10, 50 and 90 values of 0.7 (0.01), 2.1 (0.1) and 21.2 (0.7).

In order to assess the effects of increasing the drug load in the CPF nanocomposite formulation on nasal drug distribution, a study was performed to compare the modified and previously optimized formulation, together with the unprocessed CPF powder. These three formulations were administered to the nasal cavity of VCU nasal model 1 using the experiment conditions that produced highest middle passage drug delivery and lowest exhaled dose as described above (Exp. 7NASAL). The results presented in Table 5.13 show that the modified nanocomposite formulation produced a similar mean (SD) emitted dose of 85 (4.4) % compared to the previously optimized nanocomposite formulation. The regional nasal deposition profile between the two formulations was also similar, with mean (SD) deposition in the anterior nose of 11.3 (3.8) %, combined middle passage and nasopharynx deposition of 72.2 (4.2) % and exhalation losses of 17.9 (6.0) % for the modified nanocomposite formulation. It appeared that the small but significant increase in particle size for the modified formulation did not significantly affect the emitted dose or regional nasal drug delivery compared to the previously optimized nanocomposite formulation. However, using the modified formulation the dose of CPF delivered to the middle passages was tripled using the same capsule formulation loaded mass compared to the optimized formulation due to the increased drug loading. In this study, a single capsule administration of the modified ciprofloxacin nanocomposite formulation containing a mean (SD) loaded nanocomposite formulation mass of 9.3 (0.4) mg produced a mean (SD) middle passage deposited dose of 3.7 (0.3) mg of CPF. This was significantly higher than the delivery achieved using either the previously optimized nanocomposite formulation with the lower loaded mass of CPF or the unprocessed ciprofloxacin powder (100% drug). For the unprocessed CPF powder with a mean

(SD) loaded powder mass of 8.2 (0.3) mg, the mean (SD) middle passage deposition was 2.2 (0.5) mg with a significantly fraction of the dose being deposited in the DPI and anterior nose indicating poor aerosolization of the unformulated raw material powder.

Regional nasal drug deposition within the middle passages for ciprofloxacin nanocomposite formulation was tested using the segmented VCU nasal model 1. The VCU nasal model 1 was segmented into anterior nose, middle and superior meatuses, olfactory region, maxillary sinuses and the base of middle passages (Figure 5.33). Ciprofloxacin modified nanocomposite powder was administered to the segmented model based on Exp. 7NASAL (Table 5.11). Regional nasal drug deposition data is presented in Table 5.14 (based on the total drug deposited in the combined middle passage and nasopharynx region). Based on the data shown in Table 5.14, it can be seen ciprofloxacin from modified nanocomposite formulation was distributed over all the different segments. Overall, drug deposition was higher in the left side compared to the right side of the nasal cavity which was the side of drug administration (nasal cannula was placed in the left nostril). Mean (SD) for drug deposition in the left meatus was 6.7 (3.6) % and 8.4 (3.9) % in the left olfactory segment. Similar values for the left sinus was 1.0 (0.7) % and 0.1 (0.7) % in the right sinus.

Drug delivery to the non-ventilated sinuses with narrow opening is known to be challenging. Maxillary sinus drug delivery of nasal sprays is reported as non-significant, however, 7.1 ± 1.7 (% of nasal deposited dose) sinus drug delivery was reported in healthy volunteers after pulsating aerosol application using a Vibrant nebulizer prototype with the use of pressure wave of 25 Hz (PARI Pharma GmbH, Germany)[137].

The observed regional nasal deposition results for the nanocomposite formulation and novel breathing maneuver are promising in the treatment of paranasal sinuses infection as targeted drug delivery can be observed to the potentially infected regions of meatuses (where the openings of paranasal sinuses are located).

Table 5.12. Mean (SD) particle size distribution properties measured by Sympatec for the modified ciprofloxacin nanocomposite formulation and unprocessed CPF powder (n=3)

Formulation	Drug content (%w/w)	Particle size distribution (measured by Sympatec) (µm)		
		Dv10	Dv50	Dv90
Optimized nanocomposite	20.8 (0.7)	$1.7 (0.0)^{\#}$	5.6 (0.1)*	10.6 (0.1)**
Modified nanocomposite	64.5 (0.6)	$1.8 (0.1)^{\#}$	$7.7 (0.1)^{*,+}$	$13.5 (0.1)^{**,++}$
Unprocessed CPF powder	100	0.7 (0.0)	2.1 (0.1)	21.2(0.7)

$^{\#}$ $P<0.05$, significant difference in Dv10 (one-way ANOVA), $P <0.001$ for optimized and modified nanocomposite formulations compared to unprocessed powder

* $P<0.05$, significant difference in Dv50 (one-way ANOVA), $P <0.001$ for optimized and modified nanocomposite formulations compared to unprocessed powder

$^{+}$ $P<0.05$, significant difference in Dv50 (one-way ANOVA), $P <0.001$ between the optimized and modified nanocomposite formulations

** $P<0.05$, significant difference in Dv90 (one-way ANOVA), $P <0.001$ for optimized and modified nanocomposite formulations compared to unprocessed powder

$^{++}$ $P<0.05$, significant difference in Dv90 (one-way ANOVA), $P <0.001$ between the optimized and modified nanocomposite formulations
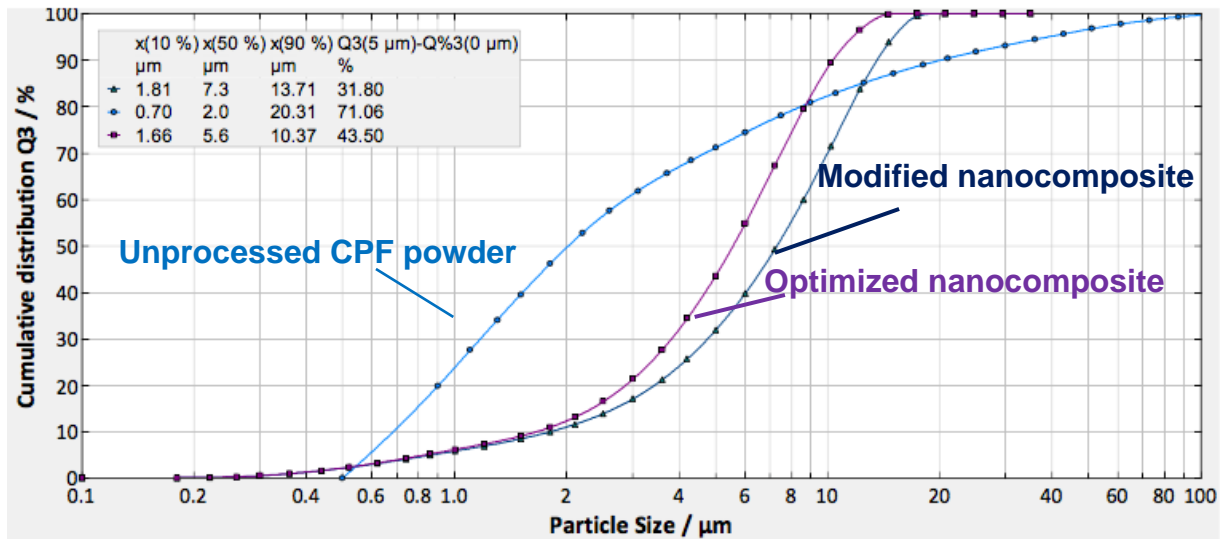
Figure 5.32. Representative cumulative volume fraction particle size distributions for the optimized and modified ciprofloxacin nanocomposite formulations (containing 20.8 (0.5) % and 64.5 (0.6) % drug content, respectively) and the unprocessed ciprofloxacin powder measured by Sympatec.

Table 5.13. Mean (SD) regional nasal drug deposition of the optimized and modified ciprofloxacin nanocomposite formulations and the unprocessed ciprofloxacin powder using the optimized VCU DPI and delivery technique. Ciprofloxacin powders were delivered using the VCU DPI 2.3 at a flow rate of 10 Lmin^{-1} with simultaneous nasal exhalation at flow rate of 90 Lmin^{-1} for 15 sec (n=4-6)

	Optimized nanocomposite formulation	Modified nanocomposite formulation	Unprocessed CPF powder
Capsule loaded mass (mg)	5.9 (0.9)	9.3 (0.4)	8.2 (0.3)
Drug content (%w/w)	20.8 (0.7)	64.5 (0.6)	100
Emitted dose (% nominal)	85.0 (1.6)	85.0 (4.4)	52.3 (4.9)*
Anterior nose deposition (% ED)	15.6 (1.1)	11.3 (3.8)	30.6 (15.1)**
Middle passage and nasopharynx deposition (% ED)	65.8 (7.6)	72.7 (4.2)	47.2 (10.9)***
Exhaled (% ED)	18.6 (2.2)	16.0 (6.0)	22.2 (5.2)
Mass of CPF in middle passages and nasopharynx (mg)	0.7 (0.1)	3.7 (0.2)	2.2 (0.5)
Recovery (%)	88.3 (4.9)	91.8 (5.2)	88.9 (3.4)

*P<0.05, significant difference in emitted dose compared to the modified nanocomposite formulation (p-value = 0.0123) (one-way ANOVA)

**P<0.05, significant difference in anterior nose deposition compared to the modified nanocomposite formulation (p-value = 0.0368) (one-way ANOVA)

***P<0.05, significant difference in middle passage drug deposition compared to the modified nanocomposite formulation (p-value = 0.0123) (one-way ANOVA)
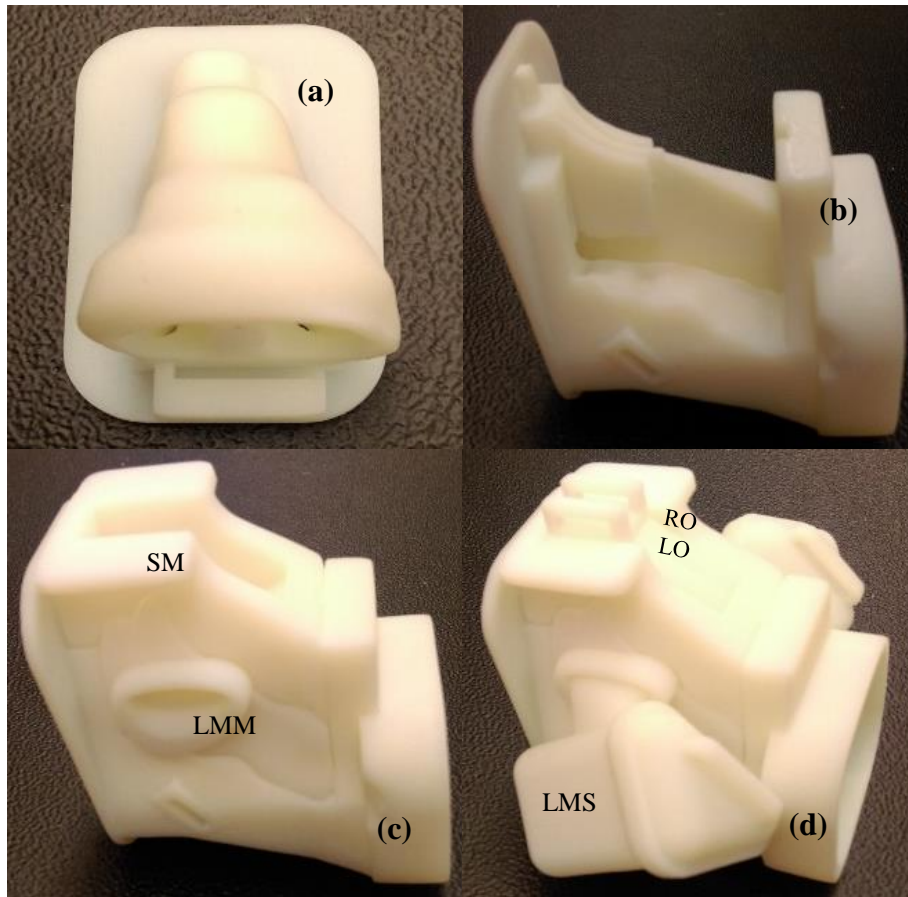
Figure 5.33. Images of segmented VCU nasal model 1 depicting (a) anterior nose, (b) base of middle passages, (c) left middle meatus (LMM) and superior meatus (SM), (d) left maxillary sinus and left – right olfactory regions attached to the base of middle passages

Table 5.14. Mean (SD) regional nasal drug deposition of the modified ciprofloxacin nanocomposite formulations using the optimized VCU DPI and delivery technique presented based on total middle passage and nasopharynx drug deposition. Ciprofloxacin modified nanocomposite powder was delivered using the VCU DPI 2.3 at a flow rate of 10 Lmin^{-1} with simultaneous nasal exhalation at flow rate of 90 Lmin^{-1}for 15 sec (n=3)

Middle passage and nasopharynx deposition (% ED)	71.3 (3.6)
Inferior meatus	76.1 (8.7)
Right Meatus	1.5 (0.8)
Left Meatus	6.7 (3.6)
Superior meatus	2.7 (0.8)
Right olfactory	3.0 (1.4)
Left Olfactory	8.4 (3.9)
Right Sinus	0.1 (0.0)
Left Sinus	1.0 (0.7)
Inferior meatus	76.1 (8.7)
Right Meatus	1.5 (0.8)

These studies have shown that the combined nasal drug delivery strategy using the VCU DPI and nanocomposite formulation did produce efficient drug delivery to the posterior part of the nasal cavity. Studies were performed using a capsule loaded formulation powder mass of approximately 10 mg of spray dried nanocomposite formulation which was efficiently aerosolized producing emitted drug doses of 80 – 85 % of the nominal CPF and good delivery to the target region in the middle passage and minimal off-target deposition. In this study, it was possible to achieve milligram levels of drug delivery to the nasal cavity (3.7 mg) that would make it feasible to deliver medications such as antibiotics including ciprofloxacin that require relatively high local doses for therapeutic effect. It is unclear as to the dose of ciprofloxacin required for efficacy within the nose to treat local infection due to a lack of literature data. A dry powder inhalation formulation of ciprofloxacin for treatment of infection in Non-CF bronchiectasis patients that are chronically infected with *P. aeruginosa* is currently being developed by Aradigm Corporation for lung delivery and has completed phase three clinical trial. For those studies, the administered dose of formulation is 50 mg, which is stated to correspond to 32.5 mg ciprofloxacin and is administered twice a day [175]. The estimated deposition of CPF in the trachea and bronchi was 22.3 % of the administered dose. Drug delivered to alveolar space was 17.2 % of the administered dose and was calculated to correspond to a delivered mass of 12.8 mg ciprofloxacin [176]. Assuming a similar dose for treatment of *P. aeruginosa* infection in the nasal cavity, this could be achieved by administration of three capsules of the modified nanocomposite formulation or by increasing the formulation capsule load. Despite powder delivery being popular in pulmonary delivery but so far rare in nasal administration. Powder formulations enhance drug stability and shelf life and its clearance by mucociliary clearance (MMC) is slower [177]. 50 to 60 % of initial nasal spray

formulations are typically removed by MCC to the nasopharynx in less than 20-30 minutes [16, 17, 140].

The dose of drug delivered by nasal sprays is limited by the ability to form a stable solution or suspension formulation and is usually delivered in a relatively low metered volume in the range of 25 – 200 µL [2]. Therefore, for high dose antibiotics, drug has to exhibit fairly good solubility to be formulated as a nasal spray product. Secondly, drug formulation from nasal sprays usually impacts closer to the site of release due to their large particle size of bigger than 40 µm which results in high drug losses in the anterior non-ciliated part of the nasal cavity near the nasal valve and base of the inferior turbinate [145] with little distribution in the middle passages and most of the deposited dose is quickly eliminated via the digestive tract. For nasal sprays, the effectiveness of the administered drug depends on mucociliary clearance of the deposited dose, which has been shown to be crucial for drug distribution and subsequent elimination [2]. *In vivo* studies show highly variable drug delivery to the middle passages for nasal sprays. However, it should be noted that mucociliary clearance may be impaired in cystic fibrosis (CF) patients with sinusitis and CRS patients who would be a potential target population for nasal antibiotic delivery. There are three targets for aerosol drug to treat sinusitis: i) the middle meatus which is a major site of drainage of maxillary and ethmoid, ii) superior and posterior regions of the nasal cavity and iii) maxillary and ethmoid sinuses [7]. In contrast to nasal sprays, nasal nebulization improves the drug deposition beyond the nasal valve and allows a larger dose to be delivered by continuous nebulization [178]. Nasal sonic jet nebulizers applying a frequency of 100 Hz have been developed to improve aerosol deposition in the sinuses compared to regular nasal jet nebulizers. The 100 Hz sonic waves generated by the sonic jet nebulizer creates a positive pressure between the ostium and the sinus allowing gas exchange within the sinus similar to a Helmholtz resonator and may increase aerosol

deposition into the sinuses by a factor two [179, 180]. Previous *in vitro* and *in vivo* experiments have demonstrated the benefit of applying an ultrasonic frequency during nebulization to improve sinus ventilation and aerosol deposition [39, 180]. Nasal sonic jet nebulizers are therefore considered the current best option for targeting aerosols to the sinus infection site. However, a disadvantage of using nasal jet nebulizers compared to nasal sprays for targeting the sinuses is that they also deliver a relatively large dose of aerosol to the lungs (33% to 58% of the dose) [17]. This has been shown to increase the risk of side effects, influence the efficiency of treating sinus infections and may result in a variable dose–response relationship. Similar levels of drug deposition in the lungs were obtained utilizing a conventional jet nebulizer and a nasal sonic jet nebulizer, indicating that the sonic effect did not have a significant influence on the level of aerosol deposition in the lungs [17]. In contrast, a new type of mesh nebulizer intended for nasal administration of drugs considerably reduced the inhaled fraction of the aerosol deposited in the lungs [137]. A similar aerosol particle size is produced by the sonic jet and mesh nebulizer. however, it appears that they do not have the same aerosol flow path through the sino-nasal cavity. The nasal sonic jet nebulizer delivers drug by inhalation through the nostrils of the patient. For this system, it is possible for the nebulized particles to reach the lungs via the nasal cavity during the patient's breathing due to their particle size and low velocity. In contrast, for the new mesh nebulizer system, the aerosol is administered using a constant air flow via one nostril and exhaled via the other nostril with the patient closing their soft palate to prevent inhalation. To achieve this, during aerosol delivery with the mesh nebulizer, the patient is instructed to breathe through the mouth. This approach bi-directional delivery is similar to the method proposed for the nanocomposite powder delivery developed in this dissertation [178]. However, using developed nasal administration technique for the dry powder nanocomposites formulation, deep penetration

into the nasal cavity and improved distribution over the nasal mucosa can be expected. Moreover, due to the smaller particle size distribution for the developed nasal powder formulation, variability in the delivered dose to the middle passages for from the novel developed delivery system is anticipated to be lower compared to the nasal spray products (with respect to nasal airway geometry variabilities due to inter and intra-subject variability including race, sex and age, along with the variability associated with the presence of the nasal disease, nasal septal deviation or the presence of the nasal cycle which can result in increased variability in delivered dose).

5.4.7 Development of a realistic nasal airway model incorporating cell monolayers into the airway passage walls to investigate transepithelial transport after realistic nasal deposition

5.4.7.1 Regional nasal deposition of ciprofloxacin after nasal administration – nasal exhalation technique with modified VCU nasal model 1

To investigate the transepithelial transport of the ciprofloxacin nanocomposite powder formulation deposited in a realistic manner on a cell monolayer modifications to the VCU nasal model 1 were made to incorporate Transwell inserts into the middle passage walls. The first task was to assess the regional nasal drug deposition of the powders in the modified nasal model in the presence of the Transwell® inserts. The results for regional drug deposition for the optimized nanocomposite formulation in the modified VCU nasal model 1 and drug deposition on the three Transwell® inserts are presented in Table 5.15. The regional nasal drug deposition did not change in the presence of the Transwell® inserts for the optimized nanocomposite formulation as shown in Tables 5.15 and 5.13. The mean (SD) mass of CPF on the three Transwell® inserts TW 1, 2 and 3 for the optimized nanocomposite formulation were 4.2 (1.4) µg, 11.3 (1.0) µg and 14.2 (2.1) µg,

237

respectively. Similar values were obtained when the unprocessed CPF powder was aerosolized into the modified nasal airway model with Transwells. The mean (SD) mass of CPF on the three Transwell® inserts, TW 1, 2 and 3 for the unprocessed CPF powder were 5.1 (3.0) µg, 11.2 (6.4) µg and 16.5 (4.2) µg, respectively. As previously described, the first and second inserts are located in the left middle meatus and the third insert is located in the superior meatus. Each Transwell insert has a surface area of 0.33 cm^2 and the total surface area of middle passage for VCU nasal model 1 is 80.24 cm^2. Therefore, each Transwell® insert represent 0.4% of the middle passage surface area [44]. The surface area of the left middle meatus is 8.76 cm^2 and the left superior meatus is 5.49 cm^2, therefore in these regions the inserts cover about 7 % of the left middle meatus region and 6% of the left superior meatus with respect to surface area. The mean (SD) percentage of the middle passage dose deposited on Transwells 2 and 3 was 1.9 (0.1) and 2.4 (0.4) %, respectively, with the optimized nanocomposite formulation. Similar values for the unprocessed CPF powder were lower with only 0.9 (0.1) % and 1.2 (0.3) % of the middle passage deposition on Transwells 2 and 3.

Table 5.15. Mean (SD) regional drug deposition for ciprofloxacin from ciprofloxacin formulations after nasal administration - nasal exhalation technique in VCU nasal model 1 with Transwell inserts (n=4)

	Optimized nanocomposite formulation	Unprocessed CPF powder
Capsule loaded mass (mg)	6.5 (0.5)	6.1 (0.3)
Emitted dose (% nominal)	77.0 (8.1)	52.1 (8.6)
Anterior nose deposition (% ED)	17.5 (6.4)	31.0 (11.0)
Middle passage and nasopharynx deposition (% ED)	62.8 (12.1)	41.3 (12.9)
Exhaled (% ED)	19.7 (6.6)	27.7 (3.1)
Mass of CPF in middle passages and nasopharynx (mg)	0.7 (0.1)	1.3 (0.4)
Drug mass on TW1 (µg)	4.2 (1.4)	5.1 (3.0)
Drug mass on TW2 (µg)	11.3 (1.0)	11.2 (6.4)
Drug mass on TW3 (µg)	14.1 (2.1)	16.5 (4.5)

5.4.7.2 Transepithelial transport across the Calu-3 cell line after realistic nasal deposition

TEER measurements performed on the Calu-3 monolayers prior to deposition studies and ranged from $780 - 950$ $\Omega.cm^2$. The Calu-3 cell monolayers were grown on the outer surface of the Transwell insert membrane using liquid covered culture (LCC) conditions, visual observation and TEER measurements provided evidence of the integrity of the cell monolayer and their confluency. Previous transport studies using this cell line reported the TEER measurements of $300 - 400$ $\Omega.cm^2$ for LCC and $700 - 1473$ $\Omega.cm^2$ and $350-600$ $\Omega.cm^2$ for air interface culture [181-183]. Transport media was maintained in the basolateral side during the deposition study to provide some structural rigidity for the membrane and monolayer during the nasal powder administration. The media on the basolateral side of the membrane prevented any movement of the insert membrane and cells during the deposition study while the airflow was passing through the modified nasal airway model. The initial deposition and transport studies were performed using HBSS as the transport media. However, it was observed that 1hr post deposition, the TEER measurements began to decrease by 50% ($350 - 450$ $\Omega.cm^2$) although they did recover to their original range of $780 - 950$ $\Omega.cm^2$ after 18 hrs. Therefore, as an alternative, EMEM growth media was used as the transport media. It appeared that the cells were very sensitive to any change in their environment and use of EMEM growth media minimized the changes experienced by the cell monolayers. Using growth media, the TEER mesurement 1 hr post deposition studies was in the range of $550 - 680$ $\Omega.cm^2$ and a second measurement after 12 hr showed TEER values of approximately 900 $\Omega.cm^2$. In both cases, there was no evident of cell leakages or changes to the monolayer cell integrity when observed visually using inverted microscope. The results from sham and deposition experiments indicate a small transient change in TEER following administration of the nasal powder. However, the measured TEER values following the 5 hr transport studies for all experiments performed were

larger than the reported literature TEER values for transport studies using Calu-3 cell lines, suggesting that the cell monolayer retained its integrity during nasal powder administration and realisitic deposition in the modified nasal airway geometry.

For all studies drug depositon on TW 1 was low and prevented analysis of the transepithelial transport due to limits of analytical detection. Therefore, the results presented below reflect drug transport studies performed on TWs 2 and 3 only. Figure 5.34 shows the cumulative mass drug transport from the optimized ciprofloxacin nanocomposite formulation across the confluent Calu-3 cells (TEER ranged 780 – 950 $\Omega.cm^2$) over 5 hours using HBSS and EMEM growth media (containing 1% PS) as the transport media at 37 °C. The data represents the combined transport data for drug deposited on TWs 2 and 3. The mean (SD) total average mass of drug deposited on the TWs 2 and 3 was 11.9 (1.4) µg and 12.6 (2.0) µg, (n=8) using HBSS and EMEM growth media as the transport media, respectively. Sham experiments reported a higher mass of drug deposited on the Transwells (Table 5.15) in the absence of the cell monolayer perhaps suggesting that the presence of cells altered the insert membrane surface properties and affected the total mass of formulation deposited. From Figure 5.34, it was observed that there was no change in the drug transepithelial transport across the Calu-3 cells when using HBSS or EMEM growth media as the transport media. The TEER measured 1 h after completion of the transport study was statistically different for the two transport media conditions (*p*-value = 0.0012) but this change in the TEER did not result in a change in the cumulative drug transport across the Calu-3 cell monolayer. The transport profile shows a linear increase in the drug transport across the Calu-3 cells using the HBSS ($R^2 > 0.9982$) and EMEM growth media ($R^2 > 0.9972$). This suggests uniform permeation across the cells as a function of time with the rate limiting step being the dissolution of drug on the cell surface and then transport across the cells. The mean (SD)

cumulative drug mass transported for the optimized ciprofloxacin nanocomposite formulation after 5 hours was 1133.2 (163.2) ng and 1179.3 (90.5) ng in the HBSS and EMEM transport media, respectively, which was 10.2 (2.3) and 9.5 (1.5) % of the amount of ciprofloxacin deposited on the Transwell cell monolayer surface.

A comparison of the transport of the optimized nanocomposite formulation with the unprocessed CPF powder delivered nasally to the modified realistic model is shown in Figure 5.35. These results reveal the effects on ciprofloxacin transport when the drug is formulated as nanoparticles compared to unprocessed micrometer sized particles. For this study, EMEM growth media was used as the transport media and the results are shown in Figure 5.35. The mean (SD) total average mass of drug deposited on the TWs 2 and 3 was 12.6 (2.0) µg and 10.6 (3.2) µg for the optimized nanocomposite and unprocessed CPF powder, respectively.

As shown in Figure 5.35, ciprofloxacin transepithelial transport from the unprocessed ciprofloxacin powder also exhibited a linear increase as a function of time ($R^2 > 0.9931$) but it was observed to be slower than compared to the optimized ciprofloxacin nanocomposite formulation. The mean (SD) cumulative percent mass transported across the Calu-3 monolayer over 5 hours for the unprocessed CPF powder was 5.4 (0.8) % which was significantly lower (p-value = 0.0198) than observed for the nanocomposite formulation (9.5 (1.5) %). Flux was calculated based on the linear slope from 1 to 5 hours and summarized in Table 5.16. There was a higher flux for the nanocomposite formulation compared to the unprocessed CPF powder. For transepithelial transport across the Calu-3 monolayer, powder drug formulations must be first dissolved. For the nanocomposite ciprofloxacin formulation, this process includes dissolution of the excipient matrix to release the ciprofloxacin nanoparticles which are then dissolved and transported across the cell monolayer. Despite this multi-step process, it appears that formulation of ciprofloxacin as

nanoparticles in the nanocomposite formulation increases the rate of drug transport compared to the unprocessed CPF powder raw material. The higher rate and extent of transport for the nanocomposite formulation compared to the unprocessed ciprofloxacin powder could be due to the transport of nanoparticles across the Calu-3 cells after dissolution of the nanocomposite matrix. However, results of dissolution test measured at pH 7 also showed the increased dissolution rate of nanocomposite formulation (Section 5.4.4) compared to unprocessed ciprofloxacin. Therefore, an alternative explanation could be that improved dissolution for nanocomposite formulation could be translated in higher transport across the Calu -3 cells.

Comparing the results obtained in this study with literature data, Ong et al. reported 33 % drug transport for ciprofloxacin (with median size of 3.6 μm) across the Calu-3 cell monolayer after 4 hours when grown at AIC [151]. In that study, ciprofloxacin was nebulized into a twin stage impinger (operating at the flow rate of 15 Lmin^{-1}) while replacing the solution in second stage with a Transwell insert which allowed deposition of 8.7 (2.0) μg ciprofloxacin on the cell monolayer [151]. The greater transport observed transport (33 %) compared to values of 5.4-9.5 % in these present studies. Differences may be attributed to the lower cell monolayer TEER reported by Ong of 550 Ω cm^2 compared to values of 780 – 950 Ω.cm^2 in the present study. Darweesh et. al [181] reported a TEER dependent transport for ciprofloxacin hydrochloride as steady state flux was significantly reduced when the TEER was over 700 Ω.cm^2.
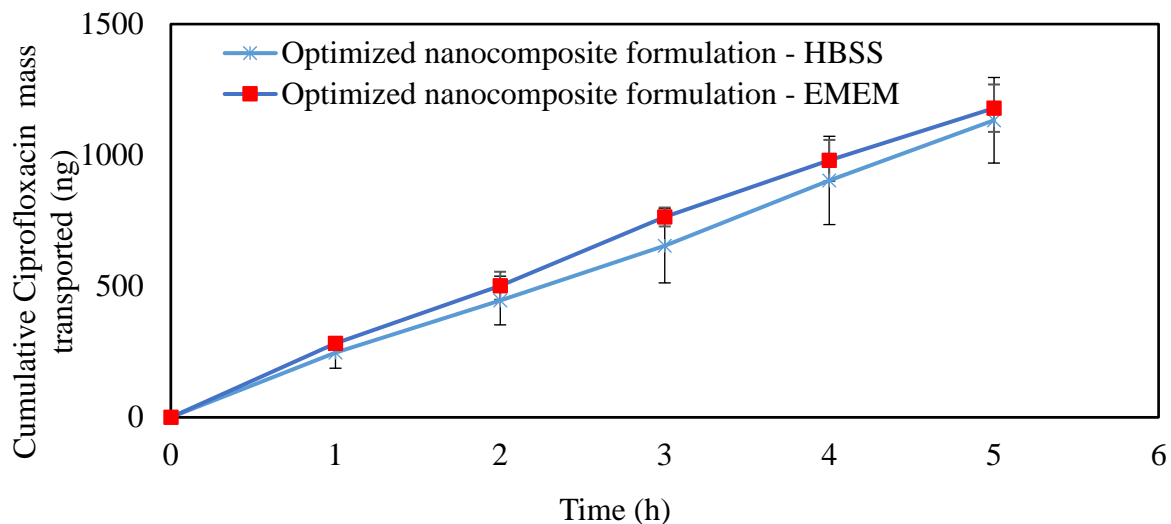
Figure 5.34. Mean (error bars are SD) cumulative ciprofloxacin transport for the optimized nanocomposite formulation across the Calu-3 cell monolayer over 5 hours using HBSS and EMEM as transport media. Linear regression was performed between for 1- 5 hr (n=3)
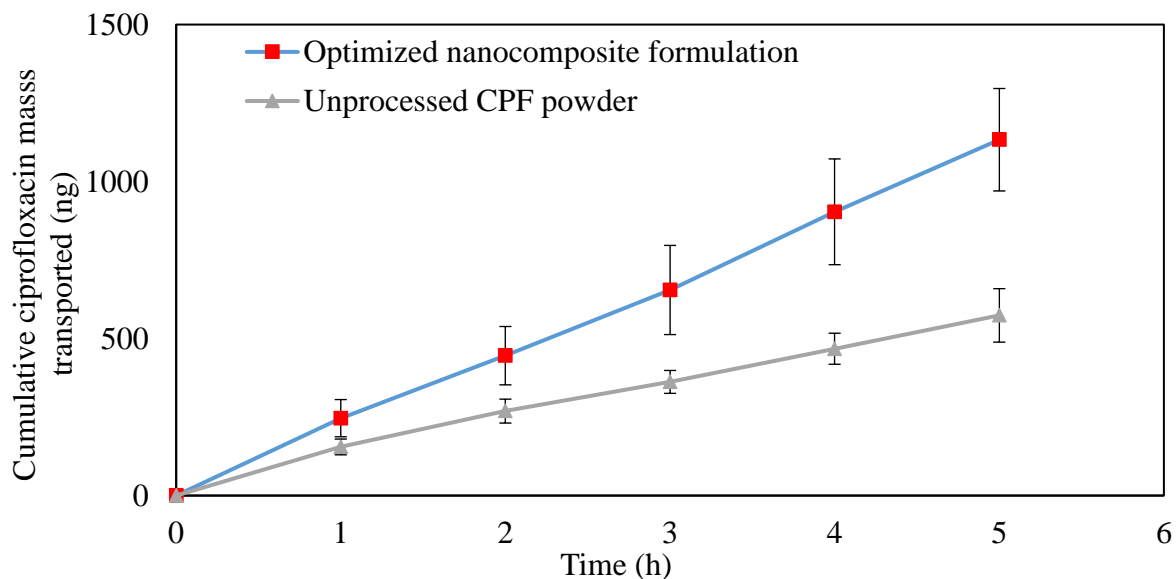
Figure 5.35. Mean (error bars are SD) cumulative ciprofloxacin transport for the optimized nanocomposite formulation and the unprocessed CPF powder across the Calu-3 cell monolayer over 5 hours using EMEM as transport media. Linear regression was performed between for 1- 5 hr (n=4)

Table 5.16. Mean (SD) steady state ciprofloxacin flux for the optimized ciprofloxacin nanocomposite formulation and the unprocessed CPF powder. Mean (SD) total drug masses of 12.6 (2.0) µg (n=8) and 10.6 (3.2) µg (n=6) were deposited on TWs 2 and 3 for the optimized ciprofloxacin nanocomposite formulation and the unprocessed CPF powder, respectively.

	Flux (ng/h/cm^2)
Optimized nanocomposite formulation	725 (92)
Unprocessed CPF powder	321 (94)

In this section, the successful deposition of ciprofloxacin powder formulations on the surface of liquid cover culture Calu-3 cell monolayer using a modified VCU nasal model was described. These studies have demonstrated the development of methodology that will allow realistic nasal deposition of drug followed by investigation of its transepithelial transport (Specific Aim 3-4). Using this newly developed technique, the transepithelial transport of a novel nanocomposite ciprofloxacin formulation was investigated following realistic nasal deposition. Its dissolution, cellular uptake and transport across the Calu-3 monolayer was compared to unprocessed CPF powder. The developed methods were able to discriminate between the two powders and identified differences in their dissolution and transport.

Future continued development of this method should focus on the incorporate of a more relevant cell model including a cell monolayer based on an air-interface culture method (AIC). In this technique, the monolayer is more morphologically similar to the airway epithelial by differentiating and developing tight junction and producing ciliated cells and goblet cells which produce mucus and has been used for both nasal and lower respiratory region cells [184-190]. Also, the use of a nasal epithelial cell model should be considered to improve the realism of the

airway model system. In these initial studies developing the technique, a Calu-3 cell monolayer was employed, however, future studies should investigate the feasibility of growing nasal epithelial cells as the monolayer. It is possible to obtain nasal epithelial cells by nasal scrape biopsies from healthy subjects or patients with allergic rhinitis (AR) or other disease states such as nasal polyps, cystic fibrosis [185, 191]. A reduced number of ciliated cells, loose tight junctions and hyperplasia of the secretory cells were observed in nasal epithelial cells from AR patients developed based using the AIC method and these characteristics may affect the transepithelial transport of nasally administered drugs [185].

5.5 Conclusions

In this chapter, the influence of crystallization variables was investigated to optimize the methods to produce ciprofloxacin nanoparticles. Conditions were identified using ultrasound energy in combination with an appropriate anti-solvent system to control nucleation and crystal growth of ciprofloxacin nanoparticles. The ciprofloxacin nanoparticles were characterized with respect to their stability, composition and particle size. Methods were also developed to produce spray dried nanocomposite particles. Composition of the spray drying feed stock mixture was optimized to produce stable and re-dispersible nanocomposites suitable for nasal administration (Specific Aim 3-1). High efficiency targeted delivery of the developed nasal nanocomposite powder was achieved using a modified VCU DPI in combination with a novel breathing maneuver (Specific Aim 3-2). The delivery of the developed formulation was assessed using the previously developed realistic airway model and showed good emitted dose characteristics together with low anterior nose deposition losses and high drug deposition in the target middle passage nasal cavity.

(Specific Aim 3-3) A modified version of the realistic airway model was developed and used to investigate the transepithelial transport of the nanocomposite formulation across a Calu-3 cell monolayer that was incorporated in the wall of the airway model to allow realistic deposition of the nasal aerosol (Specific Aim 3-4). This system was used to demonstrate improved dissolution and transport characteristics of the nanocomposite formulation in the cell system compared to unprocessed CPF powder.

Chapter 6

SUMMARY AND CONCLUSION

The nasal cavity has been widely used as a route of drug administration for topical and systemic delivery of medications. Several factors play a critical role in determining the efficacy of nasal drug delivery, including drug and formulation properties, delivery device characteristics and inter-subject variability in the nasal cavity geometry. In recent years and in this dissertation, physically realistic nasal airway models have been used to assess the delivery efficiency and drug deposition pattern of nasal spray products using *in vitro* experiments. The *in vitro* tests utilizing hollow physical models have been shown to offer realistic characterizations of regional drug deposition of nasal spray products when compared with *in vivo* studies. In contrast, some of the traditional *in vitro* tests focus on droplet size and plume geometry characteristics and the link to clinical deposition is less well established. For these realistic *in vitro* methods to capture the range of inter-subject variability found in the clinical population, it is unlikely to be achieved using a single geometry and efforts should be directed to developing a range of models or an idealized average nasal airway geometry model, similar to the approach taken for the mouth-throat models used to evaluate inhalation drug products [192].

The first part of this project focused on developing a realistic *in vitro* test for nasal spray products (Specific Aim 1-1) and investigating the influence of patient-use factors on regional drug deposition in a physically realistic model of the nasal cavity for a commercially available nasal spray product, Nasonex® nasal spray (Specific Aim 1-2). We tested the hypothesis that simulated patient-use experimental conditions can influence the *in vitro* regional drug deposition of nasal spray products in realistic nasal models. A full factorial design of experiments was conducted to

assess the effect of variables including nasal spray positioning in the nostril, head angle, nasal spray actuation force and coordination of actuation of the nasal spray with patient inhalation. Using the realistic physical nasal model, regional deposition of the nasal spray was evaluated using the simulated patient use conditions. The overall regional deposition pattern and lung delivery were similar to previous *in vivo* studies performed for nasal spray products [16-18, 140, 193]. The *in vivo* deposition results revealed regional nasal drug deposition was observed to varied widely for nasal spray products with mean middle passage deposition for the Nasonex® product being reported as 65 % [34] and about 35 % [18]. A similar range of *in vitro* middle passage deposition was observed in this study, with differences in the deposition being dependent on the patient use conditions employed. Mean *in vitro* drug delivery to middle passage ranged from 17 % to 57 % of the delivered dose when tested using VCU model 1. The presence of nasal inhalation during nasal spray delivery was observed to play a significant role in determining drug penetration through the nasal valve and into the middle passage. With simultaneous inhalation and actuation, there was a reduced fraction of drug loss due to deposition in the anterior region and improved drug deposition in the posterior nasal cavity. The DOE study using VCU nasal model 1 revealed an interaction between the nasal head angle and inhalation during actuation. Conditions were identified that would appear to enhance delivery of drug to the site of action in the middle passages and may be useful to advise patients seeking to increase the effectiveness of the Nasonex® nasal spray and minimize drug deposition losses in the anterior nose. Therefore, we can conclude that simulated patient-use experimental conditions can influence the *in vitro* regional drug deposition of nasal spray products in realistic nasal models.

The next hypothesis stated that the *in vitro* regional drug deposition of nasal spray products in realistic nasal models is determined the differences in the airway geometry of the nasal model

and the formulation / spray device properties. The initial studies were performed in a single nasal airway geometry. As described earlier, it is important to consider the effects of inter-subject variability and its effects on the nasal spray deposition. Also, having identified a series of patient use parameters which influenced deposition in VCU nasal model 1, it was important to characterize their effects in a second nasal model, with differing nasal cavity geometric dimensions. Therefore, the regional nasal deposition pattern of Nasonex® was investigated using a 2nd nasal model (VCU nasal model 2) and the effects of the patient use conditions compared with VCU nasal model 1 (Specific Aim 2-1). In general, drug deposition in the middle passage of VCU nasal model 2 was higher than observed under similar test conditions with VCU nasal model 1. The mean drug deposition fraction in the middle passages ranged from 47 to 77 % in VCU nasal model 2 compared to 17 to 57 % in VCU nasal model 1. Clearly demonstrating evidence of significant inter-subject variability which was possibly related to differences in the geometry of the nasal vestibule and valve regions. In addition, it was observed that VCU nasal model 2 was less discriminating or sensitive with respect to the varying patient use parameters which across the range of conditions tested produced only a 1.7-fold change in middle passage deposition compared to a 3.4-fold change for VCU nasal model 1. Testing with a second airway model emphasized the significant effect nasal geometry can have on the regional drug deposition of the tested nasal spray product and can be indicative of the potential range of inter-subject variability that can be expected *in vivo*. With respect to the patient use parameters, both models indicated the benefits of coordinating inhalation with spray actuation and tilting the head forward during actuation to improve drug delivery to the middle passage region and minimize anterior nose deposition. There are some limitations of the *in vitro* nasal airway models, due to their rigid inflexible structure, they are unable to simulate the Bernoulli forces present during inhalation which narrow the nasal valve with increasing inspiratory

flow rate [61]. The current *in vitro* studies indicated that deposition was independent of inhalation flow rate and that only a very small fraction of drug penetrated the nasal valve in the absence of an inhalation. The *in vitro* studies have revealed positioning of the nasal spray within the nostril, patient head angle and the coordination of inhalation and actuation all have significant influence on the ultimate deposition of the Nasonex® nasal spray and that providing detailed information regarding administration technique to the users could be used to ensure maximal drug delivery of the nasal spray.

The ability of the realistic *in vitro* nasal deposition method to discriminate between nasal sprays was also investigated using innovator and generic nasal sprays, together with sprays with differing droplet size and spray plume characteristics (Specific Aims 2-2 and 2.3). The range of drug delivery observed *in vitro* using VCU nasal models 1 and 2 for the Nasonex® and Flonase® nasal sprays were similar to the published range of *in vivo* deposition for these devices with respect to the fraction of drug penetrating the nasal valve region and depositing in posterior nose[18]. When comparing the differences in the spray characteristics of these innovator nasal sprays, differences in their droplet size distributions did significantly change their *in vitro* regional nasal drug deposition between the two nasal sprays products. The utility of the developed technique to assess regional nasal deposition of products designed to be generic copies of the innovator products, with therefore equivalent droplet size and spray plume characteristics, was also investigated using "in house" copies or marketed generic nasal spray products. The developed *in vitro* test methods were able to reliably produce similar regional nasal deposition profiles for the nasal spray products with similar spray plume characteristics. Finally, the *in vitro* test method did reveal that changes to spray plume properties could result in regional nasal deposition differences in the realistic airway geometry. Using a nasal spray with an increased spray diameter (Dmin and

Dmax), and plume angle produced higher drug deposition in the anterior nose region and lower deposition in the middle passages of VCU nasal model 1. Previous, *in vitro* and *in vivo* studies showed similar effects of increasing anterior nose deposition for nasal spray formulations with an increasing spray plume angle [16, 31]. In general, it was found that deposition in VCU nasal model 1 was more sensitive to experimental conditions (patient use and nasal spray) than VCU nasal model 2.

This comprehensive evaluation of the drug delivery to the nose for the Nasonex® spray product performed using controlled multi-variant conditions can provide guidance for the rational targeting of the nasal spray plume for delivery to the site of action within the middle passages with respect to both the device – formulation characteristics (spray plume, droplet size) and administration technique (head angle, inhalation / actuation coordination). Further studies are required to investigate the methodology as a tool for the evaluation of innovator and generic nasal spray products. It will be important to examine the nasal drug delivery efficiency of the products in a series of nasal airway models representing the variability observed in the patient population with respect to airway geometry. The selection of these representative nasal airway models and the establishment of criteria to characterize critical geometric features was beyond the scope of this study but will be essential for the future utility of this method. However, these studies have shown that the *in vitro* methods have potential advantages for the study of nasal drug delivery efficiency and for the assessing the equivalence of nasal spray products. These studies demonstrated that the combined use of physically realistic nasal airway models with simulated patient use experimental conditions could allow quantification of *in vitro* spray deposition patterns within the nose.

The developed *in vitro* nasal deposition model was also used as a tool to evaluate a novel antibiotic formulation – device combination that was developed. We hypothesized that enhanced middle passage drug delivery can be accomplished using a novel nanocomposite formulation and nasal powder delivery system. Potential applications of a nasal antibiotic include the treatment of infection in CRS. Drug nanoparticles were identified for the formulation, as it has been suggested the micrometer-sized particle delivery systems were unlikely to enhance flux through the mucus in CRS or CF patients [75, 76, 194]. Ciprofloxacin nanocrystals in the targeted particle size between 100-200 nm, suitable for penetration through mucus and potentially through biofilm layers produced by bacteria such as P. aeruginosa, were produced by an optimized sonocrystallization process. Rapid mixing of drug solution and anti-solvent, under controlled temperature conditions, was provided by application of ultrasound and crystallization variables were optimized to increase local supersaturation and increase nucleation rate of ciprofloxacin. Optimized conditions employing a mixture of aqueous and organic anti-solvent together with the use of Tween® 80 a stabilizer yielded a stable nanoparticle formulation with a mean size of 120 nm and relatively monodisperse particle size distribution.

A spray drying technique was used to convert the antibiotic nanocrystals into a nanocomposite powder in the size range of 5 - 10 μm suitable for nasal drug delivery. The goal was to produce a powder formulation suitable for use in a nasal dry powder inhaler containing dispersed nanoparticles in a matrix of water soluble excipients. On delivery to the nose, the excipients would rapidly dissolve leaving the nanoparticles on the airway surface which would then penetrate through the mucus layer and exert their antimicrobial effects. Previous studies have demonstrated that nanoparticle aggregation during spray drying was often observed which would be undesirable [102]. Water soluble excipients such as PVP K30 and mannitol were evaluated for

their ability to prevent nanoparticle aggregation during spray drying. Optimized conditions employing PVP K30 and increasing the solids concentration in the stock feed mixtures produced particles with desired size distribution (5 - 10 μm) which were readily soluble in water and released ciprofloxacin nanoparticles. The mean size of the nanoparticles before and after spray drying was 120 and 140 nm (Specific Aim 3-1). A Transwell® system, with limited fluid volume simulating the local environment within the nose, was developed to compare the dissolution of unprocessed ciprofloxacin powder (2 μm) with the nanoparticles, both as the initially produced nanosuspension following crystallization and in the spray dried nasal formulation. An increased dissolution rate was observed for the ciprofloxacin nanosuspension compared to the unprocessed ciprofloxacin powder due to reduced particle size of the nanoparticles. Spray drying and the addition of Tween™ 80 did not appear to affect the dissolution rate of the ciprofloxacin nanoparticles, with similar dissolution profiles observed for the nanosuspension and the spray dried nanocomposite powder.

High efficiency targeted delivery of the nanocomposite nasal powder formulation was achieved using a modified low flow VCU DPI used in combination with a novel breathing maneuver (Specific Aim 3-2). This method offers the ability to target delivery to the nasal middle passages and allows delivery of milligram doses that would be required for antibiotic therapy. The delivery efficiency of the developed nanocomposite formulation was assessed using the previously developed realistic *in vitro* airway model. The optimized emitted dose of the spray dried nanocomposite nasal formulation was about 80 % using the modified VCU DPI with a low actuation flow rate in a fixed air volume to prevent lung inhalation. This was significantly higher than the emitted dose for the unprocessed ciprofloxacin powder using the same DPI. For the spray dried nanocomposite nasal formulation, there was low anterior nose loss and drug deposition in the target middle passage nasal region was 72 % of the nominal dose (Specific Aim 3-3). Future

studies should evaluate the deposition in nasal airway models with varying airway geometries in the anterior nose and middle passages to assess the effects of inter-subject variability for this novel delivery technique. In this study, we demonstrated the delivery of approximately 3.7 mg of ciprofloxacin as a novel nanoparticle formulation to the site of action within the middle passages.

Finally, the realistic nasal airway model was modified to allow an *in vitro* assessment of dissolution and transepithelial transport following realistic deposition on a cell monolayer positioned in the wall of the airway model (Specific Aim 3-4). In this study, VCU nasal model 1 was modified to accommodate three Transwell® inserts with Calu-3 monolayers on the surface such that they are positioned on the walls of the middle passage. Studies were performed to determine drug deposition in the presence and absence of the cell monolayer and to confirm the integrity of the monolayer following nasal aerosol administration. Ciprofloxacin nasal aerosols were delivered to the modified airway model and the transepithelial transport of drug deposited on the Calu-3 cell monolayers was investigated. Studies revealed that the nanocomposite formulation appeared to have an increased flux compared to unprocessed ciprofloxacin delivered using the same technique. Future studies should employ a more relevant cell model; nasal epithelia cell lines would provide a more clinically relevant assessment of the fate nasally administered drugs. In addition, the effectiveness of the produced nanoparticles to penetrate through highly viscous mucus was beyond the scope of these studies. Future work should examine the functional ability of the formulated nanocomposites and nanoparticles to improve delivery of antibiotics.

LIST OF REFERENCES

1.   Illum L: Nasal drug delivery—possibilities, problems and solutions. J Control Release 2003, 87:187-198.

2.   Djupesland PG: Nasal drug delivery devices: characteristics and performance in a clinical perspective—a review. Drug Deliv Transl Res 2013, 3:42-62.

3.   Mygind N, Dahl R: Anatomy, physiology and function of the nasal cavities in health and disease. Adv Drug Deliv Rev 1998, 29:3-12.

4.   Newman SP, Pitcairn GR, Dalby RN: Drug delivery to the nasal cavity: *in vitro* and *in vivo* assessment. Crit Rev Ther Drug Carrier Syst 2004, 21:21-66.

5.   Sahin-Yilmaz A, Naclerio RM: Anatomy and physiology of the upper airway. Proc Am Thorac Soc 2011, 8:31-39.

6.   Liu Y, Johnson MR, Matida EA, Kherani S, Marsan J: Creation of a standardized geometry of the human nasal cavity. J Appl Physiol 2009, 106:784-795.

7.   Laube BL: Devices for aerosol delivery to treat sinusitis. J Aerosol Med 2007, 20:S5-S18.

8.   Wolfe TR, Bernstone T: Intranasal drug delivery: an alternative to intravenous administration in selected emergency cases. J Emerg Nurs 2004, 30:141-147.

9.   Illum L: Nasal drug delivery: new developments and strategies. Drug Discov Today 2002, 7:1184-1189.

10.   Sankar C, Rani M, Srivastava AK, Mishra B: Chitosan based pentazocine microspheres for intranasal systemic delivery: development and biopharmaceutical evaluation. Die Pharmazie 2001, 56:223-226.

11.   Pavis H, Wilcock A, Edgecombe J, Carr D, Manderson C, Church A, Fisher A: Pilot study of nasal morphine-chitosan for the relief of breakthrough pain in patients with cancer. J Pain Symptom Manage 2002, 24:598-602.

12.   Bennett WD, Zeman KL: Effect of race on fine particle deposition for oral and nasal breathing. Inhal Toxicol 2005, 17:641-648.

13.   Kesavanathan J, Bascom R, Swift DL: The effect of nasal passage characteristics on particle deposition. J Aerosol Med 1998, 11:27-39.

14.   Gambaruto AM, Taylor DJ, Doorly DJ: Decomposition and description of the nasal cavity form. Ann Biomed Eng 2012, 40:1142-1159.

15. Kimbell J, Segal RA, Asgharian B, Wong BA, Schroeter JD, Southall JP, Dickens CJ, Brace G, Miller FJ: Characterization of deposition from nasal spray devices using a computational fluid dynamics model of the human nasal passages. J Aerosol Med 2007, 20:59-74.

16. Newman SP, Morén F, S.W. C: Deposition pattern of nasal sprays in man. Rhinology 1988, 26:111-120.

17. Suman JD, Laube BL, Dalby R: Comparison of nasal deposition and clearance of aerosol generated by a nebulizer and an aqueous spray pump. Pharm Res 1999, 16:1648-1652.

18. Leach CL, Kuehl PJ, Chand R, McDonald JD: Nasal deposition of HFA-beclomethasone, aqueous fluticasone propionate and aqueous mometasone furoate in allergic rhinitis patients. J Aerosol Med Pulm Drug Deliv 2015.

19. Pu Y, Goodey AP, Fang X, Jacob K: A comparison of the deposition patterns of different nasal spray formulations using a nasal cast. Aerosol Sci Technol 2014, 48:930-938.

20. Cheng YS: Aerosol deposition in the extrathoracic region. Aerosol Sci Technol 2003, 37:659-671.

21. Xi J, Longest PW: Numerical predictions of submicrometer aerosol deposition in the nasal cavity using a novel drift flux approach. Int J Heat Mass Transfer 2008, 51:5562-5577.

22. Golshahi L, Noga M, Thompson R, Finlay W: *In vitro* deposition measurement of inhaled micrometer-sized particles in extrathoracic airways of children and adolescents during nose breathing. J Aerosol Sci 2011, 42:474-488.

23. Cheng Y-S, Yamada Y, Yeh H-C, Swift DL: Diffusional deposition of ultrafine aerosols in a human nasal cast. J Aerosol Sci 1988, 19:741-751.

24. Gambaruto AM, Taylor DJ, Doorly DJ: Modelling nasal airflow using a Fourier descriptor representation of geometry. Int J Numer Methods Fluids 2009, 59:1259-1283.

25. Churchill SE, Shackelford LL, Georgi JN, Black MT: Morphological variation and airflow dynamics in the human nose. Am J Hum Biol 2004, 16:625-638.

26. Naftali S, Rosenfeld M, Wolf M, Elad D: The air-conditioning capacity of the human nose. Ann Biomed Eng 2005, 33:545-553.

27. Cheng YS, Yeh HC, Guilmette RA, Simpson SQ, Cheng KH, Swift DL: Nasal deposition of ultrafine particles in human volunteers and its relationship to airway geometry. Aerosol Sci Technol 1996, 25:274-291.

28.   Cheng K, Cheng Y, Yeh H, Swift D: Deposition of ultrafine aerosols in the head airways during natural breathing and during simulated breath holding using replicate human upper airway casts. Aerosol Sci Technol 1995, 23:465-474.

29.   Kelly JT, Asgharian B, Kimbell JS, Wong BA: Particle deposition in human nasal airway replicas manufactured by different methods. Part II: Ultrafine particles. Aerosol Sci Technol 2004, 38:1072-1079.

30.   Wang SM, Inthavong K, Wen J, Tu JY, Xue CL: Comparison of micron- and nanoparticle deposition patterns in a realistic human nasal cavity. Respir Physiol Neurobiol 2009, 166:142-151.

31.   Cheng YS, Holmes TD, Gao J, Guilmette RA, Li S, Surakitbanharn Y, Rowlings C: Characterization of nasal spray pumps and deposition pattern in a replica of the human nasal airway. J Aerosol Med 2001, 14:267-280.

32.   Javaheri E, Golshahi L, Finlay WH: An idealized geometry that mimics average infant nasal airway deposition. J Aerosol Sci 2013, 55:137-148.

33.   Nejati A, Kabaliuk N, Jermy MC, Cater JE: A deformable template method for describing and averaging the anatomical variation of the human nasal cavity. BMC Med Imaging 2016, 16:55.

34.   Shah SA, Dickens CJ, Ward DJ, Banaszek AA, George C, Horodnik W: Design of experiments to optimize an *in vitro* cast to predict human nasal drug deposition. J Aerosol Med Pulm Drug Deliv 2014, 27:21-29.

35.   Trows S, Wuchner K, Spycher R, Steckel H: *In vitro* nasal deposition in a nasal cast model: a useful tool in nasal drug product development. In Respiratory Drug Delivery. Edited by Byron PR, Peart J, Farr SJ, Suman JD, Young PM, Traini D. DHI Publishing; River Grove, IL; 2014: 391-396.

36.   Guo Y, Laube B, Dalby RN: The effect of formulation variables and breathing patterns on the site of nasal deposition in an anatomically correct model. Pharm Res 2005, 22:1871-1878.

37.   Kundoor V, Dalby RN: Effect of formulation- and administration-related variables on deposition pattern of nasal spray pumps evaluated using a nasal cast. Pharm Res 2011, 28:1895-1904.

38.   Kundoor V, Dalby RN: Assessment of nasal spray deposition pattern in a silicone human nose model using a color-based method. Pharm Res 2010, 27:30-36.

39.   Durand M, Vecellio L, Aubert G, Chantrel G, Prades JM: *In vitro* study of sonic aerosol delivery to maxillary sinuses treatment. In Respiratory Drug Delivery. Edited by Dalby RN, Byron PR, Peart J, Suman JD. DHI Publishing; River Grove, IL; 2005: 217-220.

40.   Le Guellec S, Le Pennec D, Gatier S, Leclerc L, Cabrera M, Pourchez J, Diot P, Reychler G, Pitance L, Durand M, et al: Validation of anatomical models to study aerosol deposition in human nasal cavities. Pharm Res 2014, 31:228-237.

41.   Janssens HM, de Jongste JC, Fokkens WJ, Robben SG, Wouters K, Tiddens HA: The sophia anatomical infant nose-throat (saint) model: a valuable tool to study aerosol deposition in infants. J Aerosol Med 2001, 14:433-441.

42.   Foo MY, Cheng YS, Su WC, Donovan MD: The influence of spray properties on intranasal deposition. J Aerosol Med 2007, 20:495-508.

43.   Kelly JT, Asgharian B, Kimbell JS, Wong BA: Particle deposition in human nasal airway replicas manufactured by different methods. Part I: Inertial regime particles. Aerosol Sci Technol 2004, 38:1063-1071.

44.   Walenga RL, Tian G, Hindle M, Yelverton J, Dodson K, Longest PW: Variability in nose-to-lung aerosol delivery. J Aerosol Sci 2014, 78:11-29.

45.   Golshahi L, Finlay WH: An idealized child throat that mimics average pediatric oropharyngeal deposition. Aerosol Sci Technol 2012, 46:I-IV.

46.   Guilmette RA WJ, Wolf RK: Morphometry of human nasal airways *in vivo* using magnetic resonance imaging. J Aerosol Med 1989, 2:365-377.

47.   Schroeter JD, Kimbell JS, Asgharian B: Analysis of particle deposition in the turbinate and olfactory regions using a human nasal computational fluid dynamics model. J Aerosol Med 2006, 19:301-313.

48.   Walenga R: CFD assessment of respiratory drug delivery efficiency in adults and improvements using controlled condensational growth. Virginia Commonwealth University, Mechanical and Nuclear Engineering; 2014.

49.   Ghori MU, Mahdi MH, Smith AM, Conway BR: Nasal drug delivery systems: an overview. Am J Pharmacol Sci 2015, 3:110-119.

50.   Marx D, Birkhoff M: Multi-dose container for nasal and ophthalmic drugs: a preservative free future? In Drug development: a case study based insight into modern strategies. Edited by Rundfeldt C: InTech Open Access Publisher; 2011

51.   Inthavong K, Tian ZF, Tu JY, Yang W, Xue C: Optimising nasal spray parameters for efficient drug delivery using computational fluid dynamics. Comput Biol Med 2008, 38:713-726.

52.   Suman JD, Laube BL, Dalby RN: Validity of *in vitro* tests on aqueous spray pumps as surrogates for nasal deposition, absorption, and biologic response. J Aerosol Med 2006, 19:510-521.

53.   Hinds WC: Aerosol technology: properties, behavior, and measurement of airborne particles. John Wiley & Sons; 2012.

54.   Cheng YS: Mechanisms of pharmaceutical aerosol deposition in the respiratory tract. AAPS PharmSciTech 2014, 15:630-640.

55.   Trows S, Wuchner K, Spycher R, Steckel H: Analytical challenges and regulatory requirements for nasal drug products in europe and the u.s. Pharmaceutics 2014, 6:195-219.

56.   Li B, Jin F, Lee SL, Bai T, Chowdhury B, Caramenico HT, Conner DP: Bioequivalence for locally acting nasal spray and nasal aerosol products: standard development and generic approval. AAPS J 2013, 15:875-883.

57.   Aggarwal R, Cardozo A, Homer JJ: The assessment of topical nasal drug distribution. Clin Otolaryngol Allied Sci 2004, 29:201-205.

58.   Berger WE, Jacobs RL, Amar NJ, Tantry SK, Li J, Small CJ: Efficacy and safety of beclomethasone dipropionate nasal aerosol in children with perennial allergic rhinitis. Ann Allergy Asthma Immunol 2015, 115:130-136.

59.   Natalie S, Priemel PA, Rades T, Nielsen HM: Inhalable antimicrobials for treatment of bacterial biofilm-associated sinusitis in cystic fibrosis patients : challenges and drug delivery approaches. Int J Mol Sci 2016, 17.

60.   Durand M, Le Guellec S, Pourchez J, Dubois F, Aubert G, Chantrel G, Vecellio L, Hupin C, De Gersem R, Reychler G, et al: Sonic aerosol therapy to target maxillary sinuses. Eur Ann Otorhinolaryngol Head Neck Dis 2012, 129:244-250.

61.   Djupesland PG, Skretting A: Nasal deposition and clearance in man: comparison of a bidirectional powder device and a traditional liquid spray pump. J Aerosol Med Pulm Drug Deliv 2012, 25:280-289.

62.   Schwartz JS, Tajudeen BA, Cohen NA: Medical management of chronic rhinosinusitis – an update. Expert Rev Clin Pharmacol 2016, 9:695-704.

63.   Smith KA, Orlandi RR, Rudmik L: Cost of adult chronic rhinosinusitis: A systematic review. Laryngoscope 2015, 125:1547-1556.

64.   Piromchai P, Kasemsiri P, Laohasiriwong S, Thanaviratananich S: Chronic rhinosinusitis and emerging treatment options. Int J Gen Med 2013, 6:453-464.

65.   Stenner M, Rudack C: Diseases of the nose and paranasal sinuses in child. GMS Curr Top Otorhinolaryngol Head Neck Surg 2014, 13.

66.   Blake K, Larsen J: Management of alergic rhinitisand sinusitis. J Pharm Pract 2001, 14:228-252.

67.   Robertson JM, Friedman EM, Rubin BK: Nasal and sinus disease in cystic fibrosis. Paediatr Respir Rev 2008, 9:213-219.

68.   Merkley MA, Bice TC, Grier A, Strohl AM, Man LX, Gill SR: The effect of antibiotics on the microbiome in acute exacerbations of chronic rhinosinusitis. Int Forum Allergy Rhinol 2015, 5:884-893.

69.   Legent F, Bordure P, Beauvillain C, Berche P: A double-blind comparison of ciprofloxacin and amoxycillin/ clavulanic acid in the treatment of chronic sinusitis. Chemotherapy 1994, 40:8-15.

70.   Fombeur JP, Barrault S, Koubbi G, Laurier JN, Ebbo D, Lecomte F, Sorrel N, Dobler S: Study of the Efficacy and Safety of Ciprofloxacin in the Treatment of Chronic Sinusitis. Chemotherapy 1994, 40:24-28.

71.   Vaughan WC, Carvalho G: Use of nebulized antibiotics for acute infections in chronic sinusitis. Otolaryngol Head Neck Surg 2002, 127:558-568.

72.   Oral versus topical antibiotics for chronic rhinosinusitis exacerbations [https://clinicaltrials.gov/ct2/show/NCT01988779].

73.   Merkley MA, Bice TC, Grier A, Strohl AM, Man LX, Gill SR: The effect of antibiotics on the microbiome in acute exacerbations of chronic rhinosinusitis. In; 2015. Wiley Online Library; 2015: 884-893.

74.   Tsifansky MD, Yeo Y, Evgenov OV, Bellas E, Benjamin J, Kohane DS: Microparticles for inhalational delivery of antipseudomonal antibiotics. AAPS J 2008, 10:254.

75.   Lai SK, Wang Y-Y, Hanes J: Mucus-penetrating nanoparticles for drug and gene delivery to mucosal tissues. Adv Drug Deliv Rev 2009, 61:158-171.

76.   Lai SK, Suk JS, Pace A, Wang YY, Yang M, Mert O, Chen J, Kim J, Hanes J: Drug carrier nanoparticles that penetrate human chronic rhinosinusitis mucus. Biomaterials 2011, 32:6285-6290.

77.   Günday Türeli N, Türeli AE, Schneider M: Optimization of ciprofloxacin complex loaded PLGA nanoparticles for pulmonary treatment of cystic fibrosis infections: Design of experiments approach. Int J Pharm 2016, 515:343-351.

78.   Gunday Tureli N, Tureli AE, Schneider M: Inhalable antibiotic nanoformulations for the treatment of pseudomonas aeruginosa infection in cystic fibrosis–a review. Drug Deliv Lett 2014, 4:193-207.

79.   Yu X, Zipp GL, Davidson Iii GWR: The effect of temperature and pH on the solubility of quinolone compounds: estimation of heat of fusion. Pharm Res 1994, 11:522-527.

80.   Roca Jalil ME, Baschini M, Sapag K: Influence of pH and antibiotic solubility on the removal of ciprofloxacin from aqueous media using montmorillonite. Appl Clay Sci 2015, 114:69-76.

81.   Paton JH, Reeves DS: Fluoroquinolone antibiotics. Drugs 1988, 36:193-228.

82.   Davis R, Markham A, Balfour JA: Ciprofloxacin. An updated review of its pharmacology, therapeutic eficacy and tolerability. Drugs 1996, 51:1019-1074.

83.   Bayer: Cipro (Ciprofloxacin Hydrochloride) drug label. 2009.

84.   Lettieri JT, Rogge MC, Kaiser L, Echols RM, Heller AH: Pharmacokinetic profiles of ciprofloxacin after single intravenous and oral doses. Antimicrob Agents Chemother 1992, 36:993-996.

85.   Piercy EA, Bawdon RE, Mackowiak PA: Penetration of ciprofloxacin into saliva and nasal secretions and effect of the drug on the oropharyngeal flora of ill subjects. vol. 33. pp. 1645-1646; 1989:1645-1646.

86.   Darouiche R, Perkins B, Musher D, Hamill R, Tsai S: Levels of rifampin and ciprofloxacin in nasal secretions: correlation with mic 90 and eradication of nasopharyngeal carriage of bacteria. J Infect Dis 1990, 162:1124-1127.

87.   Endermann R, Labischinski H, Ladel C, Petersen U, Newton B; Bayer Pharma Aktiengesellschaft, Treatment of bacterial diseases of the respiratory organs. US 8034817 B2. Oct 11, 2011.

88.	Dorkin HL, Staab D, Operschall E, Alder J, Criollo M: Ciprofloxacin DPI: a randomised, placebo-controlled, phase IIb efficacy and safety study on cystic fibrosis. BMJ Open Respir Res 2015, 2:e000100.

89.	Stass H, Nagelschmitz J, Willmann S, Delesen H, Gupta A, Baumann S: Inhalation of a dry powder ciprofloxacin formulation in healthy subjects: a phase I study. Clin Drug Investig 2013, 33:419-427.

90.	Phase 3 study with dual release ciprofloxacin for inhalation in non-CF bronchiectasis (ORBIT-4) [https://clinicaltrials.gov/ct2/show/NCT02104245].

91.	Wright DH, Brown GH, Peterson ML, Rotschafer JC: Application of fluoroquinolone pharmacodynamics. J Antimicrob Chemother 2000, 46:669-683.

92.	Djupesland PG, Messina JC, Mahmoud RA: Breath powered nasal delivery: a new route to rapid headache relief. Headache 2013, 53 Suppl 2:72-84.

93.	Amidon GL, Lennernas H, Shah VP, Crison JR: A theoretical basis for a biopharmaceutic drug classification: the correlation of *in vitro* drug product dissolution and *in vivo* bioavailability. Pharm Res 1995, 12:413-420.

94.	Lipinski C: Poor aqueous solubility—an industry wide problem in drug discovery. Am Pharm Rev 2002, 5:82-85.

95.	Merisko-Liversidge EM, Liversidge GG: Drug nanoparticles: formulating poorly water-soluble compounds. Toxicol Pathol 2008, 36:43-48.

96.	Date AA, Patravale VB: Current strategies for engineering drug nanoparticles. Curr Opin Colloid Interface Sci 2004, 9:222-235.

97.	Rabinow BE: Nanosuspensions in drug delivery. Nat Rev Drug Discov 2004, 3:785-796.

98.	Möschwitzer J, Nadiem Bushrab F, Müller RH: Manufacturing of nanoparticles by milling and homogenization techniques. In Nanoparticle technology for drug delivery. Edited by Gupta R, Kompella U: CRC Press; 2006

99.	Horn D, Rieger J: Organic nanoparticles in the aqueous phase—theory, experiment, and use. Angew Chem Int Ed Engl 2001, 40:4330-4361.

100.	Liedtke S, Wissing S, Muller RH, Mader K: Influence of high pressure homogenisation equipment on nanodispersions characteristics. Int J Pharm 2000, 196:183-185.

101. Muller RH, Becker R, Kruss B, Peters K; Medac Gesellschaft Fur Klinische Spezialpraparate, Pharmaceutical nanosuspensions for medicament administration as systems with increased saturation solubility and rate of solution. US5858410 A. Jan 12, 1999.

102. Van Eerdenbrugh B, Van den Mooter G, Augustijns P: Top-down production of drug nanocrystals: nanosuspension stabilization, miniaturization and transformation into solid products. Int J Pharm 2008, 364:64-75.

103. Mullin JW: Crystallization. 4th edn: Butterworth-Heinemann; 2001.

104. Dirksen JA, Ring TA: Fundamentals of crystallization: Kinetic effects on particle size distributions and morphology. Chem Eng Sci 1991, 46:2389-2427.

105. Mudhoo A: Handbook on applications of ultrasound: sonochemistry for sustainability. CRC press; 2011.

106. Dalvi SV, Dave RN: Controlling particle size of a poorly water-soluble drug using ultrasound and stabilizers in antisolvent precipitation. Ind Eng Chem Res 2009, 48:7581-7593.

107. Castillo-Peinado LdlS, Luque de Castro MD: The role of ultrasound in pharmaceutical production: sonocrystallization. J Pharm Pharmacol 2016, 68:1249-1267.

108. Park M-W, Yeo S-D: Antisolvent crystallization of roxithromycin and the effect of ultrasound. Sep Sci Technol 2010, 45:1402-1410.

109. Dhumal RS, Biradar SV, Paradkar AR, York P: Particle engineering using sonocrystallization: Salbutamol sulphate for pulmonary delivery. Int J Pharm 2009, 368:129-137.

110. Nishida I: Precipitation of calcium carbonate by ultrasonic irradiation. Ultrason Sonochem 2004, 11:423-428.

111. Kim HN, Sander JRG, Zeiger BW, Suslick KS: Spray sonocrystallization. Cryst Growth Des 2015, 15:1564-1567.

112. Masters K: Spray drying handbook. 4th edn: George Godwin Ltd.; 1985.

113. Maa YF, Costantino HR, Nguyen PA, Hsu CC: The effect of operating and formulation variables on the morphology of spray-dried protein particles. Pharm Dev Technol 1997, 2:213-223.

114. Mansour HM, Rhee YS, Wu X: Nanomedicine in pulmonary delivery. Int J Nanomedicine 2009, 4:299-319.

115. Weers JG, Tarara TE, Clark AR: Design of fine particles for pulmonary drug delivery. Expert Opin Drug Deliv 2007, 4:297-313.

116. Vehring R: Pharmaceutical particle engineering via spray drying. Pharm Res 2008, 25:999-1022.

117. Lechuga-Ballesteros D, Charan C, Liang Y, Stults C, Vehring R, Kuo MC: Designing stable and high performance respirable particles of pharmaceuticals. In Respiratory Drug Delivery IX. Edited by Dalby RN, Byron PR, Peart J, Suman JD, Farr SJ. DHI Publishing; River Grove, IL; 2004: 565-568.

118. Van Eerdenbrugh B, Froyen L, Van Humbeeck J, Martens JA, Augustijns P, Van den Mooter G: Drying of crystalline drug nanosuspensions—The importance of surface hydrophobicity on dissolution behavior upon redispersion. Eur J Pharm Sci 2008, 35:127-135.

119. Kumar S, Gokhale R, Burgess DJ: Sugars as bulking agents to prevent nano-crystal aggregation during spray or freeze-drying. Int J Pharm 2014, 471:303-311.

120. Sham JOH, Zhang Y, Finlay WH, Roa WH, Löbenberg R: Formulation and characterization of spray-dried powders containing nanoparticles for aerosol delivery to the lung. Int J Pharm 2004, 269:457-467.

121. Doughty DV, Vibbert C, Kewalramani A, Bollinger ME, Dalby RN: Automated actuation of nasal spray products: determination and comparison of adult and pediatric settings. Drug Dev Ind Pharm 2011, 37:359-366.

122. Schoenbrodt T, Egen M, Heyder K, Kohler D, Kranz Y, Mueller C, Schiewe J: Method development for deposition studies in a nasal cast. In Respiratory Drug Delivery. Edited by Dalby RN, Byron PR, Peart J, Farr SJ, Suman JD, Young PM. DHI Publishing; River Grove, IL; 2010: 445-450.

123. Nasonex® prescribing information [www.accessdata.fda.gov/drugsatfda_docs/label/2010/020762s038lbl.pdf].

124. Guilmette RA, Wicks JD, Wolff RK: Morphometry of human nasal airways in vivo using Magnetic Resonance Imaging. J Aerosol Med 1989, 2:365-377.

125. Golshahi L, Longest PW, Azimi M, Syed A, Hindle M: Intermittent aerosol delivery to the lungs during high-flow nasal cannula therapy. Respir Care 2014, 59:1476-1486.

126.   Longest PW, Golshahi L, Behara SRB, Tian G, Farkas DR, Hindle M: Efficient nose-to-lung (N2L) aerosol delivery with a dry powder inhaler. J Aerosol Med Pulm Drug Deliv 2015, 28:189-201.

127.   Longest PW, Tian G, Hindle M: Improving the lung delivery of nasally administered aerosols during noninvasive ventilation—an application of enhanced condensational growth (ECG). J Aerosol Med Pulm Drug Deliv 2011, 24:103-118.

128.   Xi J, Longest PW: Transport and deposition of micro-aerosols in realistic and simplified models of the oral airway. Ann Biomed Eng 2007, 35:560-581.

129.   Council of Europe. European Pharmacopoeia. 5th edn; 2005.

130.   Callens C, Ceulemans J, Ludwig A, Foreman P, Remon JP: Rheological study on mucoadhesivity of some nasal powder formulations. Eur J Pharm Biopharm 2003, 55:323-328.

131.   Dayal P, Shaik MS, Singh M: Evaluation of different parameters that affect droplet-size distribution from nasal sprays using the Malvern Spraytec. J Pharm Sci 2004, 93:1725-1742.

132.   Rygg A, Longest PW: Absorption and clearance of pharmaceutical aerosols in the human nose: dDevelopment of a CFD model. J Aerosol Med Pulm Drug Deliv 2016, 29:416-431.

133.   NASONEX®   Product   Monograph [http://www.merck.ca/assets/en/pdf/products/NASONEX-PM_E.pdf].

134.   Crim C, Pierre LN, Daley-Yates PT: A review of the pharmacology and pharmacokinetics of inhaled fluticasone propionate and mometasone furoate. Clinical Therapeutics 2001, 23:1339-1354.

135.   Mometasone Furoate [www.rsc.org/merckindex].

136.   Harris AS, Nilsson IM, Wagner ZG, Alkner U: Intranasal administration of peptides: nasal deposition, biological response, and absorption of desmopressin. J Pharm Sci 1986, 75:1085-1088.

137.   Möller W, Schuschnig U, Celik G, Munzing W, Bartenstein P, Haussinger K, Kreyling WG, Knoch M, Canis M, Becker S: Topical drug delivery in chronic rhinosinusitis patients before and after sinus surgery using pulsating aerosols. PloS One 2013, 8:e74991.

138.   Foo MY: Depositin pattern of nasal sprays in the human nasal airways. The University of Iowa, 2007.

139. Benninger MS, Hadley JA, Osguthorpe JD, Marple BF, Leopold DA, Derebery M J, Hannley M: Techniques of Intranasal Steroid Use. Otolaryngol Head Neck Surg 2004, 130:5-24.

140. Shah SA, Berger RL, McDermott J, Gupta P, Monteith D, Connor A, Lin W: Regional deposition of mometasone furoate nasal spray suspension in humans. Allergy Asthma Proc 2014, 36:48- 57.

141. Doughty DV, Hsu W, Dalby RN: Automated actuation of nasal spray products: effect of hand-related variability on the *in vitro* performance of Flonase nasal spray. Drug Dev Ind Pharm 2014, 40:711-718.

142. Gungor A, Moinuddin R, Nelson RH, Corey JP: Detection of the nasal cycle with acoustic rhinometry: techniques and applications. Otolaryngol Head Neck Surg 1999, 120:238-247.

143. Clark AR, Hollingworth AM: The relationship between powder inhaler resistance and peak inspiratory conditions in healthy volunteers — implications for *in vitro* testing. J Aerosol Med 1993, 6:99-110.

144. FDA: Guidance for Industry (Draft). Bioavailability and Bioequivalence Studies for Nasal Aerosols and Nasal Sprays for Local Action. 2003.

145. Djupesland PG, Mahmoud RA: Letter to the editor: incorrect conclusions regarding deposition of conventional mometasone furoate (MF) nasal spray. Allergy Asthma Proc 2015, 36:e104.

146. Guo C, Doub WH: The influence of actuation parameters on *in vitro* testing of nasal spray products. J Pharm Sci 2006, 95:2029-2040.

147. Eron LJ, Harvey L, Hixon DL, Poretz DM: Ciprofloxacin therapy of infections caused by Pseudomonas aeruginosa and other resistant bacteria. Antimicrob Agents Chemother 1985, 28:308-310.

148. Davis R, Markham A, Balfour JA: Ciprofloxacin. An updated review of its pharmacology, therapeutic efficacy and tolerability. Drugs 1996, 51:1019-1074.

149. Guss J, Abuzeid WM, Doghramji L, Edelstein PH, Chiu AG: Fluoroquinolone-resistant Pseudomonas aeruginosa in chronic rhinosinusitis. ORL J Otorhinolaryngol Relat Spec 2009, 71:263-267.

150. Longest PW, Behara S, Farkas D, Golshahi L, Tian G, Hindle M: Efficient generation and delivery of dry powder aerosols during low flow oxygen administration. In J Aerosol Med Pulm Drug Deliv; 2015. Mary Ann Liebert, INC.; 2015: A9-A10.

151. Ong HX, Traini D, Cipolla D, Gonda I, Bebawy M, Agus H, Young PM: Liposomal nanoparticles control the uptake of ciprofloxacin across respiratory epithelia. Pharmaceutical Research 2012, 29:3335-3346.

152. Caço AI, Varanda F, Pratas de Melo MJ, Dias AMA, Dohrn R, Marrucho IM: Solubility of antibiotics in different solvents. part ii. non-hydrochloride forms of tetracycline and ciprofloxacin. Ind Eng Chem Res 2008, 47:8083-8089.

153. Behara SR, Longest PW, Farkas DR, Hindle M: Development of high efficiency ventilation bag actuated dry powder inhalers. Int J Pharm 2014, 465:52-62.

154. Son YJ, Longest PW, Hindle M: Aerosolization characteristics of dry powder inhaler formulations for the excipient enhanced growth (EEG) application: effect of spray drying process conditions on aerosol performance. Int J Pharm 2013, 443:137-145.

155. Son YJ, Longest PW, Tian G, Hindle M: Evaluation and modification of commercial dry powder inhalers for the aerosolization of a submicrometer excipient enhanced growth (EEG) formulation. Eur J Pharm Sci 2013, 49:390-399.

156. Marple VA, Olson BA, Santhanakrishnan K, Mitchell JP, Murray SC, Hudson-Curtis BL: Next generation pharmaceutical impactor (a new impactor for pharmaceutical inhaler testing). part II: archival calibration. J Aerosol Med 2003, 16:301-324.

157. Mitchell J: Practices of coating collection surfaces of cascade impactors: a survey of members of the European Pharmaceutical Aerosol Group (EPAG). Drug Deliv Lung 2003, 14:75-78.

158. Xia D, Quan P, Piao H, Piao H, Sun S, Yin Y, Cui F: Preparation of stable nitrendipine nanosuspensions using the precipitation–ultrasonication method for enhancement of dissolution and oral bioavailability. Eur J Pharm Sci 2010, 40:325-334.

159. Matteucci ME, Hotze MA, Johnston KP, Williams RO: Drug nanoparticles by antisolvent precipitation: mixing energy versus surfactant stabilization. Langmuir 2006, 22:8951-8959.

160. Lifshitz IM, Slyozov VV: The kinetics of precipitation from supersaturated solid solutions. J Phys Chem Solids 1961, 19:35-50.

161. Liu Y, Kathan K, Saad W, Prud'homme RK: Ostwald ripening of β-carotene nanoparticles. Physical Review Letters 2007, 98:036102.

162.	Iyer SR, Gogate PR: Ultrasound assisted crystallization of mefenamic acid: Effect of operating parameters and comparison with conventional approach. Ultrason Sonochem 2017, 34:896-903.

163.	Ruecroft G, Hipkiss D, Ly T, Maxted N, Cains PW: Sonocrystallization: the use of ultrasound for improved industrial crystallization. Org Process Res Dev 2005, 9:923-932.

164.	Thorat AA, Dalvi SV: Liquid antisolvent precipitation and stabilization of nanoparticles of poorly water soluble drugs in aqueous suspensions: Recent developments and future perspective. Chem Eng J 2012, 181:1-34.

165.	Kougoulos E, Marziano I, Miller PR: Lactose particle engineering: Influence of ultrasound and anti-solvent on crystal habit and particle size. Journal of Crystal Growth 2010, 312:3509-3520.

166.	Dirksen JA, Ring TA: Fundamentals of crystallization: Kinetic effects on particle size distributions and morphology. Chemical Engineering Science 1991, 46:2389-2427.

167.	Pi ZB, Zhao XY, Yang C, Fei JB, Tian XK: Preparation of ultrafine particles of azithromycin by sonochemical method. Nanomedicine 2007, 3:86-88.

168.	Ali HSM, York P, Blagden N: Preparation of hydrocortisone nanosuspension through a bottom-up nanoprecipitation technique using microfluidic reactors. Int J Pharm 2009, 375:107-113.

169.	Caço AI, Varanda F, Pratas de Melo MJ, Dias AMA, Dohrn R, Marrucho IM: Solubility of Antibiotics in Different Solvents. Part II. Non-Hydrochloride Forms of Tetracycline and Ciprofloxacin. Industrial & Engineering Chemistry Research 2008, 47:8083-8089.

170.	Chaubal MV, Popescu C: Conversion of nanosuspensions into dry powders by spray drying: a case study. Pharm Res 2008, 25:2302-2308.

171.	Turel I, Bukovec P: Comparison of the thermal stability of ciprofloxacin and its compounds. Thermochimica Acta 1996, 287:311-318.

172.	Liu Y, Wang J, Yin Q: The crystal habit of ciprofloxacin hydrochloride monohydrate crystal. J Cryst Growth 2005, 276:237-242.

173.	Weers J, Tarara T; Novartis Ag, Pulmonary delivery of a fluoroquinolone. US8834930 B2. Sep 16, 2014.

174.	Su W-C, Cheng YS: Deposition of fiber in the human nasal airway. Aerosol Sci Technol 2005, 39:888-901.

175.   Ciprofloxacin dry powder for inhalation in non-cystic fibrosis bronchiectasis (Non-CF BE) (RESPIRE 1) [https://clinicaltrials.gov/ct2/show/NCT01764841].

176.   Stass H, Nagelschmitz J, Willmann S, Delesen H, Gupta A, Baumann S: Inhalation of a Dry Powder Ciprofloxacin Formulation in Healthy Subjects: A Phase I Study. Clin Drug Investig 2013, 33:419-427.

177.   Vasa DM, O'Donnell LA, Wildfong PLD: Influence of dosage form, formulation, and delivery device on olfactory deposition and clearance: enhancement of nose-to-CNS uptake. J Pharm Innov 2015, 10:200-210.

178.   Djupesland PG, Skretting A, Winderen M, Holand T: Bi-Directional nasal delivery of aerosols can prevent lung deposition. J Aerosol Med 2004, 17:249-259.

179.   Durand M, Pourchez J, Aubert G, Le Guellec S, Navarro L, Forest V, Rusch P, Cottier M: Impact of acoustic airflow nebulization on intrasinus drug deposition of a human plastinated nasal cast: new insights into the mechanisms involved. Int J Pharm 2011, 421:63-71.

180.   Maniscalco M, Sofia M, Weitzberg E, Lundberg JO: Sounding airflow enhances aerosol delivery into the paranasal sinuses. Eur J Clin Invest 2006, 36:509-513.

181.   Darweesh R: *In vitro* lung epithelial cell transport and anti-inflammatory activity for liposomal ciprofloxacin. Virginia Commonwealth University, Pharmaceutics; 2013.

182.   Cavet ME, West M, Simmons NL: Transepithelial transport of the fluoroquinolone ciprofloxacin by human airway epithelial Calu-3 cells. Antimicrob Agents Chemother 1997, 41:2693-2698.

183.   Ong HX, Traini D, Salama R, Anderson SD, Daviskas E, Young PM: The effects of mannitol on the transport of ciprofloxacin across respiratory epithelia. Mol Pharm 2013, 10:2915-2924.

184.   Muller L, Brighton LE, Carson JL, Fischer WA, 2nd, Jaspers I: Culturing of human nasal epithelial cells at the air liquid interface. J Vis Exp 2013.

185.   Park DY, Kim S, Kim CH, Yoon JH, Kim HJ: Alternative method for primary nasal epithelial cell culture using intranasal brushing and feasibility for the study of epithelial functions in allergic rhinitis. Allergy Asthma Immunol Res 2016, 8:69-78.

186.   Mathias N, Kim K-J, Lee V: Targeted drug delivery to the respiratory tract: solute permeability of air-interface cultured rabbit tracheal epithelial cell monolayers. J Drug Target 1996, 4:79-86.

187. Yamaya M, Finkbeiner WE, Chun SY, Widdicombe JH: Differentiated structure and function of cultures from human tracheal epithelium. Am J Physiol 1992, 262:L713-724.

188. Whitcutt MJ, Adler KB, Wu R: A biphasic chamber system for maintaining polarity of differentiation of cultured respiratory tract epithelial cells. *In Vitro* Cell Dev Biol 1988, 24:420-428.

189. Lin H, Gebhardt M, Bian S, Kwon KA, Shim CK, Chung SJ, Kim DD: Enhancing effect of surfactants on fexofenadine·HCl transport across the human nasal epithelial cell monolayer. Int J Pharm 2007, 330:23-31.

190. Lee MK, Yoo JW, Lin H, Kim YS, Kim DD, Choi YM, Park SK, Lee CH, Roh HJ: Air-liquid interface culture of serially passaged human nasal epithelial cell monolayer for *in vitro* drug transport studies. Drug Deliv 2005, 12:305-311.

191. Jorissen M, Van der Schueren B, Van den Berghe H, Cassiman JJ: The preservation and regeneration of cilia on human nasal epithelial cells cultured *in vitro.* Arch Otorhinolaryngo 1989, 246:308-314.

192. Stapleton KW, Guentsch E, Hoskinson MK, Finlay WH: On the suitability of k–ε turbulence modeling for aerosol deposition in the mouth and throat: a comparison with experiment. J Aerosol Sci 2000, 31:739-749.

193. Emanuel IA, Blaiss MS, Meltzer EO, Evans P, Connor A: Nasal deposition of ciclesonide nasal aerosol and mometasone aqueous nasal spray in allergic rhinitis patients. Am J Rhinol Allergy 2014, 28:117-121.

194. Tsifansky MD, Yeo Y, Evgenov OV, Bellas E, Benjamin J, Kohane DS: Microparticles for inhalational delivery of antipseudomonal antibiotics. AAPS J 2008, 10:254-260.

Vita

Mandana Azimi

I. EDUCATION

Doctor of Philosophy, Pharmaceutical Science   2013- present
Virginia Commonwealth University (VCU), School of Pharmacy
Richmond, VA

Doctor of Pharmacy   2001- 2006
Tabriz University of Medical Sciences, School of Pharmacy
Tabriz, Iran

II. PUBLICATIONS

1. **Azimi, M.**, Hindle, M., and Longest, P. W. (2015) Towards clinically relevant *in vitro* testing of locally acting nasal spray suspension products, Proceedings of Respiratory Drug Delivery Europe, 1:121-130.
2. Golshahi, L., Longest, P. W., **Azimi, M**., Syed, A., and Hindle. M. (2014) Intermittent aerosol delivery to the lungs during high-flow nasal cannula therapy. Respir Care. 59(10):1476-86.
3. Longest, P. W., **Azimi, M.**, and Hindle, M. (2013) Optimal delivery of aerosols to infants during mechanical ventilation. J Aerosol Med Pulm Drug Deliv. 27(5):371-85.
4. Longest, P. W., **Azimi, M.**, Golshahi, L., and Hindle. M. (2013) Improving aerosol drug delivery during invasive mechanical ventilation with redesigned components. Respir Care. 59(5):686-98.
5. Golshahi L, Tian, G., **Azimi, M.**, Son, Y. J, Walenga, R., Longest, P. W., and Hindle. M. (2013) The use of condensational growth methods for efficient drug delivery to the lungs during noninvasive ventilation high flow therapy. Pharm Res. 30(11):2917-30.
6. Zakeri-Milani, P., Barzegar-Jalali, and Valizadeh, H., **Azimi, M.** (2009) Biopharmaceutical classification of drugs using intrinsic dissolution rate (IDR) and rat intestinal permeability. Eur J Pharm Biopharm 73(1):102-6.
7. Zakeri-Milani. P., Barzegar-Jalali. M., Valizadeh, H., **Azimi. M.**, and Hallaj nezhadi, S. (2008) Study of the correlation between intrinsic dissolution rate and some physicochemical and Pharmacokinetic parameters of the compounds. Pharmaceutical Sciences (Journal of Tabriz Faculty of Pharmacy), 21-31.

III. POSTER PRESENTATIONS and ABSTRACTS

1. **Azimi, M.**, Darweesh, R., Hindle, M., Farkas, R. D., Golshahi, L., Sakagami, M., and Longest, P. W. (2017) The use of a physically realistic nasal airway model for the assessment of *in vitro* transepithelial transport of nasally administered Drugs, International Society for Aerosols in Medicine (ISAM), Santa Fe, NM, June 3.

2. **Azimi, M.**, Hindle, M., and Longest, P. W. (2016) Comparison of the *in vitro* deposition of Nasonex® nasal spray product in two realistic nasal airway models, American Association of Pharmaceutical Scientist (AAPS), Denver, CO, USA, November 13.
3. **Azimi, M.**, Hindle, M., and Longest, P. W. (2016) Comparison of the *in vitro* deposition of Nasonex® nasal spray product in two realistic nasal airway models, Proceeding of Respiratory Drug Delivery (RDD), Phoenix, AZ, USA, April 17.
4. **Azimi, M.** and Hindle, M. (2016) Clinically relevant *in vitro* tests for the assessment of innovator and generic nasal spray products. Pharmaceutical Sciences Research and Career Day. Richmond, VA, USA, October 27.
5. **Azimi, M.,** Hindle, M., and Longest, P. W. (2015) Assessing the regional nasal deposition of Nasonex using two realistic *in vitro* models. Pharmaceutical Sciences Research and Career Day. Richmond, VA, USA, October 30.
6. **Azimi, M.,** Hindle, M, and Longest, P. W. (2014) *In vitro* regional deposition of Nasonex® nasal spray in a realistic nasal physical model. Pharmaceutical Sciences Research and Career Day. Richmond, VA, USA, October 17.
7. **Azimi. M.**, Valizadeh. H., Wei. H., and Leobenberg. R. (2005) Simulating intestinal absorption estimating bioequivalence of glibenclamide using *in vitro* experiments, 11th Seminar of Iranian Pharmacy Students, Shiraz, Iran, Nov 9.

IV.   PODIUM PRESENTATION

Azimi, M., Longest, P. W., Shur J., Price R., and Hindle, M. (2016) Clinically relevant *in vitro* tests for the assessment of innovator and generic nasal spray products, Drug Delivery to the Lungs, Scotland, UK, December 7.

V.   SCHOLARSHIPS/HONORS/ACHIEVEMENTS

AAPS Travelship sponsored by AstraZeneca	2016
VCU Graduate School Dissertation Assistantships (Fall 2016 & Spring 2017)	2016
VCU Department of Pharmaceutics John Wood Award for the greatest distinction in the areas of scholarship, teaching and service	2016
VCU School of Pharmacy Travel Award	2016
VCU Graduate Student Travel Grant	2016
Elected student member of AAPS Inhalation and Nasal Technology Focus Group Executive Committee	2015
Honored member of Phi Kappa Phi Society	2015
Honored member of Alpha Phi Chapter of Alpha Epsilon Lambda Society	2014
Full scholarship for six years, Awarded by Ministry of Health, Iran	2000-2006